Geological Survey of Finland

2022

Geological evolution and structure along the western boundary of the Outokumpu allochthon

Perttu Mikkola, Soile Aatos, Tapio Halkoaho, Suvi Heinonen, Jaakko Hietava, Satu Hietala, Matti Kurhila, Jani Jäsberg, Eeva-Liisa Laine, Jouni Luukas, Matti Niskanen, Maarit Nousiainen, Henrik Nygård, Anni Piispanen, Heikki Pirinen, Hanna Rantanen and Ilona Romu

GTK Open File Research Report 23/2022

GTK

GEOLOGICAL SURVEY OF FINLAND

Open File Research Report 23/2022

Perttu Mikkola, Soile Aatos, Tapio Halkoaho, Suvi Heinonen, Jaakko Hietava, Satu Hietala, Matti Kurhila, Jani Jäsberg, Eeva-Liisa Laine, Jouni Luukas, Matti Niskanen, Maarit Nousiainen, Henrik Nygård, Anni Piispanen, Heikki Pirinen, Hanna Rantanen and Ilona Romu

Geological evolution and structure along the western boundary of the Outokumpu allochthon

Unless otherwise indicated, the figures have been prepared by the authors of the report.

Front cover: Beautiful summer day on Lake Kallavesi. Shoreline outcrops north of Puutossalmi provided excellent opportunities to study the autochthonous cover series of the Karelia group; quartzites and carbonate rocks topped with pillow-structured mafic volcanic rocks.
Photo: Perttu Mikkola, GTK.

Layout of figures: Riitta Turunen, GTK
Layout: Elvi Turtiainen Oy

Espoo 2022

Mikkola, P., Aatos, S., Halkoaho, T., Heinonen, S., Hietava, J., Hietala, S., Kurhila, M., Jäsberg, J., Laine, E.-L., Luukas, J., Niskanen, M., Nousiainen, M., Nygård, H., Piispanen, A., Pirinen, H., Rantanen, H. & Romu, I. 2022. Geological evolution and structure along the western boundary of the Outokumpu allochthon. *Geological Survey of Finland, Open File Research Report 23/2022,* 117 pages, 63 figures, 10 tables, 5 appendices and 2 electronic appendices.

This report summarises nearly four years of geological work carried out in Central Finland in an area interpreted as the western boundary of the Outokumpu allochthon. The study area also includes the south-westernmost known exposures of Archaean crust in Finland, and its southwest corner is traversed by the Raahe-Ladoga suture zone. The purpose of the work was to re-evaluate the overall Palaeoproterozoic evolution of this partially poorly studied area in order to evaluate its ore potential.

The Archaean crust in the study area includes southern parts of the Kuopio complex and variably sized domes or thrust sheets south of it. Main rock types are granitoids and migmatites of the Tonalite–Trondhjemite–Granodiorite suite (TTG) and porphyritic granodiorites displaying characteristics of the sanukitoid suite (high Ba, K2O, Mg#, Cr, Ni), with smaller amounts of quartz diorites. TTGs in the study area and its vicinity yielded ages between 2.8 and 2.7 Ga. Ages of the sanukitoids and quartz diorites are poorly constrained but are likely to be close to 2.7 Ga. Overall, the observed ages and compositions support the interpretation that the domes and thrust sheets are continuations of the Kuopio complex rather than exotic terranes accreted during the Svecofennian orogeny.

The autochthonous cover series of the Karelia group along the edges of the Archaean rocks are variably preserved. The successions display a change from conglomerates to more sandy sediments and carbonate rocks topped with often pillow-structured mafic volcanic rocks and to paragneisses deposited originally as turbidites. A major change to previous interpretations is that the autochthonous paragneisses occupy significantly smaller areas than previously thought.

The voluminous paragneisses in the study area have been divided into two major allochthonous units, the Viinijärvi suite in the east, with the associated Outokumpu assemblage serpentinites, and Suonenjoki suite in the west. Based on their detrital zircon populations, yielding maximum deposition ages of 1.92–1.91 Ga, and their geochemical composition, the units are nearly identical. Thus, it is likely that the boundary between the units reflects more the structural evolution than the differences in depositional basins or the source material of the paragneisses.

Four major deformation phases can be identified from the study area, of which the first (~1.92 Ga) resulted from a collision of Archaean blocks creating thin-skinned thrusting characterizing Outokumpu allochthon consisting of Viinijärvi and Outokumpu suites. The second deformation phase (~1.91 Ga) resulted also in thrusting and folding of Archaean basement and autochthonous cover rocks in the area as a response to collision of the Savo arc from west. The third deformation phase (~1.90–1.87 Ga) was caused by approach and accretion of the next island arc from the south and, in addition to folding, the major SE-NW-trending dextral shears and their conjugates developed. The fourth deformation phase (1.84–1.80 Ga) in the study area is only observable as continued activity along the shear zones.

Granitoids with ages around 1.87 Ga are variably voluminous in the study area, present on most of the larger outcrops as veins, and locally forming major intrusions (e.g. Suvasvesi granite). Veins are variably deformed indicating intrusion during regional D3 and after it. Based on their compositional characteristics they are mainly felsic I-type with locally more mafic compositions indicating some input also from mantle.

Numerous small occurrences of Outokumpu assemblage rocks have been known north of the Suvasvesi shear zone. South of the shear zone, the number of known occurrences is significantly smaller, and they had not been studied in detail. The new data confirms that they are true members of the Outokumpu assemblage associated with specific structural features. Due to this strict spatial association, it is interpreted that the potential for new Outokumpu-type deposits southwest of the Suvasvesi shear zone is small.

As part of the project, a regional 3D model was constructed using all the available data and structural interpretations. Mineral potential modelling and exploratory data analysis methods were used to delineate areas potentially hosting rocks of the Outokumpu assemblage and to differentiate between the voluminous paragneisses in the area.

Electronic appendices 1 and 2 are available at https://tupa.gtk.fi/raportti/aineistotallenne/23_2022.zip

Keywords: paragneiss, greywackes, granitoids, granites, structural geology, thrust faults, shear zones, modelling, 3D modelling, zircon, absolute age, Archaean, Palaeoproterozoic, Raahe-Ladoga Zone, Outokumpu Area, Finland

Perttu Mikkola, Soile Aatos, Tapio Halkoaho, Satu Hietala, Jani Jäsberg, Jouni Luukas, Matti Niskanen, Maarit Nousiainen, Heikki Pirinen and Ilona Romu
Geological Survey of Finland
P.O. Box 1237
FI-70211 Kuopio, Finland

E-mail: perttu.mikkola@gtk.fi

Suvi Heinonen, Jaakko Hietava, Matti Kurhila, Eeva-Liisa Laine and Henrik Nygård
Geological Survey of Finland
P.O. Box 96
FI-02151 Espoo, Finland

Anni Piispanen
Oulu Mining School, University of Oulu
P.O. Box 3000
FI-90014 Oulun Yliopisto, Finland

Hanna Rantanen
Department of Geosciences and Geography, University of Helsinki
P.O. Box 64
FI-00014 Helsinki, Finland

CONTENTS

1 INTRODUCTION

The discoveries of Outokumpu Cu-Co-Zn ore in 1910 (Saksela 1948) and Kotalahti Ni-Cu ore in 1954 (Papunen & Koskinen 1985) have for long stimulated geological studies in these districts located in vicinity of the Archaean-Proterozoic boundary in East Finland. Vast amounts of geological and geophysical data have been collected around the most prospective geological units. The approach driven by mineral exploration left a less studied area in between, which forms the core of our current study area (Fig. 1). This selection made in 2018 was based on Geological Survey of Finland's (GTK) strategy, part of which at that time was the identification of new ore potential areas and better delineation of the boundaries of the known ones by updating basic geological data. Kotalahti type, magmatic Ni-Cu sulphide ores, are known from the core of the NW-SE-trending dextral Raahe-Ladoga suture zone, forming the boundary between Palaeoproterozoic Svecofennian domain in the west and Archaean Karelia domain in the east. Outokumpu-type ores are associated with intensively altered Palaeoproterozoic ophiolite fragments emplaced as tectonic slivers within the voluminous paragneisses covering the Archaean craton. These paragneisses and enclosed ophiolite fragments are interpreted to be allochthonous (Wegmann 1928, Koistinen 1981) and to form the Outokumpu allochthon, for which the latest definition is given by Luukas & Kohonen (2021).

Printed 1:100 000 bedrock maps surrounding the study area have been published but those from the area have not (Fig. 2). Western part of the study area is covered by a 1:400 000 bedrock map by Wilkman (1935) and eastern part by Frosterus and Wilkman (1924). Field maps (1:20 000) compiled by Outokumpu Oy ore exploration exist from parts of the area. Appendix 1 of this publication is the updated bedrock map from the core study area of the project, but it should be noted that it is not of equal quality. Certain areas have been studied in more detail than others, e.g. the north-eastern corner of the study area, consisting mainly of Archaean and Palaeoproterozoic plutonic rocks (Fig. 1) and, because regarded as economically uninteresting, it has received less attention than areas with higher ore potential. The same varying quality is also noticeable in the text, where certain units, e.g. the coarse clastic sediments and sedimentary carbonate rocks deposited on top of the Archaean units have received relatively little attention despite their scientifically interesting character. These differences arise from the main research question of the project: "Where the true western boundary of the Outokumpu assemblage is located?"

The project aimed at answering the main research question by providing answers to numerous smaller, interrelated ones, e.g. by producing new information concerning the geological unit division in the area, including both Palaeoproterozoic sedimentary and intrusive units as well as the Archaean segments. One main aim of this study is to synthesise new structural observation with the previous structural interpretations in the surrounding areas and to model a deformation sequence that is also in agreement with the current tectonic model for the Palaeoproterozoic Svecofennian orogeny. Updated structural interpretations together with abundant new gravity measurement data were relevant for the constructed regional scale 3D model. Work was also carried out to confirm that the westernmost locations preliminarily interpreted as belonging to Outokumpu assemblage indeed belong to it.

The author list of this publication is long, but far longer would be the list of people who over the last four years have been variably involved in the work, be it measuring regional gravity surveys in the field, making thin sections, picking zircons in laboratory or something completely different. Thus, a major "thank you" from all of us to all of you, and especially to Riitta for her patience in once more transforming the sometimes quite messy and equivocal drafts of the geochemical charts to something far more suitable for publication. We also thank Dr Mikko Nironen and an anonymous reviewer for comments that helped in improving the manuscript.

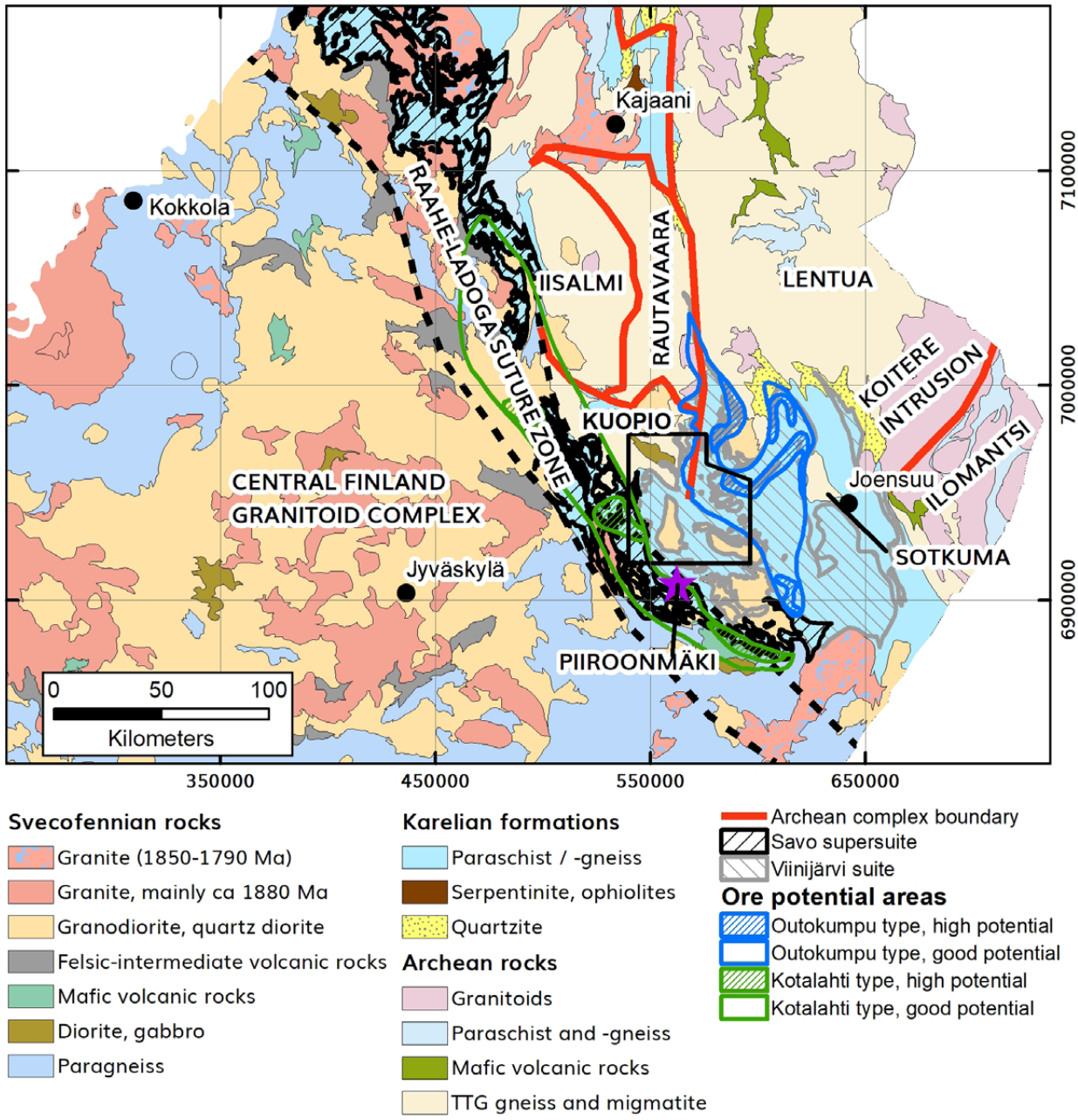

Fig. 1. Area covered by the appended bedrock map shown on bedrock map of Central Finland. Also shown are the complex division of the Archaean Craton, location of Raahe-Ladoga suture zone, Central Finland Granitoid Complex and Piiroonmäki drilling target. Outokumpu allochthon comprises of the Viinijärvi suite and the enclosed Outokumpu-type serpentinite bodies. Areas with high and good potential for Outokumpu and Kotalahti-type ores drawn according to Eilu (2012). The Savo supersuite and the Viinijärvi suite from Bedrock of Finland – DigiKP. Bedrock map simplified from Nironen et al. 2016.

2 RESEARCH AREA, METHODS AND MATERIALS

2.1 Research area, coordinate system

The study area consists of two 1:100 000 map sheets, 3243 Leppävirta and 3244 Vehmersalmi, of the obsolete national map sheet system (KKJ) covering 2,212 km^2 in municipalities of Kuopio, Leppävirta, Heinävesi and Tuusniemi. In the currently used European map sheet system the study area is covered by parts of the following map sheets N521, N522, N523, N524, P511 and P513. All coordinates in this publication and its appendices are given in the EUREF-FIN (UTM-35) system.

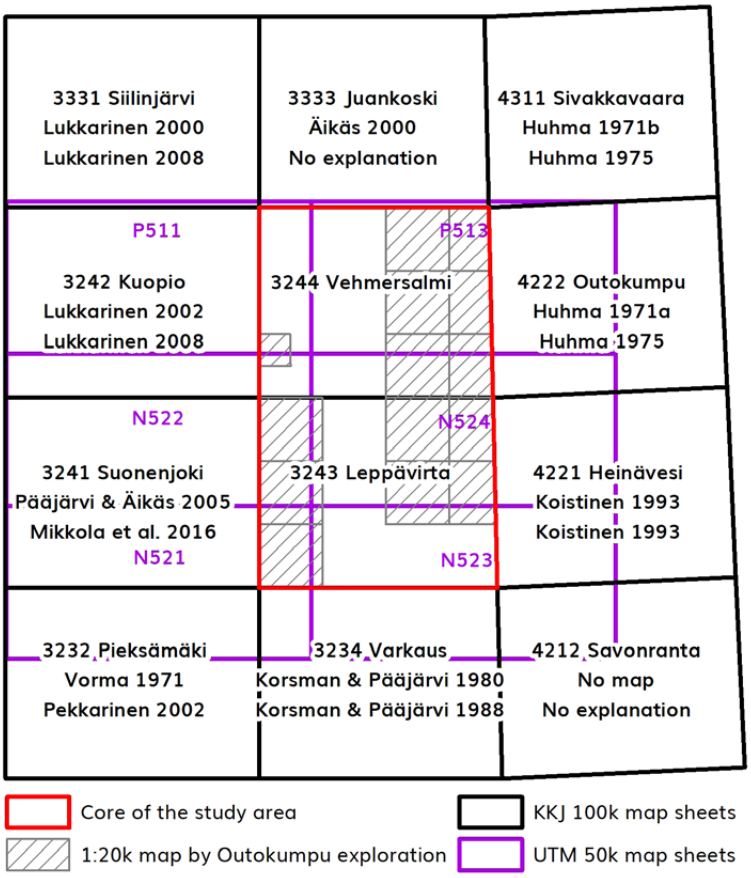

Fig. 2. Map sheets, old national KKJ system and current UTM system. Also references to surrounding bedrock maps and their explanations.

2.2 Materials and methods

2.2.1 Outcrop observations and drill cores

Prior to the onset of the project, the GTK bedrock observation database contained ca. 1,800 outcrop observations from the the study area. Also ca. 1,000 outcrop observations made by the exploration division of Outokumpu Oy were available, concentrating in the northeast and southwest corners of the study area.

A total of 2,841 new outcrop observations were made during three field seasons (Table 1, Fig. 3). All new observations were stored in digital format already in the field using either GTK's Android-based application (Mobilekapalo) on smartphones or the ArcMap-based application (Kapalo) on field computers.

Pre-existing drillings in the study area mainly consisted of short diamond exploration drill holes (Fig. 3) and drillings by Outokumpu Oyi.e. two drilled targets in southern parts of Tuusniemi and ca. 40 holes close to the village of Leppävirta. In Tuusniemi, the target had been potential Outokumpu-type

Table 1. Persons who participated in the field work, their pseudonyms and yearly numbers of observations in the area.

		2018	2019	2020	Total
Aleksi Salo	APSA	---	91		91
Antti Mäkelä	ASM$	124	---	---	124
Hanna Rantanen	HKRA	---	127	---	127
Heikki Pirinen	HAP$	---	---	29	29
Ilona Romu	KRRO	---	---	27	27
Jaakko Hietava	JOHI	---	---	15	15
Jaakko Nurkkala	JONU	---	226	---	226
Jani Jäsberg	JPJA	---	---	102	102
Joonas Sandström	JTSA	---	86	---	86
Bedrock mapping course 2018	KK7$	383	---	---	383
Mauri Luukkonen	MTL2	249	371	429	1049
Perttu Mikkola	PIM$	76	203	88	367
Rosa Malmström	SRMA	---	215	---	215
		832	1,319	690	2,841

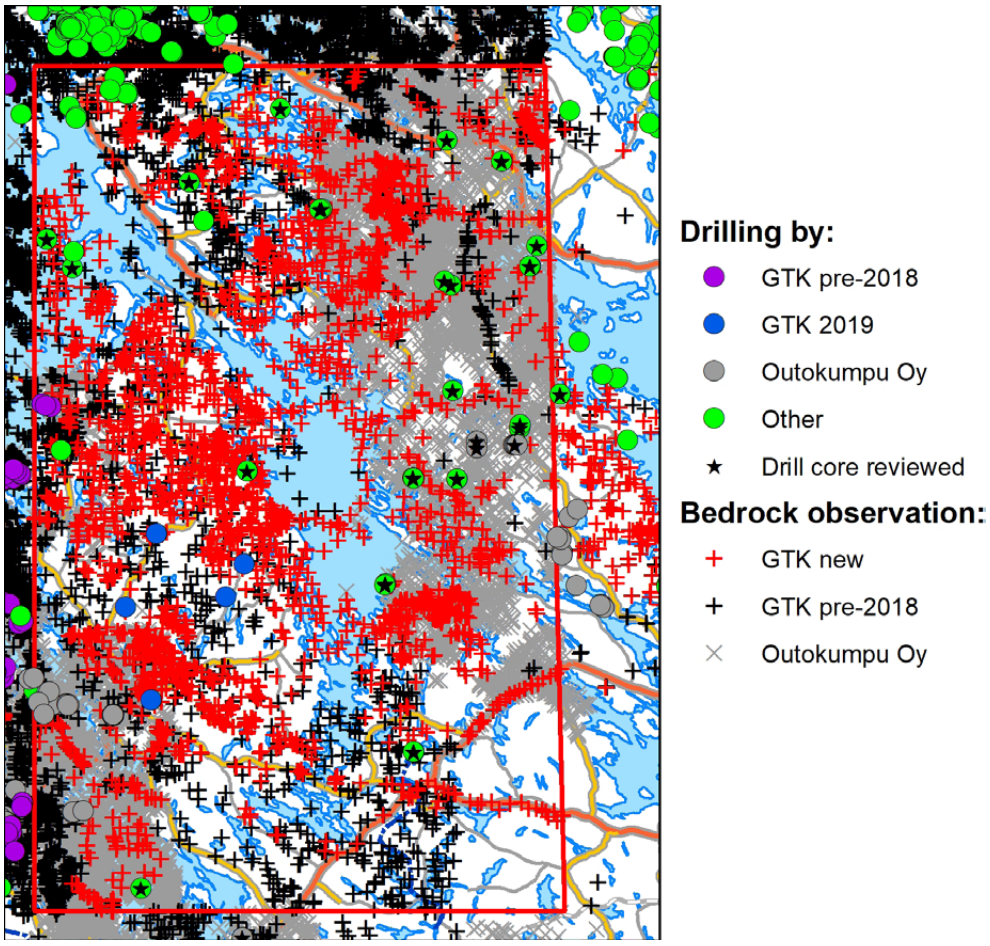

Fig. 3. Location of bedrock observations and drill holes in the study area and its immediate surroundings. See Figure 1 for location of the Piironmäki target. Basemap © National Land Survey.

mineralisations and, in Leppävirta, Kotalahti-type gabbros. The only pre-existing GTK drillings in the study area were three holes in Puutosmäki drilled for uranium exploration. Altogether 46 drill cores from the study area and its vicinity stored in the Loppi national drill core library were relogged and partially resampled in connection with this study.

In 2019, GTK drilled altogether ten holes, of which five (with a total length of 704 m) were drilled in the long-known (Koistinen, written communication, 2018) but limitedly studied Piiroonmäki area hosting rocks characteristic of the Outokumpu-type association (Pirinen & Niskanen 2020). The other five holes (with a total length of 1,045 m) were drilled northeast of Leppävirta to test the sources of varying geophysical anomaly combinations (Romu & Nousiainen 2020).

2.2.2 Whole-rock geochemical methods

In addition to previously unpublished analysis, previously published data from several studies (Glumoff 1987, Mäkinen 1995, Rasilainen et al. 2007, Lukkarinen 2008), both from the study area and areas surrounding it, have been used in the geochemical chapters of this publication. All used data is gathered in the Electronic appendix 1, and the geochemical methods are described in the original publications.

The new analyses have been made in different laboratories and with different methods. Laboratories and methods used for individual samples are distinguished in the Electronic appendix 1.

Analyses performed in the laboratory of ALS Geochemistry were done with the method package CCP-PKG03, in which the main elements together with Ba, Cr and Sr are analysed with XRF spectrometry from a disc prepared by fusing sample material with lithium borate and lithium nitrate. Loss on ignition was determined by weighing 1 g of sample, heating it in thermal decomposition furnace at 1,000°C for one hour and weighing it again after cooling. LECO induction furnace was used for determining the C and S contents of the samples. Base metals were determined with 4-acid digestion followed by ICP-AES analyses. Lithium borate fusion, together with ICP-MS method, was used for lithophile elements. The remaining analysed elements were determined using aqua regia digestion and ICP-MS method.

Whole-rock analyses performed by MSALABS from samples prepared by CRS Laboratories were performed with Lithium borate fusion and mineral acid digestion followed by analyses using the ICP-OES method for main elements (Method code WR-310). Loss on ignition was determined by heating a weighed sample at 1,000°C for one hour and reweighting it after cooling. Refractory trace elements and REEs were analysed using ICP-MS (Method code IMS-300) from Lithium borate fuse digested in mineral acids. As, Au, Bi, Hg, Sb, Se and Tl were analysed with ICP-MS from aqua regia digestion and Ag, Cd, Cu, Ni, Pb and Zn with the same method from 4-acid digested subsample. Determination of total C and S contents were carried out using LECO analyser.

2.2.3 Rutile analyses

For rutile analyses, mineral concentrate from zircon separation (see below) with mineral density >3.3 g/cm^3 was mounted in epoxy. The mount was automatically scanned with BSE and CL imaging to locate the rutile crystals for quantitative electron microprobe analyses, which were performed using the wavelength dispersive technique and a Cameca SX100 instrument at the Geological Survey of Finland, Espoo. Data were obtained with an accelerating voltage of 20 kV, a beam current of 30 nA was used for Ti, and 600 nA for the rest of the elements. Focused beam with diameter of 1 µm was used. Altogether 80 spots of 44 rutile grains were analysed for their Si, Ca, V, Fe, Cr, Mn, Zr, Nb, Ta, and Ti abundances. Natural minerals and metals were employed as standards. The analytical results were corrected using the PAP on-line correction program (Pouchou & Pichoir 1986). Points with Si≥1,000 ppm or Ca≥1,000 ppm were filtered out as they were interpreted as potentially hitting small inclusions of e.g. sphene.

2.2.4 Isotope methods

For this project, 11 new age determination samples were taken for zircon U-Pb method. Samples weighing 10–20 kg (for TIMS analyses) or 5–10 kg (for ICPMS analyses) were washed and crushed with a Fritsch Pulverisette II jaw crusher. The larger samples were further crushed in a roller mill and lighter minerals were washed out using a Wilfley table. The smaller samples were ground using a Retsch RS 200 vibratory disc mill after jaw crushing. All samples were then treated with methylene iodide and some also with Clerici® solutions for the separation of

the heavy minerals. Non-magnetic heavy fractions were separated using a Frantz isodynamic separator, and finally zircons were selected by hand-picking for analyses. Regardless of the analytical method or instrument, all the decay constant errors were ignored from age calculations, which were performed using Isoplot/Ex version 4.15. (Ludwig 2003). All plots and ages are with 2σ errors. In addition to new samples, nine previously dated samples were reanalysed.

2.2.4.1 *TIMS & CA-TIMS*

The decomposition of minerals and extraction of U and Pb for multigrain TIMS (thermal ionisation decoupled multicollector mass spectrometer) analyses followed the procedure described by Krogh (1973, 1982). For some analyses zircons were treated using the chemical abrasion (CA) method of Mattinson (2005). ^{235}U-^{208}Pb-spiked and unspiked isotopic ratios were measured using GTK's VG Sector 54 TIMS in Espoo. The measured lead and uranium isotopic ratios were normalised to the accepted values of SRM 981 and U500 standards. Common lead corrections were carried out using the age-related Pb isotope composition of the Stacey and Kramers model (1975) and errors of 0.2 (for $^{206}Pb/^{204}Pb$ and $^{208}Pb/^{204}Pb$) and 0.1 ($^{207}Pb/^{204}Pb$). The U-Pb age calculations were done using the PbDat-program (Ludwig 1991).

2.2.4.2 *Laser Ablation Multicollector Inductively Coupled Plasma Mass Spectrometer (LA-MC-ICPMS)*

Some of the single grain zircon analysis were performed using the Nu Plasma HR multicollector ICPMS together with a New Wave UP193 Nd:YAG laser microprobe at the Geological Survey of Finland in Espoo. Beam diameter was 25 µm and calibration was based on standard GJ-01 (609±1 Ma; Belousova et al. 2006) and in-house standard A1772 (2711±3 Ma/TIMS; 2712±1 Ma/SIMS; Huhma et al. 2012). See Mikkola et al. (2010) for detailed description of the method.

2.2.4.3 *Laser Ablation Single collector Inductively Coupled Plasma Mass Spectrometer (LA-SC-ICPMS)*

The majority of the performed single grain analysis were performed using AttoM single collector ICPMS, connected to a PhotonMachines Excite LA system. Calibration was based on standard GJ-01 (609±1 Ma; Belousova et al. 2006) and in-house standards A1772 (2711±3 Ma/TIMS; 2712±1 Ma/SIMS; Huhma et al. 2012) and A382 (1877±2 Ma; Huhma et al. 2012) were used as reference data. See Molnár et al. (2018) for detailed description of the method.

2.2.5 Geophysical data

In addition to the geophysical data and results described in this report, there are also geophysical field surveys done in 2019 in Piiroonmäki in Varkaus, and in the Soisalo area. They include magnetic and electromagnetic field surveys and borehole surveys measuring magnetic susceptibility, resistivity, natural gamma radiation and so-called gamma-gamma value (related to density). Magnetic data were modeled and some of the anomalies were drilled. Further information can be found from site reports by Pirinen & Niskanen (2020) and Romu & Nousiainen (2020).

2.2.5.1 *Petrophysics*

Petrophysical properties of altogether 2014 samples were measured in laboratory during the project. Sample types and areas of the samples and measured properties are presented in the Table 2.

Most of the petrophysical measurements were done in GTK's petrophysical laboratory in Kuopio using AC bridge for susceptibility and inductive resistivity, flux gate magnetometer for remanent magnetisation and AD FY-3000 scale for mass,

Table 2. Summary of samples measured for their petrophysical properties from the study area. Basic set of measurements includes: magnetic susceptibility, remanent magnetisation, inductive resistivity and density.

	Number of samples	Sample type	Basic set	Galvanic resistivity
Grab samples 2018-2020	1,849	Outcrop	X	
Reference measurements of old samples	99	Drill core	X	X
Piiroonmäki target	25	Drill core	X	X
Soisalo area	41	Drill core	X	X
Total	2,014			

volume and density. Galvanic resistivity was measured in GTK's petrophysical laboratory in Espoo using Mafrip M0 instrument. Mafrip, AC bridge and flux gate magnetometer are GTK's in-house instruments. Measurements were done by Jarmo Asikainen, Mauri Luukkonen and Timo Hallikainen in Kuopio and by Satu Vuoriainen in Espoo.

Inductive and galvanic resistivity measurements measure the same property, but their measurement range is different. Inductive measurement works with conductive samples (resistivity from ca. 10^{-2} to 10^{-7} Ωm, e.g. black schists and ores) and galvanic measurement with more resistive samples (resistivity from 10^{-3} to 10^{6} Ωm).

The Königsberger ratio Q was calculated for all measured samples. This is the ratio of remanent magnetisation to induced magnetisation. If the ratio is high, the remanent magnetisation must be considered in magnetic modelling. Also magnetite and iron contents and induced polarisation properties of some of the samples were calculated.

2.2.5.2 *Low altitude airborne data*

GTK's low-altitude aerogeophysical data includes magnetic, frequency-domain electromagnetic (EM) and radiometric survey. Line separation of the survey is 200 meters and the nominal flight altitude 30 m. The area of interest is divided between several flight areas flown between 1980 and 1992. Flight direction in all areas was east-west. The data and the methods are described by Airo (2005). Magnetic and EM data were used extensively at several stages of the work. The usability of radiometric data in glaciated areas with large lakes and bogs is more limited.

2.2.5.3 *Gravity data*

Gravity data from the study area has been acquired over a prolonged period and with variable methods (Fig. 4). Ground-measured data in eastern parts originate from exploration activities of Outokumpu Oy, whereas those in western and northern parts have been acquired by GTK before the start of this project. During this project certain ground-measured gravity data were collected from central parts of the study area. In the ground-measured dataset, the number of points varies from 1 to 8 points/km^2, most often being 4–6 points/km^2.

During this project, airborne gradiometric data were gathered from central parts of the study area by ABI Holdings Ltd in 2019. The line spacing used was 500 m and the flight area was 638 km^2. A set of ground-measured reference points were used for calibration of the results.

2.2.5.4 *Reflection seismic data*

The FIRE-3a line of the Finnish Reflection Experiment traverses the southern part of the study area (Fig. 4). Technical aspects of this crustal scale data acquisition program can be found from Kukkonen et al. (2006). Earlier interpretation of this data in the study area was made by Sorjonen-Ward (2006).

During the project, a pilot reflection seismic study was done (Fig. 4) in the area along the Otuslampi line. The seismic survey was the first one where the new GTK wireless seismic receivers were used, and it was placed in an area where the major NW-SE striking gravity anomaly is based on modelling of gravity data relatively close to the surface. The survey consisted of 80 receiver points with 40-meter intervals and 20 explosive sources that were drilled to depths of 0.9–2.4 m depending on the thickness of surficial deposits. Varying dynamite charge sizes (60–600 g) were used to evaluate the optimal size for further studies. The seismic receiver and source locations are shown in Figure 5 below. The source parameters at different locations are listed in Electronic appendix 1.

The Otuslampi seismic reflection data were processed using standard hardrock processing flow for common midpoint (CMP) imaging despite the sparse source distribution. The seismic processing workflow included setup of receiver and source coordinates into the trace headers, manual removal of noisy traces, static corrections, spherical divergence filtering to compensate for amplitude decrease due to geometrical spreading of the seismic wavefield, automatic gain control and trace amplitude balancing, frequency filtering and deconvolution with spectral whitening. The Normal Move Out corrections were done based on the velocity analysis results using velocities ranging from 5,000 m/s to 6,200 m/s, and for Stolt migration and time-to-depth conversion velocity increasing from 5,000 m/s in the surface to the 6,000 m/s in the 2 second two-way-travel time were used.

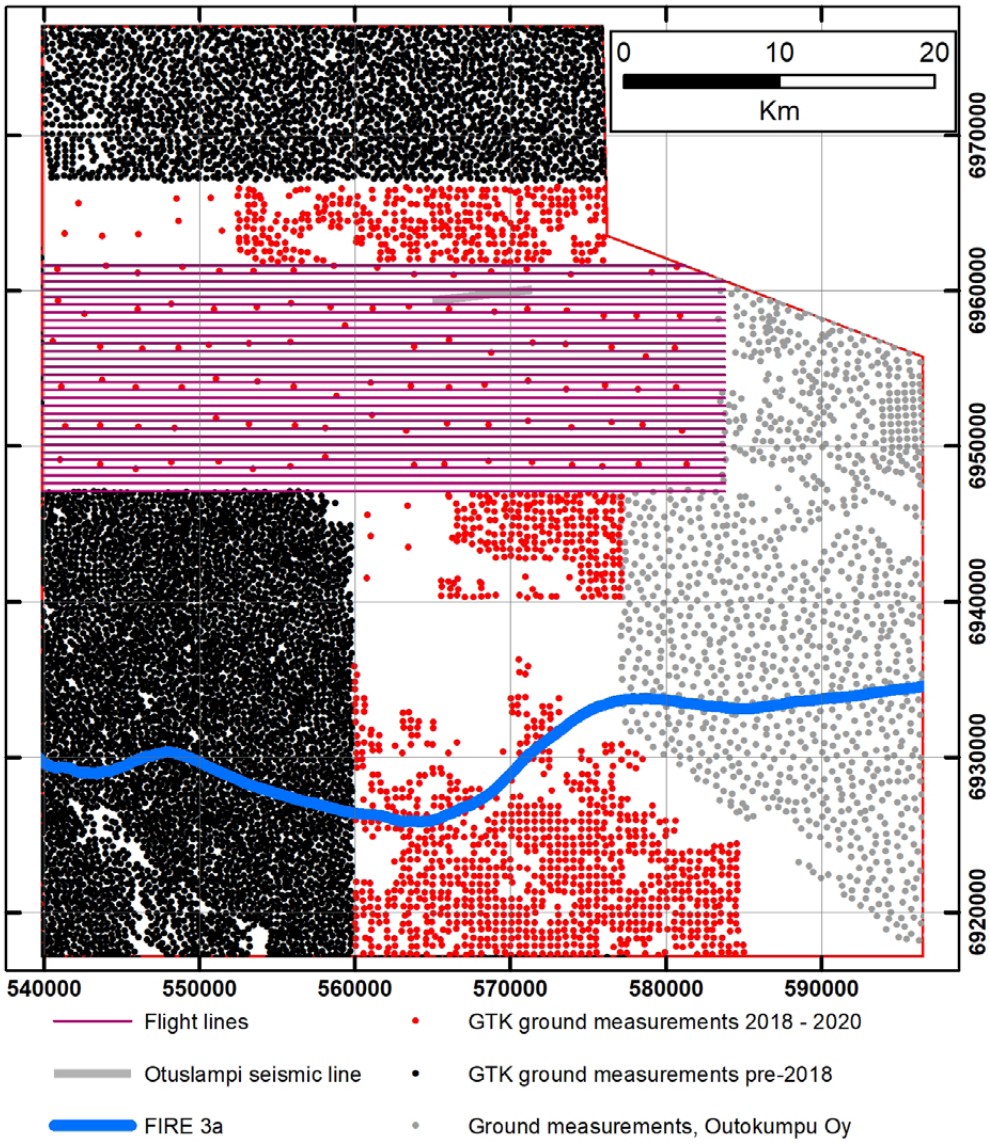

Fig. 4. Locations of ground measured gravity data, airborne surveyed area and locations of FIRE-3a and Otuslampi seismic profiles.

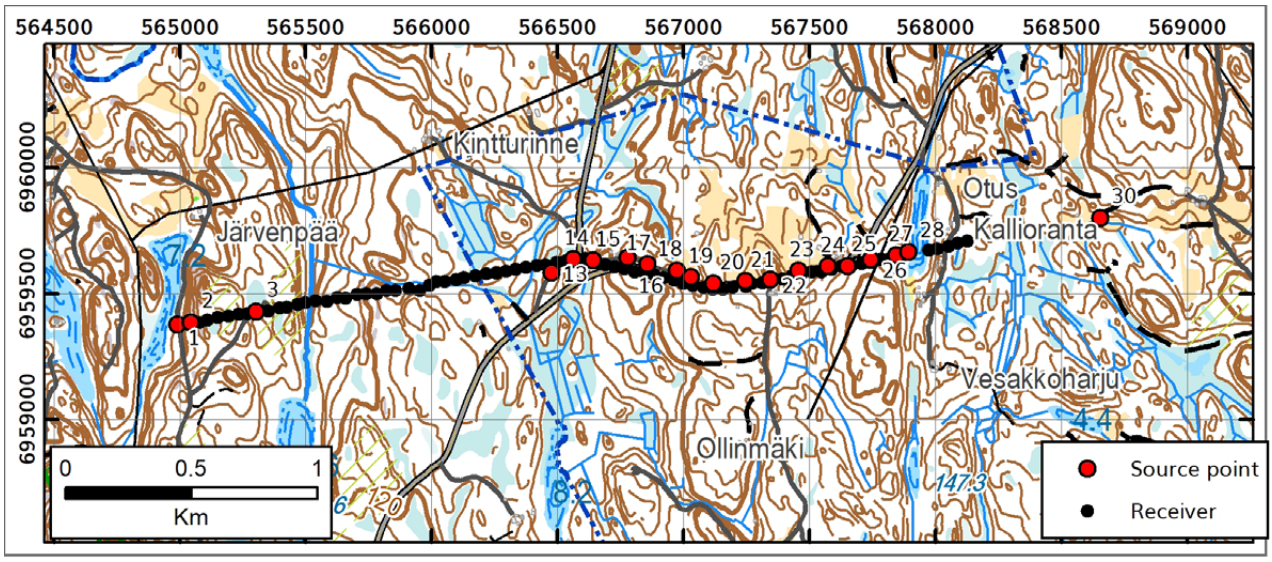

Fig. 5. Location of receivers and source points along the Otuslampi line. Basemap © National Land Survey.

2.2.6 3D modelling

3D geological model of the Okuwest area was built using mainly SKUA-GOCAD version 19 and the corresponding Mira Geoscience GOCAD Mining Suite. In addition, the complicated Archaean basement was modeled by using GeoModeller 4.0.8. Data for 3D geological modelling were imported into SKUA-GOCAD project. Data consisted of geological and geophysical maps, one seismic profile, petrophysical measurements and tectonic observations. This data collection can be regarded as a 3D data model. Not all of the data were used in the present 3D geological modelling. 3D data and geological maps were used to build 3D surface and voxet models.

The dimensions of the 3D geological were defined by the study area. The size of the geological 3D model is 57 km x 56 km x 15 km. From above, the 3D model is bounded by the topography, which is a plane approximately 100 metres above the sea level.

3 GEOLOGICAL SETTING AND PREVIOUS STUDIES

The study area is situated on the eastern side of Raahe-Ladoga suture zone that separates Karelia province in the east from the Svecofennian province in the west (Fig. 1, Kohonen et al. 2021 and references therein). The Karelia province consists of the Archaean craton and units deposited on top of or in its vicinity during an extended period of rifting, which commenced at 2.50 Ga (Vuollo & Huhma 2005) and continued sporadically before culminating in the formation of oceanic crust at 1.95 Ga (Peltonen 2005a). After ca. 1.91 Ga the Karelia province experienced several phases of compressional deformation (1.93–1.79 Ga) resulting from Svecofennian collisional events west and south of it, in present coordinates.

3.1 Archaean bedrock

In the division of Hölttä et al. (2012a), the Archaean bedrock, both the larger intact areas and the numerous thrust sheets and domes in the study area (Figs. 1 and 6) belong to the Kuopio complex, which is part of the Western Karelia subprovince. However, Luukas et al. 2017 separated the Juojärvi and Sotkuma domes into separate Joensuu complex. Whether these Archaean domes and thrust sheets represent the deformed southern boundary of the Iisalmi, Rautavaara and Lentua complexes or whether they originate, partly of wholly, from unknown source(s) is an open question (Park & Bowes 1983, Hölttä et al. 2012a).

The Kuopio complex consists of deformed Archaean granitoids, the majority of which are variably migmatised tonalites of the TTG group (Tonalite, Trondhjemite, Granodiorites) (Lukkarinen 2008), although 2.72 Ga K-feldspar porphyritic sanukitoids having distinctly higher Ba, Sr, K_2O and Mg# (Koitere suite) compared to the TTGs are also locally voluminous (Heilimo et al. 2012) as are the 2.7 Ga quartz diorites of the Jonsa suite (Hölttä et al. 2012b). Archaean greenstone belts are not known from the area (Bedrock of Finland – DigiKP, Hölttä et al. 2012a). Excluding a few small quartz diorites west of Tuusniemi, the Archaean granitoids have not been divided into different types on the digital bedrock map in the study area or its vicinity (Bedrock of Finland – DigiKP). A small number of age determinations made from Archaean rocks exists either from the study area or its immediate vicinity, but results from these are inaccurate and can only be used to prove the Archaean age of the studied units (Huhma 1976, Gaál 1980, Lukkarinen 2008), with the exception of the relatively well-defined age of 2693±13 Ma for a member of the Jonsa suite 40 km northwest of Kuopio (Lukkarinen 2008; A279).

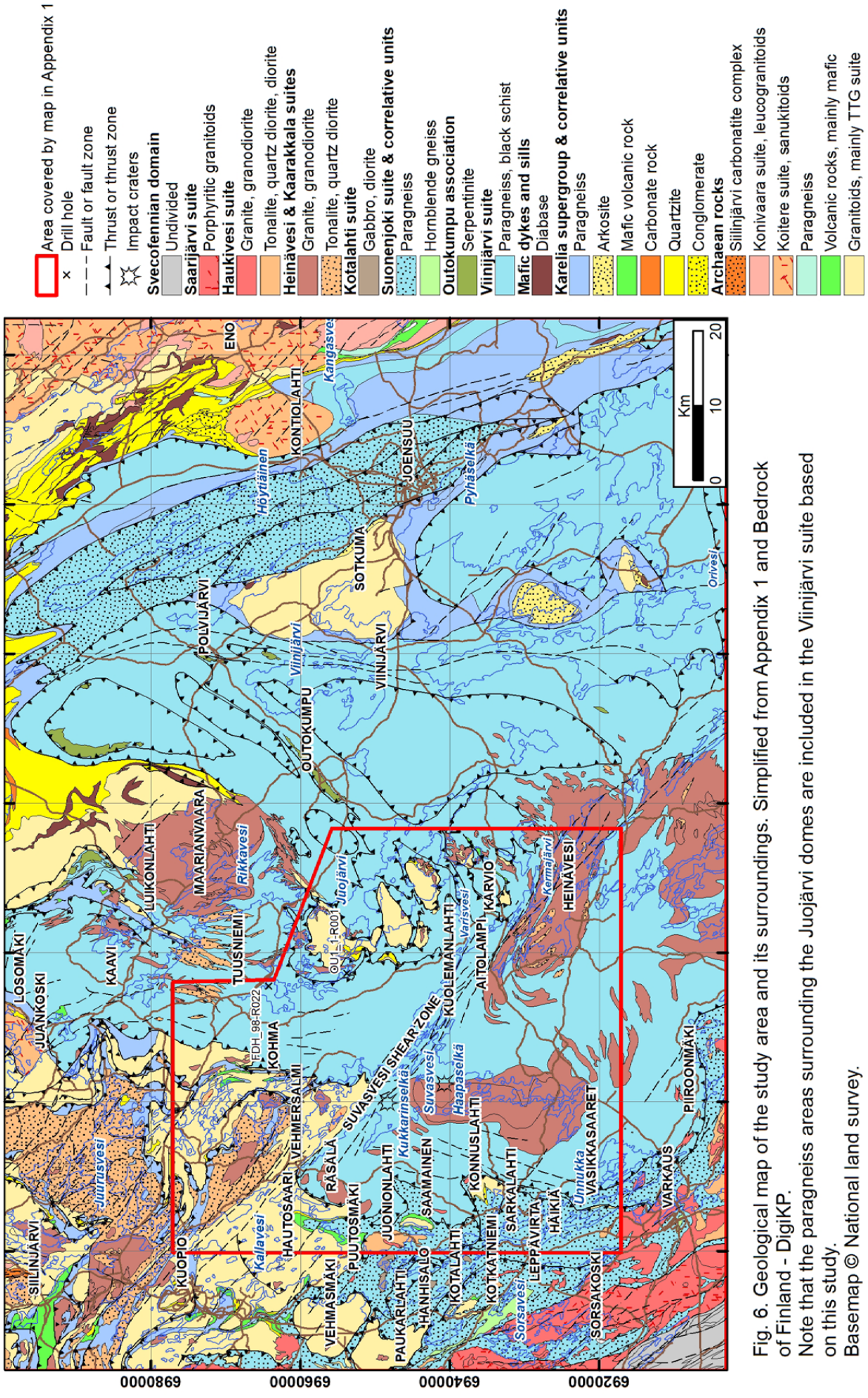

Fig. 6. Geological map of the study area and its surroundings. Simplified from Appendix 1 and Bedrock of Finland - DigiKP.
Note that the paragneiss areas surrounding the Juojärvi domes are included in the Viinijärvi suite based on this study.
Basemap © National land survey.

3.2 Proterozoic units

Variably preserved Palaeoproterozoic cover sequence (Karelia supergroup) is locally observable between the Archaean domes and thrust sheets and the vast paragneiss areas. This sequence has been interpreted as a result of extended period of episodic rifting of the Archaean craton commencing close to 2.5 Ga ago and continuing until 1.98 Ga ago as shown by the intrusion of mafic dykes in Archaean crust and overlaying Palaeoproterozoic supracrustal rocks (Vuollo & Huhma 2005, Lahtinen et al. 2015). Cover sequence has been traditionally divided into tectofacies or systems (Laajoki 2005, Hanski & Melezhik 2013). In the study area, Sariolan conglomerates represent the oldest system. On top of these were deposited quartzites, carbonate rocks and volcanic rocks of the Jatulian system. Lower Kalevian paragneisses represent the youngest sequence with turbiditic paragneisses, arkosites and garnet-dominated iron formations. Rifting culminated in formation of new oceanic crust at circa 1950 Ma (Peltonen 2005a), which is also roughly the maximum deposition age of the paragneisses belonging to the Viinijärvi suite in areas hosting Outokumpu assemblage rocks as tectonic fragments and to the Suonenjoki suite west of the Viinijärvi suite (Fig. 6, Bedrock of Finland – DigiKP, Nironen 2017 and references therein).

3.2.1 Coarse-grained clastic units

Lowest rocks of the Karelia supergroup are the rare paleoregoliths reported by Lukkarinen (2008) from two locations in the Kuopio area and by Wilkman (1938) from one location north of Puutosmäki. This calc-silicate rich rock has been interpreted as in-situ weathering product of the Archaean granitoids (Lukkarinen 2008).

In the study area, the lowest depositional unit of the cover sequence, basal conglomerate, has been reported only in connection with the Konnuslahti dome, where it is present along its western margin as a unit 100–300 metres wide. Pebbles are mainly granitoids and basement gneisses, to lesser extent amphibolites, vein quartz and metasedimentary gneisses. The matrix is formed by sandy material of varying maturity, often also containing hornblende. Arkose, greywacke and quartzite form interlayers in the conglomerate. The unit phases gradually upwards to arkosites and impure quartzites (Wilkman 1938, Parkkinen 1974). The conglomerate unit is similar to those in the Kuopio and Nilsiä areas (Aumo 1983, Paavola 1984, Lukkarinen 2008) and has been included in the same Lippumäki formation as those in the Kuopio area (Finstrati).

Quartzites and arkosites in the study area are more abundant than the basal conglomerates, and they overlie the conglomerate or directly the Archaean basement (Parkkinen 1974, Ekdahl 1977). Quartzites in the study area have been interpreted as belonging to the Nilsiä group together with the quartzites of the Kuopio area. Based on age determination from a sill intruding into the unit, these quartzites were deposited prior to 2190±15 Ma (Hanski et al. 2010) and thus typical for the whole of East Finland (Nironen 2017 and references therein).

3.2.2 Carbonate rocks

Sedimentary carbonate rocks are locally present on top of the quartzites and below or as interlayers within the overlaying volcanic sequence (Lukkarinen 2008). They have been reported from this stratigraphic position in connection with Konnuslahti and Saamanen domes, as well as from the Kohma area but are most abundant in Puutosmäki and north of it on the islands of Lake Kallavesi (Wilkman 1938, Parkkinen 1974, Ekdahl 1977). These carbonate rocks, and those in the Kuopio area in general, are impure dolomites containing typically variably abundant serpentinite, biotite, muscovite, diopside, amphiboles, quartz, garnet and olivine (ibid.). Due to the high silica content of the rock, they are sometimes referred to as calc-silicate rocks. Impurities are likely to represent both original depositional impurities and alteration associated with the following volcanic activity. All carbonate rocks in the study area in this stratigraphic position have been included into Neulamäki group, those in Puutosmäki and Saamanen area into its Petonen formation, and others into undefined formations.

3.2.3 Volcanic units

The majority of the volcanic rocks in the study area and its vicinity have been included in the Neulamäki group and those more thoroughly studied into its Vaivanen (Kuopio area) and Koivusaari formations (Siilinjärvi area, Bedrock of Finland – DigiKP). In areas close to the Juojärvi domes the mafic volcanic rocks have been included into Juojärvi suite.

In the classification of Kohonen et al. (in prep.) the volcanic rocks belong to the Ludicovian system (2060–1950 Ma). The majority of the Vaivanen and Koivusaari formations consist of mafic volcanic rocks, often with porphyritic or pillow lava structures, the latter type variably deformed to give the rock a banded appearance. The Koivusaari formation includes a felsic member, which has been dated to 2062±6 Ma. Based on their geochemical characteristics, both the Vaivanen and Siilinjärvi formations can be classified as Fe-tholeiites related to rifting of the continental crust. (Lukkarinen 2008)

3.2.4 Diabase dykes

Variably abundant diabase dykes intrude into the Archaean basement and its above-mentioned cover rocks within the study area and its vicinity. Based on observations by Lukkarinen (2008) from the Kuopio and Siilinjärvi map sheet areas, these dykes consist mainly of hornblende and plagioclase, no pyroxene-bearing variants have been observed, and in the most intensively altered dykes, biotite replacing hornblende is present as a main mineral. The dykes can be up to 30 metres wide and have been variably deformed. No geochemical or age data from these dykes in the area exist but, based on correlation with other areas, it can be presumed that they represent multiple intrusion phases between 2.5 and 2.0 Ga (Huhma et al. 2018).

3.2.5 Paragneisses

Palaeoproterozoic paragneiss units cover the majority of the study area and its vicinity (Fig. 1). Within the area covered by the map in Appendix 1, they have previously been divided into four units: Juojärvi suite, Levänen group, Viinijärvi suite and Suonenjoki suite (Bedrock of Finland – DigiKP). The Juojärvi suite and the Levänen group have been regarded as lower-Kalevian and Viinijärvi suite as upper-Kalevian. From a structural point of view, the latter has been referred to as "Outokumpu allochthon" (Nironen 2017, Luukas & Kohonen 2021 and references therein). The area covered by the Suonenjoki suite has been variably correlated with the adjacent units, and the debate remains partly open, but currently the unit is included in the Karelia province (Bedrock of Finland – DigiKP).

The nomenclature for the rocks referred to as paragneisses in this study has been highly variable, including but not limited to mica gneisses, mica schists, vein gneiss, phyllites, greywackes and pelites depending on e.g. the current grain size and focus of the study in question (Glumoff 1987, Koistinen 1993a, Forss et al. 1999, Rasilainen et al. 2007, Lahtinen et al. 2010).

3.2.5.1 *Levänen group and Juojärvi suite*

In earlier interpretations, Levänen group (part of the Karelia supergroup) comprises of scattered areas within and in the contacts of the Archaean crust in northwest parts of the study area (Fig. 6). The width of the elongated domains does not exceed 3 km. Lukkarinen (2008) interpreted that the Levänen paragneisses were deposited as turbidites conformably on top of the Neulamäki group mafic volcanic formations. The paragneisses of the Levänen group show distinct bedding and often also graded bedding textures, with bed thickness from centimetres to one metre. Pelitic parts are usually thicker than their sandy counterparts. Calc-silicate intercalations 2 to 10 cm thick are locally present. Cordierite, sillimanite and garnet porphyroblasts are locally present, especially in the clay-richer layers (Lukkarinen 2008).

Paragneisses included in the Juojärvi suite flank the Archaean Juojärvi domes as ~2 km wide zone. Note that Juojärvi suite paragneisses are not shown in Figure 6 because they are included in the Viinijärvi suite in this study. Koistinen (1993a, b) did not separate these paragneisses from the surrounding Viinijärvi suite, but instead the division and correlation to Levänen group was made by Korsman et al. (1997) and has since been carried onwards to later works (e.g. Laajoki 2005, Nironen et al. 2016).

3.2.5.2 *Viinijärvi suite*

The Viinijärvi suite is the most voluminous of the paragneiss units in the study area. Suite's contacts with all the other paragneiss units have been interpreted as thrusts and thrust zones developed during the collisions of the Archaean blocks at 1.91 Ga and followed in quick sequence by amalgamation of the Savo arc with the Karelia Province (Nironen 2017, Luukas & Kohonen 2021, Kohonen et al. 2021 and references therein). The Viinijärvi paragneisses are dark grey, thick-bedded, sand-dominated sediments, with local calc-silicate intercalations (e.g. Kontinen et al. 2006 and references therein). Migmatisation is often weak or non-existing, but the amount of neosome increases near the shear zones and towards southwest with increasing

metamorphic grade. Due to their extreme homogeneity and monotony, the paragneisses of the Viinijärvi suite have also been referred to as "monotonites" (Kontinen et al. 2006). Granitoid and quartz-feldspar dykes and intrusions are occasionally abundant (Koistinen 1993b, Rantanen 2021, Bedrock of Finland – DigiKP). The Viinijärvi suite paragneisses have been interpreted as greywackes deposited by turbidite currents, but compared to the Levänen group, they are on average clearly coarser-grained and display thicker bedding.

The contact between Viinijärvi paragneisses and metasediments east of it have also been interpreted as thrust zones (Luukas & Kohonen 2021 and references therein). As the nature of this contact and correlation of units east of it is currently in progress (Kohonen et al. in prep.), it is excluded from this study.

3.2.5.3 *Suonenjoki suite*

The Suonenjoki suite, part of the Savo supersuite, is present along the western boundary of the study area from where it and its correlative units (Lampaanjärvi and Näläntöjärvi suites) extend along the Raahe-Ladoga suture zone for 400 km (Fig. 1). Variably migmatised paragneisses are the dominate rock types of the Suonenjoki suite. The intensity of migmatisation is variable, being most intensive in the major shear zones, leaving better preserved domains in between.The migmatite structures display variation from stromatic to schollen and schlieren and, in most intensive cases, to nebulitic. In addition to variable migmatisation, local variation in metamorphic degree is also reflected by variable presence of garnet, sillimanite, cordierite and staurolite porphyroblasts, while andalusite is also locally present but interpreted as retrograde (Lukkarinen 2008).

Black schist interbeds together with small amounts of amphibolites, hornblende gneisses and quartz-feldspar gneisses are also included in the suite (Korsman & Pääjärvi 1988, Forss et al. 1999, Lukkarinen 2008, Mikkola et al. 2016). Although the exact relationship of the various gneiss types is poorly understood, it is clear that the Suonenjoki suite is more heterogeneous than the adjacent Viinijärvi suite.

3.2.5.4 *Depositional age*

There is no direct age data from the Juojärvi suite and only one sample representing the Levänen group has been analysed in this sense. This sample by Lahtinen et al. (2015) contained only one Palaeoproterozoic zircon, all others being Archaean, and thus the maximum deposition age could be Archaean but, based on the correlation with other lower-Kalevian units, their minimum deposit age is regarded as 1960 Ma (Lahtinen et al. 2010, 2013, 2015).

The same lack of direct age data is also true for the Viinijärvi suite in the study area, but detrital zircon populations of samples taken from further east define 1.92–1.93 Ga as the maximum depositional age (Lahtinen et al. 2010, 2013). The zircon populations display characteristically bimodal distribution with peaks close to 2.7 and 2.0 Ga. The minimum deposition age is defined as 1.87 Ga by granitoid veins and intrusions of the Savo supersuite (see below), but structural interpretations suggest minimum depositional age of 1.91 Ga, i.e. the timing of regional D1 (e.g. Ward 1987, Nironen 2017), linked to collision of Archaean blocks and docking of the Savo arc to the Karelia province. Age determinations from Outokumpu assemblage interpreted as part of the depositional basin of the Viinijärvi suite was deposited on have yielded crystallisation ages of 1.96–1.95 Ga (Peltonen et al. 2008, Huhma et al. 2018).

There are no detrital age data from the whole Suonenjoki suite, and the data available from correlated units to the northwest indicate similar bimodal distribution of detrital zircons as in the Viinijärvi suite, i.e. peaks at 2.7 and 2.0 Ga (Lahtinen et al. 2015) and a maximum deposition age around 1.91–1.92 Ga. Definitive minimum deposition age is 1.88 Ga given by mafic intrusions belonging to the Kotalahti suite (Gaál 1980), but like in the case of the Viinijärvi suite, on structural bases the 1.91 Ga of regional D1 could be regarded as a minimum deposition age.

3.2.5.5 *Previous correlations of the paragneiss units*

Over the years, the Suonenjoki suite has been variably divided between adjacent geological units. Simonen (1980) included the area in the Karelian formations, but later Luukkonen & Lukkarinen (1985, 1986) divided the suite into two, as they included western parts into the Svecofennian domain and the eastern part with exposed Archaean domes and thrust sheets extending from Leppävirta to Kuopio, into Karelia province. This interpretation that correlated the part included into Karelia with the Levänen group (i.e. Lower Kaleva) was later used in several large-scale compilations, e.g. Lundqvist et al. (1996) and Koistinen et al. (2001). The current

"re-inclusion" of the whole Suonenjoki suite into Karelia province is mainly based on Lahtinen et al. (2015) detrital zircon work on north-western parts of the Savo supersuite (Näläntöjärvi suite, Luukas et al. 2017), based on which the deposition ages and sources for the Viinijärvi suite and the Savo supersuite are relatively similar. However, it should be noted that no detrital zircon data exists from the area of the Suonenjoki suite.

Also, the Suonenjoki suite is dominated by paragneisses and hosts variably abundant black schist interlayers, as well as boudinaged calc-silicate layers. On average the Suonenjoki suite paragneisses are more intensively migmatised than those belonging to the Viinijärvi suite, although variation extends from completely unmigmatised into nebulitic variants. Based on geochemical composition, the paragneisses are metamorphosed greywackes. Due to differences in original composition and metamorphic degree, garnet, cordierite and sillimanite porphyroblasts are variably present in the paragneisses. (Lukkarinen 2008, Mikkola et al. 2016)

3.2.6 Outokumpu assemblage

Rocks of the so called Outokumpu assemblage (a.k.a. OKU association) have drawn significant research interest due to the world-class Outokumpu-type Cu-Co-Zn-Ni deposits they host in eastern Finland. An ideal model of an OKU assemblage is a serpentinite core enveloped, from centre outwards, by carbonate-bearing serpentinite – carbonate rock – tremolite skarn – diopside skarn – quartz rock, with an outer zone comprising of mica gneisses and black schists (Gaál et al. 1975, Peltonen et al. 2008). However, it should be noted that smaller OKU assemblage bodies can host only some of the mentioned rock types. OKU assemblage rocks are characterised by distinct geochemical features and presence of chromium-bearing minerals, most typically chromite, Cr-diopside, Cr-tremolite, fuchsite and uvarovite (e.g. Säntti et al. 2006).

Gabbroic rocks associated with the serpentinites yield ages of 1.97–1.96 Ga (Huhma 1986). Huutokoski metagabbros have neighboring outcrops of serpentinite and black schist, with no observed lithological contacts on the outcrops (Peltonen et al. 2008). The ages of gabbroic rocks associated with the Outokumpu assemblage imply that both must represent fault-bound, tectonically emplaced bodies within the Viinijärvi suite (Claesson et al. 1993, Kontinen et al. 2006).

Age determinations from replacement-type skarnoid carbonate-calc-silicate rocks in the Kylylahti Cu-Co deposit provided a zircon U-Pb age of 1926±11 Ma. Pb-Pb analyses from OKU assemblage rocks from geographically widely spaced locations provided an age indication of 1908±27 Ma (Kontinen et al. 2006).

Cu-Co-Zn-Ni deposits in the OKU assemblage are typically thin, narrow and sharply bounded sheets, lenses or rods of massive to semi-massive sulphides, located along, or close to, the interfaces between black schists and silicified or carbonated ultramafic rocks (quartz-carbonate rocks) (Peltonen et al. 2008).

Serpentinites in the OKU assemblage are elongated lenses ranging from a few metres to several hundred metres in length. Haapala (1936) defined the serpentinites of the Outokumpu area into two major zones (western and eastern) separated by the occurrence of predominant serpentine mineral, chrysotile in the western zone and antigorite in the eastern zone. Emplacement of the serpentinites seems to focus on hinge zones of isoclinal folds, with no significant effect of contact metamorphism, but rather regional metamorphism as the dominant phenomena. This can be attributed to tectonic transport during folding with the serpentinite bodies already solidified (Gaál et al. 1975). Säntti et al. (2006), suggested that the serpentinite precursors (peridotite) most likely were more or less thoroughly serpentinised before the regional metamorphism.

The Outokumpu association serpentinites are highly magnesian, with MgO concentrations averaging ca. 37%. Al_2O_3 and TiO_2 are low, as is CaO (average ca. 2.5%), significantly lower than the carbonate rocks. Fe_2O_3 concentrations are ca. 8 w-%, distinguishing the serpentinite from the quartz rock on an average basis. OKU-type serpentinites are poor in sulphides, low in copper, and their nickel to cobalt ratio is typical for ultramafic rocks. Also, the OKU quartz rocks, skarns and dolomites resemble serpentinites with their sulphide content (Huhma 1971c). Carbonate rocks in the OKU assemblage are generally thin (1-5 m) discontinuous seams between serpentinite and skarn-quartz rocks. Mineral constituents are mostly dolomite and calcite, magnesite and tremolite are locally present. With an increase in the amount of tremolite, carbonate rocks grade into tremolite-carbonate rocks or tremolite skarns. Chromite is a ubiquitous minor phase occurring as coarse to very coarse, broken, cataclastic grains.

SiO_2 content in the carbonate rocks are on average 14.65% and MgO and CaO are 20.1 and 25.2%, respectively, suggesting dolomite dominating over calcite (Kontinen et al. 2006, Peltonen et al. 2008).

Calc-silicate rocks or skarns are present in two varieties in the OKU assemblage: tremolite skarns (>50% tremolite) and diopside skarns, both occurring typically located between carbonate and quartz rocks or as bands in the quartz rock. Chromite is more common in tremolite than in diopside skarns, which also often contain uvarovite. Skarns have fairly abrupt contacts with the carbonate rocks and more gradational ones with the quartz rocks (Kontinen et al. 2006). SiO_2, MgO and CaO contents of the skarns are broadly intermediate when compared to the carbonate and quartz rock. Al_2O_3, TiO_2 and alkali element concentrations are low. (Kontinen et al. 2006, Peltonen et al. 2008).

Quartz rocks in the OKU assemblage are fine grained, strongly schistose, quartz-tremolite (± diopside) banded rocks that are dark grey to pale grey (pure quartz rocks), grey green to green (tremolite ± fuchsite-bearing quartz rocks) or sometimes brownish grey (abundant fine grained-chromite) in colour (Kontinen et al. 2006, Peltonen et al. 2008). In some datasets, quartz rocks have a high average SiO_2 content of 89.7%, with the purest quartz rocks having values of over 97% of SiO_2. Aluminum content is also very low with averages of 0.45% (Kontinen et al. 2006).

Rocks of the OKU assemblage can be identified with varying combinations of elements. The rocks are generally high in Ni, Cr, MgO and low in Th, Zr, Ba, Mn and total Fe (Kontinen 1998, Kontinen et al. 2006, Peltonen et al. 2008). Ternary relationships of Ni, Cu, and Co also have been used to classify OKU rocks into different types (Huhma & Huhma 1970). Based on e.g. occurrence and texture of chromites in quartz rocks, relative concentrations of immobile elements the quartz, carbonate and skarn rocks have been interpreted as products of complete silicification and carbonisation of ultramafic rocks of oceanic crust (Peltonen et al. 2008).

The currently preferred explanation to the sporadic presence of the OKU assemblage within the Viinijärvi suite is tectonic mixing of serpentinite lenses with paragneisses in the basal parts of the Outokumpu allochthon, further influenced by transform faults acting as initial mechanism for later obduction and development into thrust faults or detachment zones (Kontinen et al. 2006).

Based mainly on exploration activities by Outokumpu Ltd., the Outokumpu assemblage continues from the Outokumpu area west into our study area (Kontinen et al. 2006 and references therein, Bedrock of Finland – DigiKP), where numerous small serpentinite and skarn bodies have been identified within the Viinijärvi suite north of the Suvasvesi shear zone (Appendix 1). South of the shear zone, the Outokumpu assemblage is far less common and poorly studied. In respect to the OKU assemblage, this project concentrated in confirming that Kuolemanlahti, Piiroonmäki and Täilahti localities south of the Suvasvesi shear zone (Fig. 6) are true members of the group. Earlier data from these locations was limited to unpublished geological maps, passing notes or minor role in publications (e.g. Koistinen 1996, Peltonen 2005a, Säntti et al. 2006).

3.2.7 Kotalahti-type ultramafic-mafic intrusions

Kotalahti-type mafic to ultramafic intrusives within the Raahe-Ladoga suture zone have been studied intensively since the initial discovery of the Kotalahti ores in 1960s (e.g. Parkkinen 1974, Forss et al. 1999, Peltonen 2005b, Makkonen 2015 and references therein). According to Peltonen (2005b) the tholeiitic basalt source magmas ascended 1885–1880 Ma ago and intruded in transtensional setting into the Raahe-Ladoga suture zone. Age determination from the type area in Kotalahti yielded 1883±6 Ma as crystallisation age (Gaál 1980). The highly variable size of the Kotalahti-type intrusives, from plutons covering several square kilometres to fragments just tens of centimetres across, is due to both, variation in the original size and fragmentation during deformation.

Makkonen (2015) provided a summary on the evolution and genesis of the Kotalahti-type mineralisations. The mantle derived magma assimilated country rocks, both sulphur rich Palaeoproterozoic sediments and Archaean granitoids, which together with fractional crystallisation led in some of the intrusions to sulphur oversaturation and separation of sulphide melt, enriched in Ni and Cu. The mineralisations occurring near the original basal contact of the intrusion are mostly dissemination type. Fractionation of the larger magma bodies produced typically layered ultramafic-mafic intrusions.

In the present study area, small Kotalahti-type intrusions are known only along the southwestern edge, which of Outokumpu Oy drilled three; Häikiä, Kotkatniemi and Sarkalahti (Fig. 6, Karppanen 1982,

Lakanen 1983, Vihreäpuu 1993, Juurela 2012). All three contain sulphide mineralisations or indications of them, but have been regarded as too small, too low grade, in too difficult position or all of the above, to warrant exploitation or further exploration work.

3.2.8 Saarijärvi suite

The large porphyritic quartz monzonite-granite intrusions of the Saarijärvi suite in the Sorsakoski area just west of the main study area (Fig. 6) form a bimodal suite, also including mainly dioritic mafic component. These intrusions were emplaced in transtensional setting in the Raahe-Ladoga suture zone 1880–1875 Ma ago and can be regarded as typical representatives of the post-kinematic intrusives of the CFGC, despite the fact that they are not within the CFGC (Lahtinen et al. 2016, Pietilä 2020).

Based on observed petrographic and geochemical features, Pietilä (2020) concluded that the Sorsakoski intrusions can be regarded as belonging to type 3a (Elliot et al. 1998) of the post-kinematic intrusions. Although certain trace element characteristics (e.g. Ba, Rb, Zr, Sr) resemble those of type 3 the most silica-enriched parts start to resemble type 2. Pietilä (2020) also interpreted that the intrusions formed from fractionated mantle magmas which during ascent assimilated continental crust, and possibly also were contaminated by coeval felsic magmas.

3.2.9 Northern Savo supersuite

The Proterozoic granitoids and quartz diorites intruding both the Archaean basement and its Proterozoic cover as variably sized intrusions and dykes in the study area have previously been divided into Heinävesi, Kaarakkala, and Muuruvesi suites (Bedrock of Finland – DigiKP, Finnstrati). The subdivision of the granitoids is based solely on their host rocks: Kaarakkala suite intrudes Archaean crust, whereas rocks of the Heinävesi suite intrude the Viinijärvi suite paragneisses, or the Levänen group paragneisses enclosed within the Archaean granitoids. The Muuruvesi suite is the least voluminous of the three and consists of so-called microtonalite dykes and small intrusions intruding into both paragneisses and Archaean rocks. The dykes typically display magma mingling structures between finer grained quartz diorite compositions and coarser-grained trondhjemitic compositions (Huhma 1981, Lukkarinen 2008), although dykes consisting of only the mafic component are also known.

Rocks of all these suites display mineralogical variation from quartz diorites to granites and thus form bimodal suites. Suvasvesi, Heinävesi, Juurus and Maarianvaara intrusions have been dated earlier, yielding zircon U-Pb ages of 1868±7 Ma, 1865±6 Ma, 1870±2 Ma and 1850±6 Ma respectively (Huhma 1986, Lahtinen et al. 2016). The microtonalites are either coeval with the more felsic intrusions or partially somewhat younger as one of the dykes yielded crystallisation age of 1833±7 Ma (Lahtinen et al. 2016). Emplacement of the Heinävesi and Kaarakkala suites has been interpreted as taking place during continuing strike-slip deformation (e.g. Sorjonen-Ward 2006). This allowed the raise of magmas formed from metasomatised mantle (mafic members) and mafic lower crustal sources (felsic members) to present erosion level (Lahtinen et al. 2016). Contamination during ascent was variable. Rocks of the Heinävesi suite are characterised by clearly negative initial ε_{Nd} values and model ages between 2200 Ma and 2500 Ma (Lahtinen et al. 2016).

Rantanen (2021) studied the geochemical character of the Suvasvesi intrusion and dykes in its vicinity, based on their data the Suvasvesi intrusion, and the whole Heinävesi suite displays I-type mineralogy and geochemistry suggesting metaigneous source for magmas. The most likely source are Archaean TTGs and amphibolites hidden beneath a relatively shallow sheet of Viinijärvi suite paragneisses.

3.2.10 Haukivesi suite

The Haukivesi suite consists of granitoids intruding into the Raahe-Ladoga zone. This suite belongs to a group of poorly defined Palaeoproterozoic granitoids regarded as too felsic for inclusion into the Kotalahti suite. Based on the bedrock map (Pääjärvi & Äikäs 2005) rocks included in this suite vary from quartz diorite to granite in composition.

3.3 Structural geology

Similar fold styles and rock fabrics have been recognised in different parts of the Outokumpu allochthon (=rocks belonging to the Viinijärvi suite & the Outokumpu assemblage) and these observations highlight rather well-defined deformation events for the area. This is especially the case for the early events in the deformation sequence. Bedding-parallel differentiation layering and quartz veins were formed by pressure solution process even before the first deformation event (Koistinen 1981, Ward 1987). First deformation event (D1) affected the Palaeoproterozoic cover sequence and is seen as recumbent, isoclinal F1 folds in the supracrustal rocks (Koistinen 1981, Park & Bowes 1983, Ward 1987). Generally small angle between original bedding and axial planar foliation, except at fold noses, points to originally recumbent attitude of the F1 folds (Koistinen 1981).

The second deformation event (D2) affected the Archaean basement as well as cover sequence (Park & Bowes 1983). East-verging overturned folds were formed and locally the fold limbs evolved into thrusts (Koistinen 1981, Park & Bowes 1983, Ward 1987). Pervasive foliation and lineation developed in both the cover rocks and their Archaean basement during D2 stage (Park & Bowes 1983, Koistinen 1981).

In the third deformation event (D3) NW-trending shear zones developed (Koistinen 1981, Halden 1982, Ward 1987). The most significant of these is the Suvasvesi shear zone, which has at least 15 km of dextral strike-slip movement (Halden 1982, Lukkarinen 2008). Curvature of the SSW-trending to WSW-trending L2 mineral and intersection lineation is caused by D3 movement along the Suvasvesi shear zone (Heinävesi wrench fault lineament, Koistinen 1981).

Finnish Reflection Experiment (FIRE) seismic measurements across Outokumpu region revealed that the Outokumpu mining district is located on the western limb of the Viinijärvi synform and associated with northwest verging thrusts (Sorjonen-Ward 2006). Sorjonen-Ward (2006) interpreted the formation of Viinijärvi synform as folding, coeval thrusting and formation of shear zones in response to the NNW-SSE regional compression. Säntti et al. (2006) defined metamorphic isograds from serpentinite rocks of the Outokumpu assemblage and observed that metamorphic grade increases from east to west across the Outokumpu allochthon. Furthermore, Säntti et al. (2006) noted that static peak-metamorphic assemblages in the serpentinite bodies overprint high-strain fabrics. Metamorphic isograds are oblique to the major structural trends on aeromagnetic maps (Fig. 7). Sorjonen-Ward (2006) interpreted that the peak metamorphic conditions relate to regional advection of the heat from 1.87-1.855 Ga old granitoids, which give minimum age for NE-SW-trending structures on the Outokumpu allochthon.

Along the Raahe-Ladoga suture zone, near the western margin of the study area structural geological studies have been carried out during nickel-copper exploration in Kotalahti-type intrusions. Gaál (1980) carried out extensive stratigraphic and structural studies in the vicinity of the Kotalahti mine. Jokela (1994) studied structures and migmatisation of the paragneisses between Varkaus and Kuopio. Forss et al. (1999) studied structures on the western side of Vehmasmäki (Fig. 6).

Jokela (1994) observed isoclinal recumbent F1 folds in the weakly-migmatitic paragneisses of the Hanhisalo islands. These folds are most likely related to thrusting of Proterozoic allochthonous units over Archaean craton (Jokela 1994). Further to the west, at Täilahti, Outokumpu-type serpentinite body has been been discovered (Forss et al. 1999). All the other known Outokumpu-type serpentinites are tectonically emplaced to Viinijärvi suite paragneisses, which indicates the presence of an allochthonous klippe at Täilahti (Kontinen et al. 2006).

Within the Raahe-Ladoga zone major shear zone structures and schollen migmatites show spatial correlation with each other (Jokela 1994). Forss et al. (1999) observed folded biotite schistosity in F2 folds, which indicates former pervasive S1 schistosity, although F1 folds are difficult to detect from the Raahe-Ladoga zone because of long-lasting and intensive deformation. East-verging asymmetric folds with subhorizontal fold-axes and locally thrusted limbs formed during the second deformation phase on the western side of Vehmasmäki (Forss et al. 1999, Fig. 6). These folds correspond to east-verging D2 folds with thrusted limbs at the Kaavi area (Park & Bowes 1983). Minor formation of neosome is related to the thrusting in the second phase (Forss et al. 1999). During the third deformation phase upright folds formed, and fold limbs developed into shear zones and main migmatisation occurred (Forss et al. 1999).

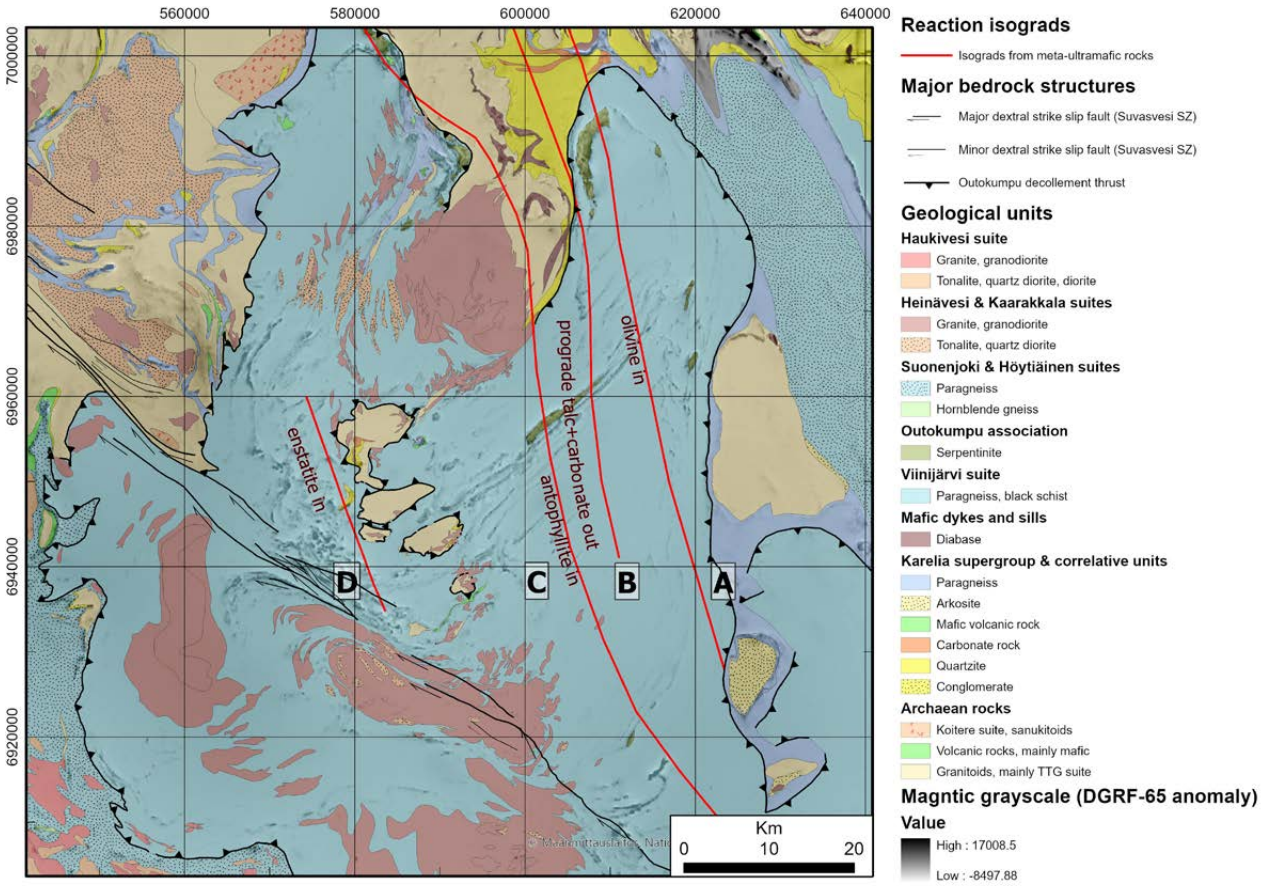

Fig. 7. Metamorphic reaction isograds, defined from meta-ultramafic rocks of the Outokumpu suite (Säntti et al. 2006), are discordant with the structural trend shown by aeromagnetic anomalies in the background. Sorjonen-Ward (2006) interpreted that the peak metamorphic conditions relate to the outcropping granitoids (Heinävesi and Kaarakkala suites). According to Säntti et al. (2006), mineral assemblages in the meta-ultramafic rocks are A: Antigorite ± olivine ± tremolite, B: Olivine ± talc, C: Olivine ± antophyllite ± cummingtonite ± talc, D: Olivine ± enstatite ± antophyllite ± MgAl-spinel.

3.4 Suvasvesi impact structures

Suvasvesi North (Kukkarinselkä) and South (Haapaselkä) impact structures (Fig. 6) are covered by two circular open waters of Lake Suvasvesi separated by several islands. Before age determinations, the Suvasvesi N and S were regarded as a doublet produced by the single impact of a binary asteroid, similarly as e.g. Clearwater Lakes, Canada. However, $^{40}Ar/^{39}Ar$ geochronologic data indicate age of ~85 Ma for Suvasvesi North and ~710 Ma for Suvasvesi South (Schmieder et al. 2016).

3.4.1 Suvasvesi North

The Late Cretaceous (~85 Ma) Suvasvesi N is a simple impact crater ~3.5 km in diameter and ~260 m deep. The crater is located just south of the Suvasvesi shear zone near the contact between the Viinijärvi suite and Archaean rocks (Fig. 6) and was first studied as a possible kimberlite pipe. The interpretation was based on magnetic features in high-altitude aeromagnetic data and detailed ship-borne magnetic survey.

Drilling of the negative magnetic anomaly to a depth of ~260 m revealed a ~80 m thick layer of impact breccia and impact melt rock. Drilling was finished before penetrating the impact melt layer (Matti Tyni, personal communication, 2020). Impactites (depth 228–252 m) consist of impact melt-bearing breccias and impact melt. The clast-rich and clast-poor impact melt have a cryptocrystalline matrix with fluidal (schlieren) texture and a spinifex matrix with ferrosilite-pyroxene. According to Schmieder et al. (2016), the composition of the melt matrix has a ternary feldspathic composition (63–69% SiO_2, 0.9–12.6% K_2O, 2.9–7.1% Na2O, 0.6–5.4% CaO). Quartz is the most abundant mineral and shows up to three sets of PDFs (planar deformation features), which proved the structure

to be of impact origin (Pesonen et al. 1996, Werner et al. 2002). The PDFs are partially decorated, e.g. containing tiny fluid inclusions produced from fresh PDFs by secondary annealing (Grieve et al. 1996). Clasts with rare ballen-textured silica and zircon grains with planar fractures have been observed (Pesonen et al. 1996, Schmieder et al. 2016). The impactites show only minor alteration comprising chlorite filled vesicles. The Fe-rich Si-Al-oxides and Fe-Ti-oxides, bravorite (Ni-rich pyrite), and pyrite are the common opaques (Schmieder et al. 2016).

After initial discovery the low-altitude airborne magnetic data delineated a circular negative magnetic anomaly ~0.8 km in diameter with an amplitude of ~160 nT, coinciding with the lake's bathymetric maximum (96 m). This anomaly has been interpreted as being produced by a reversely magnetised allochthonous impact melt-bearing breccias and impact melts (Pesonen et al. 1996, Werner et al. 2002). The peak minimum is surrounded by a weaker, round anomaly with a diameter of 3.5 km. Anomalies in two perpendicular gravity profiles 9 km in length also reveal a crater diameter of ~3.5 km (Werner et al. 2002).

3.4.2 Suvasvesi South

The Suvasvesi S impact structure, 3.8 km in diameter, in the contact of the Viinijärvi suite paragneisses and Suvasvesi intrusion was first perceived in satellite images due to its round shape (Pesonen et al. 1996). Evidence for its impact origin is based on the shatter cones on outcrops at the central part of the lake (Schmieder et al. 2016) and well-formed shatter cones in biotite paraschist and granite boulders found southeast of the crater. Also, a number of impact melt boulders have been found a few kilometres east-southeast of the Haapaselkä lakeshore (Lehtinen et al. 2002, Pesonen et al. 2003, Öhman et al. 2003). It has been proposed that the boulders could have originated from Suvasvesi N, but the direction of the regional ice flow is 140°, and thus the transportation theory from the northern structure is unlikely (Donaldini et al. 2006).

The impact melt boulders contain granitic clasts, supporting Suvasvesi S as the source as Suvasvesi N formed in paragneiss dominated area. The glassy melt matrix has a fluidal texture and contains rare diaplectic plagioclase glass (maskelynite) inclusions (Öhman et al. 2003, Donaldini et al. 2006). The shocked quartz grains and oligoclase show decorated PDFs with common impact diagnostic crystallographic orientations. Various shock metamorphic features indicate pressures in the 15–25 GPa range. In addition, impact melt glass contains opaque crystals, commonly tiny, 10–100 µm in size, with Ni-Co core surrounded by Fe-oxide rim, occasionally mixed with Ni-Si phase. Enrichment of Ni-Co is suggested to be from the projectile (Öhman et al. 2013).

According to Puura & Plado (2015), Suvasvesi S impact structure is deeply eroded but partly preserves crater fill deposits. In addition, the actual depth of the structure is still unknown, but bathymetric features are more shallow than in Suvasvesi N, with a maximum water depth of 29 m, and the structure shows no magnetic anomalies.

4 ARCHAEAN ROCKS

The Archaean bedrock of the study area has in this study been divided into three main groups based on field observations, petrography and geochemical composition. The most voluminous groupconsists of variably deformed equigranular tonalites, granodiorites and granites, with biotite as the main mafic mineral. The group will be in this text referred to as TTGs despite the fact that they would be more correctly referred to as "TTGs sensu lato" as the group includes rocks with K_2O/Na_2O >0.5 not fulfilling the classical definition of "true TTGs" (Martin et al. 2005). The second main group are the granodiorites. Based on geochemical characteristics these typically porphyritic granodiorites are referred to as 'sanukitoids'. The third, and least voluminous, group consists of equigranular quartz diorites.

The sanukitoids and TTGs are also divided on the updated bedrock map (Appendix 1). However, the reader should note that, due to low and variable observation density, the areal distribution of the rock types should be taken as tentative.

4.1 Field observations and petrography

4.1.1 Tonalites, Granodiorites and Granites (TTGs)

The majority of the Archaean crust exposed in the study area and its vicinity consist of small to medium-grained (1–3 mm) equigranular tonalites and granodiorites. Also granites exist, but they form a minority. Biotite is the most common mafic mineral, hornblende being observed only locally and always in smaller proportions than biotite. Typical accessory minerals include sphene, apatite, epidote and zircon. Post-crystallisation alteration is typically weak, but small amounts of secondary muscovite and chlorite are relatively common.

The TTGs sensu lato are always variably oriented, the nature of the orientation varying from gneissic foliation to strong and penetrative mineral lineation (Fig. 8), the latter being dominant especially in the Konnuslahti dome (see location in Fig. 6). Banded structures can be observed locally, and in some places the leucocratic material appears to be local, in situ melt, as indicated by biotite rich seams between the leucosome and the mesosome, whereas in other places this dark band is missing, and it seems more likely that the leucocratic material represents narrow granitoids veins, later deformed to structure resembling banded migmatite (Fig. 8D).

4.1.2 Porphyritic granodiorites, i.e. sanukitoids

In certain parts, the dominant Archaean granitoid is K-feldspar porphyritic granodiorite displaying variably intensive augen gneiss texture. The size of the K-feldspar megacrysts is typically 2 to 4 cm, but individual ones can be up to 10 cm. In more strongly sheared areas the size of the phenocrysts has been

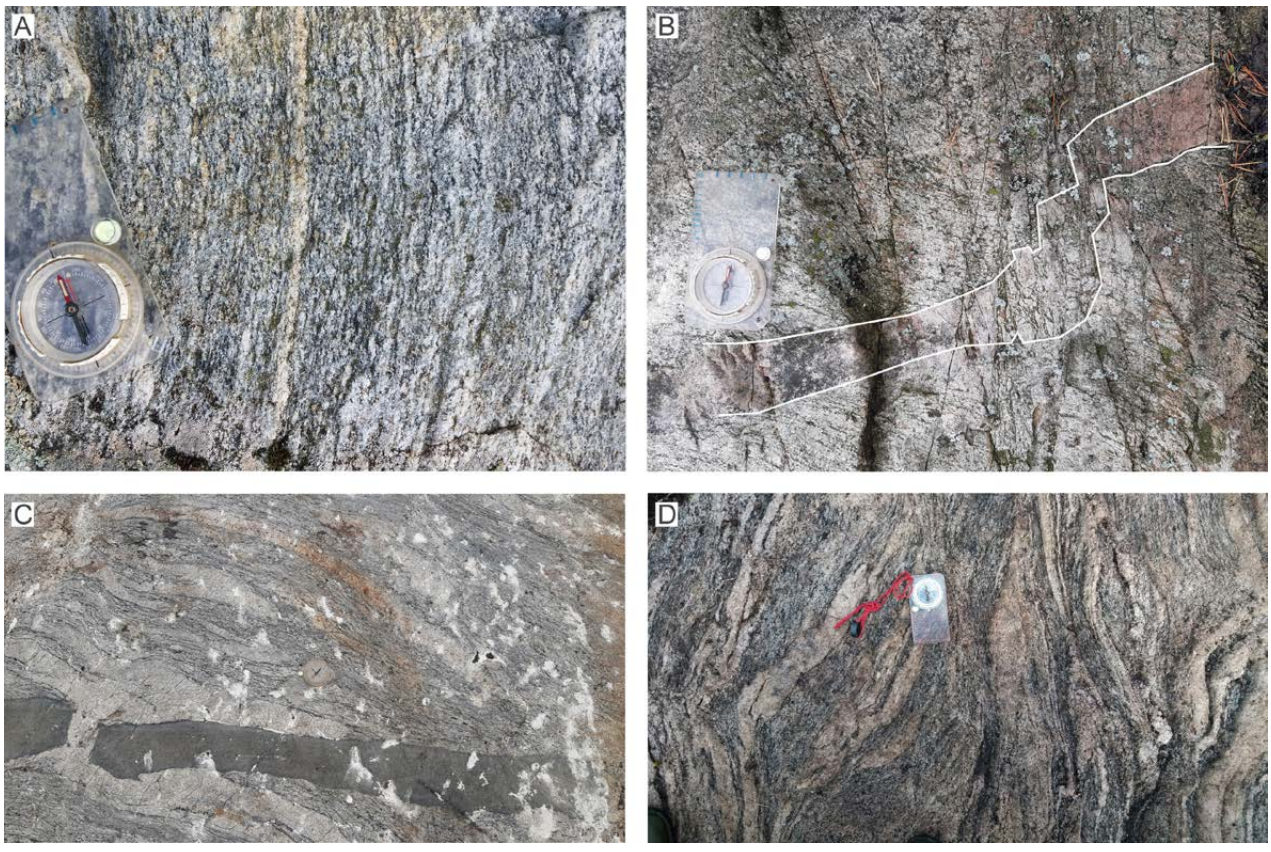

Fig. 8. Archaean granitoids from the study area. Length of compass 12 cm. A) Unmigmatised, strongly foliated biotite tonalite of the TTG suite at observation PIM$-2019-76 (E=541 910, N=696 2427). B) Proterozoic leucogranitoid crosscutting TTG tonalite at observation PIM$-2019-168 (E=545 164, N=696 4643). Dyke is crosscut by N-S striking sinistral brittle fault. C) TTG gneiss hosting two generations of leucogranitoid dykes, the older is tightly folded and the younger crosscuts the relatively undeformed diabase dyke in the lower left-hand corner of the photo. Observation PIM$-2020-35 (E=560 944, N=696 0797). Note, that the white spots are recent guano deposits. D) Intensively veined and folded TTG. Observation MTL2-2018-218 (E=543 584, N=694 3705). Photo: Mauri Luukkonen, GTK.

Fig. 9. Archaean sanukitoids and quartz diorite from the study area. Length of compass 12 cm. Photos: Mauri Luukkonen, GTK. A) Weakly deformed porphyritic sanukitoid with mafic enclave and crosscutting leucogranite dyke at observation MTL2-2019-28 (E=556 395, N=697 3043). B) Typical augen gneiss structure of sanukitoid at observation MTL2-2019-8 (E=560 251, N=697 2527). C) Intensively sheared porphyritic sanukitoid in which the K-feldspar phenocrysts have diminished in grain size at observation MTL2-2019-124 (E=556 356, N=696 0557). D) Archaean quartz diorite crosscut by trondhjemite vein at observation MTL2-2019-357 (E=565 761, N=696 6836). The few observable larger phenocrysts are plagioclase.

mechanically diminished (Fig. 9). Hornblende and biotite are present as the mafic mineral in various proportions, the first typically being altered to the latter variably. Typical accessory minerals are sphene, apatite and zircon. Secondary chlorite and muscovite are also present.

4.1.3 Quartz diorites

The Archaean quartz diorites are variably oriented and more mafic than the TTGs (Figs. 8 vs. 9D), but distinction between these two groups in the field is not always simple and the sparse observation network hinders reliable delineation of these rock types on the Appendix map. It should also be noted that some of the more mafic equigranular quartz diorites and tonalites are, from a geochemical point of view, members of the sanukitoid suite. Similar observation has also been made e.g. in Lieksa area where quartz diorites are divided between the Koitere suite (i.e. sanukitoids) and the Jonsa suite (i.e. not sanukitoids, Mikkola et al. 2013).

In the study area, quartz diorites are most common in the eastern part of the Kuopio complex and especially in the Kohma area (see location in Fig. 6). Similar leucocratic veins, as in TTGs, are less abundant but still common in quartz diorites. Quartz diorites typically display moderate to strong gneissic foliation. Grain size is close to 2 mm and plagioclase is in some places present as small (≤ 1 cm) sporadic phenocrysts (Fig. 9D). The amount of quartz varies so that some of the samples are actually tonalites, if mineralogically classified. Hornblende and biotite are typically present in roughly equal proportions. Common accessory minerals include sphene, apatite, epidote (both magmatic and secondary) and zircon. Secondary chlorite is also common.

4.2 Areal distribution of the Archaean granitoids

4.2.1 Main Kuopio complex

Southern parts of the Kuopio complex in the study area are dominated by TTGs sensu lato intruded by diabase dykes and leucocratic dykes. TTGs are typically strongly deformed but homogeneous gneisses. Sanukitoids are more abundant east of Vehmersalmi where they form elongated areas, typically a few kilometres long and less than 2 kilometres wide. The Archaean quartz diorites are most abundant in the Kohma area where they form separate areas. They exist also further west, but due to limited observation density cannot be delineated on the map.

4.2.2 Konnuslahti area

In the Konnuslahti area, there are two separate occurrences of Archaean rocks; larger Konnuslahti dome and smaller Monganlahti thrust sheet. The Konnuslahti dome is ca. 8 km long and 2.5 km at widest and elongated in north-south direction (Fig. 10, for location see Fig. 6). Monganlahti thrust sheet (2*0.2 km) is located west of it. Both are surrounded mainly by paragneisses, with thrust contacts. Only along its western contact the Konnuslahti dome is flanked by autochthonous cover sequence belonging to the Karelia supergroup.

The Archaean rocks consist of relatively homogeneous biotite tonalite, typically displaying strong lineation towards southwest at a relatively shallow angle. The abundant mafic rocks hosted by the tonalite have been interpreted as Proterozoic diabase dykes, although Archaean volcanic origin is possible for certain more heterogeneous variants. The tonalite is not migmatised but crosscut by narrow, typically <30 cm wide, pegmatitic granitoid veins that are relatively undeformed.

4.2.3 Saamanen dome

The Archaean section in Saamanen area (for location see Fig. 6) displays a classical mantled gneiss dome structure (Eskola 1949) similar to the Kuopio area where the Archaean granitoids are symmetrically mantled by Palaeoproterozoic quartzites, carbonate rocks and mafic volcanic rocks. In the case of Saamanen, the mafic volcanic rocks predominate. The Archaean core of the dome consists of intensively deformed tonalite, which has a banded structure. It is arguable if the leucocratic bands represent in-situ partial melting of the hosting tonalite or narrow deformed veins, as in most cases the dark biotite rich melanosome is absent.

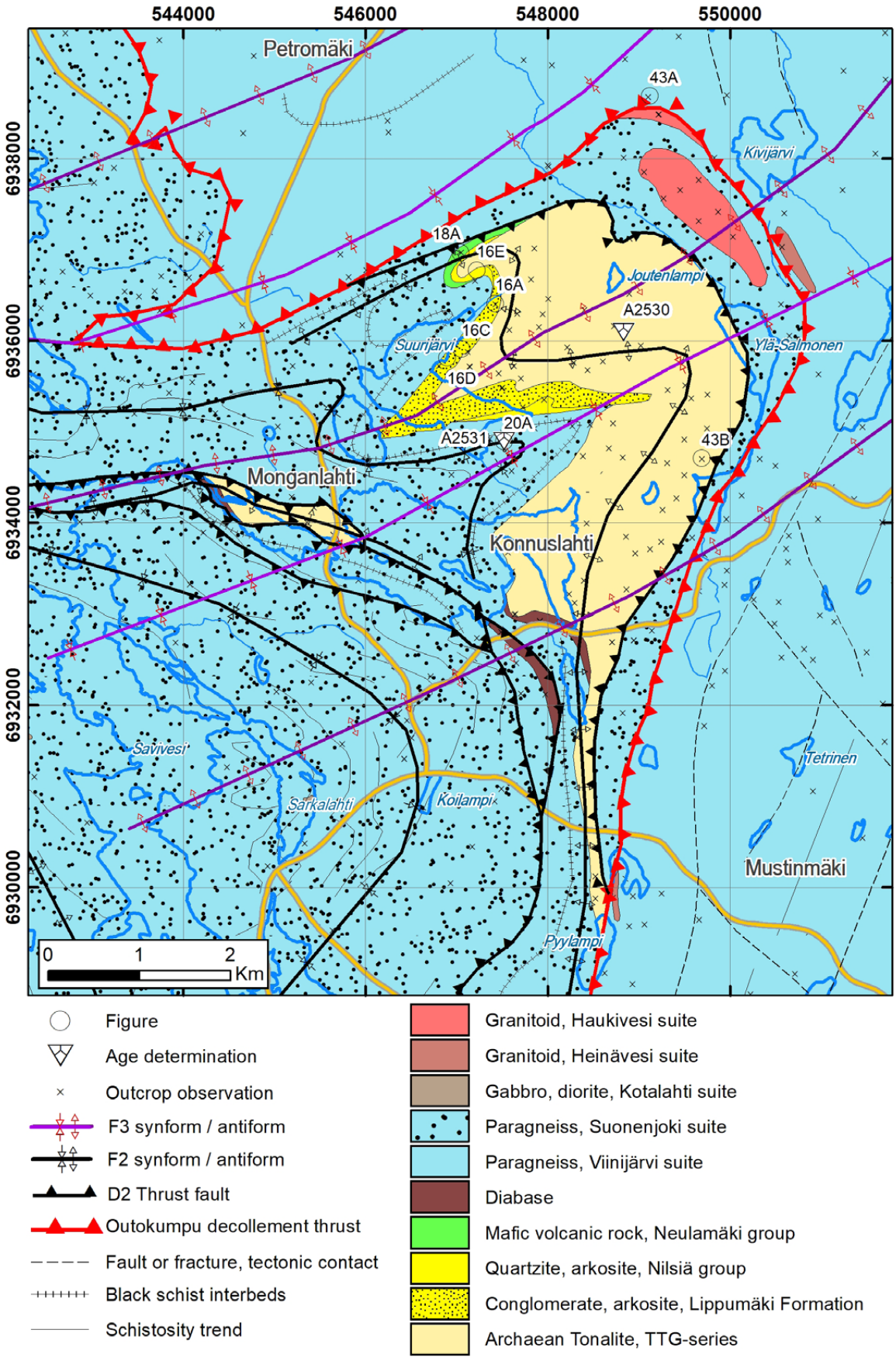

Fig. 10. Bedrock map of the Konnuslahti area, located in the vicinity of the interpreted contact between Viinijärvi and Suonenjoki suites. Structurally the area is dominated by thrust faults developed during the initial collisional phases at ~1910 Ma (D1 and D2) and folds generated during D3 phase observable as fold axis and strong lineation plunging to southwest at a relatively low angle. See text for further discussion.

4.2.4 Vasikkasaaret thrust sheet

The ca. 5 km long Vasikkasaaret thrust sheet is located approximately 10 kilometres south of Leppävirta (for location see Fig. 6) and consists of highly deformed biotite tonalite hosting abundant homogeneous amphibolites interpreted as diabase dykes (Fig. 11). Based on field observations and a weak magnetic anomaly caused by the dykes, the width of the fragment is likely to be 200–300 metres but cannot be reliably determined.

Fig. 11. Strongly sheared TTG gneiss and homogeneous amphibolites interpreted as diabase dykes at observation PIM$-2019-124 (E=545 491, N=692 2193) from the Archaean Vasikkasaaret thrust sheet. Proterozoic granitoid vein has intruded along the contact between the gneiss and the diabase. Length of compass 12 cm.

4.3 Geochemistry

Geochemical data from Archaean bedrock consists of 79 samples, out of which 14 are new analysis and the remaining 65 collected from various publications. Sample locations are shown in Figure 12. See the Electronic Appendix 1 for data and references.

4.3.1 TTG s.l.

TTGs s.l. (n=45) in the area are felsic, SiO_2 62.7–75.4%, average 70.1% and have relatively low Mg# (Mg#=Mg^{2+}/(Mg^{2+}+FeT^{2+})*100) varying from 17 to 61 with average of 42 (Fig. 13). Furthermore, they are leucocratic with FeOt+MgO+MnO+TiO2=1.4–7.1%, average 4.0% and low Cr and Ni contents, mainly below 50 ppm and 30 ppm respectively. K_2O is highly variable, with values from 0.7 to 5.0%, with an average of 2.3, whereas Na_2O is less scattered and varies from 3.7 to 5.7%, excluding an outlier at 1.0%. All of the above-mentioned characteristics are typical for Archaean TTGs but, due to elevated K_2O contents, some of the samples have $K_2O/Na_2O>0.5$, which was considered by Martin et al. (2005) as the limit of "true TTGs" produced by partial melting of mafic protoliths.

The TTGs s.l. are further divided in this study based on main and trace element geochemistry, term "transitional TTGs" will be used for samples with $K_2O/Na_2O>0.5$ (n=16, Fig. 13). Samples with $K_2O/Na_2O<0.5$ are referred in this text as TTGs and have been further divided into low-HREE-type (n=18) and high-HREE-type (n=7). The HREE division is based on work by Halla et al. (2009) who interpreted it as a result of variable amount of garnet in residue reflecting variable melting depths. Additionally, the TTGs include samples which, due to limited trace element data, cannot be assigned to either of the HREE groups.

Low-HREE TTGs display variable enrichment in LREE (La_N=30–315), REE fractionation (La_N/Yb_N=14–169) and Eu anomaly (Eu/Eu*=0.65-2.50), which correlate so that the samples with low La_N have positive Eu anomalies (Fig. 14A). Respectively, samples more enriched in LREE display weakly negative Eu anomalies. On primitive mantle normalised spider diagrams samples display scatter in LILE (large ion litophile elements) in addition to distinct negative Nb and P anomalies.

High-HREE TTGs display more uniform enrichment in LREE (La_N=43–115) than the low-HREE variants, but due to higher HREE the fractionation is weaker (La_N/Yb_N=11–20). Eu anomalies are mainly weakly negative (Eu/Eu*=0.78–1.08) (Fig. 14A). On primitive mantle normalised spider diagram the high-HREE TTGs display mainly similar patterns as the low-HREE ones, i.e. scatter in LILE and negative Nb and P anomalies, with the only difference being the negative Ti anomaly.

On the CIPW normative feldspar triangle of O'Connor (1965) both low- and high-HREE TTGs plot in the tonalite and trondhjmite fields (Fig. 15)

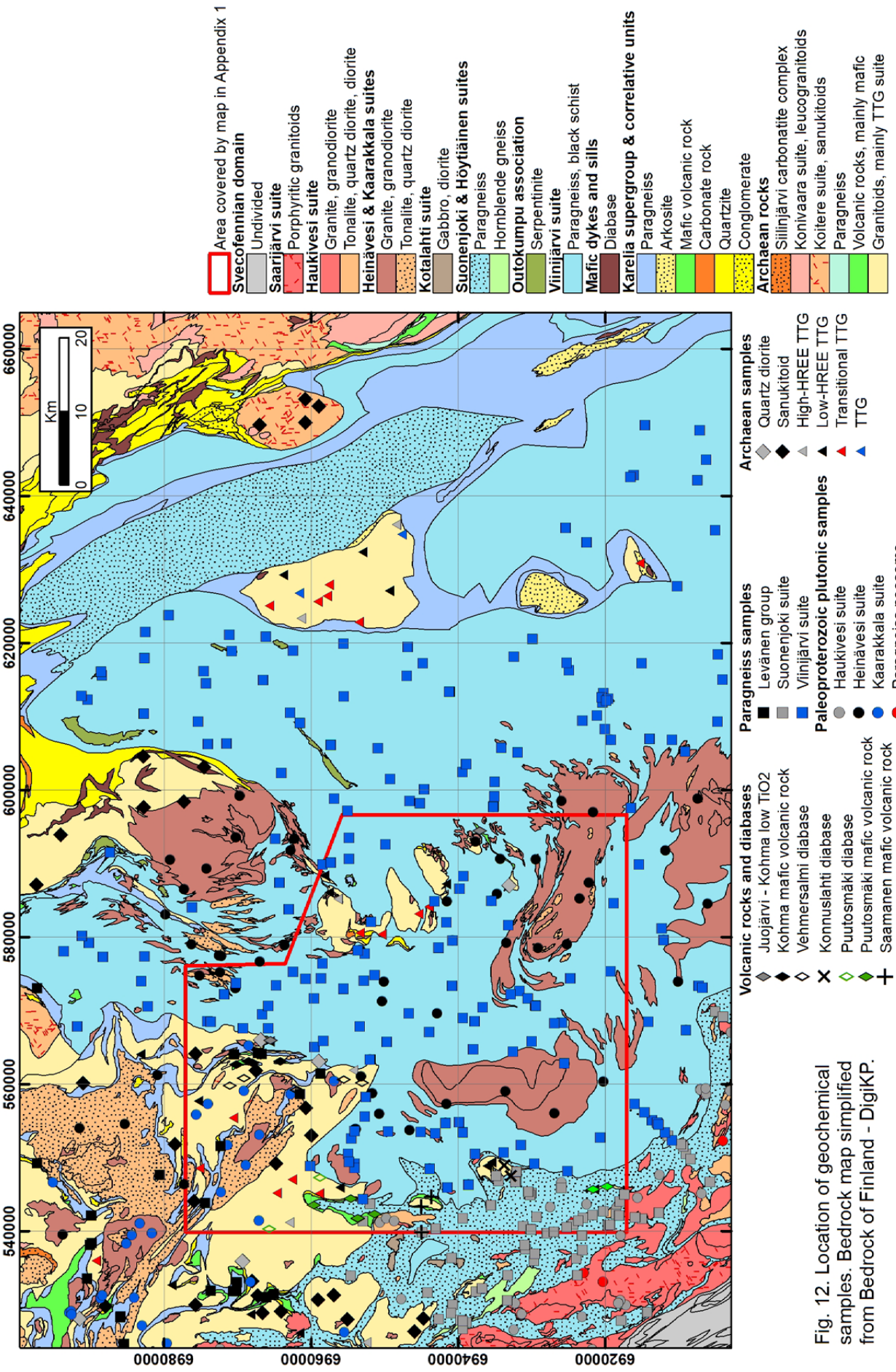

Fig. 12. Location of geochemical samples. Bedrock map simplified from Bedrock of Finland - DigiKP.

and in the classification diagrams of Laurent et al. (2014) in the TTG field. The difference in the HREE composition is visible on the classification diagram of Heilimo et al. (2010). Based on source classification diagram of Laurent et al. (2014), low- and high-HREE TTGs were derived from low-K mafic rocks.

Transitional TTGs have similar variation in LREE enrichment and REE fractionation as the low-HREE TTGs, La_N=18–345 and La_N/Yb_N=10–122. The Eu anomaly is negative in 12 of the 14 samples and only one sample displays a strongly positive anomaly (Eu/Eu*=0.51–1.90, Fig. 14). On primitive mantle normalised spider diagram also the transitional TTGs display scatter in LILE, but the levels are, on average, higher than in the other TTG groups, while Sr concentrations are lower. Negative Nb and P anomalies are similar to the other groups, whereas the Ti anomaly is distinctly clearer than in high-HREE TTGs.

The transitional TTGs potentially form two separate populations, divided by Ba contents. Ba content does not correlate with any of the main elements and out of the trace elements the only observable differences are somewhat higher Zr, Hf and REE, and especially HREE, contents of the samples enriched in Ba. This question is not discussed further because it could be an artefact of limited sample number as the transitional TTGs in the Lentua complex form a continuum from low to high concentrations (Mikkola et al. 2012, 2013) and thus would require additional field work and sampling to be properly addressed.

On O'Connor's (1965) feldspar triangle the transitional TTGs plot near the junction between trondhjemite, granodiorite and granite fields, with the majority of them in the last (Fig. 15). On Laurent et al.'s (2014) classification diagram, samples plot in the biotite granite and hybrid granite fields and, on the source discrimination diagram, in fields interpreted as derived from tonalites and high-K mafic rocks.

4.3.2 Sanukitoids

Despite significant scatter, overall the sanukitoids are, on average, less felsic than the TTGs (SiO_2=55.0–72.6%, average 65.0, n=29, Fig. 13) and have higher Mg# varying from 38 to 57, with an average of 48. Observed K_2O concentrations (1.6–5.0%, average 3.3%) are slightly higher than and Na_2O similar (3.5–5.3%) to those in TTGs, resulting in higher K_2O/Na_2O ratios on average. Ba+Sr varies from 930 to 3130 ppm. Cr and Ni concentrations are slightly higher than in TTGs, being 20–85 ppm and <40 ppm respectively. All of the above-mentioned characteristics are typical for Neoarchaean sanukitoids in East Finland (Heilimo et al. 2010). The most significant difference between the typical sanukitoids and those from the study area is the mainly low Sr of the latter (Sr=237–1300 ppm, average 569 ppm, Fig. 13), which is similar to the TTGs from the study area. Yet the Ba concentration of the sanukitoids is clearly higher than in TTGs, a typical feature for the suite.

REE patterns of the sanukitoids are enriched in LREE (La_N=63–416), variably fractioned (La_N/Yb_N=10–126) and Eu anomaly varying from small to significant (Eu/Eu*=0.47–0.96, Fig. 14). On spider diagram normalised with primitive mantle, the sanukitoids display negative anomalies of Nb, Sr, P and Ti in addition to the scatter in LILE.

On the feldspar triangle, the sanukitoids plot mainly as granites and granodiorites (Fig. 15) and, on the discrimination diagrams of Laurent et al. (2014) and Heilimo et al. (2010), as sanukitoids. Based on source discrimination diagram of Laurent et al. (2014), sanukitoids were derived from high-K mafic rocks.

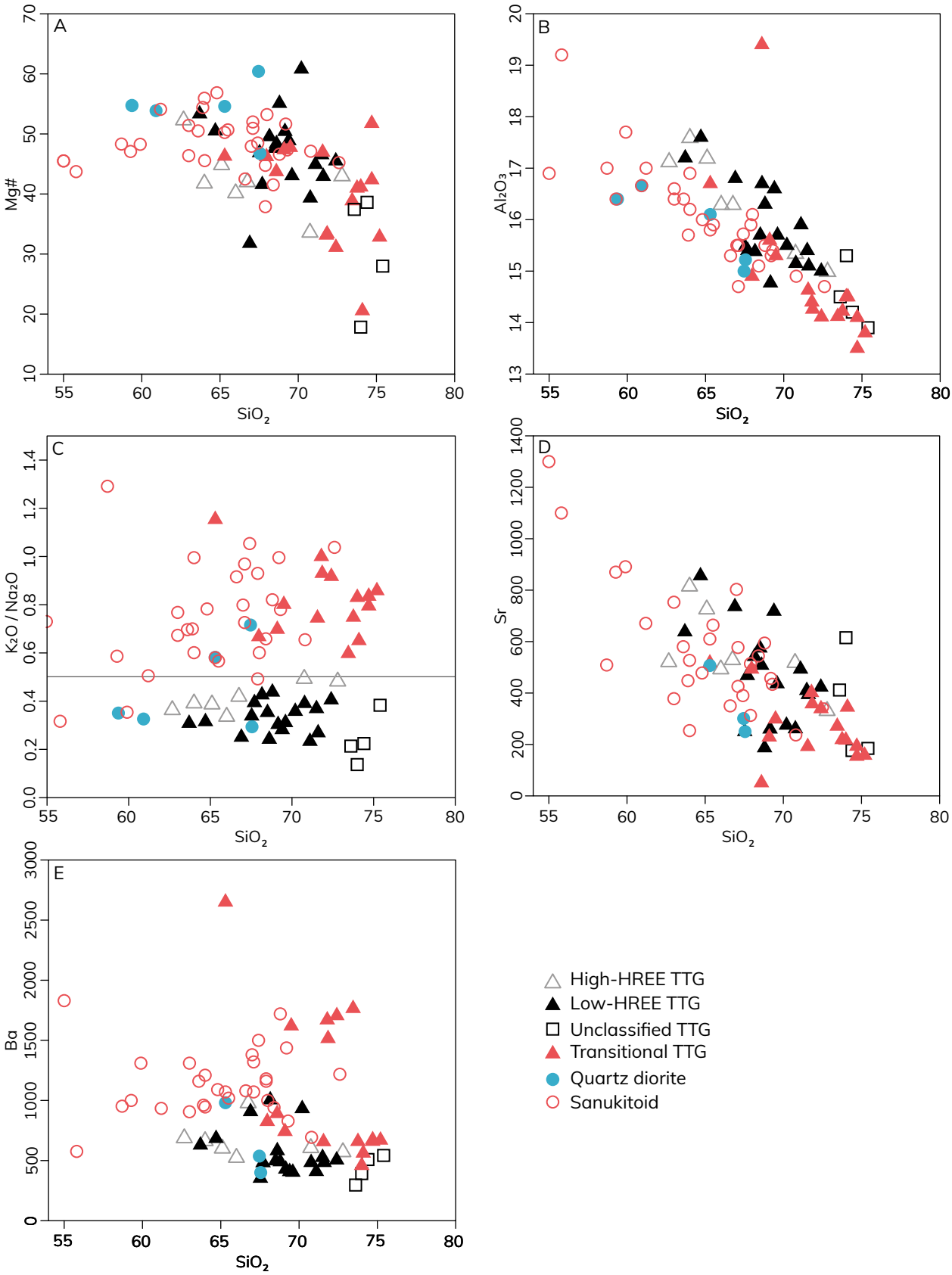

Fig. 13. Selected Harker diagrams for the Archaean granitoids.

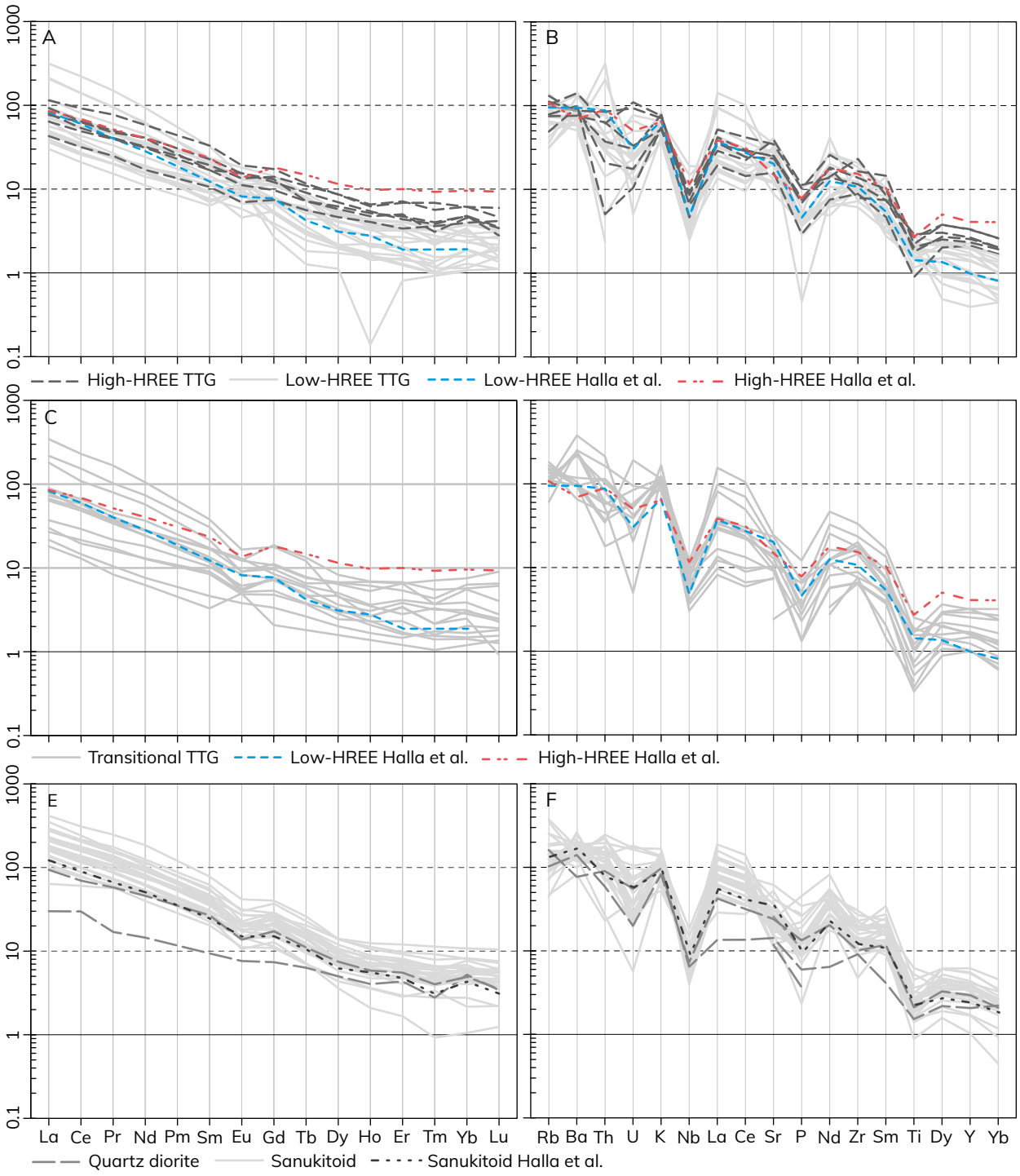

Fig. 14. Chondrite-normalised REE diagrams and mantle-normalised spider diagrams for TTGs (A, B), transitional TTGs (C, D) and quartz diorites and sanukitoids (E, F). Averages by Halla et al. (2009) shown for reference. Chondrite values from Boynton (1984) and mantle values from Sun & McDonough (1989).

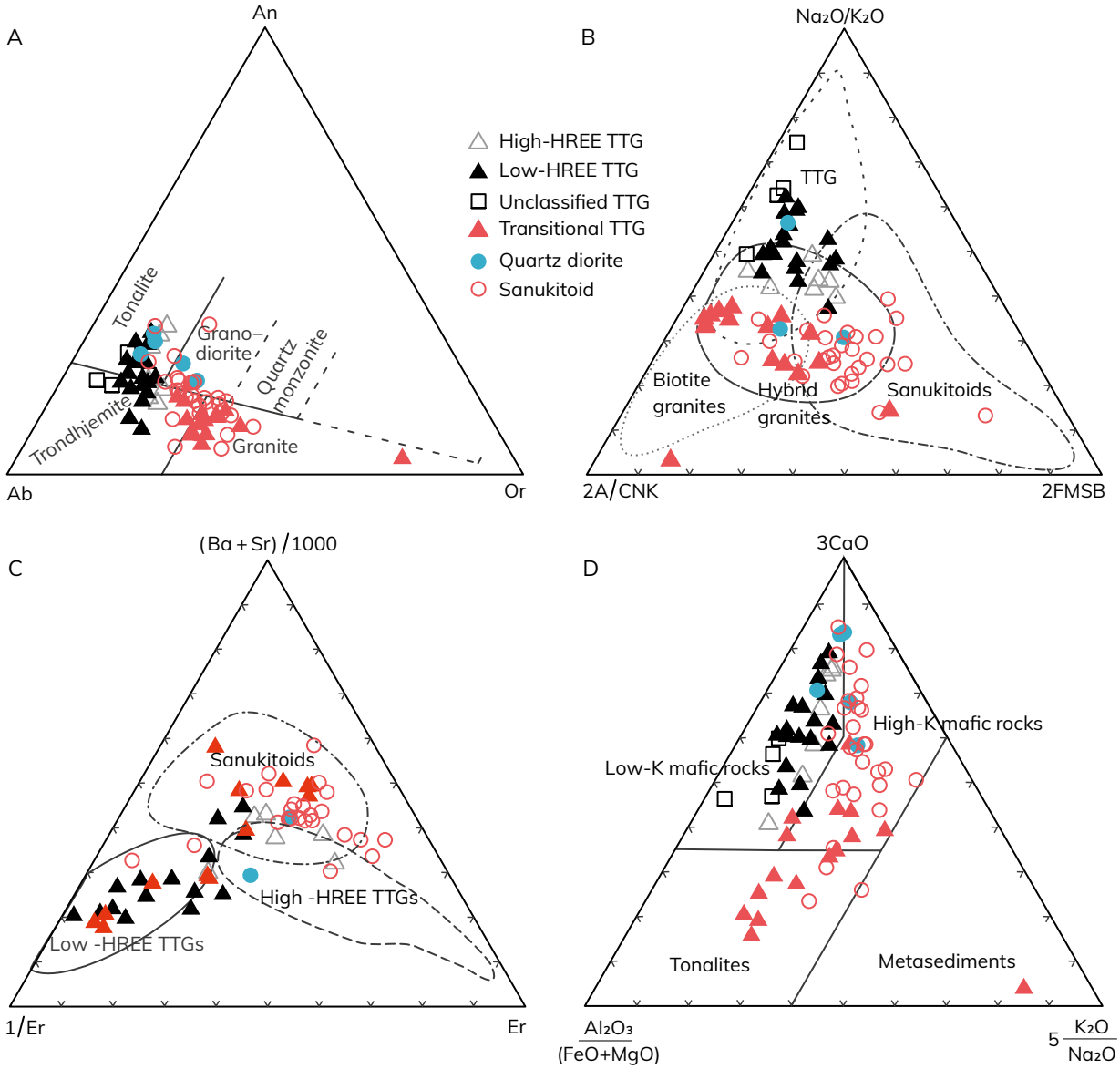

Fig. 15. Classification diagrams for Archaean granitoids. A) Feldspar triangle of O'Connor (1965). B) Classification diagrams of Laurent et al. (2014) and C) Heilimo et al. (2010). D) Magma source discrimination diagram of Laurent et al. (2014).

4.3.3 Quartz diorites

The number of quartz diorite samples is very limited (n=5), and only two of these include all trace elements. SiO_2 of the samples varies from 59.4 to 67.6% and Mg from 47 to 60. K_2O/Na_2O varies from 0.29 to 0.72 and is on average lower than that of sanukitoids, as is also Ba+Sr which varies from 650 to 1,488 ppm.

REE patterns of the quartz diorites are less enriched in LREE and more weakly fractioned than those of the sanukitoids as La_N is 30 and 94 and La_N/Yb_N 6 and 19 for those samples that the data exists. On primitive mantle normalised spider diagram, (kuten edellä) the quartz diorites display the same negative Nb, P and Ti anomalies as sanukitoids but, due to lower REE concentrations, they are weaker.

On the normative feldspar triangle the quartz diorites plot in the tonalite and granodiorite fields. On Laurent et al.'s (2014) classification diagram (Fig. 15), the quartz diorites are divided between the TTG and sanukitoid fields, and similar division is also observable on the source rock discrimination diagram where samples are divided between low- and high-K mafic rocks.

5 PROTEROZOIC SUPRACRUSTAL UNITS AND DYKES

5.1 Paleoregolith

During the field work, the paleoregolith between the Archaean basement and its Proterozoic cover rocks was found only from location north of Puutossalmi as already described by Wilkman (1938). The paleoregolith consists mainly of carbonate and diopside and forms a 1.5-metre-thick layer between gneiss tonalite and quartzite and contacts to both units are sharp (Fig. 16A).

Fig. 16. Rocks of the supracrustal cover sequence. Length of compass 12 cm. A) In the middle of the photo paleoregolith at observation PIM$-2018-95 (E=542 056, N=695 5717). On the left, quartzite of the Nilsiä group and, on the right, Archaean tonalite gneiss. View to southwest. B) Poorly sorted basal conglomerate with greenish matrix at observation KK7$-2018-1102 (E=547 433, N=693 6401), clasts are mainly leucogranites. C) Arkosite at observation PIM$-2018-11 (E=547 051, N=693 5910) showing penetrative lineation plunging southwest at a shallow angle. Note the small lithic fragments and the one larger quartzite clast. D) Conglomerate interlayer in the upper parts of the Lippumäki formation in Konnuslahti. In addition to leucogranite fragments also schist fragments are abundant. Observation KK7$-2018-1502 (E=546 899, N=693 5805). E) Brecciated arkosite at observation KK7$-2018-1214 (E=547 208, N=693 6769) in Konnuslahti, dark veining consists of phlogobite and actinolite. F) Quartzite from observation MTL2-2020-375 (E=550 853, N=697 2496) displaying weak compositional layering and schistosity.

5.2 Conglomerates and arkosites

Conglomerates correlative to the basal Lippumäki formation (Lukkarinen 2008) were found only from Konnuslahti where they occur along the folded western contact of the Archaean dome. On the outcrops, the clasts are mainly leucogranitic in composition and highly variable in size, the largest one being up to 50 cm in diameter (Fig. 16B). The matrix has locally greenish colour hue similar to that described by Aumo (1983) from the Kuopio region. In addition to outcrops, conglomerate was observed as thin layers in drill core N5242019R1 where the clasts are quartzite pebbles <5 cm in diameter (Fig. 10).

The basal conglomerates grade into arkosites with sporadic larger lithic clasts (Fig. 16C) and matrix-supported conglomerate interlayers of varying thickness. Aluminium enrichment indicating origin from deeply weathered sources is suggested by local presence of andalusite in the arkosites. In the conglomerate interlayers the leucogranites are the main lithic clast type, but schist clasts are locally abundant (Fig. 16D). Presence of schist clasts is not typical for the Lippumäki formation (Lukkarinen 2008), but their presence does not hinder correlation of the arkosites and conglomerates from the Konnuslahti area in the formation.

Along the northern contact of the Konnuslahti dome, the arkosite displays breccia structure in which the quartz plagioclase clasts are surrounded by veining consisting of phlogopite and actinolite (Fig. 16E).

5.3 Quartzites

Quartzites are relatively abundant in the study area, but their thickness rarely exceeds a few tens of metres. Thus, large number of the occurrences cannot be shown on the appendix map. In most places the quartzites are adjacent to the Archaean rocks, but the exact contact is typically more deeply eroded, preventing direct observation of its nature on outcrops.

Orthoquartzites are not common, more often the quartzites contain variable amounts of feldspars, biotite, muscovite and andalusite, and grade with the arkosites without clear contacts. This feature is typical also for the quartzites in the Kuopio area (Lukkarinen 2008). The quartzites do not display clear primary structures and most often the only observable structures are weak to moderate schistosity and compositional variation which might or might not represent original compositional layering (Fig. 16F).

5.4 Carbonate and calc-silicate rocks

The most voluminous and purest carbonate rock layers were observed in Puutosmäki and north of it in the Hautosaari area (for location see Fig. 6). In these areas, also a number of small historical quarries exist. Carbonate rocks were also observed in Saamanen and Kohma areas. Like in the surrounding areas, the carbonate rocks are rarely pure, thus in most cases calc-silicate rock would be a more appropriate name.

In the Hautosaari area, the relationship of the carbonate rocks and overlying volcanic units is well preserved and easily observable on shoreline outcrops. The lowermost parts of the carbonate rock are the purest, with centimetre-scale siliceous layers alternating with the carbonate rock (Fig. 17A). Further up in the sequence, similar thin bedding continues, but the volcanic material starts to dominate (Fig. 17B) and finally the carbonate layers disappear entirely.

The calc-silicate rock observations around the Saamanen dome are limited to a single outcrop. The only outcrop observations in the Kohma area are also from calc-silicate rocks but, based on material from well drilling, also purer carbonate rocks exist in this area. Typical silicate minerals in the calc-silicate rocks and interlayers of the carbonate rocks include diopside, epidote, phlogobite, plagioclase and quartz.

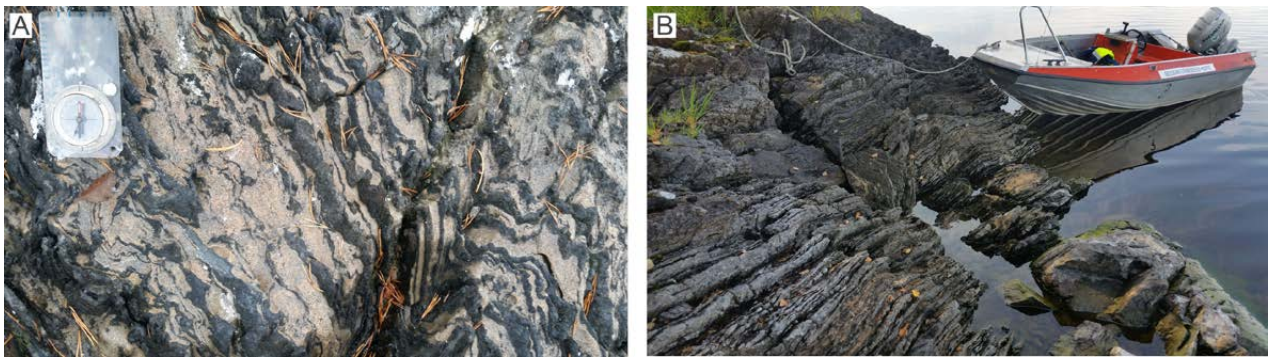

Fig. 17. A) Folded carbonate rock alternating with dark silicate-richer layers at observation location PIM$-2018-82 (E=545 021, N=696 0355) in the Hautosaari area. Length of compass 12 cm. B) Narrow interbedding of carbonate rock and volcanic material at observation location PIM$-2018-88 (E=544 609, N=696 0727) in the Hautosaari area. Length of boat ca. 5 metres.

5.5 Volcanic rocks and diabases

5.5.1 Volcanic rocks

In our interpretation, volcanic rocks in connection with the Konnuslahti dome are present only along the northeastern contact, where a clearly heterogeneous foliated mafic rock is observable (Fig. 18A). Parkkinen (1974) interpreted that rocks in the southwestern contact of the dome are volcanic, whereas in our opinion they are diabase dykes, based on their homogeneity (Fig. 19A).

Fig. 18. A) Heterogeneous foliated mafic volcanic rock from the northwesten contact of the Konnuslahti dome. Handle of the hoe pointing north. Observation JPJA-2020-57 (E=547 053, N=693 6968). B) Pillow lava from the Hautosaari area with well developed lineation towards south. Hammer handle pointing north. Observation PIM$-2018-85 (E=544 647, N=695 9890). C) Well-preserved pillow lava with wide intrapillow parts. Observation MTL2-2019-96 (E=563 065, N=696 4194). D) From the same outcrop as the previous photo, a more intensively deformed part with less intrapillow material.

Volcanic rocks surrounding the Saamanen dome and in the Puutosmäki, Hautosaari and Kohma areas are heterogeneous on outcrop scale and interpreted as variably deformed pillow lavas or pillow lava breccias. In areas of more intensive deformation, the rocks have banded appearance and locally display well-preserved primary structures (Fig. 18B, C).

The texture of volcanic rocks is typically variably granoblastic or lepidoblastic. Only one sample (PIM$-2019-197.1) from Juojärvi shows clearly porphyroblastic texture. The grain size of the mafic volcanic rocks varies from 0.05 to 4 mm. Main minerals in the volcanic rocks are amphibole (hornblende or actinolite), plagioclase, quartz, diopside, biotite and chlorite. Minerals are variably present in different areas; diopside in Kohma and Länsi-Saamanen areas, actinolite in Juojärvi and Länsi-Saamanen areas, and biotite in Kohma and Puutosmäki areas.

5.5.2 Diabase dykes

Diabases within the study area are relatively abundant within the Archaean basement and in the quartzite cover (Fig. 19A). They display sharp contacts with host rocks (Fig. 19B) and in some cases coarser-grained central parts, but proper chilled margins were not observed. The typical orientation of the dykes varies from area to area. This is interpreted as more of a result of later deformation than differences in original emplacement directions as the host gneisses often display Proterozoic orientations (Fig. 19C). In the field, distinction between deformed diabase and a mafic volcanic rock was done mainly based on homogeneity in outcrops; homogeneous mafic rocks were regarded as dykes (Fig. 19D), whereas those displaying small-scale heterogeneities were regarded as volcanic rocks.

Fig. 19. Diabases from the study area. Length of compass 12 cm. A) In the middle of the photo ~50 cm wide E-W striking diabase dyke, which crosscuts the bedding striking 160 and schistosity of the quartzite (lower part of the photo). Upper part of the photo consists of a leucogranitoid from which an apophyse intrudes into the diabase. Observation PIM$-2019-131 (E=542 562, N=695 8550). B) N-S striking diabase dyke at observation PIM$-2019-68 (E=540 838, N=696 7016) parallel to the foliation of the hosting Archaean gneiss. Length of hammer handle 60 cm, handle pointing north. C) Banded Archaean gneiss hosting boudinaged diabase dyke at observation PIM$-2019-67 (E=541 573, N=696 6215). Diabase is intruded by younger granitoid vein. D) Homogeneous diabase displaying clear foliation. Observation MTL2-2018-205 (E=543866, N=6945603). Photo: Mauri Luukkonen, GTK.

The texture of diabases varies between granoblastic to lepidoblastic. Only one sample (PIM$-2019-45.1) from Vehmersalmi has preserved glomeroporphyric texture. The grain size of diabases varies between 0.2 and 2.5 mm. Characteristic main minerals of the diabases are hornblende, plagioclase and quartz. In the Konnusmäki and Puutosmäki areas they can also contain biotite as a main mineral and in Vehmersalmi also diopside and epidote. Sericite alteration is most common in Vehmersalmi and Vasikkasaaret areas.

5.5.3 Geochemistry

Due to significant similarities, the geochemistry of volcanic rocks (n=17) is here described together with the diabases (n=11) and they have been grouped based on their spatial location (Fig. 12). Number of samples is limited, but some regional features are visible on the various geochemical diagrams (Figs. 20–22). Data from the Siilinjärvi and Kuopio areas (Lukkarinen 2008) was used as reference material.

On various bivariate diagrams (Fig. 20), both diabases and mafic volcanic rocks plot in the same field as the analyses from the Kuopio and Siilinjärvi areas with a normal titanium content. Only the mafic volcanic rocks of Juojärvi-Kohma-E and the diabases from Konnuslahti differ from the others. Out of these, the two analyses from Konnuslahti plot together with the TiO_2-rich mafic volcanic rocks of Siilinjärvi (Fig. 20C). The two samples from Juojärvi and one from Kohma form a distinct low TiO_2 group. The two samples of Juojärvi have clearly the highest Ni and Cr contents, and the lowest TiO_2 content. The

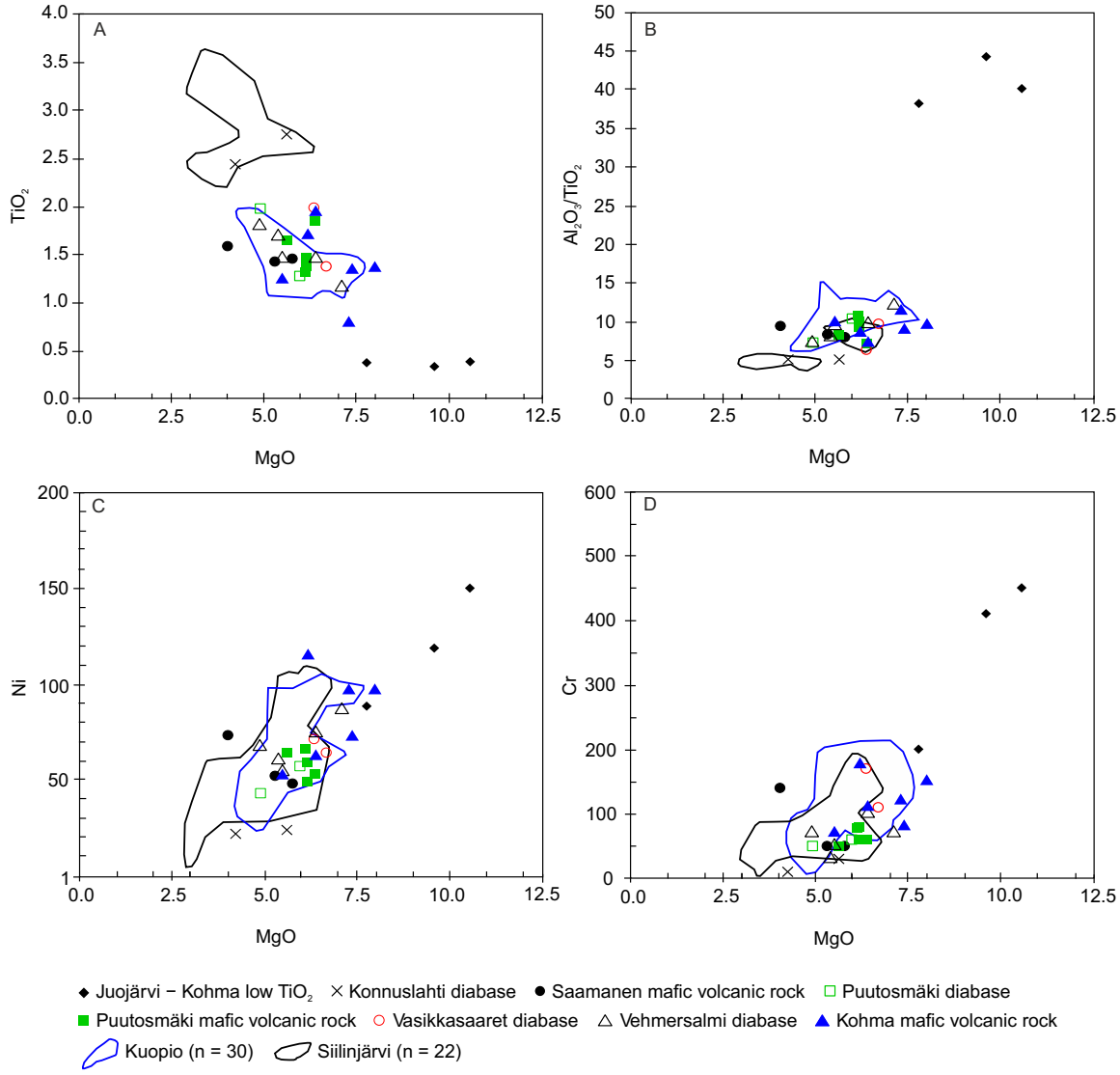

Fig. 20. Ni, Cr, TiO2 and Al2O3/TiO2 vs. MgO diagrams for the diabases and mafic volcanic rock types. Fields for volcanic rocks from Siilinjärvi and Kuopio have been drawn based on data in Lukkarinen (2008) and Rasilainen et al. (2007).

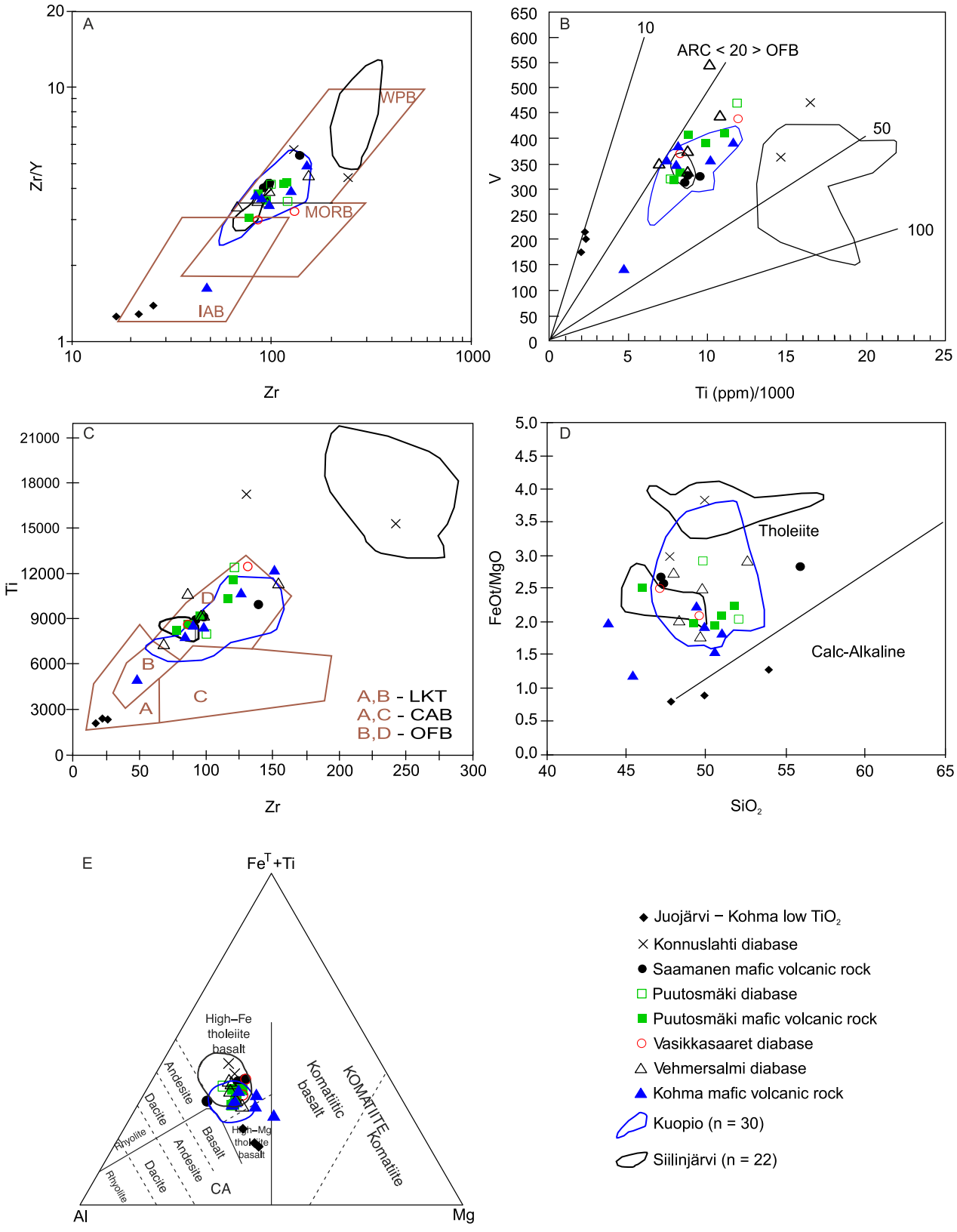

Fig. 21. Discrimination diagrams for the diabases and mafic volcanic rocks from the Kuopio-Leppävirta-Tuusniemi-Heinävesi region: A) Zr/Y vs. Zr, B) V vs. Ti/1000, C) Ti vs. Zr, D) FeOt/MgO vs. SiO2 and E) Jensen (1976) ternary plot. Names of the fields: A) WPB = Within Plate Basalts, MORB = Mid Ocean Ridge Basalts and IAB = Island Arc Basalts, B) ARC = Island Arc Basalts and OFB = Ocean Floor Basalts, C) LKT =Low-potassium tholeiites, CAB = Calc-alkaline basalts and OFB = Ocean Floor Basalts and E) CA = calc-alkaline. Fields for volcanic rocks from Siilinjärvi and Kuopio have been drawn based on data in Lukkarinen (2008) and Rasilainen et al. (2007).

Kohma-E sample has lower Ni and Cr contents, but also lower MgO content, which explain this feature. The chemistry of those three samples greatly resembles the chemistry of the so-called Losomäki-type low-TiO_2 rocks (Fig. 6, Kontinen et al. 2006).

On diagrams discriminating between various geotectonic settings (Figs. 21A–D), the majority of the samples classify as ocean floor basalts and within plate basalts, with clear tholeiitic affinity. An exception are the low-TiO_2 samples from Juojärvi and Kohma, which classify as (island) arc basalts with calc-alkaline affinity. The Konnuslahti diabases plot quite near the field of titanium-rich mafic volcanic rocks of Siilinjärvi (Figs. 21A–D). In Jensen's (1976) cation diagram almost all samples plot in the high-Fe tholeiite basalt field, with, again, the exception of the Juojärvi-Kohma low-TiO_2 samples which classify as high-Mg tholeiite basalts, together with two of the samples from Kohma. The Länsi-Saamanen sample, which differs in all diagrams from the other two, settles on the boundary between andesite and high-Fe tholeiite basalt fields in the Jensen diagram, being clearly more intermediate than the other two Länsi-Saamanen samples. The chemical difference from the other two samples can therefore be explained by its more intermediate composition (Fig. 21E).

Most of the samples display similar REE patterns, i.e. no Eu anomaly and moderate fractioning (Fig. 22, La_N=21–53, Lu_N=8–24), an exception being the Vasikkasaaret diabases which display nearly flat REE patterns (La_N=16-24, Lu_N=13-19) and the low TiO_2 samples which display slightly ascending REE patterns (La_N=2–8, Lu_N=9–12) like observed from the Losomäki-type volcanic rocks (Kontinen et al. 2006).

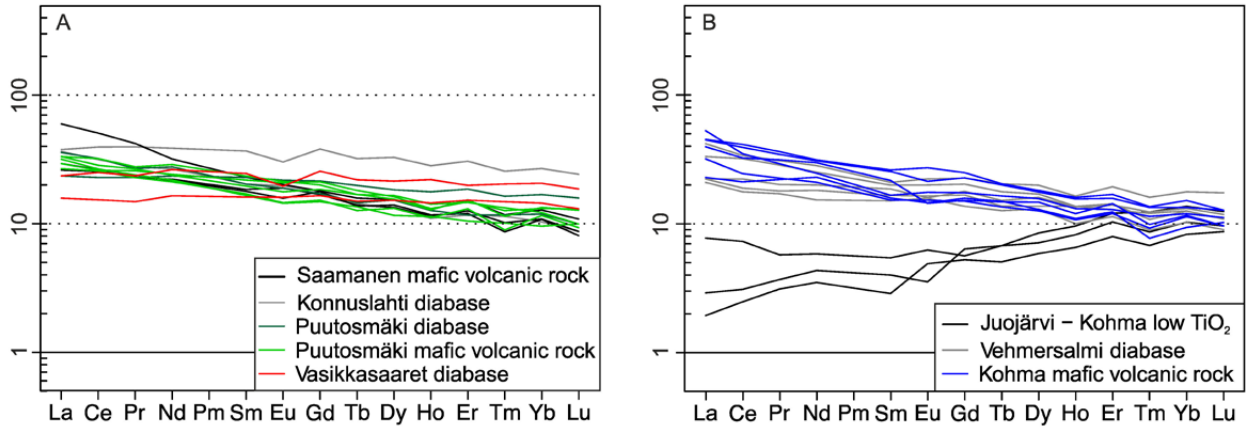

Fig. 22. Chondrite-normalised REE patterns for the diabases and mafic volcanic rocks. Chondrite values from Boynton (1984).

5.6 Paragneisses

5.6.1 Levänen group

Members of the Levänen group occur within the Archaean rocks of the Kuopio complex and flank them in the Kohma (Fig. 6) area. The protoliths for this group include arkosites and clay-rich greywackes and muds. Paragneisses of this group vary from those displaying clear cm-scale bedding (Fig. 23A) to more massive variants (Fig. 23B). Locally, especially in proximity to larger granitoid intrusions of the Kaarakkala suite within the Archaean complex, the paragneisses are clearly migmatised (Fig. 23C). In the Kohma area, a new Hiidenlahti formation was established (Appendix 5). The formation consists of the arkosite Matinlahti member interbedded with garnet paragneiss of the Kohma member (Appendix 5, Fig. 23D).

Grain size of the groundmass of the greyish paragneisses is typically 1–3 mm. The main minerals in the porphyroblastic Levänen group paragneisses are quartz, cordierite, albite-oligoclase, ±garnet, ±K-feldspar. Accessory minerals variably present include apatite, zircon, pyrrhotite, graphite and ilmenite. Cordierite can in most cases be identified only in microscopic study but the patchy texture it forms together with garnet is distinctive (Fig. 23E). Sillimanite is present typically in the northern parts of the Kohma area. Garnet is commonly present in the Levänen group paragneisses but most abundant (Fig. 23F) just above the underlying volcanic rocks.

This corresponds to the stratigraphic position of the iron formations in the Kuopio area (Lukkarinen 2008). The variability of minor mineral phases are indicative of heterogeneous chemical composition of Levänen group paragneisses (see Chpt. 5.6.4).

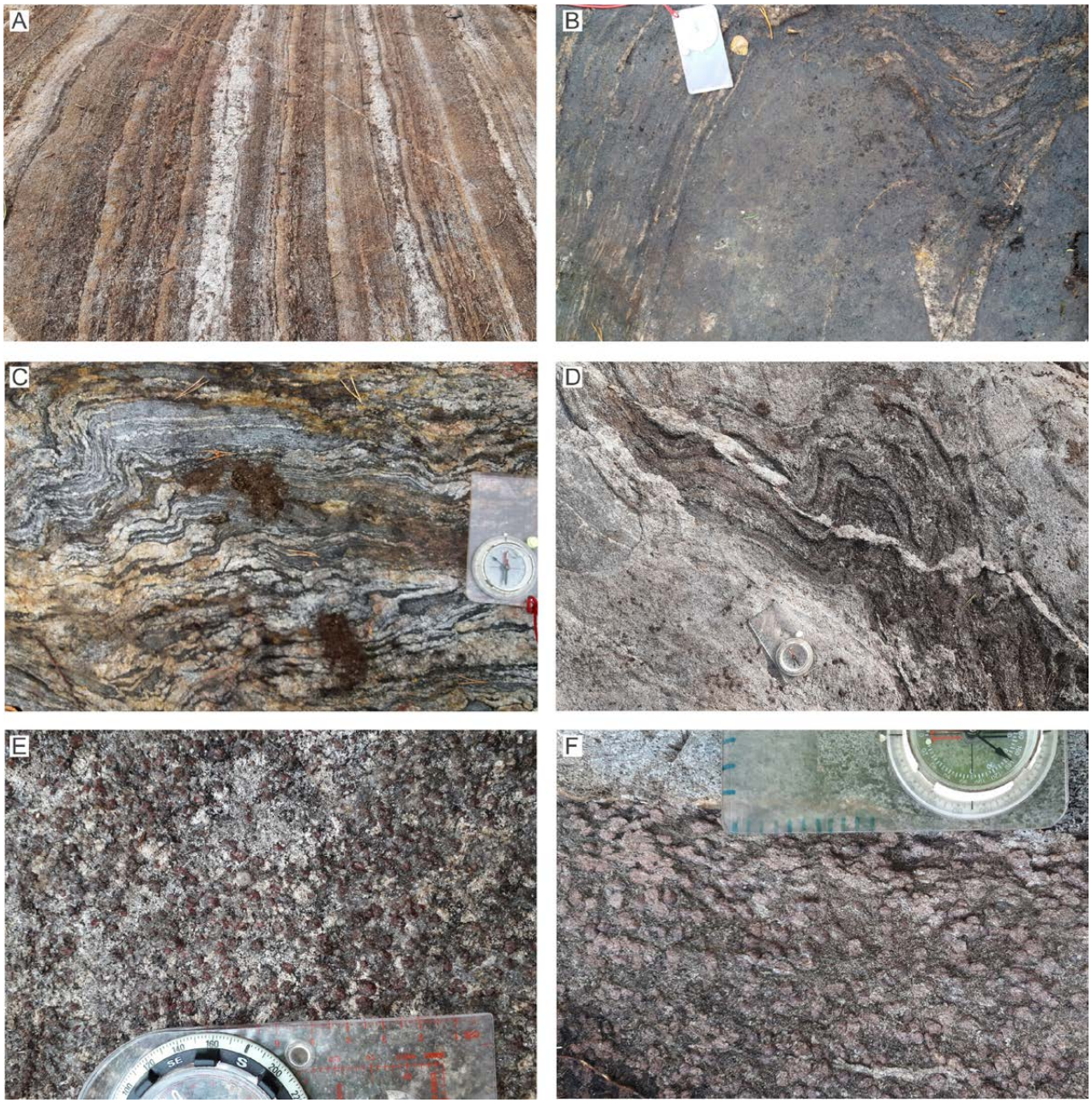

Fig. 23. Examples of rocks included in the Levänen group. Length of compass 12 cm. A) Paragneiss with cm-scale bedding with variable amounts of garnet and sillimanite in different layers as porphyroblasts, the three white layers are bedding parallel trondhjemite veins. Observation MTL2-2020-18 (E=564 327, N=696 8173). B) Homogeneous paragneiss, granitoid material is interpreted as intrusive veins, not as in situ melting. Observation MTL2-2020-424 (E=556 034, N=696 4818). Photo: Mauri Luukkonen, GTK. C) Migmatised paragneiss, observation MTL2-2020-343 (E=549 935, N=697 2359). Photo: Mauri Luukkonen, GTK. D) Arkosite of Matinlampi member with thin interbed of garnet-paragneiss of the Kohma member. Observation MTL2-2020-15 (E=564 349, N=696 8948). E) Porphyroblastic sillimanite-garnet-cordierite meta-quartzwacke. Note medium-grained, evenly distributed garnet porphyroblasts with grey patches of cordierite, sillimanite, albite, and K-feldspar. Observation SRMA-2019-189 (E=564 244, N=696 7248). F) Garnet rich paragneiss in sharp contact with arkosite layer. Observation MTL2-2020-13 (E=564 254, N=696 9023).

5.6.2 Viinijärvi

Paragneisses of the Viinijärvi suite, covering the majority of the eastern and southern parts of the study area, are dark grey, thick-bedded, sandy sediments in which pelitic layers, when present, are relatively thin. Boudinaged calc-silicate layers or ovoid shaped "concretions", consisting mainly of epidote and plagioclase are locally present (see Fig. 42). Crosscutting granite, granodiorite, and pegmatic quartz rich dykes with only minor feldspar are locally abundant, and the narrowest of those may misleadingly resemble migmatitic neosome. The amount of neosome increases near the major shear zones but is on average relatively low or non-existent (Figs. 24A, B). West of our study area, this feature has been recognised earlier by Jokela (1994). The lithological similarity of the Viinijärvi and Suonenjoki paragneisses and -paraschists makes them impossible to distinguish in the field.

The main minerals in the Viinijärvi suite paragneisses are quartz, plagioclase (albite-andesine), biotite and locally K-feldspar. Metamorphic index minerals include garnet, cordierite and sillimanite. Sillimanite is rare and only two samples with co-existing garnet-cordierite were identified in thin sections. Cordierite occurrences are limited to Suvasvesi shear zone and to the vicinity of the Archaean domes. Typical accessory minerals are apatite, zircon, rutile, titanite, epidote and muscovite, carbonate is rare. Opaque minerals, present in variable amounts, include pyrrhotite, graphite, pyrite, and ilmenite. Graphite is common and occurs as euhedral fibres and flakes. Relatively coarse (2–3 mm in diameter) graphite co-exists with biotite in biotite-quartz-cordierite association. Petrography of graphite indicates that organic material was deposited along the clastic detritus.

The primary bedding has been deformed and the main minerals have been recrystallised (blastoclastic texture). Primary clastic texture has, nonetheless, been occasionally preserved in fine-grained (< 1mm) schistose parts. These clasts include quartz, andesine, zircon, and occasionally rutile. The surface of these mineral grains is clean and their shape well-rounded. The grain boundaries of cross-hatch twinned microcline crosscut the twin lamellae. Decisive determination if these rounded grains are primary clasts or shaped by grain boundary dissolution during the metamorphism would require further studies. Migmatic neosome of the studied samples is granite in composition.

5.6.3 Suonenjoki suite

Paragneisses of the Suonenjoki suite (meta-greywackes) are on average more intensively migmatised than those of the Viinijärvi suite. Although variation in migmatisation extends from completely unmigmatised into nebulitic ones, with the better-preserved variants being more abundant near the eastern boundary of the suite against the Viinijärvi suite (Figs. 24C, D). Especially in the vicinity of the Konnuslahti dome the rocks are completely unmigmatised. In areas where the amount of veining material is smaller, it is difficult to distinguish if the observed veining is in-situ melt or deformed intrusive granitoid veining. However, in the westernmost parts of the study area, closer to the core of the Raahe-Ladoga suture zone, the abundant veining is a result of melt generation through anatexis.

The paragneisses contain black schist, chlorite schist, and meta-arenite interlayers. The black schists are rarely exposed and their presence is mostly interpreted from geophysical data. Similarly to the Viinijärvi suite the Suonenjoki suite also contains locally calc-silicate layers/concretions. Mafic layers possibly representing volcanic interlayers are rare, but are found on a few outcrops and in drill hole N5242019R1.

Main minerals are biotite, quartz, cross-hatch twinned K-feldspar and plagioclase (oligoclase-andesine). Metamorphic index minerals, when present, are garnet, amphibole, chlorite, and cordierite. Accessory and ore minerals variably present include apatite, monazite, zircon, muscovite, pyrrhotite, pyrite, graphite, and sphalerite. Migmatic neosome of the studied thin section samples is K-feldspar granite in composition, when present.

Fig. 24. A) Layered paragneiss of the Viinijärvi suite, hosting concordant deformed tonalite veins crosscut by younger undeformed tonalite vein. Observation MTL2-2020-144 (E=553 062, N=694 6134). B) Intensively migmatised paragneiss neosome of the Viinijärvi suite close to the interpreted contact with the Viinijärvi suite. Observation MTL2-2019-277 (E=548 151, N=692 5128). C) Unmigmatised Suonenjoki suite paragneiss with folded calc-silicate layers near the Konnuslahti dome, observation PIM$-2018-15, location of age determination sample A2531 Eteläjoentausniitty (E=547 526, N=693 4882). Length of compass 12 cm. GTK. D) Intensively migmatised paragneiss of the Suonenjoki suite with calc-silicate concretions. Observation MTL2-2019-275 (E=547 712, N=692 5099). Photo: Mauri Luukkonen, GTK.

5.6.4 Geochemistry

Geochemical dataset (n=382) used for this study includes both new analyses and those published earlier. The entire dataset and references can be found from Electronic appendix 1. It should be noted that the list of elements analysed varies between the studies, and e.g. carbon and REE are missing from significant number of analyses. Based on field observations and map interpretation, the data were classified into Levänen group (n=36) and Viinijärvi (n=265) and Suonenjoki suites (n=81).

On the log (SiO_2/Al_2O_3) vs. log (Na_2O/K_2O) diagram, commonly used for chemical classification of clastic sediments, the samples, regardless of unit, classify as greywackes (Fig. 25A). Excluding the C- and S-enriched samples, correlation between SiO_2 and Al_2O_3 diagram is good, forming a continuum from SiO_2-rich sandier compositions to clay mineral-enriched muds (Fig. 25B, Kontinen & Sorjonen-Ward 1991, Kontinen et al. 2006). Deviation of the carbon and sulphide-richer samples from the main trends is due to variable amounts of metal and sulphur precipitation from sea water and possibly detrital carbon sediments (Kontinen et al. 2006). Although individual samples cannot be distinguished and the ranges overlap, the Levänen group and the Suonenjoki suite are, on average, slightly SiO_2-poorer than the Viinijärvi suite, respective averages being 62.5, 63.2 and 67.1%. Also the correlation between SiO_2 and MgO is good, but a subgroup of six samples from the Suonenjoki suite deviates from it with higher MgO contents (Fig. 25C). On the other hand, e.g. Na_2O shows no correlation with SiO_2 (Fig. 25D). In respect to Cr content, the Levänen group stands out from the two others as it contains both

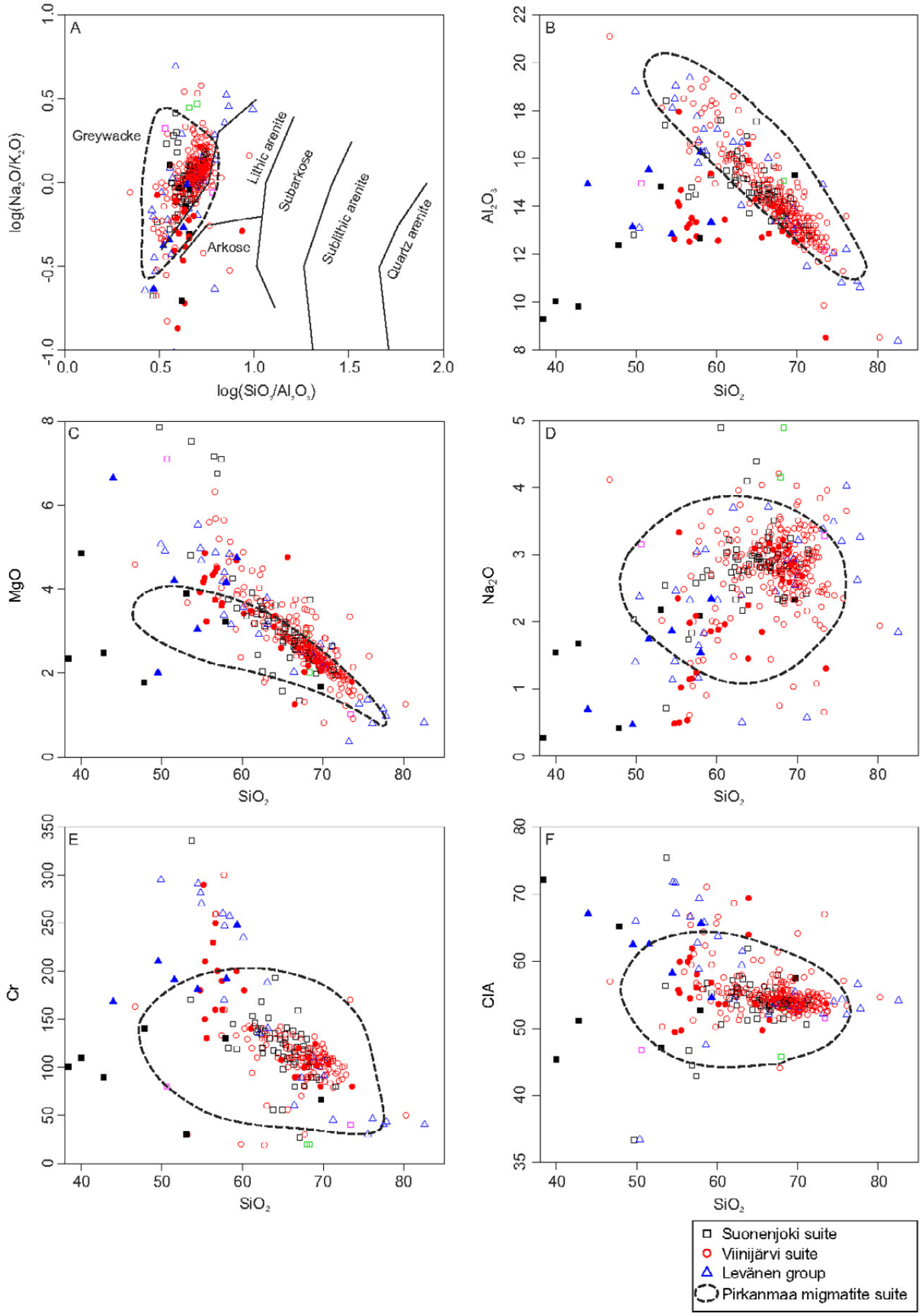

Fig. 25. Paragneiss samples from the study area and its vicinity plotted on A) log (SiO2/Al2O3) vs. log (Na2O/K2O) classification diagram of Pettijohn et al. (1972) with lines modified by Herron (1988) and Harker diagrams (B-F). Note that in E the samples from Glumoff (1987) are not shown as it seems evident that the results for Cr were systematically high. Reference data for eastern parts of the Pirkanmaa migmatite suite from Mikkola et al. (2018a). Note that samples not analysed for carbon are symbolised as those with C<1%.

the highest and lowest Cr contents (Fig. 25E). The calculated CIA (Chemical Index of Alteration) values are typically close to 55, with higher values being most common in the Levänen group (Fig. 25F).

Chondrite-normalised REE pattens are also uniform with LREE enrichment (La_N=14–231, average=93) and moderate fraction ($(La/Yb)_N$=2.4–47.5, average=9.7) in all units, with a small negative Eu anomaly (Eu/Eu*=0.39–3.51, average=0.75, Fig. 26). In the Levänen group, the samples with the lowest La_N are the SiO_2-richest and three of the samples represent the exceptionally garnet-rich layers from the Kohma area. A number of Viinijärvi suite samples with the lowest LREE concentrations also display a distinct positive Eu anomaly. The Eu anomaly does not correlate with major or trace elements, but all samples with La_N<50 are located within 10 km of the unit's western contact, extending from Kohma southwards to Konnuslahti dome, but this area also includes samples with REE patterns typical for the unit. Four Suonenjoki suite samples close to the contact with the Konnuslahti dome deviate from the main population in their REE patterns (Fig. 26E), with two of these samples displaying stronger than average REE fractionation ($(La/Yb)_N$=26.2 and 47.5) and two displaying low LREE contents with weaker than average REE fractionation (La_N=14 and 22, $(La/Yb)_N$=4.4 and 3.0). The samples with low HREE and strong fractionation are Na_2O-richer and K_2O-poorer than the main population, but otherwise the deviations are smaller or nonexistent. On primitive mantle-normalised spider diagrams the samples display relatively large scatter in LILE and negative anomalies of Nb, Sr, P and Ti. The samples with the highest uranium contents are black schists.

5.6.5 Rutile thermometry

Heavy fractions of all the paragneiss age determination samples were studied for presence of rutile. The idea was to test the usability of Zr-in-rutile thermometer (Watson et al. 2006) in evaluation of peak metamorphic conditions. Only samples A2528 Piiroonmäki (n=22), A2531 Eteläjoentausniitty (n=20) and A2534 Salkolahti (n=2) contained rutile grains (Fig. 46). The grains show variable shapes of rounded round, rounded angular, angular and euhedral, angularity likely to have been caused by crushing and grinding. Analytical data can be found from Electronic appendix 1 and description of individual samples from chapter 9.2.

The rutile of sample A2528 Piiroonmäki, representing the SW parts of the Viinijärvi suite (Fig. 46), is 100–300 microns in diameter. The grains are dominantly rounded (round and rounded angular types). The rutile shows significant variation of Zr content (266–1064ppm) between analysed grains. Rutile is also variable in Cr (547–2122 ppm), Fe (111–2339 ppm) and Nb (1814–20809 ppm) (Fig. 27). The grains were large enough for separate analyses from rim and core parts, but analyses from these do not display clear differences in concentration of any elements, although Zr concentrations of cores are slightly higher than those from rims, averages being 745 and 673 respectively, but in some grains the core displays lower values. Correlation between the trace elements is weak and especially for Zr nonexistent. Based on the Zr-in-rutile thermometer, the analysed spots have equilibrated in 630–760°C (Fig. 27).

Grain size of the rutile in sample A2531 Eteläjoentausniitty, representing Suonenjoki suite's easternmost parts (Fig. 46), is 40–100 microns. Due to small grain size, only a single spot per grain was analysed from this sample. Most of the rutile is angular in shape, only a few rounded grains were present. Rutile in this sample has variable Cr (80–1143, outliers at 2838 and 6363 ppm), Fe (109–3225 ppm) and Nb (442–6683 ppm) associated with low Zr (49–207 ppm). Based on Zr-in-rutile thermometer (Watson et al. 2006), rutile of sample A2531 equilibrated in 515–613 °C (Fig. 27).

The two rutiles found from sample A2534 Salkolahti, representing the Viinijärvi suite in Tuusniemi area (Fig. 46), are rounded and ~50 microns across. They are low in Cr (30 and 180 ppm), variable in Nb (1490 and 8278 ppm) and moderately high in Zr (616 & 620 ppm). Based on their Zr contens both of them equilibrated at 705 °C.

Based on the morphology of the studied rutile grains, it cannot be decisively concluded to which extent they represent detrital grains and to which extent they represent metamorphic growth during the Svecofennian orogeny. Rutile shows highly variable diffusion rates for different trace elements, with Zr being among the elements with fastest diffusion rates (e.g. Dohmen et al. 2018). This is in line with our data, as the thermometer results from individual samples are consistent within the ±50°C regarded as the uncertainty for the calculation (Watson et al. 2006). This was expectable as the Zr-rutile system is reset in metamorphic

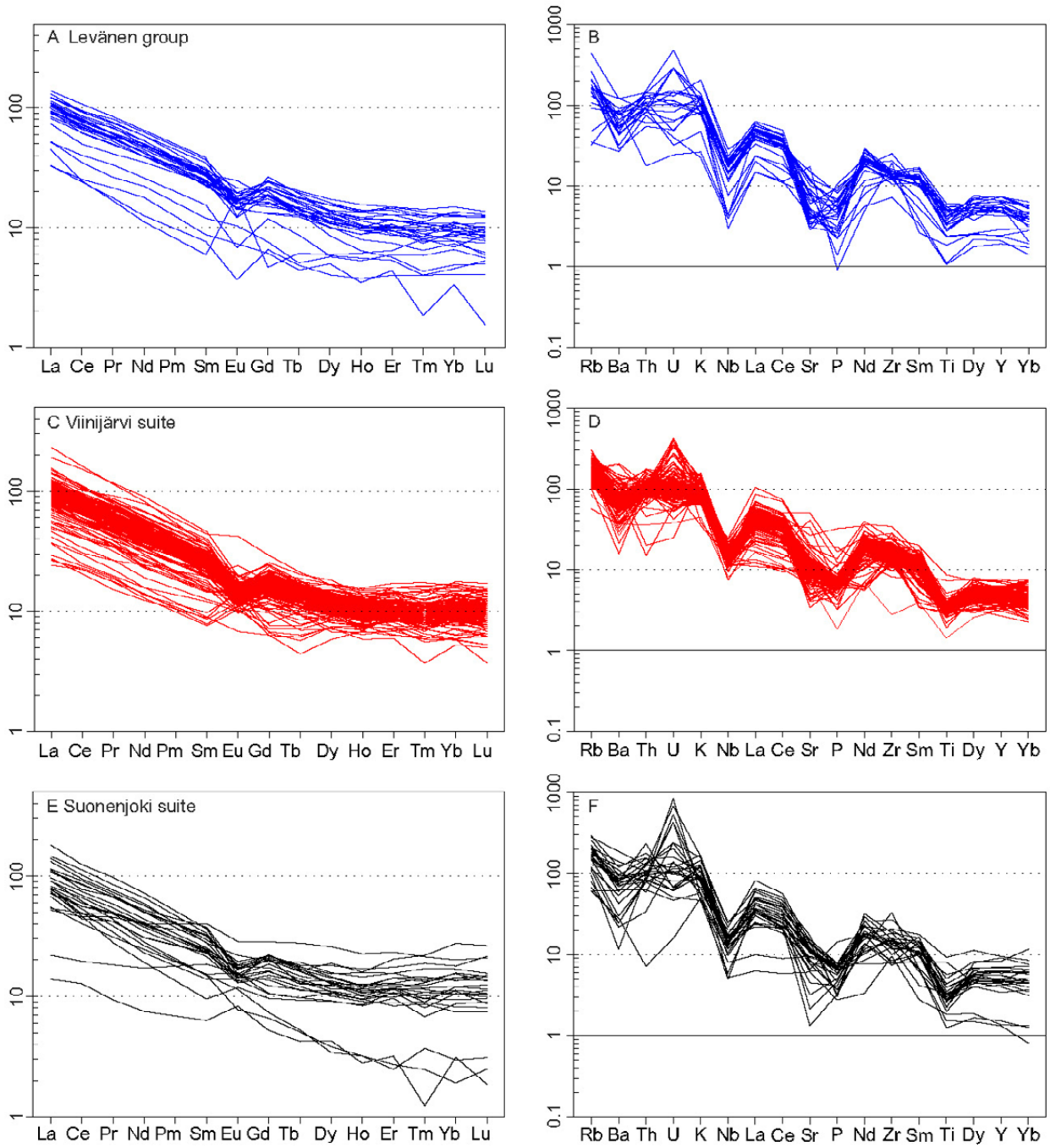

Fig. 26. Chondrite-normalised REE patterns and primitive mantle-normalised spider diagrams for samples representing Levänen group (A, B), Viinijärvi (C, D) and Suonenjoki suite (E, F). Chondrite values from Boynton (1984) and primitive mantle values from Sun & McDonough (1989).

conditions exceeding subgreenschist facies (Zack et al. 2004a). The field observations also support the calculated values, as sample A2528 that yielded an average temperature of 715°C is from an area where the Viinijärvi suite paragneisses display clear signs of partial melting, indicating metamorphic peak temperatures well in the partial melting field of metapelites (e.g. Spear et al. 1999). Sample A2531 from an area displaying no signs of partial melting yielded a significantly lower average temperature estimate, i.e. 575°C. Values from sample A2534 (~705°C) are higher than expected as the sample does not display signs of partial melting, but it should be remembered that only two rutiles were found from this sample.

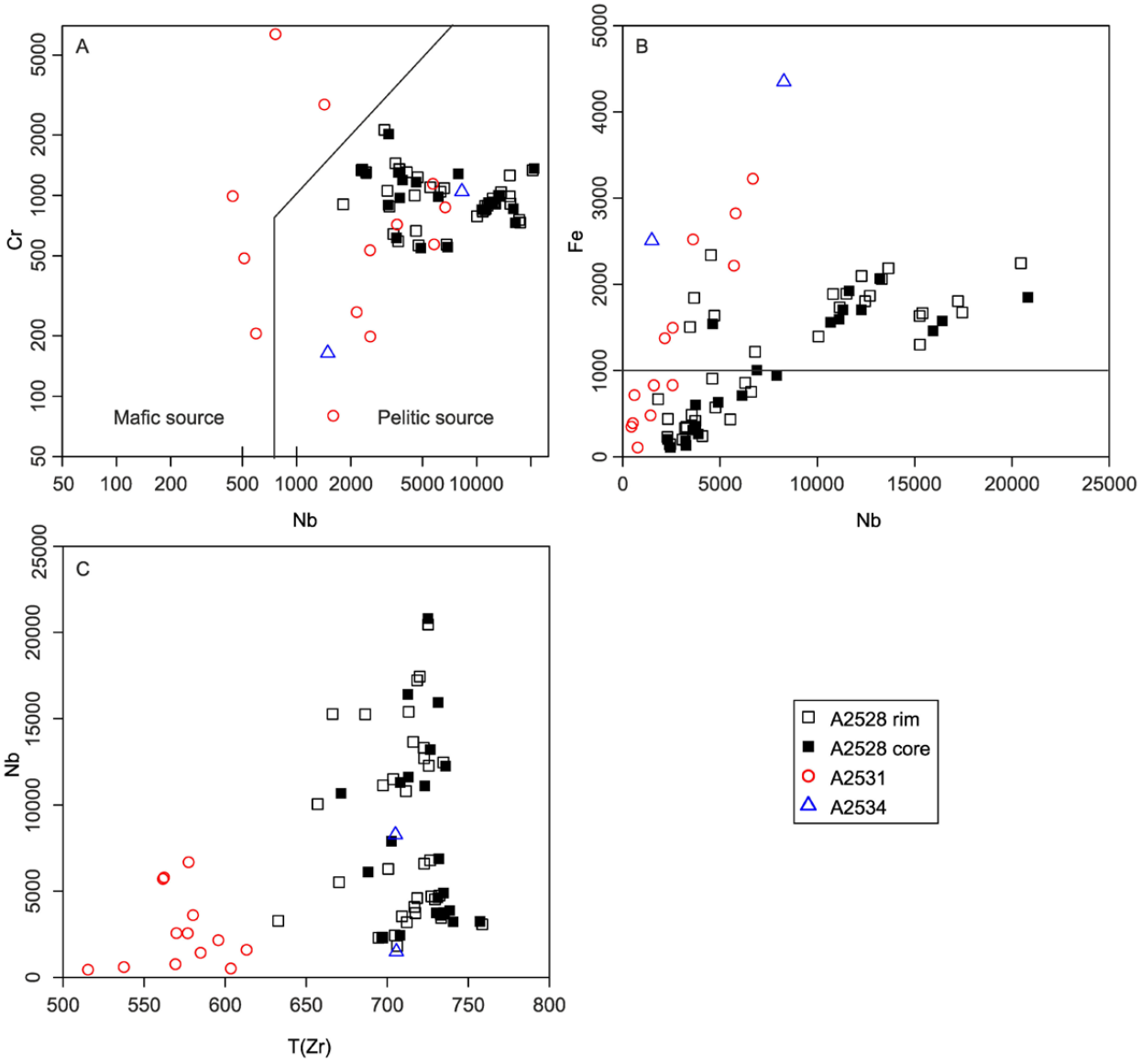

Fig. 27. Rutile compositional plots for analysed points. A) Nb vs Cr plot with source fields defined by Meinhold et al. (2008). B) Nb vs Fe plot, Zack et al. (2004a) regarded as Fe >1000 ppm as characteristic for metamorphic rutile. C) Plot of equilibrium temperature (T(Zr)) based on Zr-in-rutile thermometer of Watson et al. (2006) and observed Nb concentrations.

In the classification proposed by Meinhold et al. (2008), nearly all of the analysed spots (68 out of 73) classify as originating from metasedimentary or felsic source, i.e. Nb>800 ppm and $\log_{10}$(Cr/Nb)<0. The partially very high Nb of sample A2528 could be attributed to stability of Ti-rich biotite, which would incorporate most of Ti, but no Nb, resulting in a low modal rutile enriched in Nb (Zack et al. 2004b). This low modal rutile percentage would also explain the fact that only two out of seven parag-neiss age determination samples yielded a larger amount of rutile. Iron contents >1000 ppm have been regarded as characteristic for metamorphic rutiles (Zack et al. 2004a), a boundary splitting the rutiles studied here, although averages from all samples are higher than the threshold (A2528 1130 ppm, A2531 1335 ppm, A2534 2507 and 4350 ppm). To conclude, the rutiles from the paragneisses seem to record the peak-T of metamorphism, and likely either crystallised during metamorphism of the host rocks or were extensively re-equilibrated during it.

6 OUTOKUMPU ASSEMBLAGE

6.1 Kuolemanlahti

Huhma (1971c) identified multiple skarn rock occurrences in the Kuolemanlahti area just south of the Suvasvesi shear zone and classified them as belonging to Outokumpu assemblage. Based on written communication (Koistinen 2018), a narrow seam of quartz rocks can be followed at least semi-continously for several kilometres in a WNW direction before it turns south along with the general structural trend (Appendix 1, Fig. 28). Skarn rock boulders were also known ca. 2 km south of this "seam" (Fig. 28).

In order to more closely study this seam of quartz rock, a research trench was dug (Hietava 2022). In the trench, the main rock type is a paragneiss of the Viinijärvi suite, which gradually phases into a slightly altered paragneiss with some quartz-carbonate veins and greenish hue. East of the trench, the rock type is a clearly foliated quartz skarn rock with boudinaged inclusions of green chromian minerals, along with brown weathered carbonate portions. This rock type was not however observed in the trench.

Within the trench, the rock type continues from the gradually altered paragneiss to a coarse-grained, non-foliated and pervasively silicified type of quartz skarn rock, with brown weathered carbonate and felsic veins also present. A green-coloured tremolite diopside skarn rock is observed as small (0.5–1 m) inclusions or lenses within the quartz skarn rock in the trench and outside the trench. Tremolite and/or diopside are present as medium to coarse-grained pale green crystals, with rounded

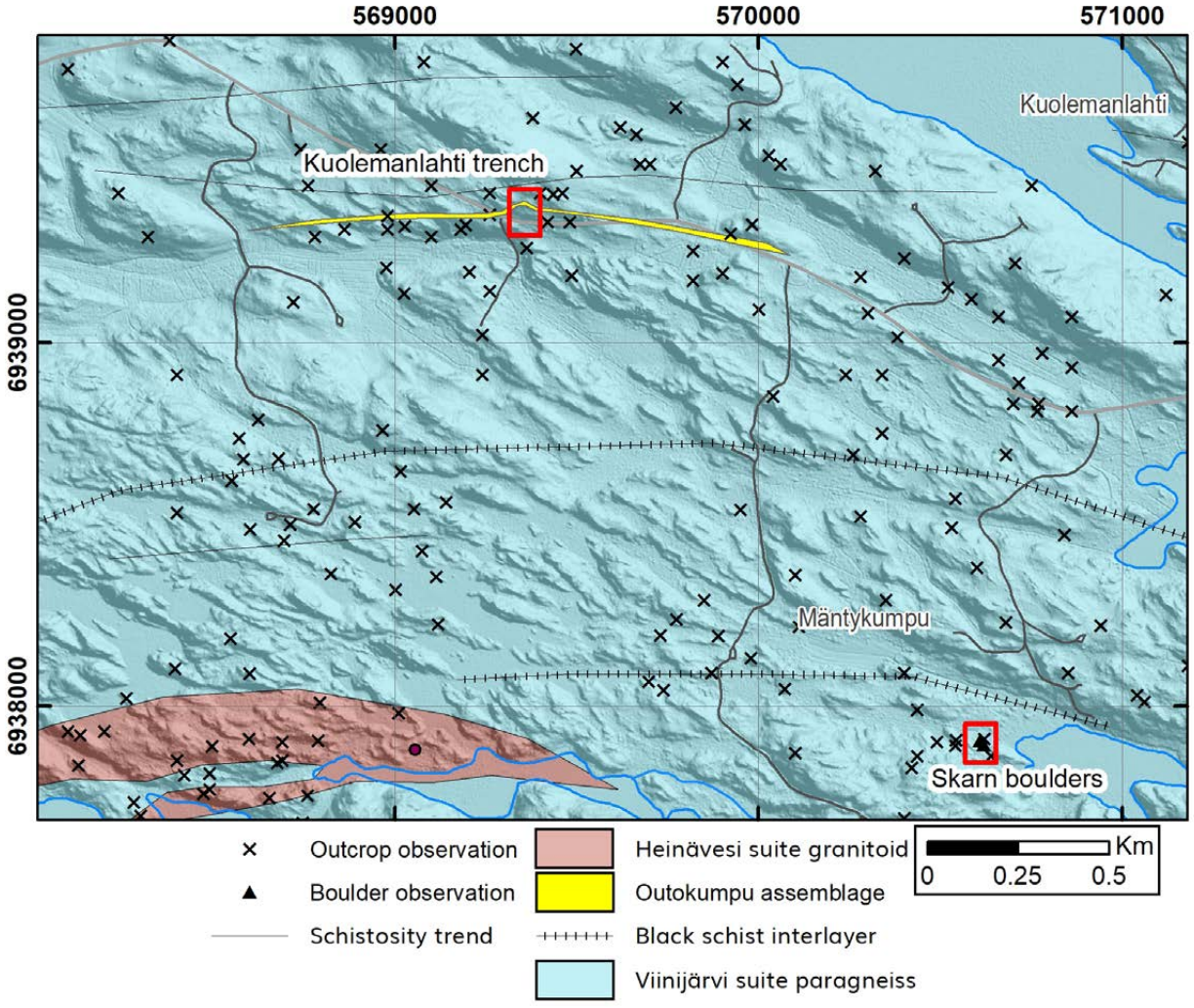

Fig. 28. Geological map of Kuolemanlahti (Bedrock of Finland – DigiKP). Basemap and LiDAR data ©National Land Survey.

rectangular crystal shapes. No observable contacts between the different rock types could be made within the trench. Contacts were either buried by mud in the steeply undulating bedrock surface or were undetectable due to phasing or graduality of the contacts.

The green-coloured chrome-bearing minerals observed in the tremolite diopside skarn rock, quartz skarn rock and the foliated quartz skarn rock identified in the field included fuchsite, chromian diopside, and uvarovite, which are diagnostic for OKU assemblage (e.g. Säntti et al. 2006, Peltonen et al. 2008). High Cr concentrations provided by the rock sample analyses provide initial support for the visual identification.

No direct observations of black schists, typically associated with OKU assemblage (e.g. Gaál et al. 1975), were made. However, LiDAR data (Light Detection and Ranging) indicates a clear depression on the southern flank of the seam hosting OKU assemblage, possibly indicating a rock type or a fault/thrust zone more prone to weathering under glacial sediments. Serpentinites were also not observed from the trench.

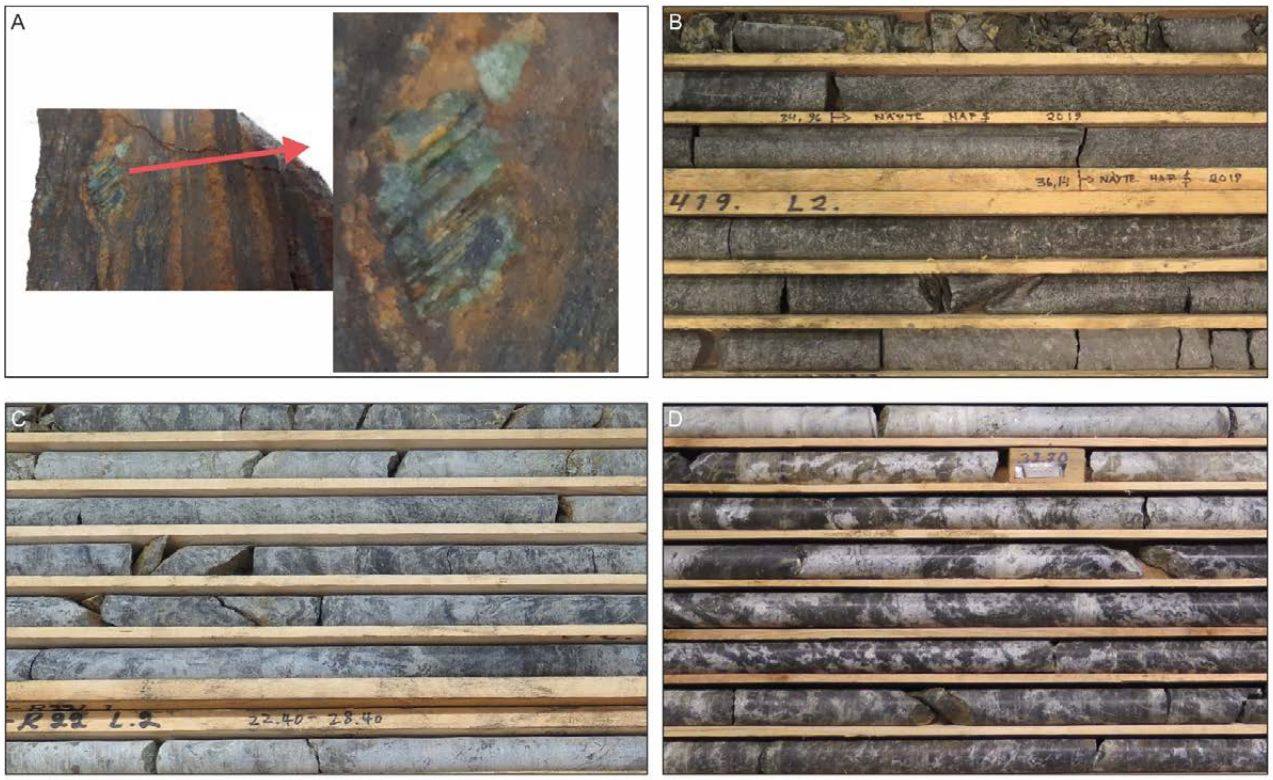

Fig. 29. A) Foliated quartz skarn rock from Kuolemanlahti with boudinaged chromium diopside. B) Drill core M324196R419 from Täilahti medium to coarse-grained serpentinite. C) Drill core FDH_98-R022. Serpentinite with patchy texture at depth 14–22 m. D) Drill core OU_1-R001, depth approximately 33–36 m. Serpentinite soapstone with patchy texture and brown carbonate in upper portions.

6.2 Piiroonmäki

A small outcropping serpentinite-diopside-quartz rock occurrence 10 km east of Varkaus in Piiroonmäki was located by Outokumpu Ltd. in the 1980s (Koistinen, written communication, 2018) and drilled by GTK in 2019 (Pirinen & Niskanen 2020). Three of the five drilled holes intersected rocks of the Outokumpu assemblage as interlayers a few metres thick, hosted by the Viinijärvi suite paragneisses with black schist interbeds and variably abundant pegmatite and granitoid dykes.

In thin sections, serpentinites from the Piiroonmäki drillholes display pseudomorphic spherical or patchy textures, with either spherical or elongated patches of serpentine minerals or talc grains forming rims around other mesh-like textured serpentine patches or altered olivines or pyroxenes. Serpentine minerals along with fibrous talc are either a main or an accessory mineral in all observed

samples, indicating a high degree of alteration. Both olivine and pyroxenes are intensively altered but in some samples preserved well enough to be identified. Other accessory minerals include carbonates, opaques, quartz, pyroxenes and olivines.

Skarn rocks from Piiroonmäki are mostly comprised of medium to coarse-grained talc and tremolite crystals with different serpentine minerals. Texturally the skarn rocks have patchy features similarly to the serpentinites, and in thin sections serpentine, tremolite or talc minerals form rims around serpentinised coarse-grained olivine or pyroxene crystals. Tremolite crystals also form larger clumps in some sections, and mesh-like serpentine is also common. In thin sections, quartz rocks display an equigranular, foliated quartz with elongated clinopyroxene crystals and anhedral roundish small orthopyroxenes and/or olivines forming the foliated structure.

6.3 Täilahti

During exploration for Kotalahti-type nickel deposits in Täilahti (Figs. 6 and 44), significantly west of other known occurrences of the OKU assemblage, a serpentinite which was later tentatively included in the OKU assemblage was intersected by drilling (Peltonen 2005a, Kontinen et al. 2006).

Drillhole M324196R419 (29.1-45.65 m, Fig. 29B) comprises of medium to coarse-grained serpentinite with intermittent talc-bearing pegmatitic portions. The analysed sample was taken from a talc-bearing serpentinite with minor pyrite dissemination. In thin section, it is a fine-grained serpentinite with a slightly foliated structure, formed by orientated talc crystals. A faint pseudomorphic spherical texture can also be observed, with talc crystals forming rims around a serpentine matrix.

6.4 Revision of pre-existing drill core samples

Two of the diamond exploration drill cores south of Tuusniemi revised in drill core archive (Fig. 29C, D), FDH_98-R022, OU_1-R001) contained serpentinite resembling those of the Outokumpu assemblage. The serpentinite in FDH_98-R022 is small to medium grained, non-foliated and gray, partly with a vaguely patchy texture.

Drillholes TN_VUO-3 and TN_VUO-4 were added to the dataset using modern analytical methods, with previous drilling data from the area not being up to date. The drillholes are comprised of paragneiss or graphite gneiss with pegmatite portions, along with smaller serpentinite and tremolite and diopside skarn rock segments. A similar patchy texture can be observed in the serpentinites and some of the skarn rocks.

Drillhole OU_1-R001 is comprised of serpentinite soapstone and soapstone, with the soapstone containing tremolite. Serpentinite soapstone contains vaguely shaped (>10 mm) serpentine-carbonate patches, with brownish carbonate. Talc is also present as fibrous (1-7 mm) crystals. Thin sections display mostly metaperidotite or serpentinite with a spherical pseudomorphic texture with serpentine and talc being the main minerals. Accessory opaque minerals include chromite, magnetite and pyrrhotite. Serpentine minerals form a mesh-like texture within the coarse-grained roundish pseudomorphs, most probably consisting of relict olivines. The pseudomorphic patchy texture is also observed elsewhere in OKU assemblage serpentinites or metaperidotites (Säntti et al. 2006) and can be observed in thin sections from the Piiroonmäki serpentinites and skarn rocks.

6.5 Geochemistry

All geochemical data can be found from Electronic Appendix 1 and summary of samples from Table 1. Despite significant variations in mobile element concentrations of more mobile elements (e.g., Al_2O_3, MgO, U, Figs. 30 and 31), the quartz rock, skarn and serpentinite samples display similar patterns and concentrations (e.g., TiO_2, Zr, Ta, HREE, Figs. 31 and 32) in respect to more immobile elements. They are also rich in Cr and Ni with low TiO_2, unfractionated REE patterns lacking significant Eu-anomaly. K_20 and Na_2O are low in all rock types, with some outlier behaviour for Al_2O_3/Na_2O in the quartz skarn rocks. In respect to e.g. MgO, MnO and CaO, the samples from all locations display a gradual decline

from serpentinites through skarns into quartz skarn rock without significant breaks. This decline is balanced by an increase in SiO_2 concentrations from serpentinite to quartz rocks. These features match those summarised by e.g. Kontinen et al. (2006) and Peltonen et al. (2008) as characteristic for the OKU assemblage.

The data from Kuolemanlahti, including samples from both Outokumpu assemblage and Viinijärvi suite paragneisses, demonstrate the fact that, in addition to mineralogical contacts, the chemical contacts are sharp. Composition of paragneisses close to the contact display no significant alteration, i.e. even the LILE are similar to paragneisses taken further away from occurrences of the Outokumpu assemblage. Even the quartz-richest rocks from Kuolemanlahti have elevated Fe2O3 values compared to those characterising the true quartz rocks of the assemblage. Average Fe2O3 values for Kuolemanlahti quartz skarn rocks is 6.2%, with the highest values exceeding 11%. Average Fe2O3 values for quartz rocks from Outokumpu and Vuonos areas are 1.65%, respectively (Kontinen et al. 2006). Thus, the term quartz skarn rock is regarded appropriate.

The relatively high CaO (avg. 11.2%) of the tremolite diopside skarns is hosted by tremolite, diopside and carbonate minerals. The foliated quartz skarn rock also displays one higher value of 5.04% (JOHI-2020-4.1), supporting the visual indicators of weathered brownish carbonate in the quartz skarn-type rocks. Compared to the data in Kontinen et al. (2006), the major oxide concentrations of Kuolemanlahti are very similar, with some variety in skarn rocks, which is however expected due to e.g. varied nomenclature and complex mineralogy of the rocks. Most notable differences in

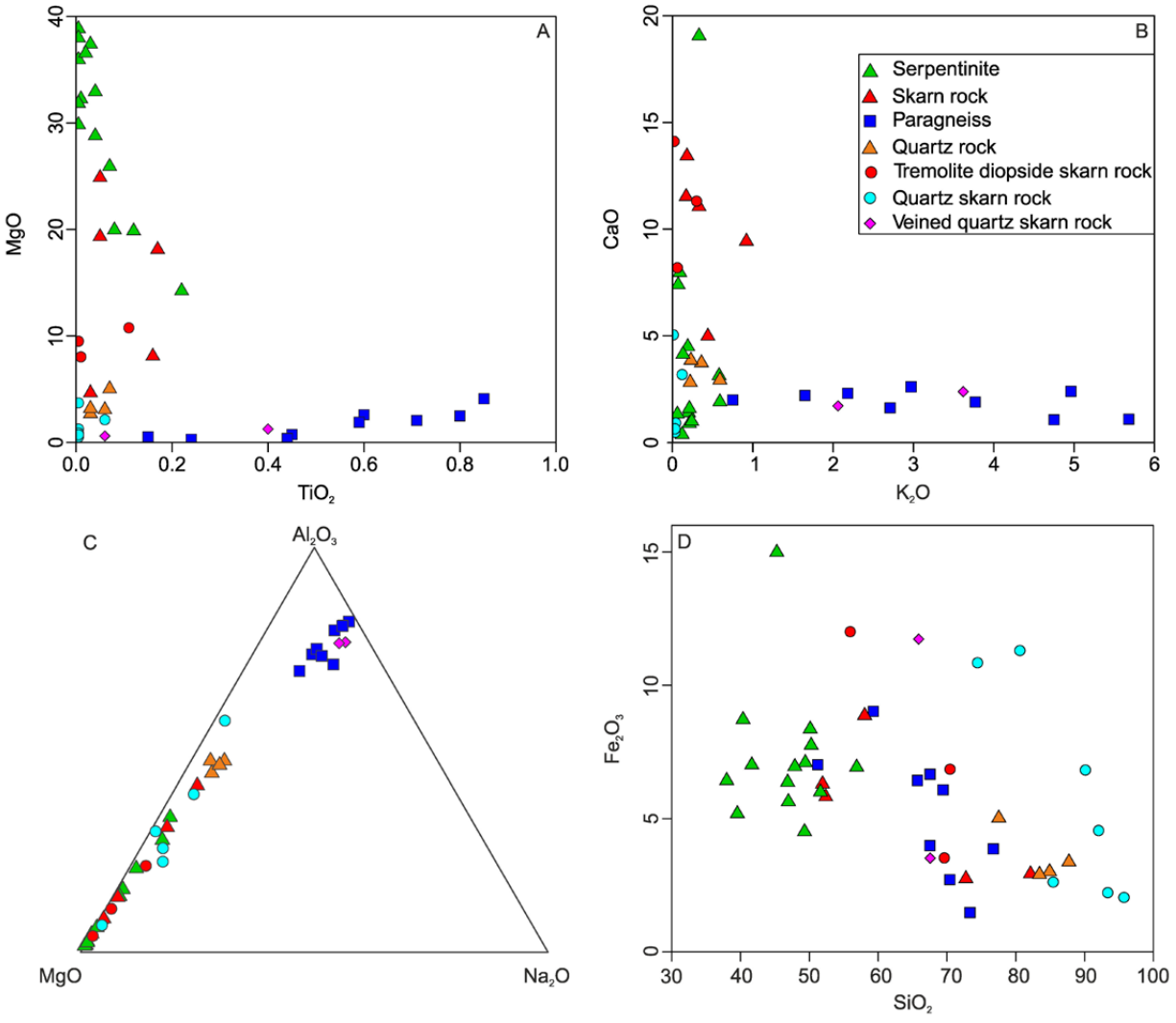

Fig. 30. Geochemical diagrams for the Outokumpu assemblage and paragneisses from the Kuolemanlahti trench. Triangles represent drill core samples and circles represent the Kuolemanlahti trench samples. For samples with TiO2 below detection limit (0.01%), ½ of the detection limit has been used.

Table 3. Sample types, rock types, location and sample numbers used in the study.

Sample type	Rock types	Location	Number of samples
Drill core sample	Serpentinite, skarn, paragneiss	Tuusniemi, Täilahti	12
Drill core sample	Serpentinite, skarn, quartz rock	Piiroonmäki	12
Trench sample	Quartz skarn rock, tremolite diopside skarn rock, paragneiss	Kuolemanlahti	20
		Total	44

major oxides are in Fe2O3 values in the quartz skarn rocks against the quartz rocks, and MgO values in tremolite diopside skarns (avg. 9.42%) against average values for carbonate rocks in Outokumpu and Vuonos (19.28%) and tremolite and diopside skarns in the Outokumpu-Jormua belt (18.97 and 16.25), respectively. Skarn rocks from Piiroonmäki display much lower SiO2 and higher values in Fe2O3 and MgO, with CaO and MnO concentrations also higher than samples from other locations.

On a primitive mantle-normalised spider diagram (Fig. 31), all rock types of the Outokumpu assemblage display similar patterns, especially positive Ta, Pb and negative Nb and Ti anomalies are characteristic. Uranium shows the largest variation, being low in the serpentinites and high in skarns and quartz rocks, which is also characteristic for the assemblage (Kontinen et al. 2006). In paragneisses all of the aforementioned anomalies are either missing or less pronounced.

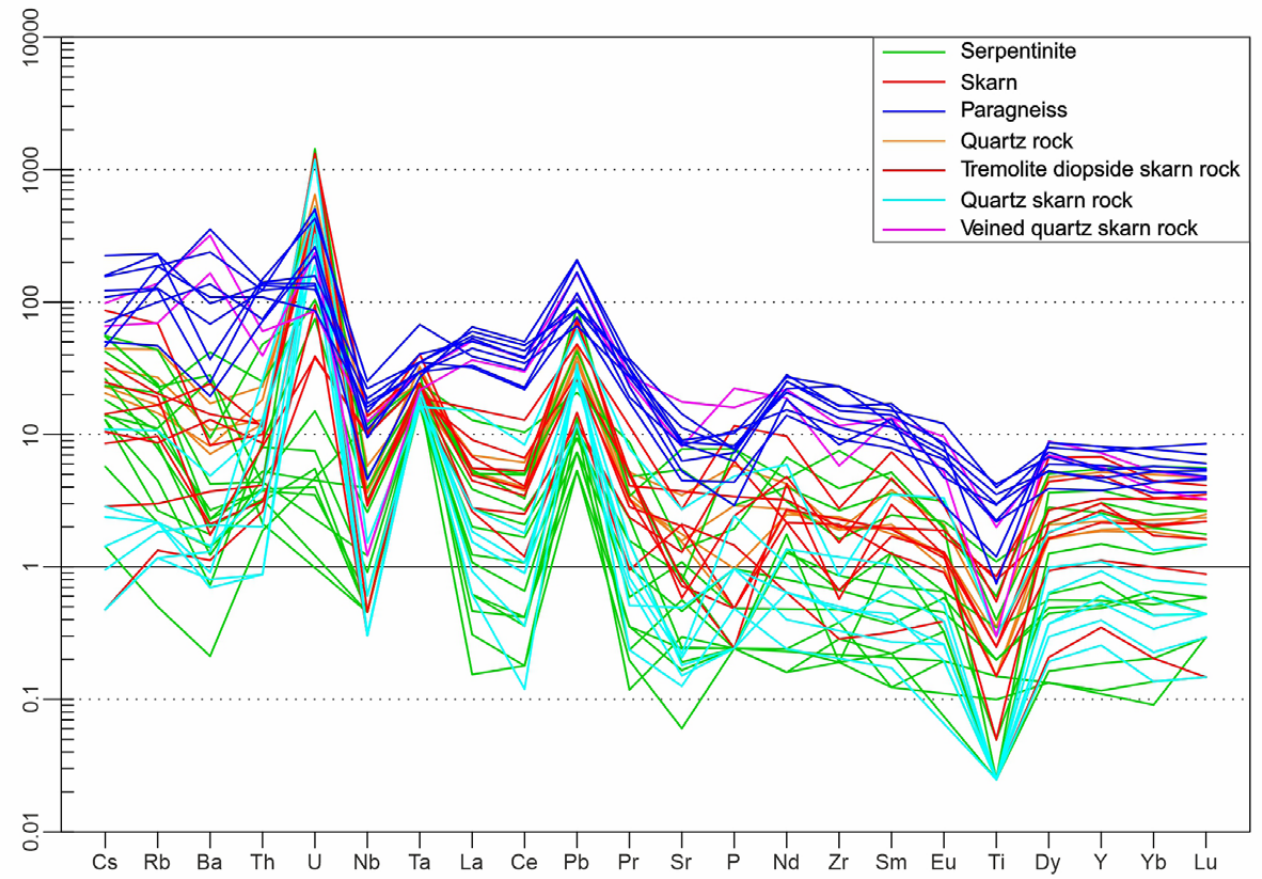

Fig. 31. Trace element patterns of the Outokumpu assemblage rocks and paragneisses from Kuolemanlahti and revised drill cores normalised with primitive mantle values of McDonough & Sun (1995).

In terms of the REE fractionation patterns, the rock types of the Outokumpu assemblage behave relatively consistently (Fig. 32), without significant LREE/HREE fractionation and small Eu anomalies, either positive or negative, and are concordant with the data of Kontinen et al. (2006). Some of the samples display possible weak signs of REE mobility, i.e. small spikes not congruent with smooth magmatic fractionation patterns. Paragneisses from Kuolemanlahti differ by having clear LREE/HREE fractionation.

As a whole, the samples on the Ni-Co plot show good correlation with some outlier samples (Fig. 31A, R^2 = 0.783), while the Ni-Cr ratios display a weaker one (Fig. 31B, R^2 = 0.4195). The Ni-Co data displays a Ni/Co ratio of ca. 20:1 regarded typical for the OKU assemblage serpentinites already by Huhma & Huhma (1970). Lithological groups differentiate to certain extent on both, but Ni-Co plot performs better, especially in respect to serpentinites, however skarn rocks and quartz rocks cannot be differentiated. Serpentinite sample from Täilahti (M324196R419) deviates from the trendline in the Ni-Co and Ni-Cr plots and the other sample from drillhole FDH_98-R022 on the latter.

On a ternary diagram of Co-Cu-Ni ratios (Fig. 33C), used by Huhma (1971c) and Puustjärvi (1984) to differentiate the rock types and visualise the abundances and relationships of these elements in the OKU assemblage rocks, most of the serpentinites, quartz, and skarn rocks plot in the close to the Ni apex, while the paragneisses plot away from the Ni apex. This behavior is very similar to that observed by Huhma & Huhma (1970), Huhma (1971c) and Puustjärvi (1984). On ternary Ni-Ti-Cr (Fig. 33D), the paragneisses plot in the Ti apex, while the OKU-type rocks plot between Ni and Cr apexes as one group, not displaying differences between lithological groups. Data presented by Huhma (1971c) differs from that presented here in one aspect: it has a larger concentration of data points near the Cr apex.

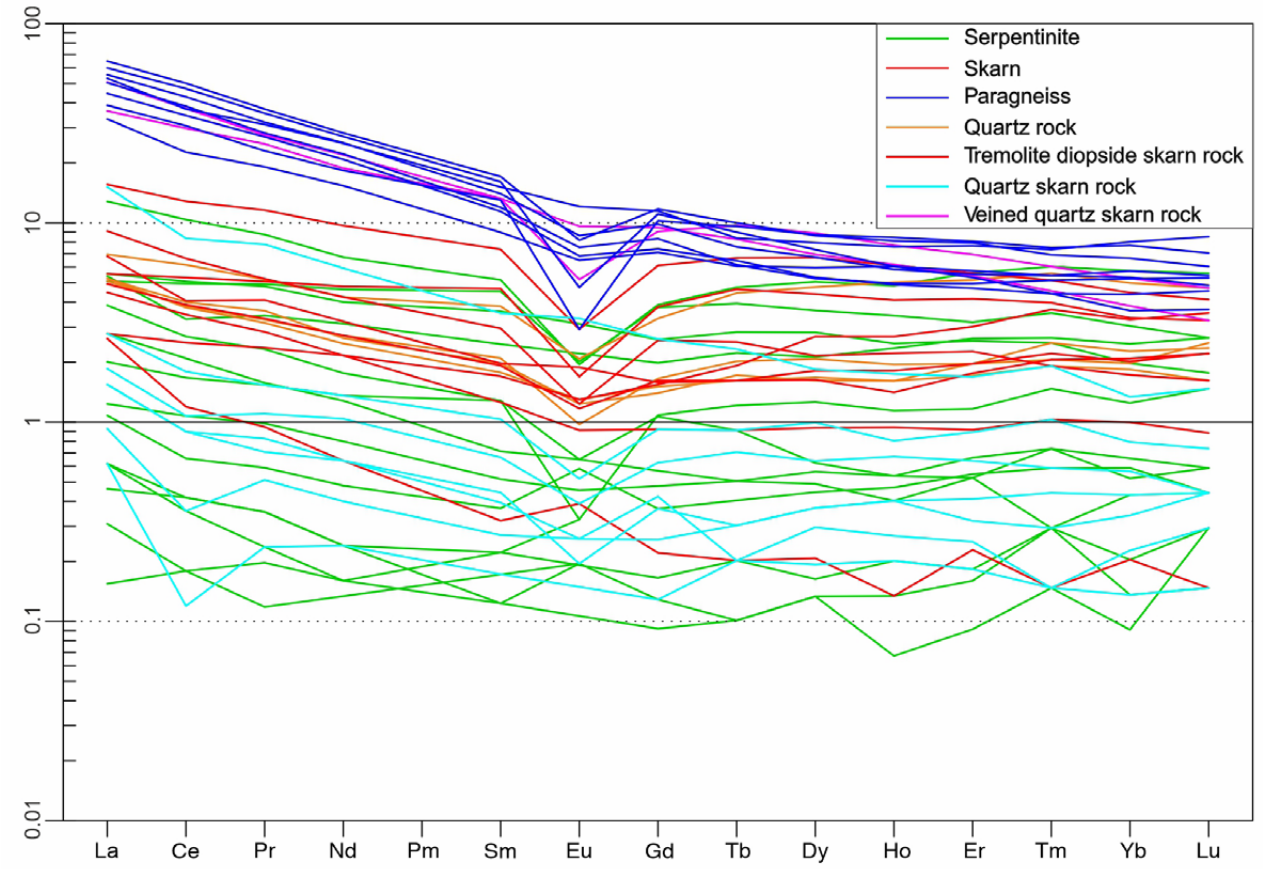

Fig. 32. REE patterns of the Outokumpu assemblage rocks and paragneisses from Kuolemanlahti and revised drill cores normalised with primitive mantle values of McDonough & Sun (1995).

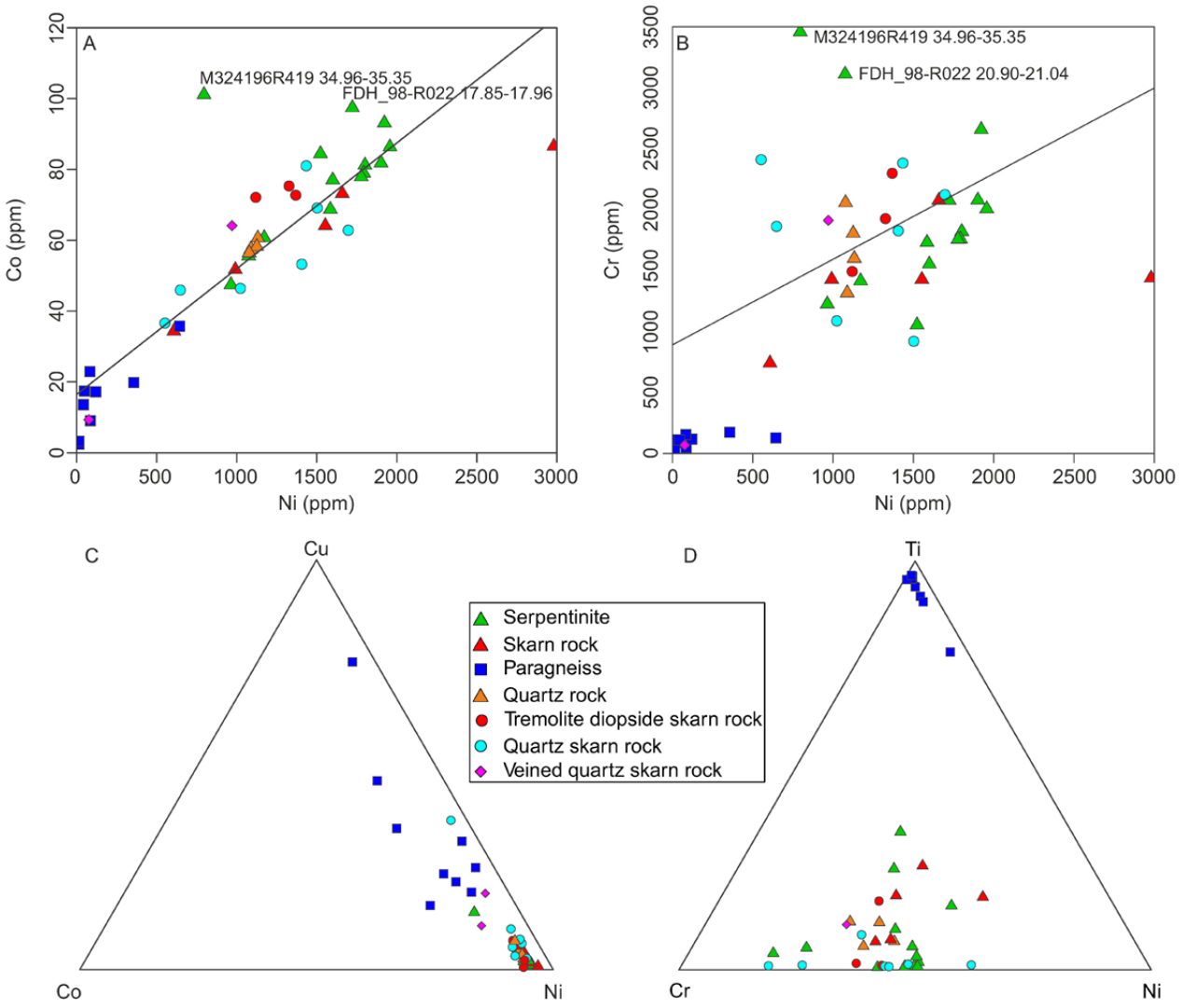

Fig. 33. A) Ni vs. Co and B) Ni vs. Cr plots and ternary diagrams for Co-Cu-Ni (C) and Cr-Ti-Ni (D) (n=44).

The OKU-type skarn is being referred by previous research to be low-Ti and lacking feldspars and biotite. (Huhma 1971c, Puustjärvi 1984). Our data is consistent with this and displays e.g. low K_2O, indicating the lack of micas in the OKU-type rocks (Fig. 30B). In the $MgO-Al_2O_3-Na_2O$ diagram (Fig. 30C), the last two serve as nominators for the presence of feldspars in the samples and most of our data plot away from the "feldspar apexes" with some quartz skarn rocks from Kuolemanlahti as outliers. The same outliers concerning the quartz skarn rocks can also be seen in Figure 30B. These are most likely due to more felsic vein material in the original samples and are referred to as veined quartz skarn rocks in the plots. It should however be noted that the skarn rocks associated with Luikonlahti and Kokka ores are rich in feldspar and Ti, and thus denote the complexity and overlapping nature of OKU assemblage mineralogy (Puustjärvi 1984).

Subtypes or mixed types of the OKU assemblage rocks have been observed before (e.g. Huhma 1975) within the study area. Mixed lithotypes within the OKU assemblage rocks are more than likely common, as is evidenced by the observations from the Kuolemanlahti trench where mixed-type rocks such as the quartz skarn rock and tremolite diopside skarn lenses with very variable geochemistry were observed. Given the complex mineralogy, specific naming of these units based on their verified quantitative mineralogy is not warranted at this point.

Lithological groupings formed by the binary plots also correlate between the ternary diagrams in that clustering of the OKU assemblage rocks is occurring in all diagram types, further highlighting the validity of the interpretation that the Kuolemanlahti trench samples and drill core samples share common geochemical features.

The new data from Piiroonmäki and Kuolemanlahti is in our opinion abundant and uniform enough to confirm the earlier preliminary inclusions of these locations into locations with the Outokumpu assemblage, although a serpentinite member was not encountered in Kuolemanlahti. The rock types present in these locations display both mineralogical and geochemical characteristics of the Outokumpu assemblage. Chromium-bearing green minerals, fuchsite, uvarovite and Cr-diopside observed in Kuolemanlahti are diagnostic to the assemblage. Despite major differences in mobile elements, they display uniform concentrations of immobile elements (e.g. low Ti, high Cr) and unanimous trace element patterns (negative Ta and Ti, positive Pb and Nb anomalies), which are compatible with the data from the core area of the Outokumpu assemblage (Peltonen et al. 2008 and references therein). Thus, there is no reason to doubt the validity of the earlier proposed hypothesis of intensively altered peridotite as the protolith of the quartz and skarn rocks.

In respect to the drill core samples FDH_98-R022, OU_1-R001, and the one from Täilahti, the situation is somewhat different, the amount of sample material from these locations is relatively low and thus the uncertainties are higher. The existing data, however, displays the same characteristics as the samples from Piiroonmäki and Kuolemanlahti, allowing at least their preliminary inclusion into locations with Outokumpu assemblage rocks, which for Täilahti has already been done before (Forss et al. 1999).

7 PROTEROZOIC INTRUSIVES

7.1 Kotalahti suite

The field mapping and drillings did not result in locating new intrusions of the Kotalahti suite. In addition to the intrusions, the gabbros of the Kotalahti suite are present as variably sized tectonic fragments in Suonenjoki suite paragneisses, but these are not as abundant as further west in the core of the Raahe-Ladoga suture zone.

7.2 Savo supersuite

The Kaarakkala and Heinävesi suites in the study area do not display significant differences in mode of occurrence or texture. On average, the Kaarakkala suite, intruding into the Archaean complex, is more mafic of the two and spans mineralogically from diorites to tonalites. In the Heinävesi suite, intruding the Viinijärvi suite paragneisses, the variation spans from quartz diorites to granites. Quartz diorites are relatively common on the southeast side of the Suvasvesi intrusion and rarer west and north of it. Both suites occur as larger intact intrusions and veins of variable width, which can be locally abundant, especially in the Viinijärvi suite area where it is practically impossible to find a larger outcrop without crosscutting granitoid dykes varying in width from centimetres to metres. Dykes occur both as schistosity parallel deformed ones and undeformed ones crosscutting them (Figs. 34A, B), indicating multiple magma pulses over prolonged periods. Also, the larger intrusions display sharp compositional internal boundaries on outcrop scale (Figs. 34C, D), making formation from multiple magma pulses more likely than fractional evolution within a single magma chamber.

The rocks are either unoriented or weakly oriented, signs of postcrystallisation alteration are limited mainly to chloritisation of biotite and seritisation of plagioclase, both are locally moderately strong but are mainly weak or nonexisting. The rocks are typically equigranular, and clearly K-feldspar porphyritic varieties are only found within the Suvasvesi intrusion, the core of which is formed by the porphyritic variety. Biotite is the dominant mafic mineral in granodiorites and granites, accompanied variably by hornblende especially in more mafic compositions. Accessory garnet is rare.

Magma mingling structures resembling those described from the so-called microtonalites (Huhma 1976, Lukkarinen 2008) were observed from a few locations within the Archaean rocks. In all of these cases medium-grained, relatively

leucocratic tonalite was in contact with distinctly more mafic and finer-grained quartz diorite (Fig. 34E). Xenoliths of the country rocks displaying variable degrees of assimilation are locally present, especially within the Suvasvesi intrusion (Fig. 34F).

Fig. 34. Granitoids of the Heinävesi and Kaarakkala suites. Length of compass 12 cm. Scale bar with cm division. A) Older deformed granitoid vein intruding into Viinijärvi suite paragneiss and crosscut by younger undeformed one at observation MTL2-2020-117 (E=552 538, N=694 3596). B) Granitoid of the Kaarakkala suite intruding Archaean basement (bottom of photo) and brecciating diabase dyke. Observation PIM$-2019-48 (E=562 616, N=695 1908). C) Sharp contact between two different porphyritic granite phases within the Suvasvesi intrusion at observation HKRA-2019-49 (E=558 974, N=693 4880). D) Contacts between different equigranular phases of the Suvasvesi intrusion at observation HKRA-2019-100 (E=558 864, N=692 6798). E) Contact between fine-grained and medium-grained quartz diorites at observation MTL2-2020-408 (E=547 894, N=696 8624), interpreted as possible magma-mingling structure. F) Variably assimilated unmigmatised paragneiss xenoliths in porphyritic variant of the Suvasvesi intrusion at observation HKRA-2019-27 (E=562 958, N=692 6144).

7.3 Granitoids of the Haukivesi suite

Mineralogically, in our study area, the rocks of the Haukivesi suite vary from quartz diorite to granite, although in adjacent areas the suite also includes diorites and gabbros. Most of the occurrences are veins and elongated intrusions less than 2.5 km long, with the exception of the Juonionlahti intrusion, 10 by 2.5 km in size. The veins crosscut the schistosity and folded veining of the Suonenjoki suite paragneisses sharply (Fig. 35A). In most cases these equigranular or weakly plagioclase porphyritic rocks are homogeneous and weakly oriented or unoriented (Fig. 35B). Especially in the Juonionlahti intrusion more mafic and finer-grained enclaves are quite common and are locally so abundant that they resemble deformed magma-mingling structures (Fig. 35C). Biotite is present as mafic mineral in all cases, variably accompanied by hornblende in quartz diorites and tonalites. Excluding the immediate vicinity of partially assimilated paragneiss, xenoliths garnet was observed only in the relatively leucocratic Juurikkamäki granite (Fig. 35D) intruding into the Juonionlahti intrusion.

Fig. 35. Granitoids of the Haukivesi suite. Length of compass 12 cm. A) Schistocity parallel openly folded leucogranodiorite veins are truncated by practically undeformed biotite tonalite vein, which is in turn cut by leucogranodiorite closely resembling the older generation in appearance. Observation PIM$-2018-71 (E=544 484, N=693 1323). B) Homogeneous hornblende-biotite tonalite of the Juonionlahti intrusion at observation MTL2-2019-214 (E=541 369, N=695 0386). C) Tonalite from the Juonionlahti intrusion with abundant finer-grained and more mafic enclaves which could represent deformed magma mingling structure. Observation PIM$-2019-181 (E=541 944, N=694 7899). D) Garnet-biotite granite of the Juurikkamäki intrusion at observation MTL2-2019-209 (E=541 326, N=694 8713).

7.4 Geochemistry of the Proterozoic granitoids and paragneiss neosomes

Geochemical data from Heinävesi (n=72), Kaarakkala (n=23) and Haukivesi suites (n=31), in addition to six samples from paragneiss neosomes both from the study area and its vicinity, are handled together due to their significant resemblance. SiO_2 contents of the samples vary from 47.3 to 77.8%, the majority having concentrations above 60%. The Haukivesi suite samples are on average somewhat more basic, although the compositional range is similar to that of the other groups (Fig. 36). In respect to CaO, FeOt and MgO, the samples display clear trends, which are for the first two similar to all of the groups but, in respect to MgO, the Haukivesi suite seems to deviate from the others with a higher trend line. In respect to other main elements, the data displays significant scatter, although it can be noted that at lower SiO_2 concentrations Haukivesi suite has, on average, lower Na_2O and P_2O_5 contents than the other suites. Based on commonly used classification diagrams, the samples can be characterised as mainly weakly magnesian, calc-alkaline and slightly peraluminous (ASI=1.0–1.2, Fig. 37). However, the more mafic variants of the Haukivesi and Kaarakkala suite rocks are metaluminous in composition.

On mantle-normalised spider diagrams, the suites are characterised by variably negative Nb, P and Ti anomalies in addition to major scatter in the LILE (Fig. 38). All of the negative anomalies are strongest in the Heinävesi suite and weakest in the Haukivesi suite. Additionally, most of the neosome samples display a negative Sr anomaly. REE patterns of all of the suites are mainly LREE enriched with variable LREE/HREE fractionation and either display variably negative or no Eu anomaly (Figs. 37 and 38). Heinävesi suite also contains samples with strongly positive Eu anomaly ($Eu/Eu^* \leq 2$) and/or weak LREE/HREE fractionation ($(La/Yb)_N \leq 5$). Heinävesi suite also includes the samples with the strongest negative Eu anomaly ($Eu/Eu^* \leq 0.3$). Especially in the Heinävesi suite, the scatter in Eu anomaly increases with increasing SiO_2 content.

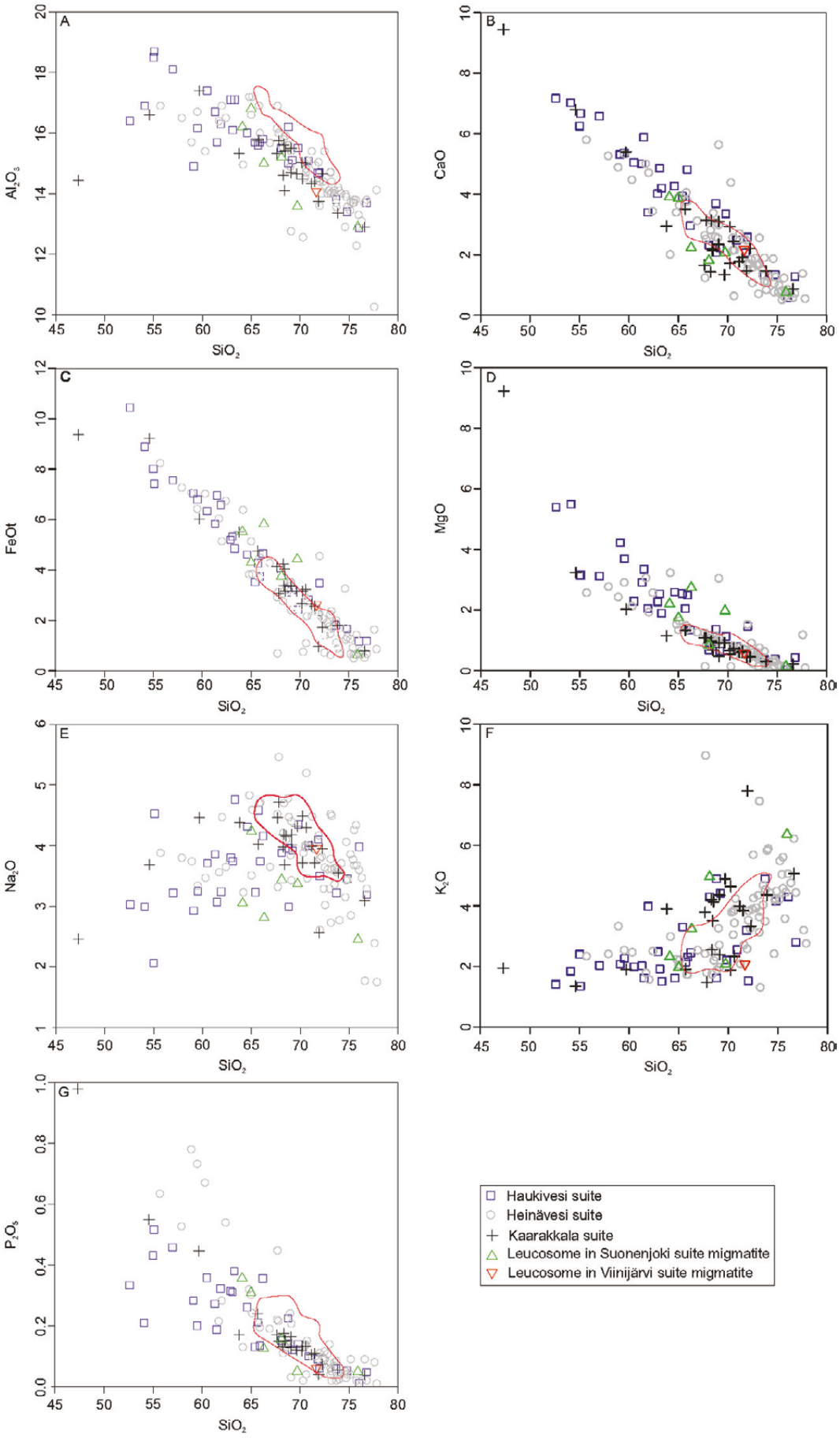

Fig. 36. Harker diagrams for samples representing Heinävesi, Kaarakkala and Haukivesi suites and paragneiss neosomes. Compositional field for Suvasvesi intrusion drawn based on unpublished data of Rantanen & Heinonen.

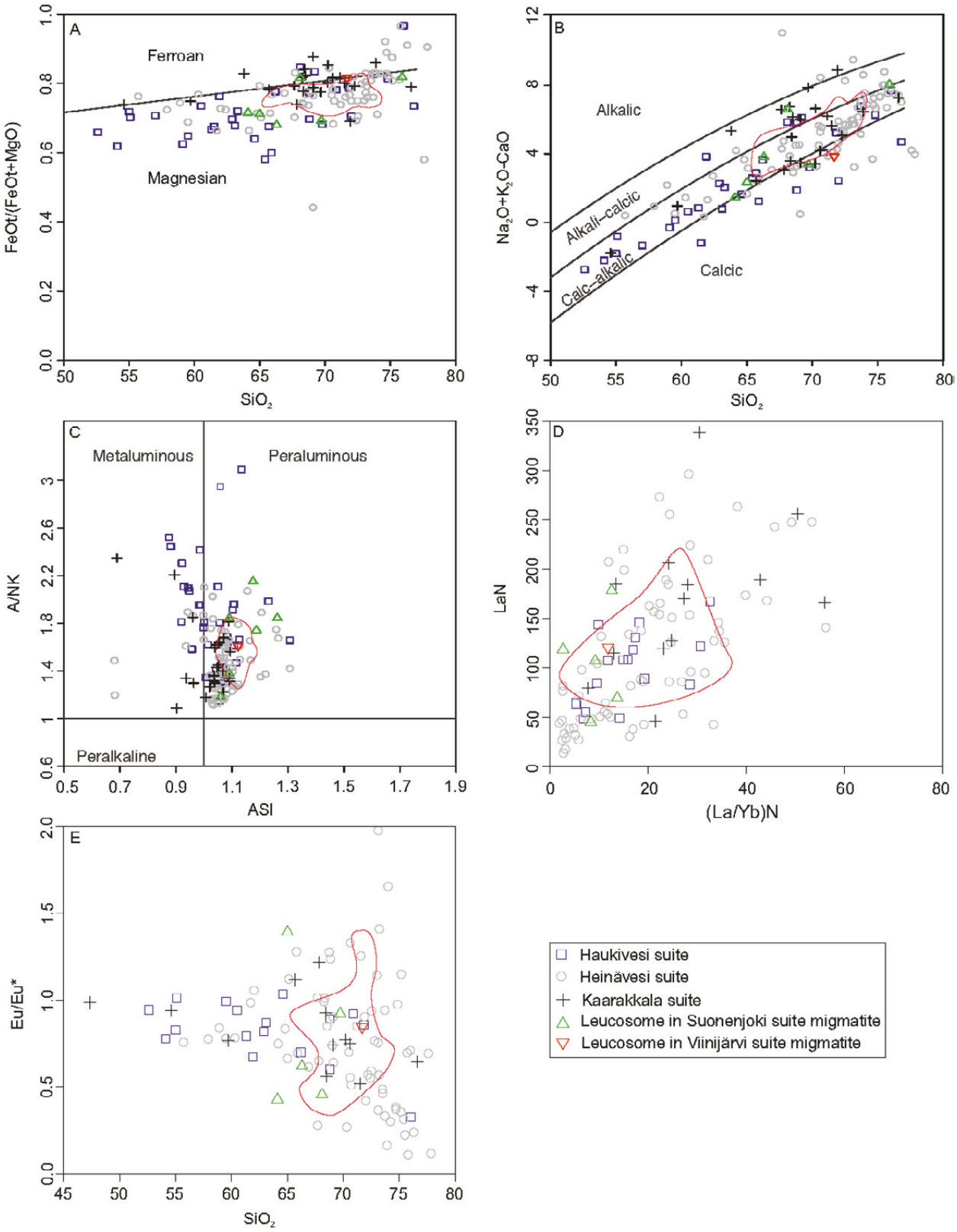

Fig. 37. Proterozoic granitoids plotted on various diagrams. A, B, C) classification diagrams of Forst et al. (2001). D) Chondrite-normalised La/Yb ratio versus La, E) SiO2 versus Eu anomaly.

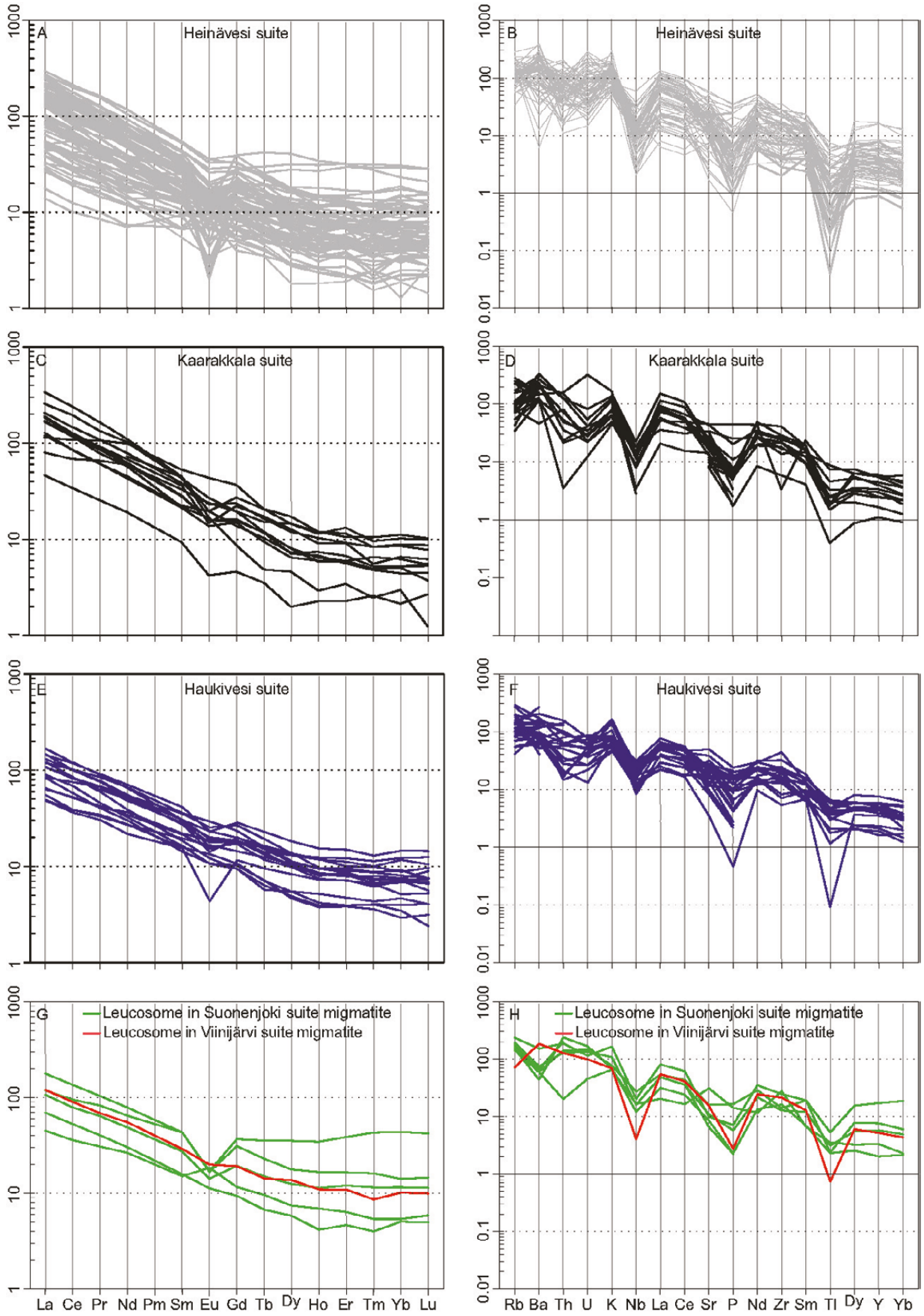

Fig. 38. Chondrite-normalised (values from Boynton 1984) REE patterns and primitive mantle-normalised spider diagrams (values from Sun and McDonough 1989) for samples representing Heinävesi (A, B), Kaarakkala (C, D) and Haukivesi (E, F) suites and paragneiss leucosomes (G, H).

8 STRUCTURAL OBSERVATIONS

Our approach in structural studies was to concentrate on a few key areas identified by geophysical data and previous studies. The aim was to link our observations and interpretation with previously defined structural interpretations from Outokumpu allochthon and the Raahe-Ladoga zone between Kuopio and Varkaus. We also related different deformation phases to tectonic events and in this way updated interpretation of the structures.

8.1 Kohma

The Kohma area is located on the eastern contact of the Archaean Kuopio complex, and the whole stratigraphy from Archaean basement, through rocks of Jatulian system, and to autochthonous Ludicovian and allochthonous Kalevian paragneisses is present. Large-scale fold structures can be observed in magnetic anomalies of the aerogeophysical data (Fig. 39).

Oldest structure in the Kohma area is the inferred Outokumpu decollement thrust along which the Outokumpu allocthon was emplaced on the attenuated Archaean continent. North-south to northeast-southwest-trending folds with west to northwest dipping axial planes can be observed in the Viinijärvi suite paragneiss. The large scale Kolonjärvi synform is observable from aerogeophysical data (Fig. 39) and small folds related to it can be seen on the outcrops (Fig. 40A). The Honkajärvi basement-cored antiform is present west of Kolonjärvi synform. Open folding and south plunging fold axis with a dip of 35° was observed on the western limb of the antiform (Fig. 40B). Further west, the Ylä-Nurjonen synform is defined (Fig. 39). Because basement and cover are folded together in these major folds, we infer that these were formed in a thick-skinned manner during the second deformation event.

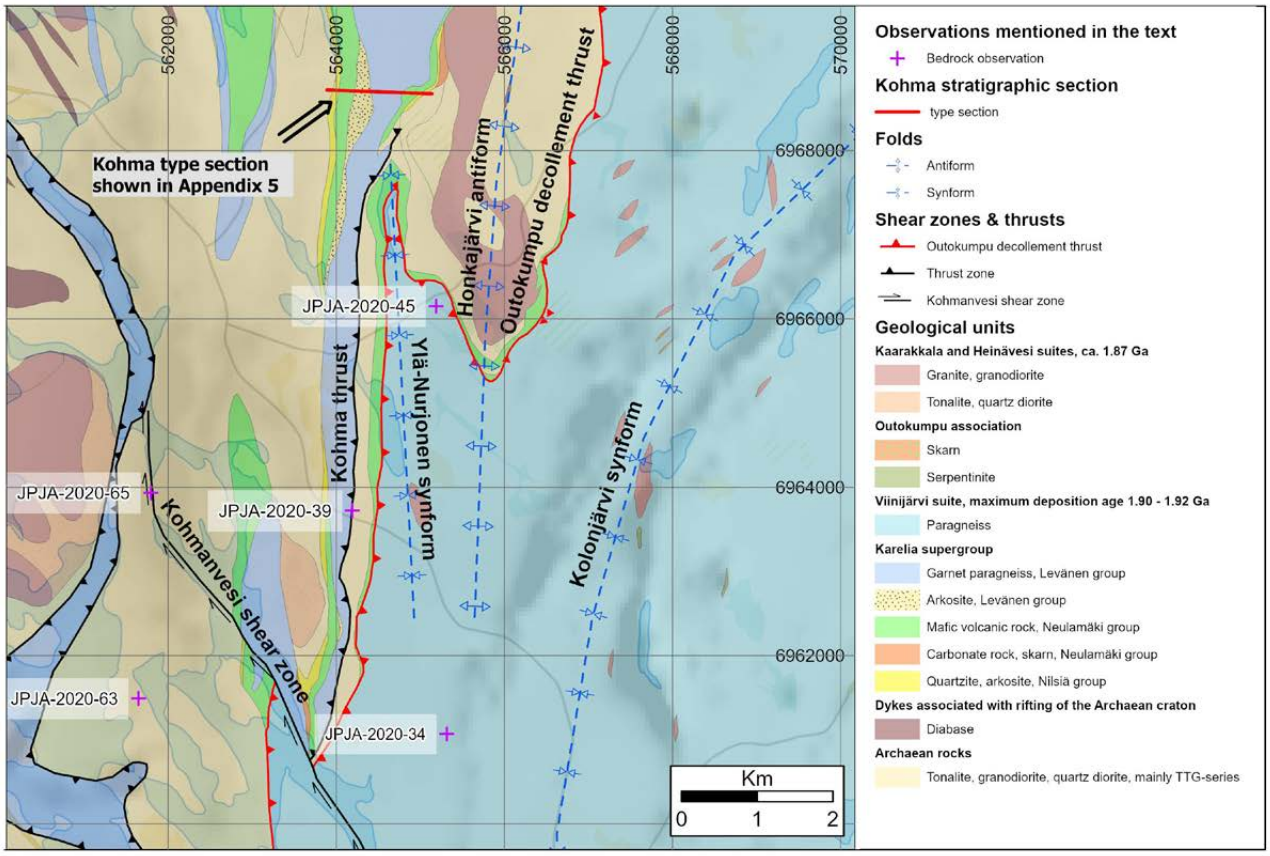

Fig. 39. Geological map of the Kohma area with interpreted structures mentioned in the text. Aeromagnetic data on the background. Basemap ©National Land Survey. See Figure 6 for location of the area.

Strongly foliated and banded Archaean basement gneiss was observed on the western side of the Ylä-Nurjonen synform (Fig. 40C). Paragneisses and arkoses of the Hiidenlahti formation, part of the Levänen group, are located on top of the Archaean basement. Because of intensive deformation and discontinuous stratigraphic sequence, a thrust, named as the Kohma thrust, is inferred between the basement and the cover (Fig. 39).

A younger Kohmanvesi shear zone with dextral strike-slip movement crosscuts the structures described above and the Kohma thrust (Fig. 39). The shearing is particularly well observable in the porphyritic Archaean granodiorite gneisses of the Koitere suite (Fig. 40D). Conjugate structures related to this shear zone with sinistral movement were observed along the limbs of SW-NE-trending folds (Fig. 40E). Granitic veins have intruded the axial plane of these SW-NE-trending folds (Fig. 40F). These granitic veins must have been intruded simultaneously with the folding and could give the absolute age of the folding. We infer that the Kohmanvesi shear zone is coeval with the major D3 Suvasvesi shear zone and that the folding with SW-NE-trending axial planes predated formation of the shear zone.

Fig. 40. A) Dextral minor folds in the Viinijärvi suite paragneiss on the western limb of the Kolonjärvi synform, handle pointing north, observation JPJA-2020-34 (E=565 315, N=696 1070). B) Folded quartz-feldpar segregations and boudinaged calc-silica layers in the Viinijärvi suite paragneiss on the western limb of the Honkajärvi antiform, observation JPJA-2020-45 (E=565 188, N=696 6151). C) Deformed Archaean basement gneiss with north-south-trending foliation next to the Kohma thrust, observation JPJA-2020-39 (E=564 192, N=696 3721). D) Kohmavesi shear zone in Archaean porphyritic granodiorite gneiss belonging to the Koitere suite, observation JPJA-2020-65 (E=561 794, N=696 3935). E) NW-SE-trending open folds in Archaean granodiorite gneiss cut by sinistral shear zone interpreted as conjugate structures of the Kohmavesi shear zone, observation JPJA-2020-63 (E=561 651, N=696 1489). Length of compass 12 cm. F) SSW-NNE-trending open fold in Archaean porphyritic granodiorite. Note the granitic veins in axial plane. Handle pointing north, observation JPJA-2020-63 (E=561 651, N=696 1489).

8.2 Räsälä

The Räsälä subarea is located south of the Suvasvesi shear zone (Figs. 6 and 41). North-east of Räsälä, isoclinal, recumbent F1 folds, with NNE-trending axial plane, were observed in the paragneisses of the Viinijärvi suite (Fig. 42A). Folded bedding forms sharp hinges, whereas folds in calc-silicate layers have round hinges. These folds are similar to the ones that were described by Koistinen (1981) from Outokumpu, Park & Bowes (1983) from Kaavi and Jokela (1994) from Hanhisalo. We infer that these isoclinal folds with limbs subparallel to bedding were formed while the Outokumpu allochthon was emplaced over the attenuated Archaean continent during the first deformation phase (D1).

West of Räsälä, the basement rocks form the core of the large scale, slightly east-verging Tomperi antiform, which is partly surrounded by autochthonous Jatulian units on the eastern and western side of the antiform. To south, on the eastern limb of the antiform, Viinijärvi suite paragneisses have been thrusted directly on the foliated basement (Fig. 42B). When moving north along the eastern limb of the antiform, a thrust wedge of Archaean basement was observed above Palaeoproterozoic quartzites (Fig. 42C) and volcanic rocks (Fig. 41, Archean basement wedge observationsd JPJA-2010-10 and JPJA-2010-8). Previously, classification of this migmatised rock unit was unsure, but our observations confirm Archaean origin for the migmatised tonalite gneiss rock unit (Fig. 42D). On the southern end of the Tomperi antiform, a north-south-trending shear zone with dextral horizontal movement was observed (Fig. 42E). On the western side of Tomperi antiform is Tervassalo F2 synform. Suonenjoki suite paragneiss forms the core of the synform, followed by mafic volcanic rocks of the Vaivainen formation and quartzites of the Kolmisoppi formation. The nature of the contact between Vaivanen and Suonenjoki formations could not be observed in the field.

We infer that the folding of the basement together with the supracrustal cover at Räsälä occurred during the second deformation event. This folding progressively evolved to thrusting of tectonic wedges as in Vehmasmäki (Forss et al. 1999) and Kaavi (Park & Bowes 1983). We also infer that the shear zone at the southern end of the Tomperi antiform was first activated as a thrust in the second deformation event.

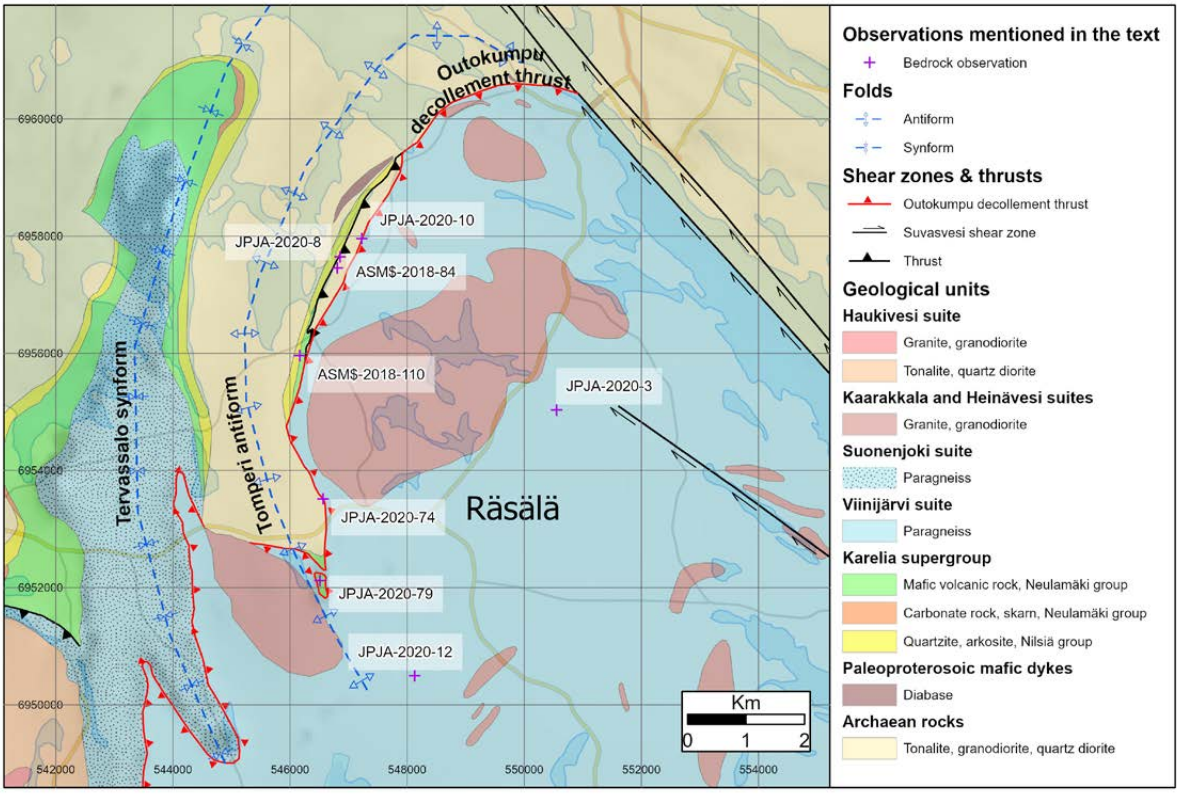

Fig. 41. Geological map of the Räsälä area with observations and interpreted structures mentioned in the text. Aeromagnetic data in the background. Basemap ©National Land Survey. See Figure 6 for location of the area.

Well-developed crenulation cleavage with SW-NE-trending axial plane was observed in the Viinijärvi suite paragneiss south of the hinge of the Tomperi antiform (Fig. 42F). Here the pervasive foliation, formed during D2, was refolded in the third deformation event. The crenulation cleavage has formed in the SE-NW main stress direction of the D3 deformation.

Fig. 42. A) Isoclinal F1 folds in Viinijärvi suite paragneiss, length of hammer 64 cm, handle pointing north, observation JPJA-2020-3 (E=550 551, N=695 5032). B) Deformed Archaean tonalite gneiss with inclined foliation at Tomperi, view towards NW. The thrust contact to the allochthonous Viinijärvi suite paragneiss is less than 10 metres east, observation JPJA-2020-74 (E=546 562, N=695 3517). C) Autochthonous quartzite deposited on the Archaean basement, observation ASM$-2018-110 (E=546 165, N=695 5956). Length of compass 12 cm. D) Migmatitic Archaean tonalite gneiss, observation AMS$-2018-84 (E=546 809, N=695 7456). E) Shear zone at the hinge of Tomperi antiform where dextral movement is indicated by folded granitic vein above the hammer head, hammer handle pointing north, observation JPJA-2020-79 (E=546 511, N=695 2121). F) NE-SW-trending crenulation in the Viinijärvi suite paragneiss, handle pointing north, observation JPJA-2020-12 (E=548 131, N=695 0494).

8.3 Areas surrounding Konnuslahti and Saamanen domes

Upright folds with SW-NE-trending axial planes and almost horizontal fold axes were observed from outcrops of the Konnuslahti dome (Fig. 43A). West of the Konnuslahti dome, magnetic anomalies on aerogeophysical data also repeat this folding pattern. These folds form predominant deformational structure in the Konnuslahti area and have the same trend as the crenulation cleavage observed at the southern side of the Tomperi antiform (Fig. 42F). The structural trend at the southwestern end of the Outokumpu area also have the same strike as above-described folds at Konnuslahti. We infer that these folds developed in the D3 phase.

In the Archaean basement rocks of Konnuslahti moderately SW-plunging lineation was observed (Fig. 43B). Pervasive lineation in the cover rocks and Archaean basement has been interpreted as a D2 structure in earlier studies (Koistinen 1981, Park & Bowes 1983). Measured lineations form curvature on the Outokumpu allochthon, with SSW-NNE trend at Miihkali changing into WSW-ENE trend at Juojärvi (Koistinen 1981). This same curvature can be seen on the aeromagnetic anomaly map (Fig. 7). We interpret that the moderately plunging lineation at Konnuslahti is a D2 structure that was transposed during NNW-SSE regional D3 compression.

Crenulation cleavage and shear bands were observed in well-preserved and only weakly migmatitic Suonenjoki suite paragneisses on the eastern side of the Saamainen Archaean dome. Here pelitic paragneisses show extensional crenulation cleavage with dextral shear bands (Fig. 43C). These ESE-WNW-trending dextral shear bands are subparallel to the Suvasvesi shear zone. We infer that crenulation cleavage and shear bands formed in NNW-SSE regional compression in the D3 phase.

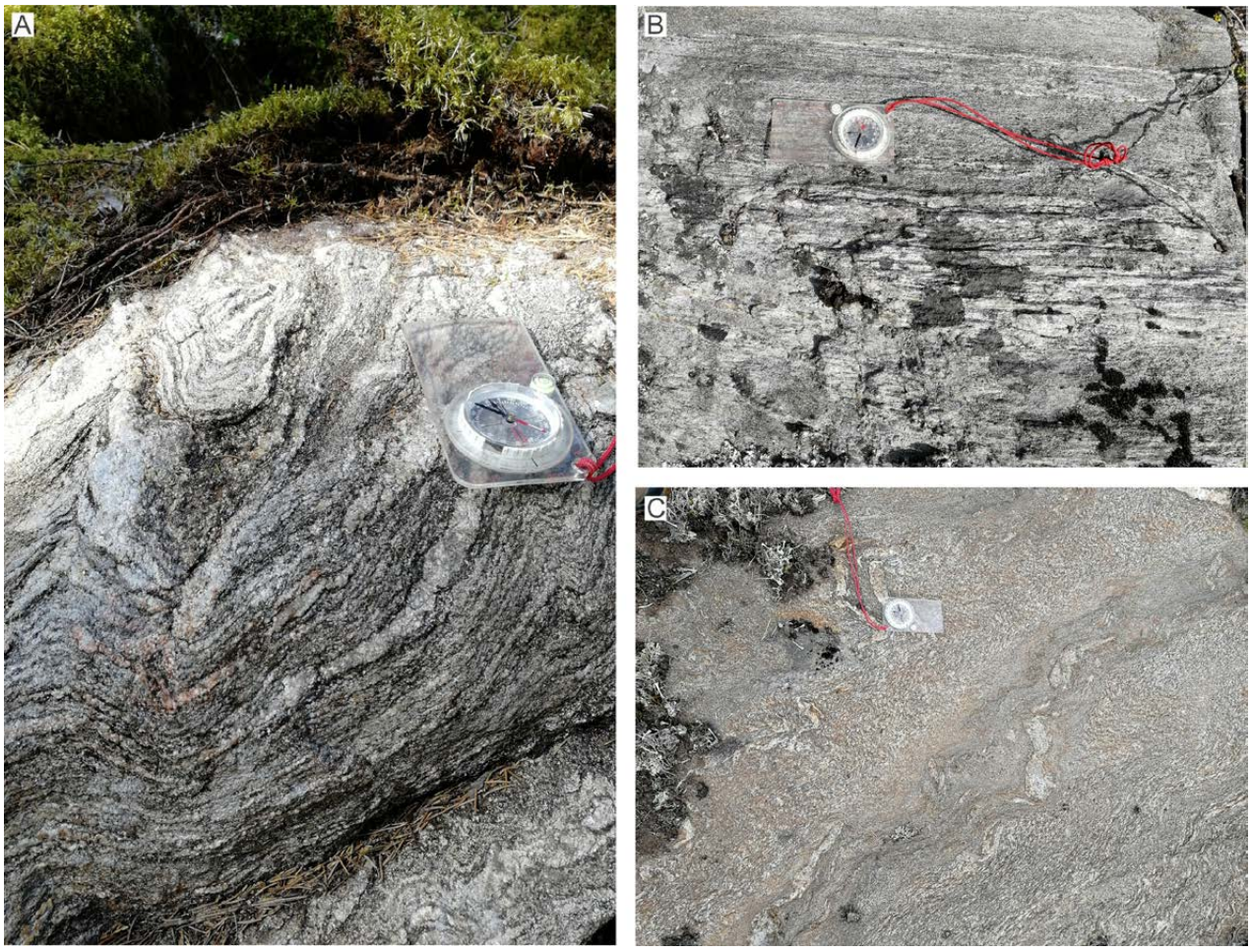

Fig. 43. A) Open fold with almost horizontal fold axis dipping SW in a shallow angle in a paragneiss on the northern side of Konnuslahti Archaean dome, observation MTL2-2007-43 (E=549 111 N=693 8690). B) Distinctive lineation in Archaean gneiss at Konnuslahti with dip direction 220 deg. and dip of 65 deg., observation JPJA-2020-56 (E=549 694, N=693 4703). C) Asymmetric crenulations and dextral shearing in weakly migmatitic paragneiss of the Suonenjoki suite, observation JPJA-2020-85 (E=547 850, N=694 3822).

8.4 Hanhisalo klippe

Jokela (1994) reported isoclinal folds with axial planar biotite schistosity in weakly migmatised turbiditic paragneisses at Hanhisalo. Biotite schitosity is bedding parallel and forms combinated S_0-S_1 foliation. Turbidites are dominantly psammitic with boudinaged calc-silicate layers.

Furthermore, a serpentinite body was found at Täilahti in a GTK nickel exploration program (see Fig. 44). The Täilahti peridotite is an Outokumpu-type serpentinite as shown by whole-rock and olivine analyses (Forss et al. 1999, this study). As all the other Outokumpu-type serpentinites are tectonically emplaced in the Viinijärvi suite paragneiss, Kontinen et al. (2006) tentatively suggested a klippe of Viinijärvi suite paragneisses at Täilahti.

We did reconnaissance field observations along cape Multniemi and observed psammitic paragneisses similar to those at Hanhisalo. Because of 1) similar lithology, 2) early deformation style associated with the thrusting of Outokumpu allochthon, and 3) the discovery of an Outokumpu-type serpentine body, we interpret a unit of Viinijärvi suite rocks between Multniemi, Hanhisalo and Täilahti referred to as Hanhisalo klippe (Fig. 44). This unit can also be observed in geophysical data, since originally clay-rich, pelitic beds in Suonenjoki suite paragneisses show as conductors around the unit (Fig. 44). We further favour the klippe interpretation of Kontinen et al. (2006) for the Hanhisalo unit. Although both the Suonenjoki suite and Viinijärvi suite are interpreted as allochthonous (Luukas & Kohonen 2021) and the thrusting of the Suonenjoki allochthon was related to a later D2 event, the explanation for the klippe at Hanhisalo is the D3 deformation which occurred from SE and thrust the Viinijärvi suite paragneisses further NW along the Suvasvesi shear zone.

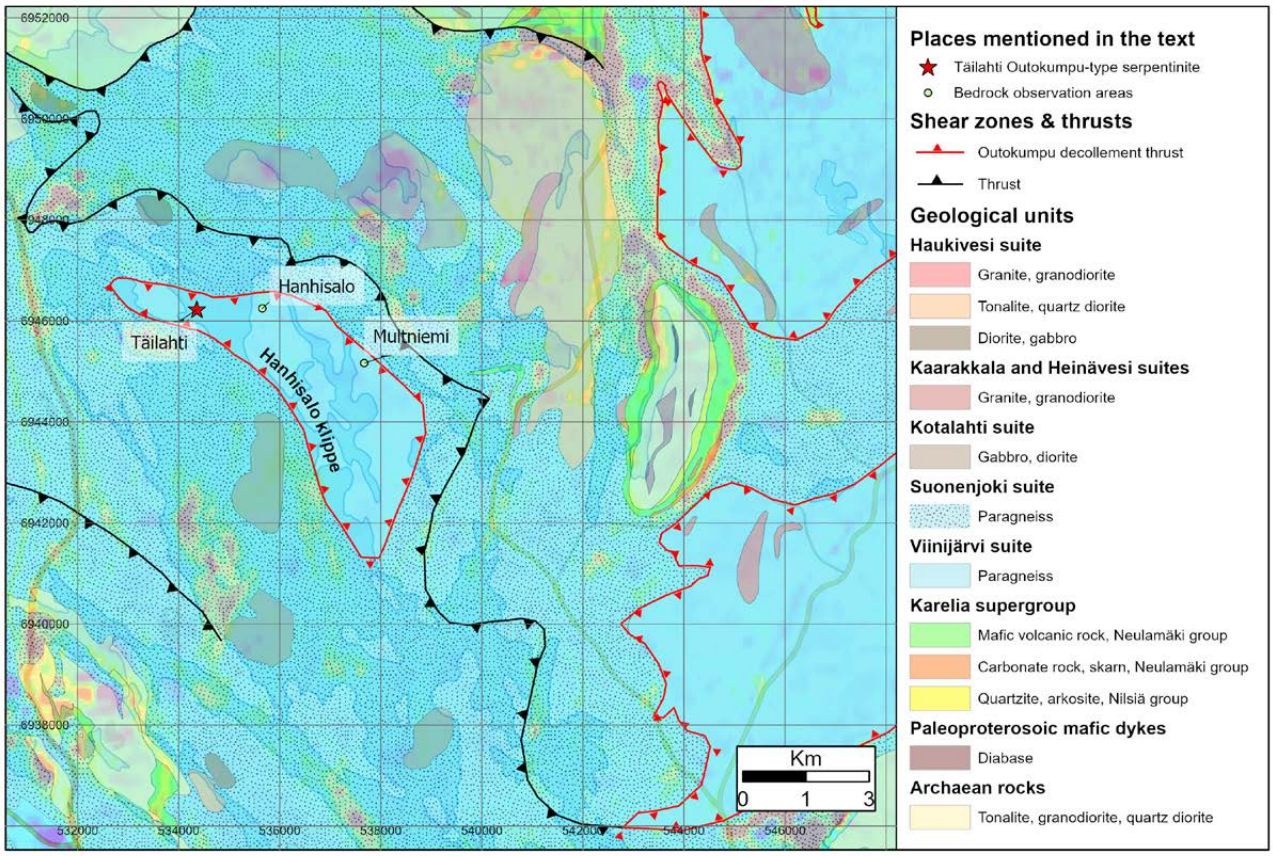

Fig. 44. Location of bedrock observation areas and Täilahti serpentinite on the Hanhisalo klippe west of the main allochthonous units. Aero-electromagnetic data in the background. Basemap ©National Land Survey.

8.5 Structures within the Raahe-Ladoga suture zone

The location of the R-L suture zone is indicated in Figure 1. Folds in Suonenjoki suite paragneiss with ESE-WNW-trending axial plane and fold axis plunging 70° WNW were observed near Leppävirta (Fig. 45A). Pelitic layers have molten in the paragneiss and thicker neosome layers have been boudinaged. After melting the paragneiss with the neosome has been folded. Tectonic stress that caused the folding did not exist when the melt formed or else the melt would have escaped to the pressure minimum along the axial plane. From Vehmasmäki, Forss et al. (1999) interpreted that the main migmatisation occurred after folding in their third deformation phase along major shear zones. Our observation indicates that some migmatisation also occurred before folding. Linear tonalite dykes cut the relict foliation in the migmatised paragneisses near Leppävirta (Fig. 45B). These tonalite dykes postdate the migmatisation and have a U-Pb zircon age of ca. 1.87 Ga (this study). The linear appearance of these dykes indicates that strain must have been localised in shear zones before their emplacement.

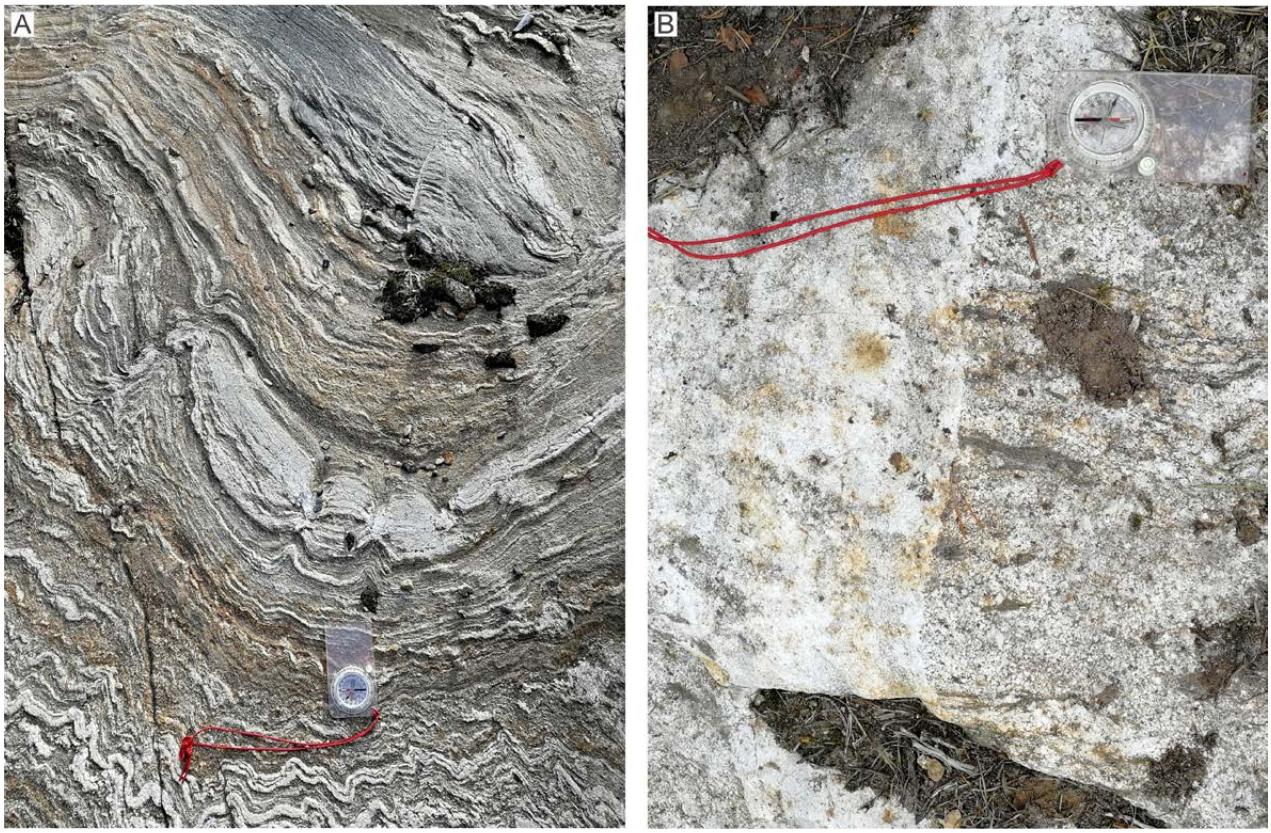

Fig. 45. A) Fold in Suonenjoki suite paragneiss with ESE-WNW-trending axial plane. Neosome has formed from the pelitic layers in the paragneiss, observation MTL2-2019-267 (E:545 824 N:692 5694). B) Tonalite dyke of the Haukivesi suite cuts relict foliation in nebulitic Suonenjoki suite paragneiss, observation MTL2-2019-262 (E:543 257, N=692 7485).

9 AGE DETERMINATIONS

New age data and the most relevant previously published results from the study area and its vicinity are summarised in Table 4. Locations of the age determination samples are shown in Figure 46. All analytical data and BSE images of the zircons can be found in Electronic appendix 1.

Table 4. Summary of age data from study area and its vicinity.

Sample	Location	Rock name	Geological unit/ area	N-EUREF	E-EUREF	Method	Crystallization age (Ma)	Metamorphic age (Ma)	Deposition age max (Ma)	Reference
A356	Vehka	Trondhjemite gneiss	Kotalahti dome	6938022	531486	LA-SC-ICPMS	2850–2750	1900–1800	----	This study
A362	Valkeinen	Granite migmatite	Kotalahti dome	6937762	532506	LA-SC-ICPMS	2850–2750	----	----	This study
A2530	Aumakivenkangas	Tonalite	Konnuslahti dome	6936093	548838	LA-SC-ICPMS	2803±6	----	----	This study
A38	Kuorevaara	Granodiorite	Sotkuma dome	6966115[a]	624682	CA-TIMS	2784±2	----	----	This study
A37	Sotkuma	Granodiorite	Sotkuma dome	6959069	625531	CA-TIMS	2774±2	----	----	This study
A2533	Vasikkasaaret	Tonalite	Vasikkasaaret thrust sheet	6921460	545652	LA-SC-ICPMS	2800–2700	1950–1850	----	This study
A2532	Kolmoset	Tonalite	Kuopio Complex	6962952	541170	LA-SC-ICPMS	2708±7	2600–2500?	----	This study
A75	Kapustaniemi	Tonalite	Juojärvi domes	6956336	585127	CA-TIMS	2704±2	----	----	This study
A448	Hoikanmäki	Quartz diorite		6966880	566032	LA-SC-ICPMS	2750–2650	----	----	This study
A449	Litmaniemi	Quartz diorite		6959013	563133	LA-SC-ICPMS	~2700	----	----	This study
A36	Heinävaara	Granodiorite	Koitere suite	6962881[a]	653230	CA-TIMS	2714±2	----	----	This study
A1033	Petosenmäki	Granodiorite	Koitere suite	6968319	531596	LA-MC-ICPMS	2750–2700	----	----	This study
A242 & A481	Koivusaari	Felsic volcanic rock		6994569	527158	TIMS	2062±6	----	----	Huhma et al. 2018
A2528	Piiroonmäki	Paragneiss	Viinijärvi suite	6907062	559200	LA-SC-ICPMS	----	----	1900	This study
A2529	Valkeinen	Paragneiss	Viinijärvi suite	6939373	553383	LA-SC-ICPMS	----	----	1920	This study
A2534	Salkolahti	Paragneiss	Viinijärvi suite	6960745	574276	LA-SC-ICPMS	----	----	1910	This study
A2535	Hepomäki	Paragneiss	Viinijärvi suite	6943256	584820	LA-SC-ICPMS	----	----	1930	This study
A2536	Iso-Patalampi	Paragneiss	Viinijärvi suite	6965158	565766	LA-SC-ICPMS	----	----	1900	This study
A2526	Kakonniitty	Paragneiss	Suonenjoki suite	6925965	545824	LA-SC-ICPMS	----	----	1900	This study
A2531	Eteläjoentausniitty	Paragneiss	Suonenjoki suite	6934882	547526	LA-SC-ICPMS	----	1900–1875	1910	This study
A446 & A701	Välimalmio & Mertakoski	Gabbro	Kotalahti suite			TIMS	1883±6	----	----	Gaál 1980

[a] significant error in coordinates

Table 4. Cont.

Sample	Location	Rock name	Geological unit/ area	N-EUREF	E-EUREF	Method	Crystallization age (Ma)	Metamorphic age (Ma)	Deposition age max (Ma)	Reference
A2527	Ryönänpelto	Tonalite	Haukivesi suite	6925958	546614	LA-SC-ICPMS	1872±9	----	----	This study
A134	Puijo	Granodiorite	Savo supersuite	533335	6975537	TIMS	1872±6	----	----	Lukkarinen 2008
A23	Juurus	Granodiorite	Savo supersuite	547809	6996068	SIMS	1870±2	----	----	Lahtinen et al. 2016
A24	Suvasvesi	Granite	Savo supersuite	559605	6926397	SIMS	1868±7	1863±3	----	Lahtinen et al. 2016, Huhma 1986
A25	Kermajärvi	Granodiorite	Savo supersuite	576798	6933894	SIMS	1865±6	----	----	Lahtinen et al. 2016
A60	Maarianvaara	Granite	Savo supersuite	585902	6988645	SIMS	1850±6	1843±3	----	Lahtinen et al. 2016, Huhma 1986

[a] significant error in coordinates

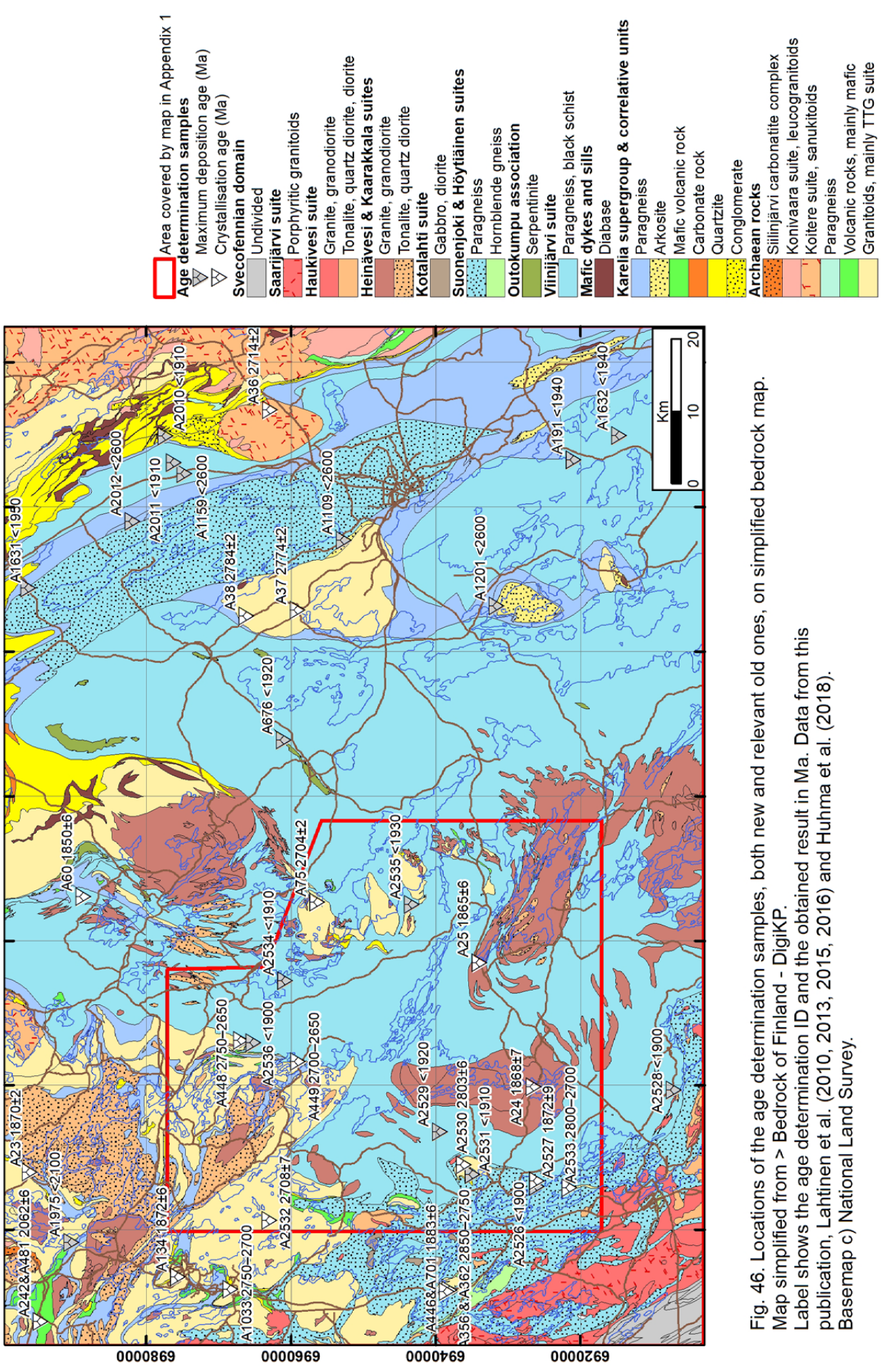

Fig. 46. Locations of the age determination samples, both new and relevant old ones, on simplified bedrock map.
Map simplified from > Bedrock of Finland - DigiKP.
Label shows the age determination ID and the obtained result in Ma. Data from this publication, Lahtinen et al. (2010, 2013, 2015, 2016) and Huhma et al. (2018).
Basemap c) National Land Survey.

9.1 Plutonic rocks

9.1.1 A36 Heinävaara gneiss granodiorite

Results for the Heinävaara sample (A36) were originally published by Wetherill et al. (1962). The sample is K-feldspar porphyritic granodiorite gneiss characteristic of the Kontiolahti dome. The dome has been regarded as a displaced part of the nearby Koitere intrusion (Bedrock of Finland – DigiKP), which belongs to the Neoarchaean sanukitoid suite (Heilimo et al. 2010). The original data by Wetherill et al. (1962) consists of one borax fusion analysis, the results of which indicated Archaean age for this sample.

A single CA-TIMS analysis was made from this sample which yielded a concordant age of 2714±2 Ma, which we interpret as the crystallisation age of this sample. This age is also within error limits with the 2722±6 Ma age of the main intrusion (Heilimo et al. 2011).

9.1.2 A37 Sotkuma gneiss granodiorite

Results for the Sotkuma sample (A37) were originally published by Wetherill et al. (1962). The sample is from the central parts of the Sotkuma dome and it represents the deformed granodiorites forming the majority of the dome. Wetherill et al. (1962) only published data for a single borax fusion analysis, based on which the rock was confirmed as Archaean in age.

Later, four additional zircon fractions have been analysed using the TIMS method and one with the CA-TIMS method. The fraction analysed with CA-TIMS yielded a concordant age of 2774±2 Ma, which we regard as the best estimation for the crystallisation age of the sample. The four TIMS fractions are highly discordant, but do not contradict the interpretation made as they define a discordia line with an upper intercept of 2687±28 Ma (Fig. 47A).

9.1.3 A38 Kuorevaara granodiorite

Results for the Kuorevaara sample (A38) were originally published by Wetherill et al. (1962). The sample is from the northern part of the Sotkuma dome and it represents the deformed granodiorites forming the majority of the dome.

Based on the single borax fusion analysis by Wetherill et al. (1962), the sample is Archaean in age. A fraction analysed with the CA-TIMS method yielded a concordant age of 2784±2 Ma which we regard as the crystallisation age of this granodiorite.

9.1.4 A75 Kapustaniemi gneiss tonalite

The strongly oriented Kapustaniemi (A75) tonalite originates from the northernmost one of the so-called Juojärvi domes. The first data for the sample by Huhma (1976) consist of a single borax fusion analysis clearly proving the Archaean age of the sample.

Later, four fractions have been analysed using the TIMS method and one with the CA-TIMS method. The fractions analysed using the TIMS method are strongly discordant but fall on a discordia line and define an upper intercept of 2714±38 Ma (Fig. 47B). The CA-TIMS analysis is concordant and yields an age of 2704±2 Ma, which we regard as the best estimate for the crystallisation age of this sample.

9.1.5 A356 Vehka trondhjemite gneiss

Sample A356 Vehka was taken from the trondhjemite gneiss wall of the Vehka ore body within the Kotalahti dome (Fig. 45) by Gaál (1980). The analysed two fractions were highly discordant, although clearly of Archaean age. The zircon population has two distinct morphological types; light cloured, oscillatory-zoned and relatively equidimensional versus darker-coloured, unzoned and elongated grains. Altogether 42 spots were analysed from 41 grains using LA-SC-ICPMS, all of which are concordant or nearly concordant. Two spots were discarded due to high common lead. The $^{207}Pb/^{206}Pb$ ages vary from 1796 to 2843 Ma and form two clusters at 1800–1900 Ma and 2600–2840 Ma (Fig. 47C). All ages belonging to the younger group are from the dark unzoned crystals, but some of this morphological type belong to the older group. All of the unzoned crystals display low U (<40 ppm). No meaningful concordia or average ages can be calculated. We interpret the 1800–1900 Ma cluster as marking Svecofennian metamorphism, and the zoned crystals as the original magmatic population variably affected by lead loss during the later events. The trondhjemite most likely crystallised between 2850 and 2750 Ma.

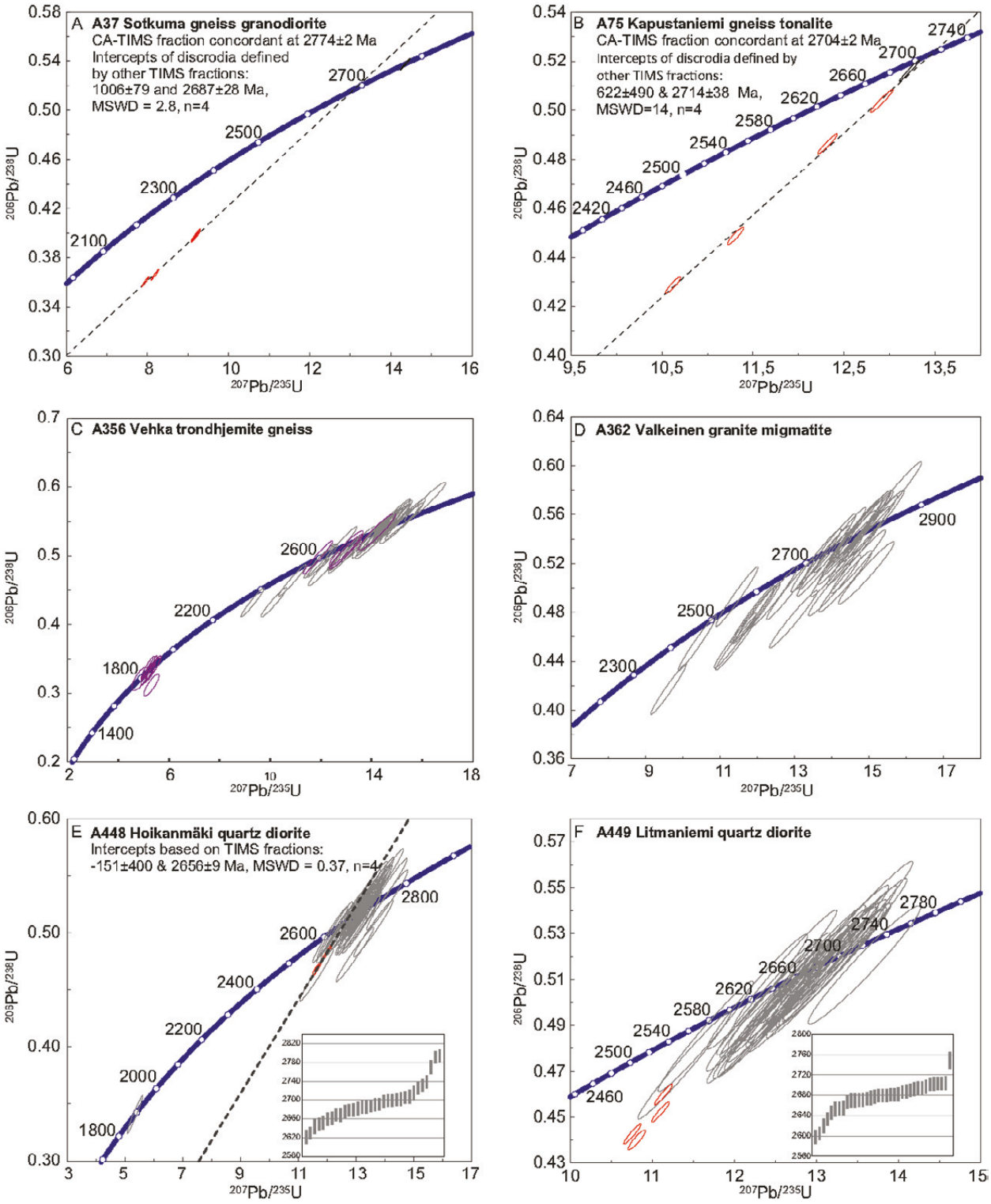

Fig. 47. Concordia diagrams for samples A37, A75, A356, A362, A448 and A449. Red ellipses mark the TIMS fractions and black the CA-TIMS fractions. Grey ellipses represent single grain analyses that are either unclassified (D, E, F) or from oscillatory-zoned grains (C). Purple ellipses in (C) represent unzoned homogeneous rims and grains. All data are plotted at the 2σ confidence level.

9.1.6 A362 Valkeinen granite migmatite

Sample A362 is a granite migmatite from the Kotalahti dome originally taken by Gaál (1980). The four reported fractions analysed with TIMS are highly discordant but indicate an Archaean age for this sample. The zircon population is morphologically homogenous and consists of weakly zoned crystals containing abundant inclusions. A total of 35 spots from 35 crystals were analysed with LA-SC-ICPMS for this study. All of the analysed spots are concordant or nearly concordant. The common lead concentrations are often relatively high, but only two crystals with $^{206}Pb/^{204}Pb$ <500 were rejected. Lead-lead ages span from 2508 to 2914 Ma (Fig. 47D) and the youngest ages tend to have higher common lead. Our interpretation is that the rock originally crystallised at 2850–2750 Ma and the large observed scatter is caused by periodic lead loss to which the grains with high common lead contents were more prone. It is also possible that some of the scatter is caused by inherited crystals.

9.1.7 A448 Hoikanmäki quartz diorite

Sample A448 Hoikanmäki was taken from the vicinity of the Archaean Proterozoic boundary 10 kilometres west of Tuusniemi (Fig. 45) by Huhma (1976). The sample represents quartz diorites which are abundant in this subarea (unpublished field maps of Outokumpu Oy, Huhma 1976). The original data, consisting of a single discordant analysis confirmed the Archaean or most likely Neoarchaean age of the sample but did not allow calculation of discordia or concordia age.

Later, three additional fractions were analysed with the TIMS method, also all of these analyses are discordant. Based on the four fractions, a discordia with an upper intercept of 2658±5 Ma can be calculated. Despite low error margins and an MSWD of 1.4, this age should be regarded dubious because it is based on four fractions that cluster closely together.

Altogether 33 spots from 33 zircon grains were analysed using LA-SC-ICPMS. Different morphological groups are not apparent as all of the grains are weakly zoned, and contain abundant inclusions and fractures in BSE pictures. Thirty-two of the spots are concordant or nearly concordant and form a continuum with $^{207}Pb/^{206}Pb$ ages spanning from 2621 to 2794 Ma, with a peak close to 2700 Ma (Fig. 47E). No correlation between age or composition of the zircon grains is observable. The one remaining spot yielded a concordia age of 1890±15 Ma. Our interpretation is that the sample crystallised most likely at 2750–2650 Ma and the observed scatter is due to lead loss caused by metamorphic event(s), the one distinctly younger age possibly representing complete resetting during Svecofennian.

9.1.8 A449 Litmaniemi quartz diorite

The Litmaniemi quartz diorite sample (A449) represents the same rock type as sample A448 and was taken 10 kilometres south of it (Fig. 45) by Huhma (1976) from a geologically similar location, i.e. close to the Archaean Proterozoic boundary. The original single analysis confirmed the Archaean, most likely Neoarchaean, age of the sample but did not allow more precise age determination.

Also the three fractions analysed later with the TIMS method were discordant. Due to all points plotting closely together and scattering, no meaningful age could be calculated with them, although the Neoarchaean age could be regarded as confirmed based on the obtained $^{207}Pb/^{206}Pb$ ages.

A total of 35 spots from 35 zircon grains were analysed using LA-SC-ICPMS. The grains are morphologically similar to those of A448, i.e. weakly zoned and containing abundant inclusions, but fracturing is less intense. All of the spots are concordant or nearly concordant. No meaningful age can be calculated as the lead-lead ages span from 2598 to 2749 Ma, with a cluster at 2650–2700 Ma (Fig. 47F). The oldest analysed spot could be inherited as it does not overlap with the others. The youngest ages tend to have higher common lead concentrations than the older ones, but exceptions exist both ways. Thus we interpret that this quartz diorite most likely crystallised close to 2700 Ma, and the significant scatter is caused by lead loss caused by younger events.

9.1.9 A1033 Petosenmäki gneiss granodiorite

The Petosenmäki sample A1033 is a porphyritic granodiorite gneiss (Lukkarinen 2008), representing sanukitoids of the Kuopio complex (Heilimo et al. 2012). The original U-Pb data by Lukkarinen (2008) consisted of five highly discordant zircon fractions, based on which a meaningful age could not be calculated, although Archaean age seemed most likely.

Later, 50 spots were analysed from 47 different zircon crystals using LA-MC-ICPMS. Data are

mostly concordant, but the $^{207}Pb/^{206}Pb$ ages form a nearly continuous range from 2.3 to 2.75 Ga, with an outlier at 2.15 Ga (Fig. 48A). Based on the data it is not possible to calculate meaningful ages. Our interpretation is that significant lead-loss was induced by Palaeoproterozoic thermal event(s) in the zircon crystals of this Neoarchaean granodiorite, which most likely was roughly coeval with the sanukitoids of the West Sanukitoid Zone, i.e. ~2.72 Ga (Heilimo et al. 2011).

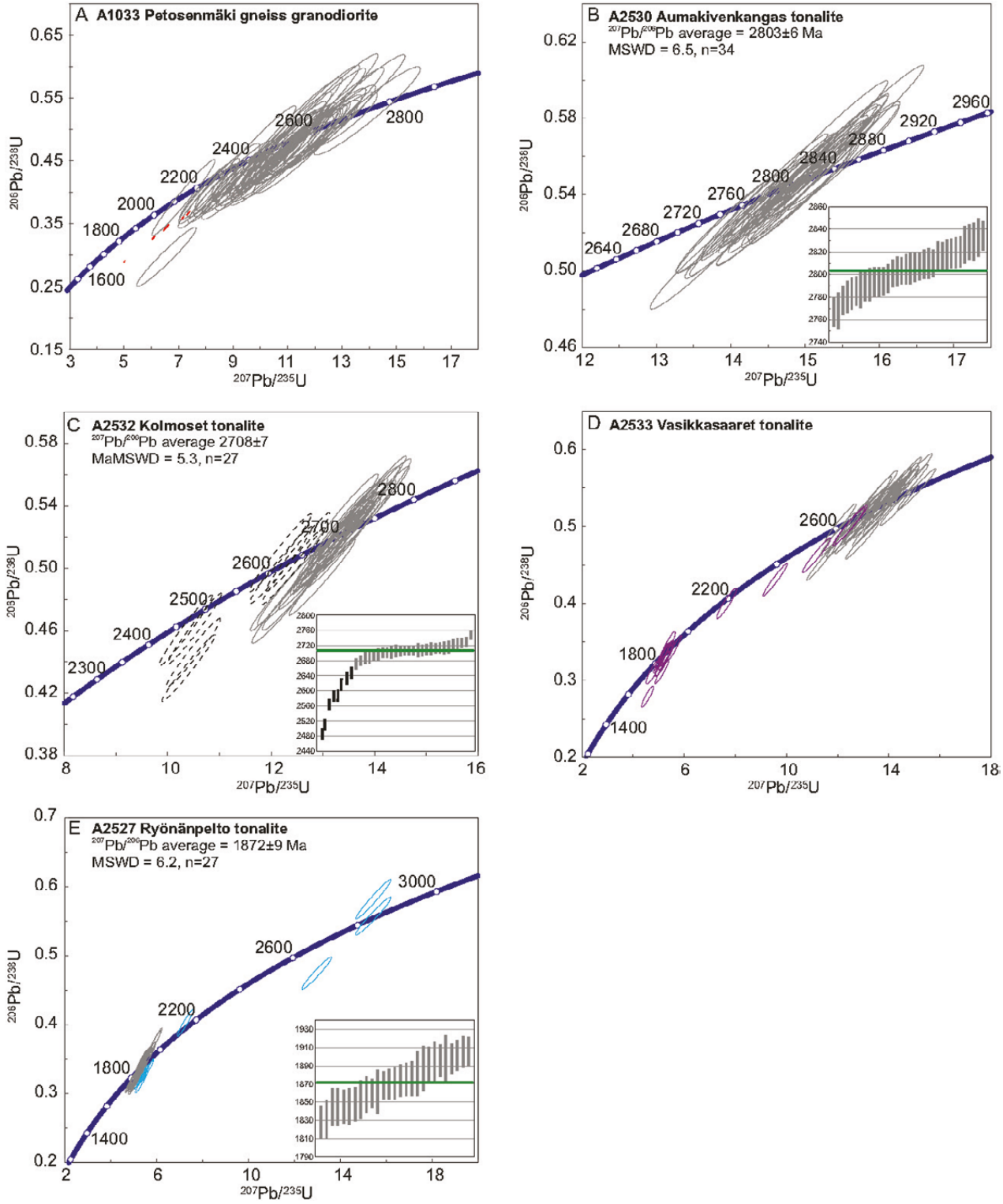

Fig. 48. Concordia diagram for samples A1033, A2530, A2532, A2533 and A2527. TIMS fractions as red ellipses and unclassified or oscillatory-zoned spot analyses as grey ellipses. In (C) spots excluded from calculation of the $^{207}Pb/^{206}Pb$ average age shown with black line. In (D) purple ellipses are from homogeneous rims or grains and turquoise ellipses in (E) mark spots interpreted as inherited. All data plotted at 2σ confidence level.

9.1.10 A2530 Aumakivenkangas tonalite

Aumakivenkangas tonalite (A2530) represents the strongly lineated homogeneous biotite tonalites forming the bulk of the Archaean Konnuslahti dome (Fig. 45). Zircons exhibit oscillatory zoning, in addition to which a limited number of core-rim structures are observable. Using LA-SC-ICPMS, 34 spots from 31 crystals were analysed. The observed rims yield similar ages with the rest of the population. Data scatters so that concordia age cannot be calculated, thus we interpret the weighted average of $^{207}Pb/^{206}Pb$ ages, 2803±6 Ma as the best estimate of crystallisation age of this rock (Fig. 48B). Scatter is likely caused by lead loss associated with later event(s).

9.1.11 A2532 Kolmoset tonalite

Kolmoset tonalite (A2532) is a strongly oriented biotite tonalite and represents the dominant Archaean rock type north of Puutosmäki. Zircon grains of the sample mainly display oscillatory zoning and in some cases core-rim structures. Altogether 39 spots from 31 grains were analysed with LA-SC-ICPMS, out of which 4 spots with central concordance ≤90% were rejected. The remaining 35 spots display $^{207}Pb/^{206}Pb$ ages from 2488 to 2747 Ma with a distinct cluster at 2700 Ma (Fig. 48C). The four youngest spots are all from rims. If the eight youngest spots not overlapping in age with the main group are removed, a weighted average of 2708±7 Ma can be calculated, which we regard as the best estimate for the crystallisation age of this tonalite. The meaning of the <2600 Ma rims remains open as metamorphic ages from this period have not previously been reported from the region.

9.1.12 A2533 Vasikkasaaret tonalite

Vasikkasaaret tonalite sample (A2533) originates from a thrust sheet of biotite tonalite hosting abundant diabase dykes within the Raahe-Ladoga zone 9 kilometres south of Leppävirta (Fig. 45). Abundant core-rim structures characterise the zircon population and 54 spots from 34 grains were analysed. Three spots were rejected due to high discordance. The remaining spots have $^{207}Pb/^{206}Pb$ ages varying from 1831 to 2823 Ma with clusters at 1850–1950 Ma and 2600–2800 Ma (Fig. 47D). All of the ages younger than 1950 Ma are from analysed rims, which also display lower U concentrations (<75 ppm) than the analysed cores. The older cluster consisting of all of the analysed cores and grains lacking core-rim structures in addition to four rims form a continuum and do not display significant differences in composition. Thus, in respect to crystallisation age it can be only said that the sample is Archaean. The younger cluster is interpreted as a result of metamorphic overgrowth during Svecofennian orogeny.

9.1.13 A2527 Ryönänpelto tonalite

Ryönänpelto tonalite sample (A2527) represents a biotite tonalite dyke belonging to the Haukivesi suite and intruding into migmatitic paragneisses of the Suonenjoki suite. Morphologically the zircon population can be divided into two groups; larger, more equidimensional, and strongly prismatic, smaller grains. A total of 39 spots from 39 grains were analysed and 2 of the these were rejected due to high common lead. The remaining spots have $^{207}Pb/^{206}Pb$ ages varying from 1828 to 2834 Ma (Fig. 48E). We interpret the ten oldest ages, all from larger, equidimensional group, to be from inherited zircons as they are older than 1910 Ma, which is the maximum age of this dyke based on the maximum deposition age of the paragneiss it intrudes into (A2526, see below). The remaining spots scatter, preventing calculation of a concordia age. Weighted average $^{207}Pb/^{206}Pb$ age of 1872±9 Ma calculated from them is, in our interpretation, despite high MSWD (6.2), the best estimate for the crystallisation age of this dyke. The prismatic zircon grains likely represent crystallisation from the magma and similar ages from the equidimensional larger crystals are caused by complete resetting of U-Pb systematics of the inherited zircons. Extensive scatter in ages is associated with emplacement during high grade metamorphic conditions into a major shear zone.

9.2 Paragneisses

In paragneiss samples, results with concordance lower than 90% were automatically rejected. The term patchy is used to characterise zircon grains displaying inhomogeneities but not typical magmatic oscillatory zoning in BSE images. Spots from homogeneous grains or overgrowths have been interpreted as metamorphic.

9.2.1 Viinijärvi suite

9.2.1.1 A2528 *Piiroonmäki paragneiss*

Piiroonmäki paragneiss sample (A2528) is from a drill core intersecting also rocks of the Outokumpu assemblage south of our main study area (Fig. 45). The sample is interpreted to represent the Viinijärvi suite. Zircon grains are typically either patchy or display oscillatory zoning, homogeneous grains are rare. Core-rim structures are relatively common, but often too narrow for dating. Altogether 63 spots were analysed from 55 grains, of which 2 were rejected based on discordance. Lead-lead ages of the Palaeoproterozoic spots vary from 1855 to 2070 Ma and Archaean spots from 2651 to 2870 Ma, respectively. Morphology of the grains and the observed age do not display clear correlation. The youngest observed ages are mainly from grains with higher than average common lead. It could be that these grains were more prone to periodic lead-loss in addition to higher analytical uncertainties. Likelihood of lead-loss is increased by the sample being metamorphosed in a higher degree than the rest of the Viinijärvi suite (Hölttä & Heilimo 2017). Thus, our interpretation is that the maximum deposition age of this sample is 1.90 Ga (Fig. 49).

9.2.1.2 A2529 *Valkeinen paragneiss*

Valkeinen paragneiss sample (A2529) is taken west of the Suvasvesi intrusion from a drill core intersecting rocks of the Viinijärvi suite. The majority of the zircon grains are either patchy or display clear oscillatory zoning. Homogeneous ones exist, but their number is small. Grains are characterised by abundant inclusions and narrow overgrowths, similar to those in the Piiroonmäki sample. Metamict domains are also common. Altogether 51 spots from 45 zircon grains were analysed, of which three were rejected based on high discordancy. Palaeoproterozoic $^{207}Pb/^{206}Pb$ ages vary from 1911 to 2489 Ma and Archaean from 2632 to 3094 Ma (Fig. 49). Morphology of the analysed spot and its lead-lead age do not display any clear correlation. Based on the data, the maximum deposition age for this sample is interpreted as 1.92 Ga.

9.2.1.3 A2535 *Hepomäki cordierite paragneiss*

Hepomäki cordierite paragneiss was taken from the vicinity of the Juojärvi domes, from an area earlier interpreted as part of the Juojärvi suite which is correlative with the Levänen group of the Karelia supergroup. The zircon population is dominated by grains with clear oscillatory zoning, patchy and homogeneous grains are clearly less abundant. Morphoplogy of the analysed spot and its lead-lead age do not display any clear correlation. A total of 71 spots from 65 grains were analysed, out of which 18 spots were rejected due to high discordance. Lead-lead ages of the Palaeoproterozoic spots varied from 1923 to 2280 Ma. Ages of the Archaean zircons varied from 2684 to 2942 Ma (Fig. 49). Our interpretation is that maximum deposition age of this sample is ca. 1.93 Ga.

9.2.1.4 A2534 *Salkolahti paragneiss*

Salkolahti paragneiss sample (A2534) was taken from between the Juojärvi domes and the main Kuopio complex and represents typical unmigmatised paragneiss of the Viinijärvi suite in this area. Zircon population is dominated by grains displaying patchy or weak oscillatory zoning, homogeneous ones are rarer. Homogeneous overgrowths too narrow for dating are common. Altogether 66 spots were analysed from 61 grains. Three spots were rejected due to discordance. Palaeoproterozoic spots yielded ages from 1848 to 2453 Ma and Archaean ones from 2651 to 2935 Ma (Fig. 49). Morphoplogy of the analysed spot and its lead-lead age do not display any clear correlation. Two youngest spots contain relatively high common lead and are interpreted as a result of ancient lead-loss. When these two spots are excluded, the maximum deposition age of the sample is 1.91 Ga.

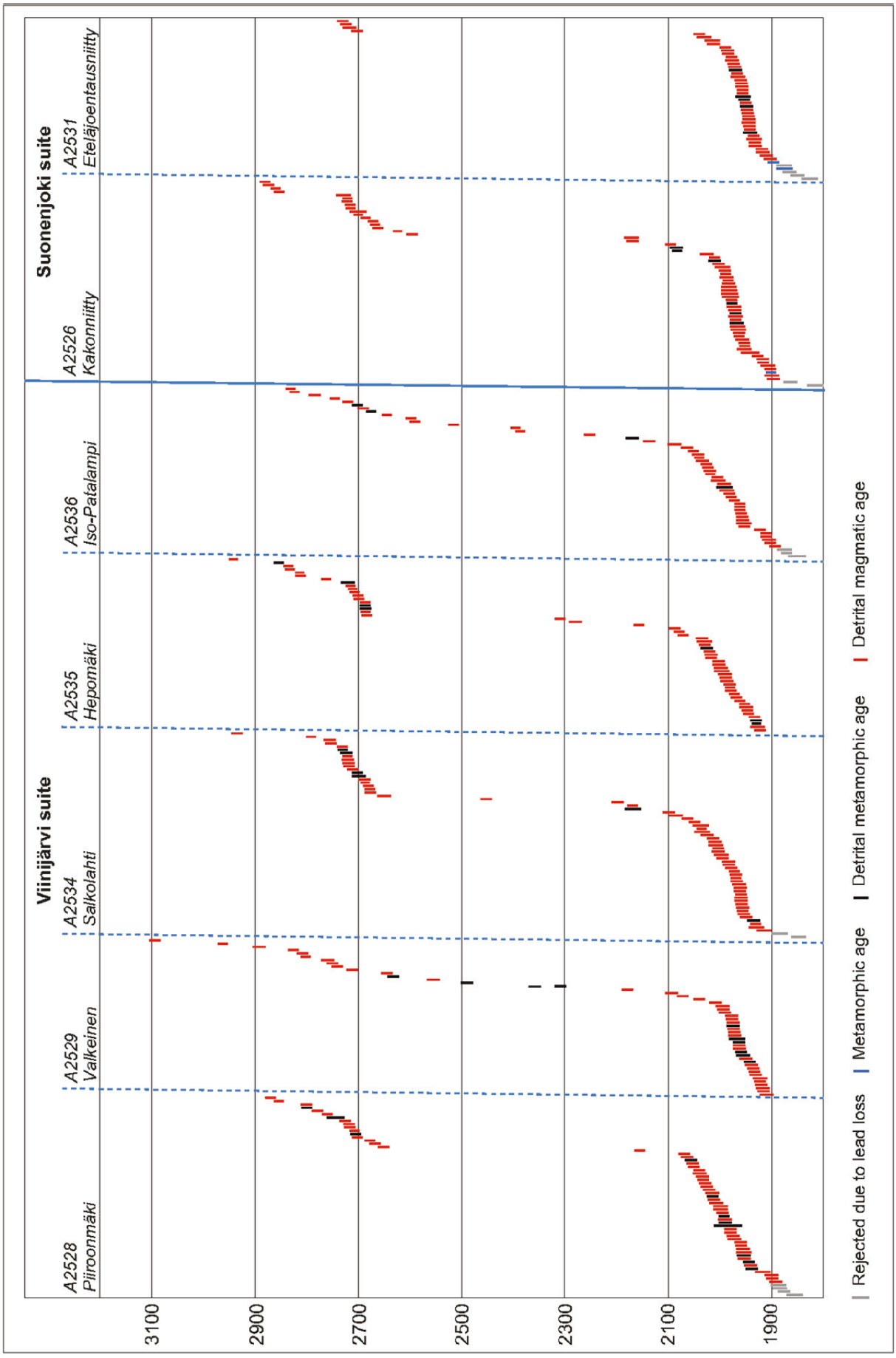

Fig. 49. $^{207}Pb/^{206}Pb$ Ages of all analysed spots from the paragneiss samples. Error bars drawn at 2σ.

9.2.1.5 A2536 Iso-Patalampi kyanite-cordierite paragneiss

Iso-Patalampi kyanite-cordierite paragneiss sample (A2536) was taken near the contact between the Kuopio complex and Viinijärvi suite paragneisses from an area earlier interpreted as belonging to the Levänen group. Zircon population consists mainly of patchy and oscillatory zoned crystals, often with narrow overgrowths. Homogeneous crystals are typically more rounded and smaller than the other morphological types. Altogether 53 spots from 51 grains were analysed and out of these one rejected due to high discordance. Lead-lead ages of the Palaeoproterozoic grains vary from 1851 to 2396 Ma and Archaean from 2516 to 2831 Ma (Fig. 49). Morphoplogy of the analysed spot and its lead-lead age do not display any clear correlation. The three youngest ages are from spots yielding relatively high common lead concentrations, which could indicate crystal properties making them more prone to periodic lead loss. Based on the remaining spots, we interpret 1.90 Ga as the likely maximum deposition age of this sample.

9.2.2 Suonenjoki suite

9.2.2.1 A2526 Kakonniitty migmatitic paragneiss

Kakonniitty migmatitic paragneiss sample (A2526), taken from the Suonenjoki suite, consists of narrow bands of trondhjemite neosome and relatively coarsely-grained paragneiss (Fig. 45A). Morpohologically most of the zircon grains are oscillatory-zoned or patchy. Homogeneous grains are less common and a small number of clear core-rim structures are also observable. Relatively large inclusions and metamict domains are common, especially in the patchy grains. Altogether 63 spots from 56 grains were analysed. All of the spots are concordant or nearly concordant and $^{207}Pb/^{206}Pb$ ages of the spots fall in two groups: 1814–2172 and 2596–2880 Ma. No clear correlation between the morphology and observed age exists, although all of the homogenous grains are Palaeoproterozoic. Two youngest analysed zircon grains are patchy, display high common lead concentration (>1%) and likely display signs of later lead loss, and were thus excluded from estimation of maximum deposition age which, based on the remaining spots, is in our opinion ca. 1.90 Ga (Fig. 48). Out of the ca. 1900 Ma spots one is from a homogeneous rim and could represent a post-depositional metamorphic event, however the youngest morphologically clearly magmatic spots are of the same age.

9.2.2.2 A2531 Eteläjoentausniitty paragneiss

Eteläjoentausniitty paragneiss (Fig. 21C, A2531) is from the vicinity of the Konnuslahti dome and represents the well preserved, intensively folded paragneisses of the Suonenjoki suite flanking the dome on its west side. Again, the majority of the zircon grains display oscillatory zoning or are patchy in BSE pictures, homogeneous ones are a minority. A certain number of rim structures is also observable. Altogether 55 spots were analysed from 50 grains, and out of these six were rejected based on discordance. The zircon population is dominated by Palaeoproterozoic grains (40 out of 44) with $^{207}Pb/^{206}Pb$ ages from 1827–2040 Ma. The limited Archaean population yielded ages from 2703 to 2730 Ma. Morphoplogy of the analysed spot and its lead-lead age do not display any clear correlation. Again, the youngest obtained ages have relatively high common lead concentrations, making them more prone to post-crystallisation disturbance. Thus we interpret 1.91 Ga as the maximum deposition age of this sample. The two remaining youngest ages are from a homogeneous rim and grain, which could possibly indicate metamorphism of the sample at 1900–1875 Ma.

10 GEOPHYSICAL DATA

10.1 Petrophysics

Densities of the 12 most common rock types among the petrophysical samples are presented in Figure 50. Amphibolite, diabase, and mafic vulcanite samples have clearly higher density than other common rock types, whereas differences between granitoids and paragneisses are more subtle.

Magnetic properties of the 12 most common rock types among the petrophysical samples are presented in Figure 51. Magnetic susceptibility is typically low varying from -100 to 1000 (SI 10^{-6}) and remanent magnetisation below 100 mA/m. If the remanent magnetisation is high compared to the induced magnetisation, it is particularly important to take remanent magnetisation into account in magnetic modelling. Induced magnetisation is proportional to magnetic susceptibility. Magnetic susceptibility is displayed in logarithmic scale so negative values are cut of out the chart.

Figure 52 compares densities and magnetic susceptibilities of the 12 most common rock types, which helps to classify rock types geophysically. For example, serpentinite stands out from the other samples by its high magnetic susceptibility and low density. As in Figure 50, the use of field names may cause large deviation in the data.

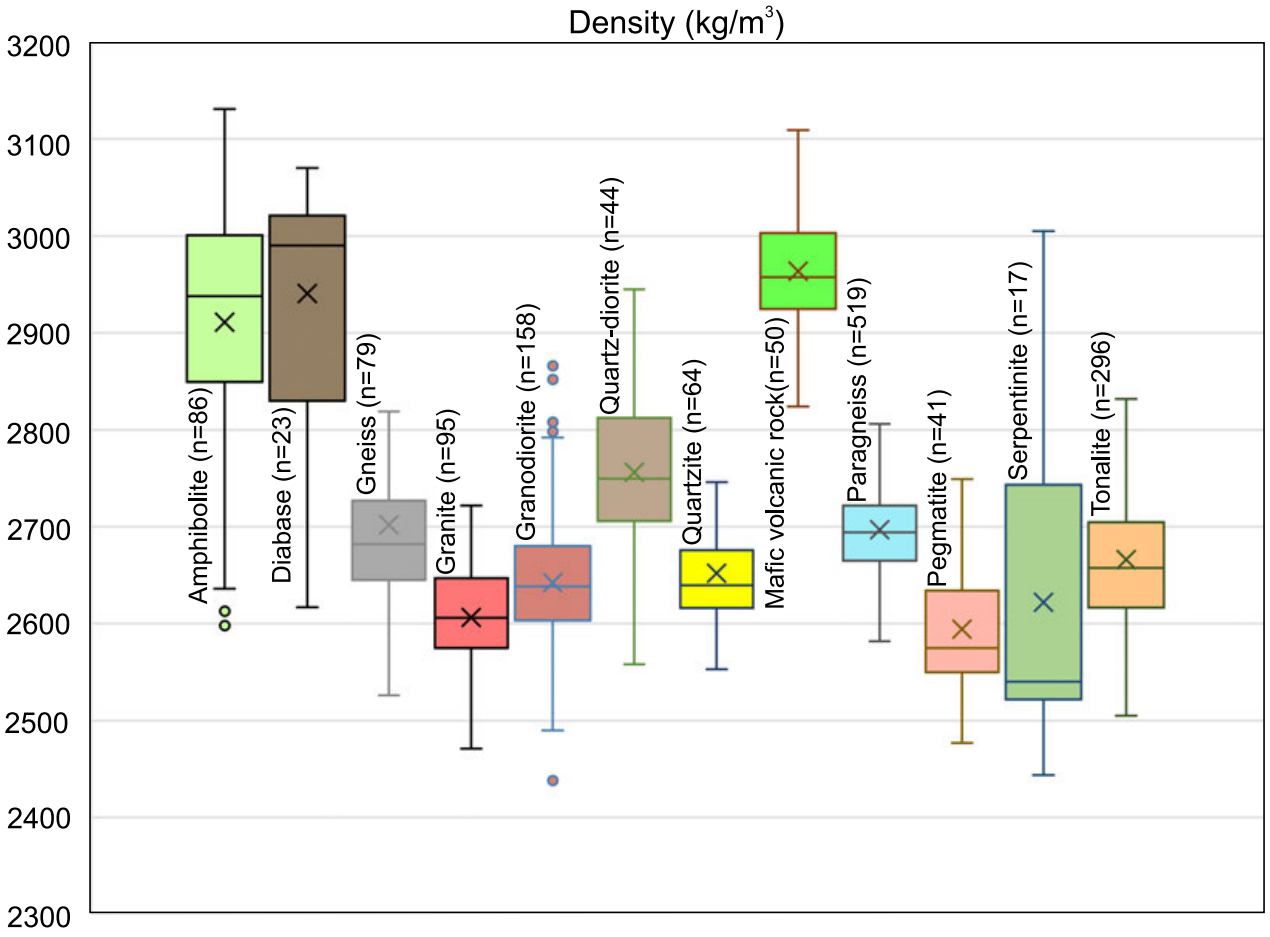

Fig. 50. A) Densities of the 12 most common rock types of the petrophysical samples, which represent 71% of the 2,014 samples measured for their petrophysical properties. The rock type of some of the samples was missing. The boxes range from the 1st to 3rd quartile of the data and whiskers extend to the farthest point in the dataset that is not an outlier. Outliers are data points which are more than 1.5 * IQR above the third quartile or below the first quartile. (The interquartile range (IQR) is defined as the distance between the 1st quartile and the 3rd quartile.). Within each box, X stands for average value and line for median. Classification is based on the field name used by the observer and e.g. amphibolite group consists of unclassified diabases and mafic volcanic rocks. Use of field names likely results in larger than real deviation for each rock type and explains also the outliers, e.g. granodiorites with density >2800 kg/m^3.

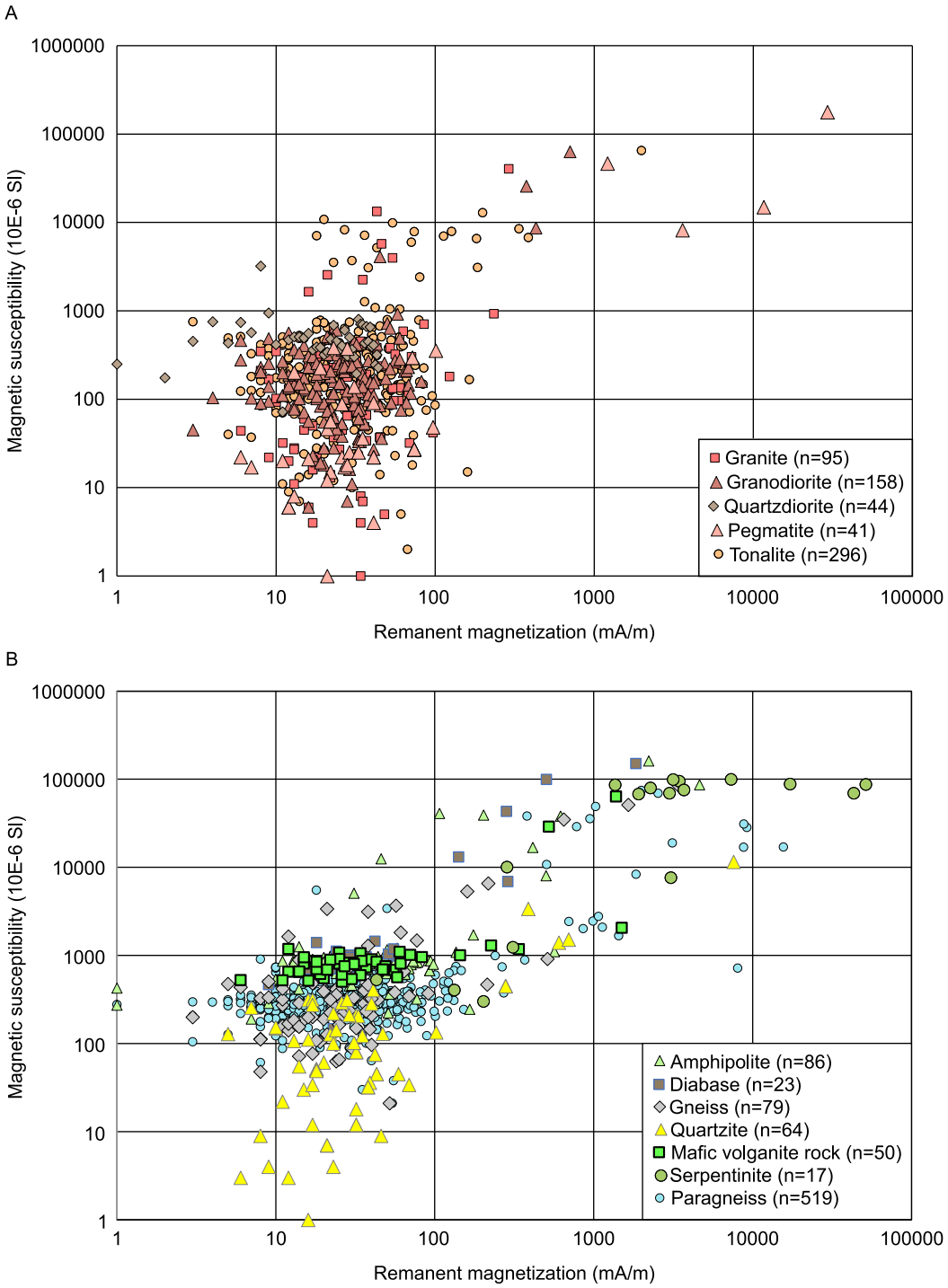

Fig. 51. Comparing magnetic susceptibilities and remanent magnetisations of A) felsic to intermediate plutonic rocks B) other rock types.

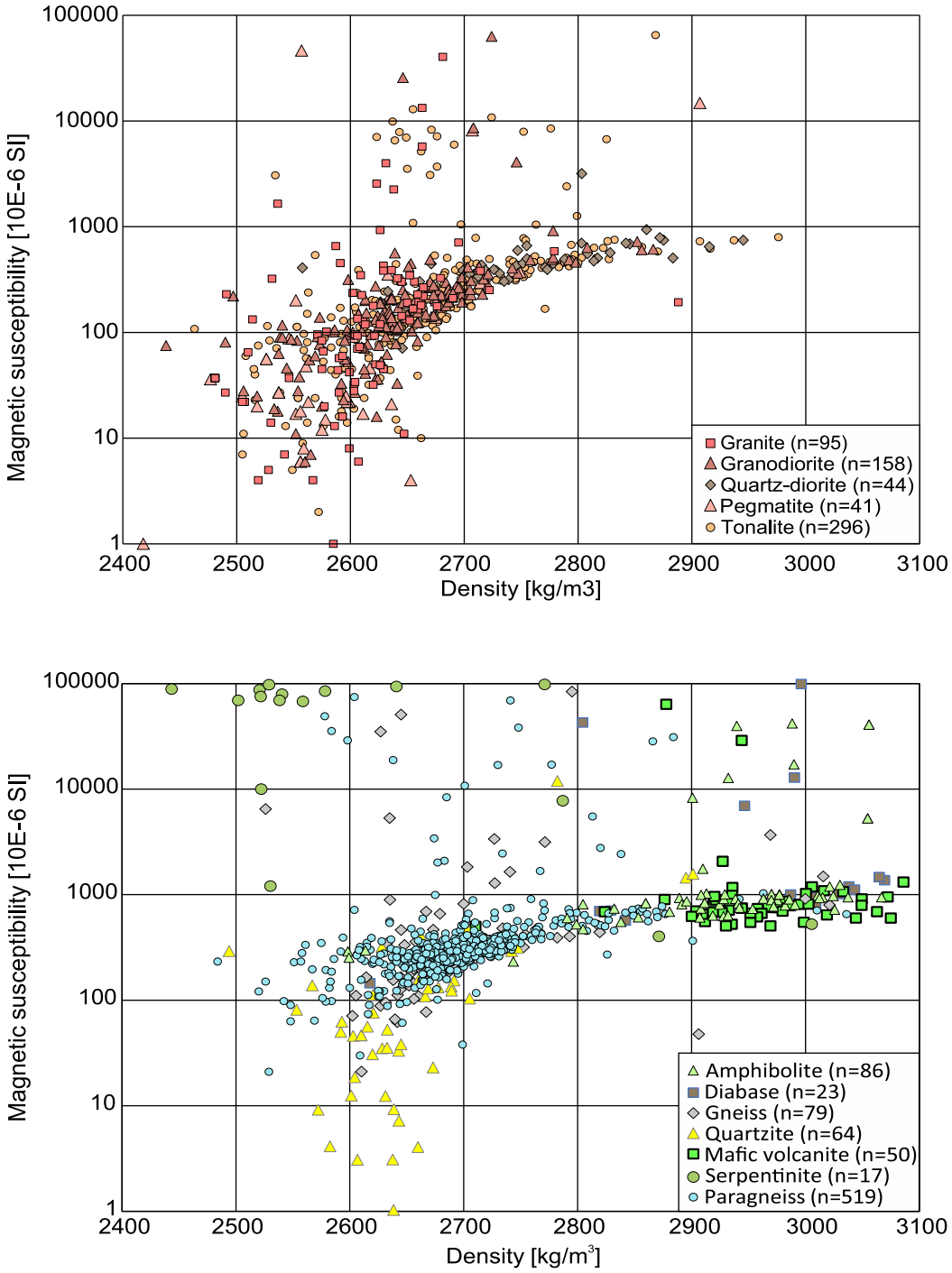

Fig. 52. Comparing magnetic susceptibilities and densities of A) felsic to intermediate plutonic rocks B) other rock types. Magnetic susceptibility values higher that 100,000 [10^{-6} SI] are cut out of the chart.

10.2 Airborne data and processings

East of the Suvasvesi granite and the Kuopio complex, the Viinijärvi suite hosts abundant, linear magnetic anomalies, which mostly coincide with similar conductivity anomalies. These anomaly combinations are interpreted as black schist interbeds in the paragneisses. The amount of outcrop observations from black schists are limited, but the existing drill core logging results confirm this interpretation (e.g. Vihreäpuu 1985a, 1985b).

West and north of the Suvasvesi granite, both the number and intensity of both magnetic and conductivity anomalies is distinctly smaller, but the existing anomalies are caused by black schists (Romu & Nousiainen 2020). In this subarea the background level of the anomaly is also higher than further east. As at the current erosion level the bedrock consists of similar paragneisses in both areas which, based on laboratory measurements, do not display differences in susceptibility the source of the magnetic anomaly is considered to be hidden. This is clearly visible by comparing the total magnetic intensity in Appendix 1 to the processing where the longer wavelengths have been removed (Appendix 4).

The anomaly pattern within the Suonenjoki suite resembles that of the Viinijärvi suite, abundant linear coinciding magnetic and conductivity anomalies. Also in this case the anomalies are interpreted as black schist interbeds.

The Suvasvesi shear zone is clearly visible as a conductivity anomaly, like few smaller faults within the Archaean Kuopio complex. In an area where paragneisses occur between the Archaean domes magnetic and conductivity anomaly similar to Suonenjoki and Viinijärvi suites are present, indicating that black schists are also present within these smaller paragneiss domains. Within the Archaean rocks, also linear magnetic anomalies missing an associated conductivity anomaly are present and interpreted as diabase dykes.

10.3 Gravity data and interpretation

On the Bouguer anomaly map (Appendix 1), the most striking feature is the large positive NNW-SSE striking anomaly that traverses the whole study area. Based on field observations, there is nothing in the surface geology that would explain the anomaly. The anomaly also cuts, in a small angle, the mainly N-S to NNW-SSW trends of the rocks in the area, observable both in the structural field and aeromagnetic data. Furthermore, it crosscuts even the Archaean-Proterozoic boundary, which is well constrained in the area. The anomaly seems to be bounded by the Suvasvesi shear zone, but in respect to it gives the impression of sinistral movement, contrary to the dextral character of the zone on the surface.

Based on numerical modelling, the anomaly described above is most likely caused by flat-lying sheet-like source. Depending on the density parameter (2.9–3.3 g/cm^3) used for the source, the upper surface is placed at a depth of 300–400 metres. For the smallest used density value, the thickness of the source is 1,500 metres and, for the largest, 550 metres.

The Suvasvesi granite is located in a strong negative anomaly, with the lowest values in central parts of the intrusion. This supports the interpretation made from the FIRE-3 line that the intrusion has considerable depth extent. If the extent was smaller, the relatively small difference in density between the Viinijärvi suite paragneisses and the intrusion (Fig. 50) would not result in significant anomaly.

The positive anomaly in the western part of study area coincides mostly with the boundary of the Viinijärvi and Suonenjoki suites. Based on geological observations, the regional positive anomaly is caused by a combination of abundant diabase dykes in the Archaean domes, mafic volcanic units on top of them and, to a lesser extent, by Proterozoic mafic intrusions belonging to Kotalahti and Haukivesi suites. Bedrock surface in the anomaly area, however, consists mainly of paragneisses. Thus it can be concluded that especially in this area the paragneiss thrust sheets overlaying the Archaean basement are relatively thin.

In the northwest corner of the study area an elongated SE-NW striking minimum is observable within the Archaean complex. The area is transsected by the Suvasvesi shear zone, and as the area, based on observations and aeromagnetic data, does not differ from the surroundings in respect to bedrock, the anomaly is interpreted as a result of tectonic brecciation. This interpretation is supported by elevated conductivity of the bedrock in the area.

10.4 Otuslampi seismic reflection profile

Based on outcrop mapping along the Otuslampi seismic reflection profile (for the location see Fig. 4), the bedrock consists of homogeneous paragneisses of the Viinijärvi suite. The seismic image has low fold because of sparse source distribution, but some reflectivity is observed in the stacked data. The quality of seismic images is best in the middle of the seismic section, and reflectivity is thus most prominent at these locations (Fig. 53). The quality of the seismic data is limited near the surface, but if the reflector marked with transparent yellow colour between CMP 120 and 160 is projected to the surface, it coincides with magnetic anomalies at CMP 170–180. These reflectors could originate from the black schist interlayers hosted by the Viinijärvi suite paragneisses. In the unstacked data, a reflector was observed at 560 ms two-way-travel time, corresponding with a depth of approximately 1,400–1,600 m. These reflections are also seen in the stacked data. The overall reflectivity characteristics show more prominent discontinuous reflectivity at 800–1,000 m depths, suggesting lithological changes.

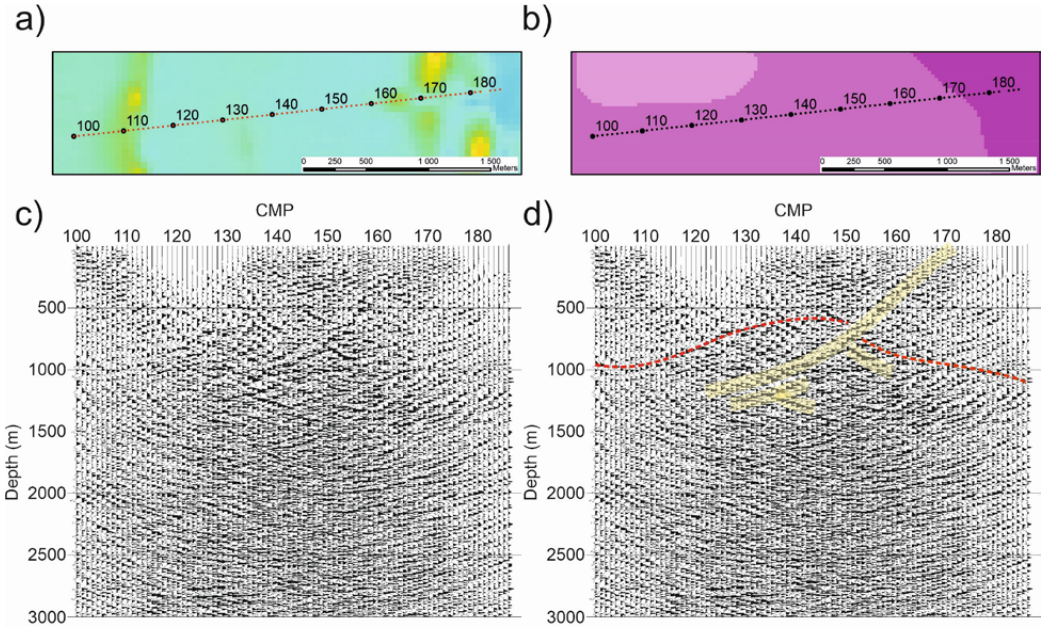

Fig. 53. Seismic reflection sections from Otuslampi and location of profile plotted on (a) an aeromagnetic and (b) gravity map (section 10.3). Data is of best quality where fold is highest, in the middle of the profile. c) Unmarked seismic image of the Otuslampi line. d) Seismic image of the Otuslampi line with the reflectors coinciding the magnetic anomalies discussed in the text marked with yellow and the dashed red line m.

11 3D INTERPRETATIONS

The main features included in the 3D model are the Suvasvesi shear zone, Archaean basement, Suvasvesi granite intrusion, granodioritic and dioritic intrusions, thrust zones and lithodemic units dominated by paragneisses of the Suonenjoki and Viinijärvi suites (Fig. 54). The 3D model can be found in pdf format as an Electronic appendix 2 of this publication.

Archaean basement outcropping, as extensive areas in the NW corner of the model and as several smaller domes and thrust sheets elsewhere, forms a continuos “bottom” of the model at depths of 1–3 kilometres. GeoModeller implicit approach was used to build the interface between the Archaean basement and younger suites as modelling these irregular boundaries with triangulated surfaces would have been difficult. This approach resulted in a randomly uneven surface. Dip of the contact between Archaean basement and the younger units was based on surface observations and structural interpretations based on them.

Interpreted major thrust planes (Outokumpu decollement thrust) taken to be associated with the D1 at 1910 Ma were included in the model. In addition to major synforms from D1, D2 and D3, shear fold surface associated with the Suvasvesi shear zone was included in the model (Fig. 54).

Suvasvesi shear zone is transected by the FIRE-3 line, and its behaviour at depth can be interpreted from it with some degree of certainty. In our model the shear zone changes orientation from nearly vertical to nearly horizontal in the depth of 12 km, marking a change from brittle to ductile deformation.

The Viinijärvi suite was divided into an area southwest of the Suvasvesi shear zone, an area inside the block bounded by a possible discontinuity in the north, D1 thrust in west and Suvasvesi shear zone in south (Fig. 55A). The third group consisted of the rest of the Viinijärvi suite paragneisses together with those of the Levänen suite.

Along the eastern boundary of the Suonenjoki suite against the Viinijärvi suite, a boundary zone (Fig. 56A) was separated from the rest of the unit. This zone contains outcropping Archaean rocks (Saamanen and Kotalahti domes). The zone is also visible as a positive gravity anomaly on a regional Bouguer anomaly map (Appendix 1).

The large positive NNW-SSE striking Bouguer anomaly traversing the study area and crosscutting the Archaean–Proterozoic boundary was modelled using 3D gravity modelling and included into the 3D model. Based on field observations, this anomaly must be caused by an unknown subsurface body or bodies, as the surface does not contain suitable sources. Possible source for this anomaly could be a relatively thin and dense layer (see 10.3) formed by mafic volcanic rocks (Fig. 55B) overlaying the Archaean basement, like typically observed along the craton boundaries.

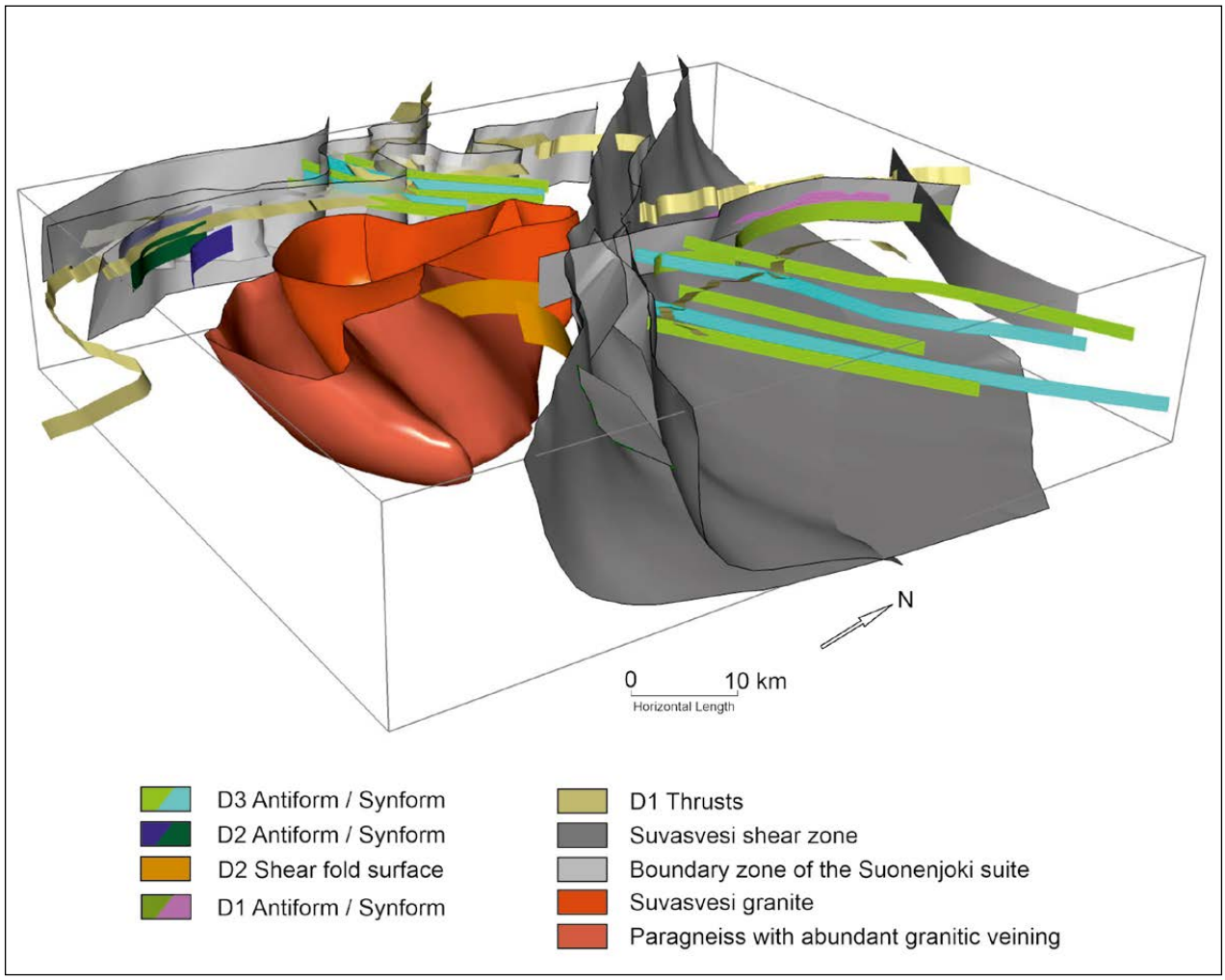

Fig. 54. Geological surfaces used in building the voxet model.

The Suvasvesi intrusion is clearly visible in the FIRE3 data as an area of low reflectivity extending down to ca. 10 km (Fig. 56). If this would be taken as the depth extent of the intrusion, its thickness would be roughly similar to the significantly larger rapakivi intrusions in SE Finland (Rämö & Haapala 2005). Based on field observation, the area of low seismic reflectivity continues SE of the intrusion to an area consisting of paragneisses with abundant granitoid veining. Analogously, if the intrusion is underlied by similar paragneisses with abundant veins (feeding the intrusion?) the depth of the granitoid mass could be significantly smaller than the mentioned 10 km.

The preliminary 3D geological model represents one possible alternative 3D interpretation. In the future, geophysical modelling and new interpretations of the regional geology will improve or totally change the presented subsurface 3D geological interpretation of the area.

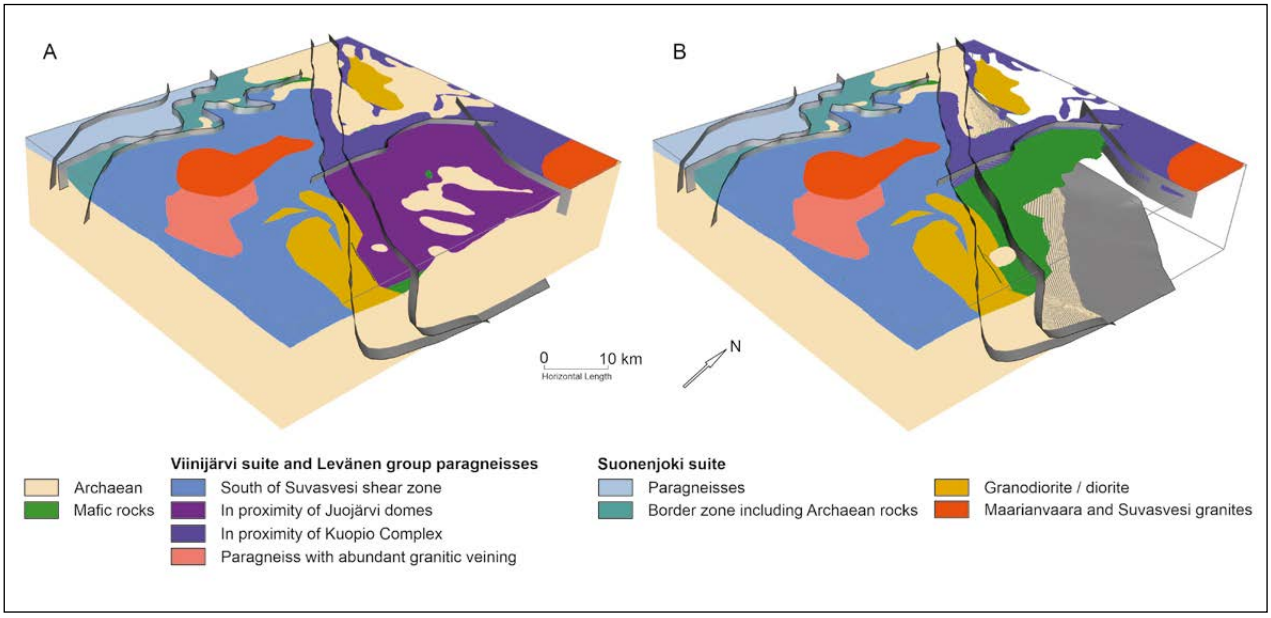

Fig. 55. A) Surface view of the 3D geological voxet model. B) 3D voxet model with units covering and underneath the hidden dense layer (in green) modelled based on gravity data removed.

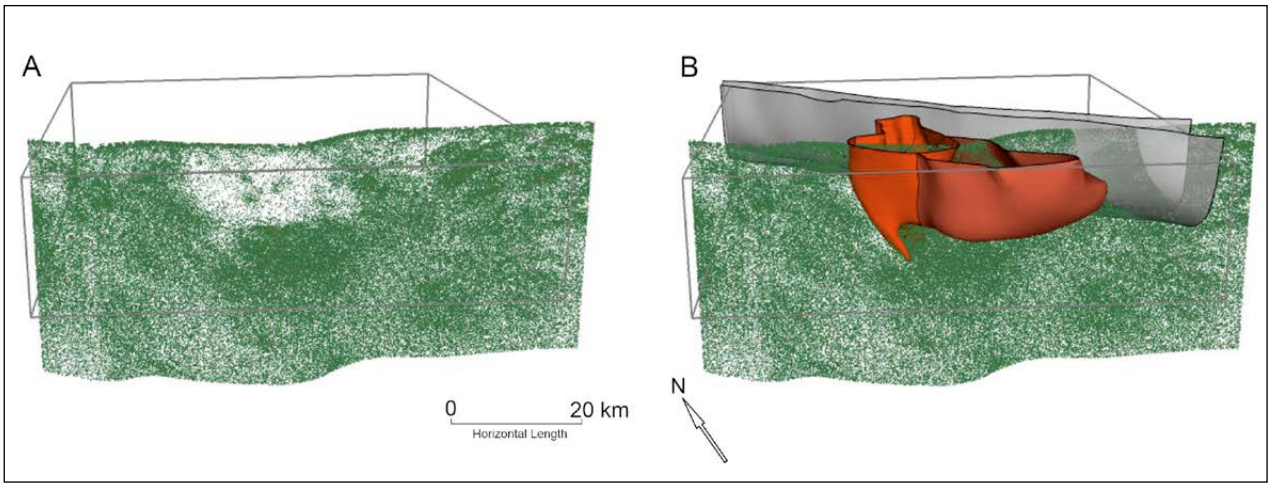

Fig. 56. A) Outlines of our 3D model together with seismic data from FIRE3 line, with absolute amplitude values (absamp) greater than 2.6 presented as a point cloud. B) 3D surfaces for the Suvasvesi intrusion (bright red), paragneiss domain with abundant veining (burgundy) and Suvasvesi shear zone (grey).arking the change in reflectitivity characteristics that might suggest lithological changes.

12 ORE POTENTIAL

12.1 Kotalahti type

In respect of Kotalahti-type ores, earlier projects in the area (e.g. Parkkinen 1974, Forss et al. 1999) concentrated in the Raahe-Ladoga suture zone. One of the research questions of the project was related to evaluating the likelihood of Kotalahti-type intrusions within the easternmost parts of the Viinijärvi suite. This was done by re-evaluating the existing layman's samples in this area and by testing some of the suitable geophysical anomalies with drilling. Neither of these approaches revealed any significant evidence for Kotalahti-type intrusions east of the potential areas delineated by Eilu et al. (2012) and Rasilainen et al. (2012). Also, the lack of suitable large structures between the Suvasvesi shear zone and contact of the Viinijärvi and Suonenjoki suites should be regarded as a factor lowering the possibilities for Kotalahti-type intrusions in this specific area.

12.2 Potential model for Outokumpu assemblage

Image processing of point-form, georeferenced geochemical data and low-altitude airborne geophysical data has been a part of mineral potential modelling and prospectivity mapping in Finland since the 1980's (e.g., Gaál 1988, Kuosmanen 1988, Aarnisalo 1990, Nykänen 2008, Leväniemi et al. 2017, Niiranen et al. 2019, Torppa et al. 2019, Torppa et al. 2021). The general aim of this study was to compute a set of regional pseudolithological GIS raster models using low-altitude aerogeophysical data (Fig. 57) and evaluate them together with lithogeochemical data in order to outline the most prospective areas for the ore potential Outokumpu-type assemblage. The main objective was to see if indications of Outokumpu-type mineralisation (Ekdahl 1993) and alteration zones enriched in Cu, Ni, Co, Cr, and S could be derived from large sets of aerogeophysical data with data analytical or raster calculation methods.

Special emphasis was given to the surroundings of the three "spatial outliers" southwest of the Suvasvesi shear zone: Kuolemanlahti, Piiroonmäki and Täilahti (Figs. 6, 58, 59 and 60). These targets are considered as allochthonous, structurally bound Outokumpu assemblage occurrences outside the essential area, but consisting of typical serpentinites, skarns, and quartz rocks, all with distinctive and characteristic concentrations of MgO, Cr and Ni (high), TiO_2 and Zr (low). Some members of the assemblage are variably missing from these locations as Kuolemanlahti does not contain serpentinite and Täilahti only contains serpentinite.

Another objective of the modelling was to investigate whether the approach could be used to distinguish between different paragneiss units of the region. It was regarded possible that subtle but systematic differences in composition could reveal differences in distributions between model class categories in the raster models.

12.2.1 Data and methods

Exploratory data analysis methods and tools were used to produce raster model and model evaluation data. The raster models (Figs. 57–60) were calculated from airborne electromagnetic (real or in-phase, imaginary or quadrature, and apparent resistivity or reversed conductivity) and magnetic image data (Airo 1999, Airo et al. 2014) available as raster data. The result model data were produced as GIS raster, vector, and text datasets.

The clustering tools of the ArcGIS application were used for each combination of three aerogeophysical electric evidence layers, with one magnetic evidence layer set to produce three model output layers with categorical classification representing pseudolithological response class for interpretation. Coverage of the model area was based on the extent of lithogeochemical data of the project. Model evaluation data were also extracted from the result raster model layers with ArcGIS tools per labelled bedrock sample with geochemical analysis of the project data (Table 5).

Output models are so-called pseudolithological models, i.e. geological interpretations of model values or categories. All raster data and models are of regional scale due to original airborne image data source (cell size 50 m x 50 m, raster size 3,601 columns x 2,521 rows). Derived datasets consisted of unsupervised iso-cluster models (text format), and categorical GIS model representation of them (raster format).

Data analyses of evaluation data were target-scale due to original lithogeochemical point data source (number of bedrock samples = 1,281). Pseudolithological model data for evaluation consisted of individual raster model pixel values that were extracted with ArcGIS tools from derived cluster models in Table 5 below (cell size 50 m x 50 m, number of model evaluation pixels = 1,281). The lithogeochemical data were explored with the IBM SPSS Statistics software to produce derived lithogeochemical variables for interpretation and model evaluation purposes.

Raster model evaluation data were combined as a table from the variables of the lithogeochemical dataset, including original concentration data and categorical bedrock type information of the project, computationally derived lithogeochemical variables, and the extracted sets of raster model data (Tables 5–9). The geo-referenced raster model datasets were visualised as maps (Figs. 57–61), and they can be visualised also in 3D GIS or geomodelling applications if a digital terrain model (DTM) is available, and the delivered file formats are being supported.

Geological expert opinion based on the existing knowledge of the authors on the Outokumpu-type lithogeochemistry was used to evaluate the suitability of using k-means clustered lithogeochemical main element oxide and rare earth element (REE) variables. Also, lithogeochemical data interpretation, especially related to Outokumpu-type rock and/or paragneiss, was used to evaluate clustered airborne geophysical GIS raster and point-form model datasets.

Table 5. Exploration and other study criteria, input evidence and lithogeochemical data for evaluating the GIS cluster models of airborne geophysical data.

Outokumpu assemblage: Sulphides present	BLACK SCHIST	Concentration of S (ppm)	High positive in-phase, paramagnetic to diamagnetic	In-phase and magnetic input layers combined by clustering
Outokumpu assemblage: Serpentinite present	SERPENTINITE	Concentration of MgO (%), FeO (%), Ni (ppm)	High magnetic susceptibility, negative in-phase or apparent resistivity	Apparent resistivity and magnetic input layers combined by clustering (Fig. 57, class 3)
Outokumpu assemblage: Skarn or calc-silicate rock present	SKARN	Concentration of Co, Cu, Cr, Ni (ppm)	Positive quadrature and magnetic responses	Quadrature and magnetic input layers combined by clustering
Outokumpu assemblage: Quartzite or quartz rock present	QUARTZITE, QUARTZ ROCK	Concentration of SiO_2 (%)	Low-magnetic or diamagnetic, low conductivity or non-conductive	In-phase or quadrature combined by clustering with magnetic data
Metasedimentary domain: paragneiss present	PARA	Concentration of K_2O, Na_2O, Al_2O_3, TiO_2 (%), Zr (ppm)	Various EM and magnetic responses	Areas with texturally uniform or zoned internal variation of various model units in clustered raster models

12.2.2 Outokumpu assemblage-type model responses

Classes of pseudolithological raster model set were mapped as spatial entities visually resembling bedrock geological interpretation (Fig. 57) and they were used as an aid in exploring the Outokumpu assemblage-type ore potential model classes. Known Outokumpu assemblage skarn occurrences display unique rock types that overlap each other in terms of their mineralogical content. Pseudolithological maps from Täilahti, Kuolemanlahti and Piiroonmäki (Figs. 58–60) all seem to have different compositions reflected on the maps. This may be due to the overlapping and complex mineralogy of the Outokumpu assemblage skarn rocks. For example, Kuolemanlahti pseudolithology shows skarn occurrences while Täilahti does not. However, regional resolution of the data may be too coarse to distinguish e.g. various skarn types.

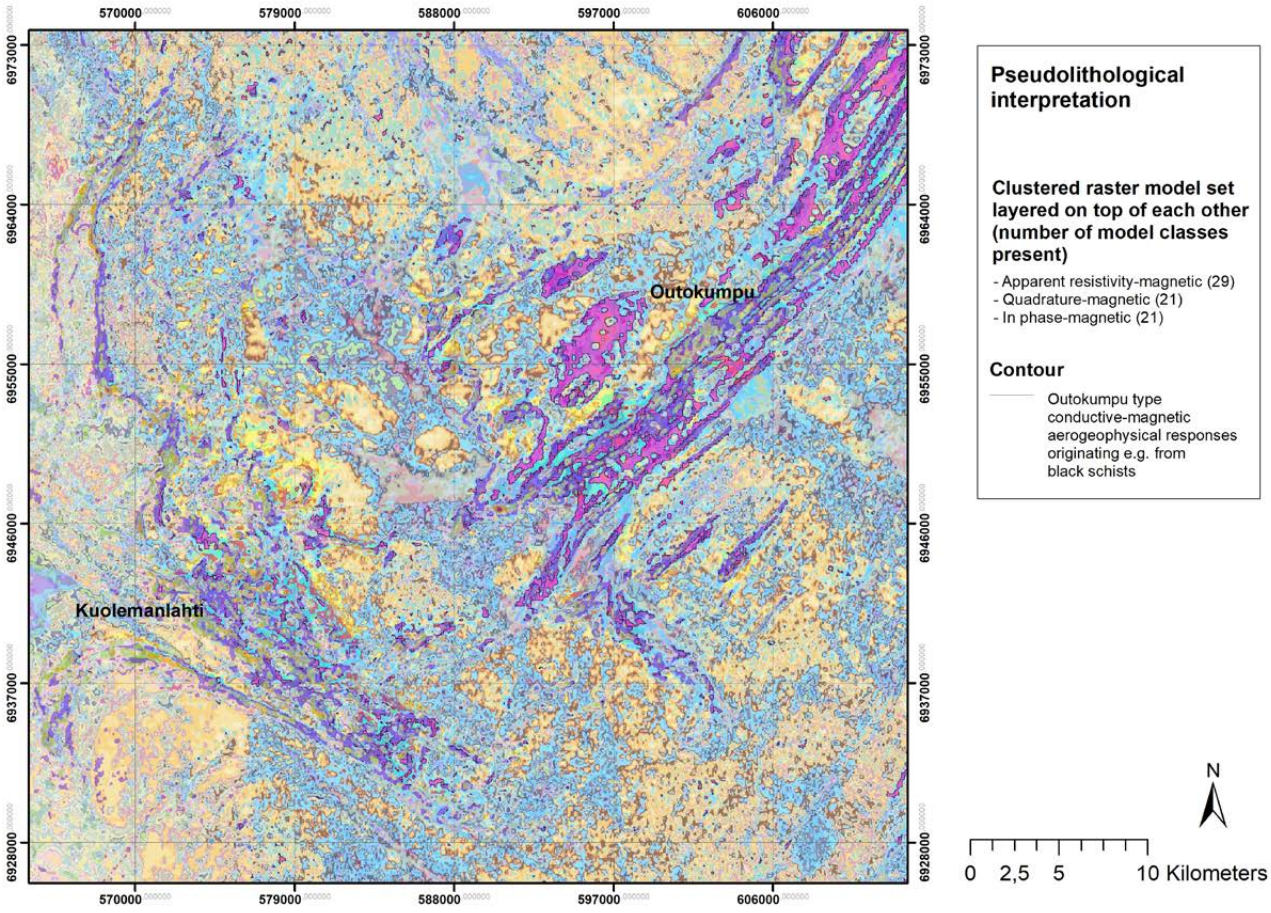

Fig. 57. The pseudolithological model set consisted of three clustered output layers, derived from originally continuous variables of airborne magnetic and electromagnetic raster data. The combined model set has been visualised class by class according to preliminarily interpreted bedrock type characteristics of each model class, the result is a combination of raster models resembling a bedrock map.

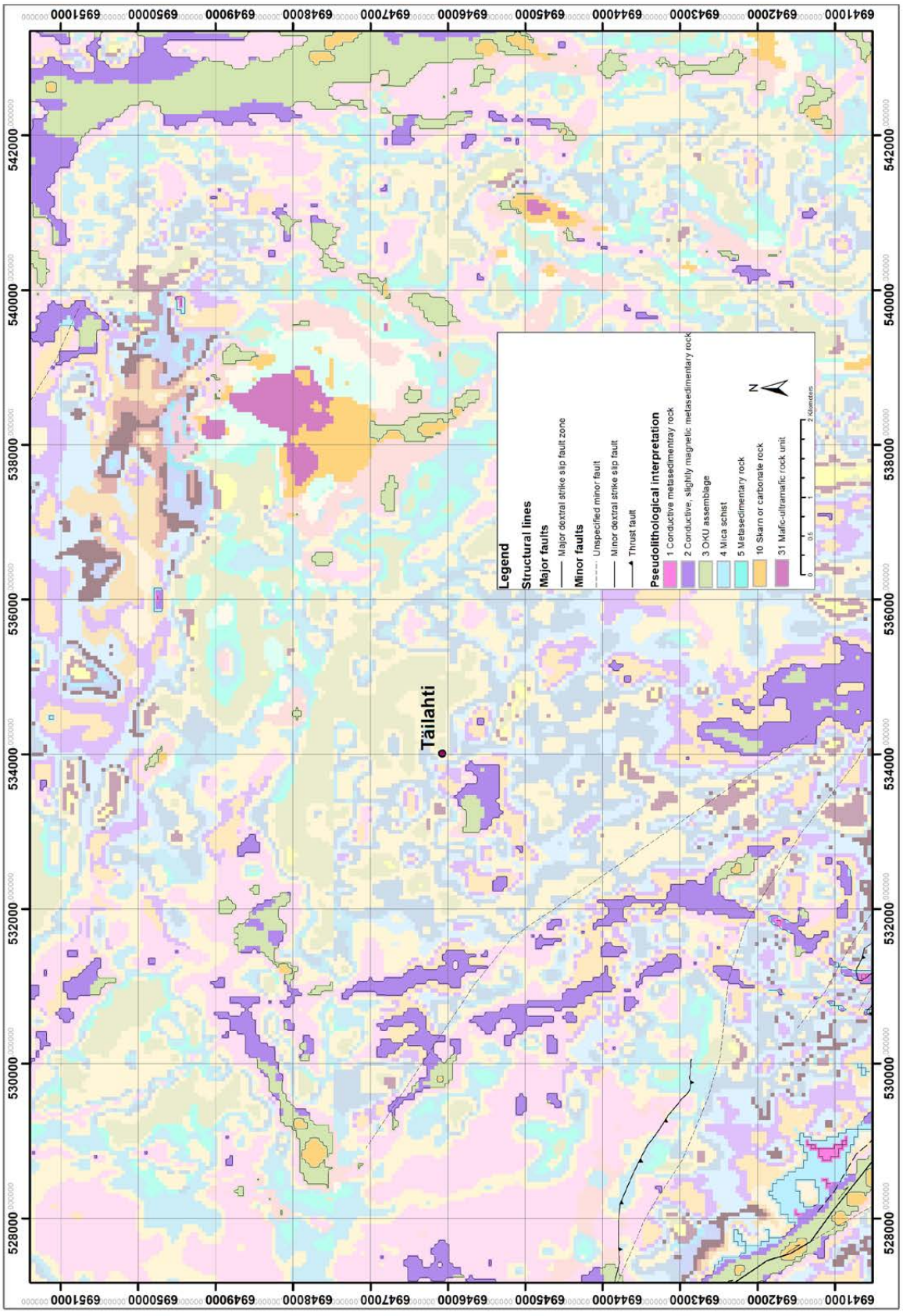

Fig. 58. Preliminary pseudolithological apparent resistivity–magnetic cluster model for areas surrounding the Täilahti occurrence. In this area, the model does not work well as a single model layer and most of the locations interpreted as Outokumpu assemblage (model class 3 = green pixels) are black schists and to a lesser extent mafic to ultramafic intrusives of the Kotalahti suite. The Täilahti occurrence does not show up in the model, most likely due to its small size relative to the cell size (50*50 m) of the used source data.

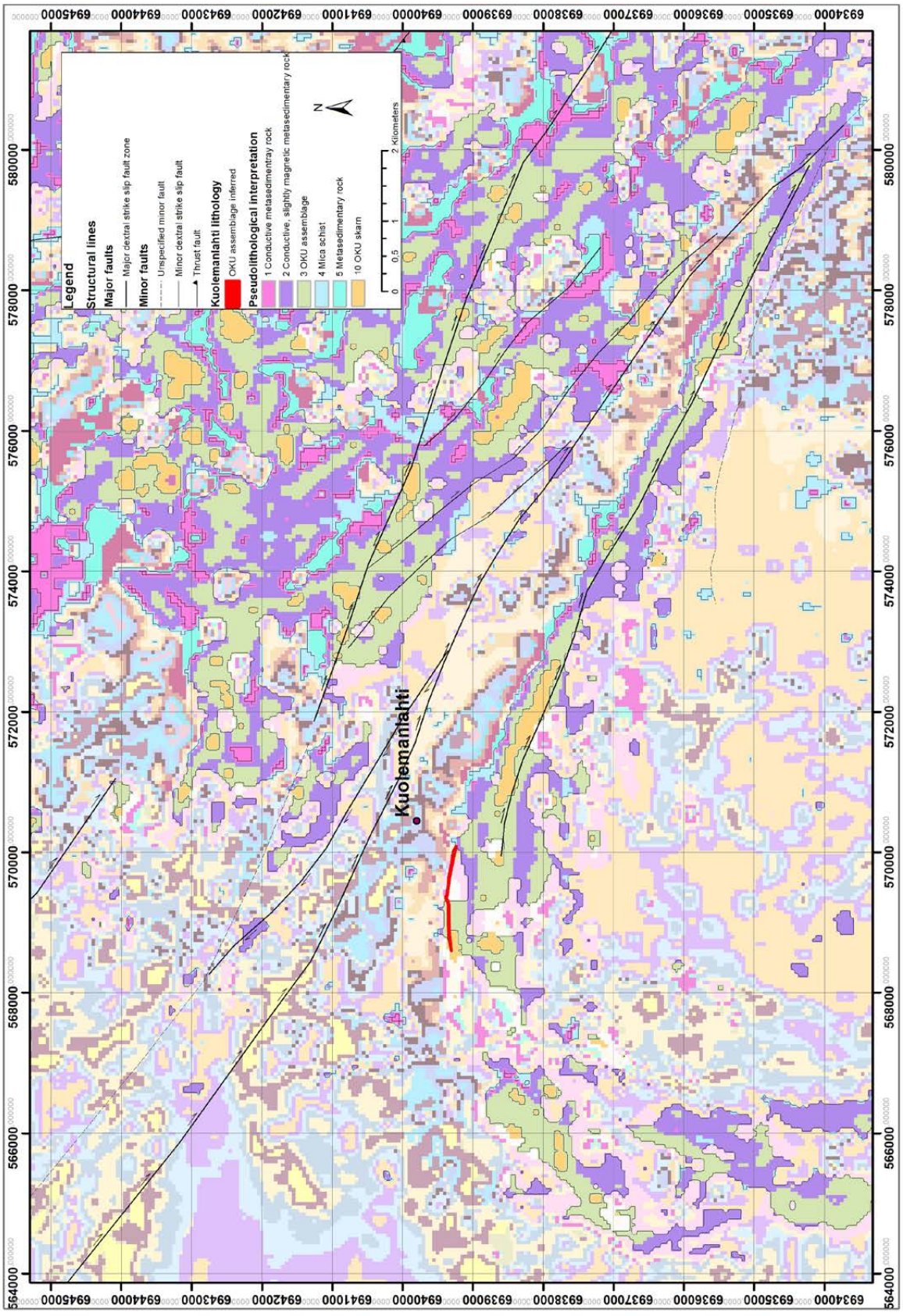

59. Preliminary pseudolithological apparent resistivity-magnetic cluster model for areas surrounding Kuolemanlahti. South of the Suvasvesi shear zone, transecting the map area in NW–SE direction, only a single "arc" of rocks classified as Outokumpu assemblage can be seen. This coincides well with the known locations shown as a red line. North of the Suvasvesi shear zone, the Outokumpu assemblage is more abundant, both in the model and based on the known occurrences (Appendix 1).

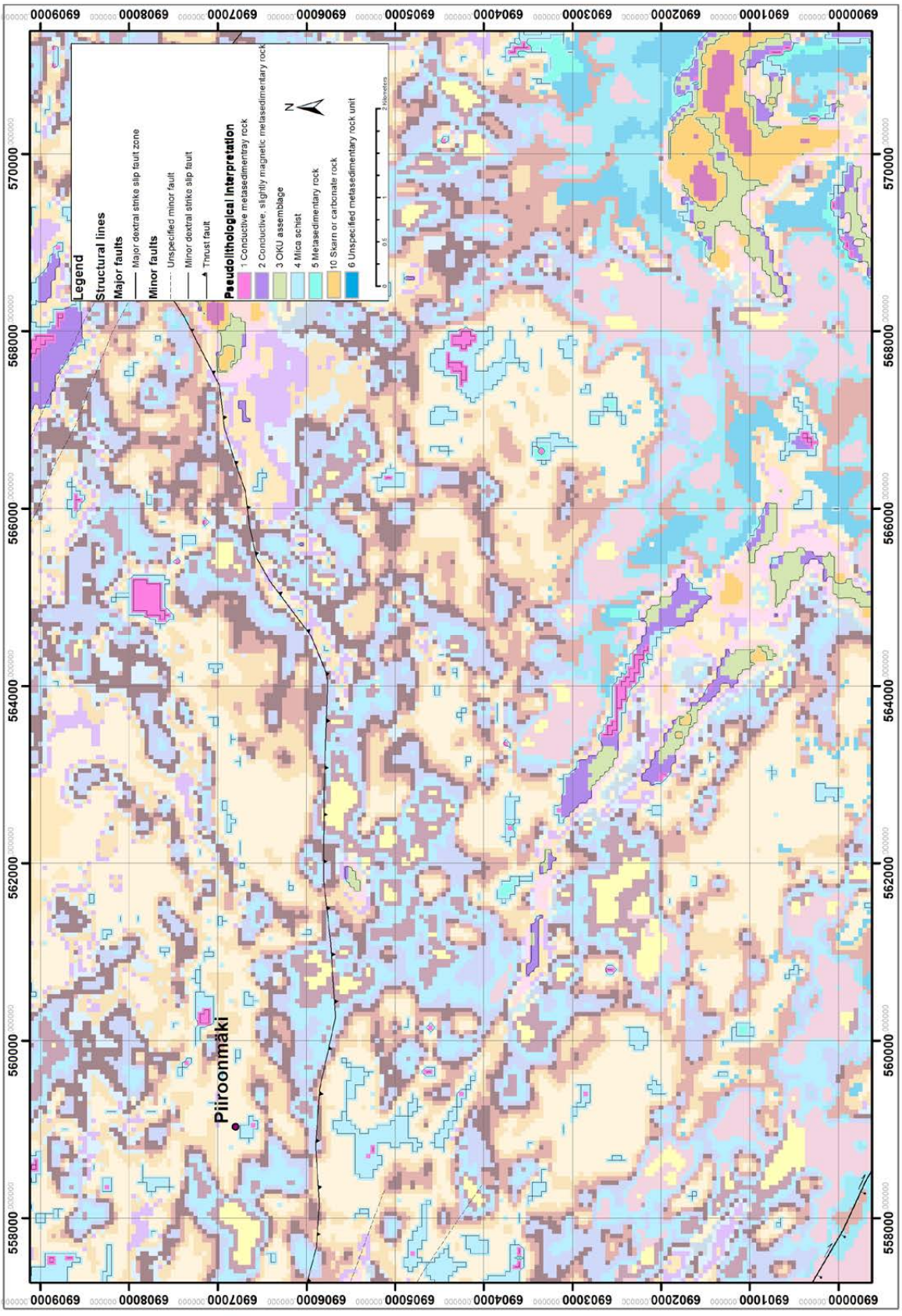

Fig. 60. Preliminary pseudolithological apparent resistivity-magnetic cluster model class values suggesting Outokumpu assemblage-type geophysical responses, originated e.g. from serpentinite or other mafic-ultramafic rock (model class 3 = green pixels) have been delineated with GIS tools from Piironmäki and its vicinity. The known occurrence in Piironmäki does not show in the model, most likely due to its small size relative to the cell size (50*50 m) of the source data. Structural lines from Bedrock of Finland – DigiKP.

The project's lithogeochemical database (n of rock samples = 1,281) served as the source of data for statistical evaluation. There was some variation in the naming of the rock types in the original database due to several generations of geologists responsible for the observations affecting the classification of rocks. While producing the k-means cluster values of the main element and REE data, the number of the clusters was determined experimentally (Tables 6–10).

The clustering results reveal some lithogeochemical differences between clusters, e.g. main element cluster centres resemble concentration typical to mafic (cluster 1), metasedimentary or non-mafic plutonic (clusters 3, 4, and 5) or carbonate rocks (clusters 2 and 6). Outokumpu assemblage-type trace elements Co, Cr, Cu, Ni, and S have somewhat higher concentrations in clusters 1, 4, and 5. Categorical values in mode of individual raster model layers may be overlapping between different layers, i.e. giving the same type of response classes to several bedrock types in clusters, thus making the interpretation or evaluation of the modelling results more ambiguous (Table 6).

Table 6. Lithogeochemical main element evaluation data were processed with a statistical k-means tool to produce clusters. The dataset consisted of 1,188 data rows of which the number of valid sample cases for clustering was 1,109. The number of missing cases was 79. The number of the final main element cluster center vectors was 6. Trace element concentration related to each cluster was presented as median values (n of valid cases).

Cluster	**1**	**2**	**3**	**4**	**5**	**6**
Number of cases in cluster	166	2	248	227	464	2
SiO_2 %	50,89	27,29	74,14	59,66	67,90	14,74
TiO_2%	1,36	0,20	0,37	0,99	0,65	0,08
Al_2O_3 %	13,95	1,92	13,11	16,71	14,89	1,12
FeO %	12,10	2,71	2,94	8,71	5,03	0,70
MnO %	0,19	0,13	0,04	0,10	0,07	0,29
MgO %	7,04	13,93	1,15	3,94	2,27	24,04
CaO %	10,03	31,14	1,84	3,28	2,63	57,41
Na_2O %	2,33	0,10	3,10	2,67	3,32	0,84
K_2O %	1,09	0,53	3,08	3,25	2,93	0,63
P_2O_5 %	0,23	0,29	0,10	0,25	0,17	0,16
Concentration (ppm) (number of cases)						
Co	46.5 (83)	7.5 (2)	5.5 (142)	24.0 (120)	13.0 (266)	0
Cr	110 (159)	40 (1)	73 (200)	146 (216)	102 (444)	0
Cu	83 (142)	1 (1)	17 (121)	54 (186)	23 (290)	0
Ni	74 (158)	21 (2)	31 (175)	85 (211)	46 (391)	0
S	879 (97)	300 (2)	499 (134)	1866 (208)	840 (358)	0
Zr	98 (162)	16 (2)	171 (248)	158 (225)	185 (464)	50 (2)
Pseudolithological model/Bedrock type (Categorical model class in mode)						
Apparent resisitivity-magnetic	MAFIC VOLCANITE (3)	CARBONATE ROCK (2)	MICA SCHIST (7)	MICA SCHIST (11), MICA GNEISS (14), MICA GNEISS MIGMATITE (15)	GRANODIORITE (8), PORPHYRITIC GRANITE (8)	CARBONATE ROCK (19, 21)
Quadrature-magnetic	MAFIC VOLCANITE (6)	CARBONATE ROCK (11, 18)	GRANODIORITE (6)	MICA SCHIST (6)	MICA SCHIST (6)	CARBONATE ROCK (8)
In-phase-magnetic	MAFIC VOLCANITE (12)	CARBONATE ROCK (15, 18)	GRANODIORITE (12)	MICA SCHIST (12)	GRANODIORITE (12), MICA SCHIST (12)	CARBONATE ROCK (12)
Pseudolithological interpretation by main groups	Mafic rocks dominating	Coarse clastic rocks	Paragneisses and non-mafic magmatic rocks, with slight Archaean flavor	Paragneisses dominating	Paragneisses somewhat dominating non-mafic magmatic rocks, with Archaean flavor	Coarse clastic rocks

The clustering results of evaluation raster model data were also compared to the distribution of the main geologically labelled bedrock groups of the study area to enhance the interpretation and evaluation of the modelling results (Tables 7 and 8).

Table 7. Distribution of main characterised bedrock groups of the project area.

Main group	Frequency (n)	Valid (%)
Archaean	81	6,3
Coarse clastic sediment	40	3,1
Not identified	11	0,9
Outokumpu assemblage	51	4,0
Paragneiss	646	50,4
Mafic rocks	119	9,3
Proterozoic plutonic rocks	333	26,0
Total	1281	100,0

In the k-means clustered lithogeochemical evaluation data, Outokumpu assemblage rocks were mostly classified as cluster number 1, as were almost 90% of mafic rock samples, too. Coarse clastic rock samples were mostly occurring in cluster number 3. Cluster number 4 was characterised by paragneisses with over 70% dominance of the cluster samples, while cluster number 3 had paragneisses and Proterozoic plutonic rocks almost evenly with over 40% share of both. Over 50% of Archaean rock samples were present in cluster number 5, which was the most abundant cluster in frequency. Almost 60% of cluster number 5 comprised of paragneisses, also representing almost 50% of all paragneiss samples in the clustered lithogeochemical dataset. Clusters number 2 and 6 consisted only of 2 samples each. According to more detailed bedrock classification information of the sample database, these 4 samples appeared to be carbonate rocks (Tables 6 and 8).

Table 8. Distribution of cases of k-means clustered lithogeochemical data representing main geological group labels in different clusters. Unevenness of the total count of samples between tables 7 and 8 is due to some bedrock samples missing lithogeochemical main element oxide data needed to the clustering.

Main group/Cluster	1	2	3	4	5	6	Total
Archaean	0	0	21	8	48	0	77
Coarse clastic sediment	3	2	12	4	9	2	32
Not Identified	3	0	1	1	4	0	9
Outokumpu assemblage	7	0	1	1	1	0	10
Paragneiss	23	0	105	165	278	0	571
Mafic rocks	102	0	5	9	1	0	117
Proterozoic plutonic rocks	28	0	103	39	123	0	293
Total count	166	2	248	227	464	2	1109

All 17 project serpentinite samples had missing lithogeochemical clustering results due to some lacking main element oxide concentration data, so the evaluation was conducted by comparing the distribution of serpentinite labels to the model classes of extracted evaluation data (Table 9).

If the results are considered qualitative but in accordance with raster layer model characteristics, cluster 1 could represent Outokumpu-type and other mafic rocks, and cluster number 4 sulphidised metasedimentary rocks, e.g. black schists. Cluster number 3 could be considered more quartz-bearing (the highest number of SiO_2 in cluster) and biotite-bearing (a higher number of K_2O in cluster), and not as much as sulphidised (conductive) paragneisses or Proterozoic plutonic rocks in cluster number 5 (Tables 6–9).

Table 9. Rock type samples with label 'SERPENTINITE' were scattered to more than one model class categories in all three evaluation datasets of raster values extracted from the clustered raster model datasets. This suggests that more than one type of serpentinite occurs in the study area.

		Cluster number of cases	Raster value of the apparent resistivity-magnetics cluster model	Raster value of the quadrature-magnetics cluster model	Raster value of the in-phase-magnetics cluster model
N (rock samples)	Valid	0	17	17	17
	Missing	17	0	0	0
Mode (model class)			3	6	12
Frequency of model class in mode (%)			7 (41.2)	5 (29.4)	7 (41.2)

12.2.3 Paragneiss type model responses

Usability of the modelling results in identifying any spatial or other sub-groups of paragneisses were studied with k-means clustered REE and Zr data. Lithogeochemical REE model clusters were crosstabulated with raster model values to calculate the mode of occurence of the most abundant raster model value in each REE cluster (Table 10 and Fig. 61). Differences between lithogeochemical REE clusters were not very distinctive but, when combined with other lithogeochemical data and interpretation of raster model evaluation data, the differences between regional spatial distributions were notable (Fig. 61).

Most of the evaluation rock samples were of metasedimentary origin (Tables 7 and 8), which was also the case in regional interpretation of computationally derived mapping of pseudolithological units of the bedrock of the study area (Figs. 57 and 61). Paragneisses were interpreted to be distributed in individual clusters of metasedimentary rock units and e.g. Levänen suite paragneisses seem to differ from other paragneisses.

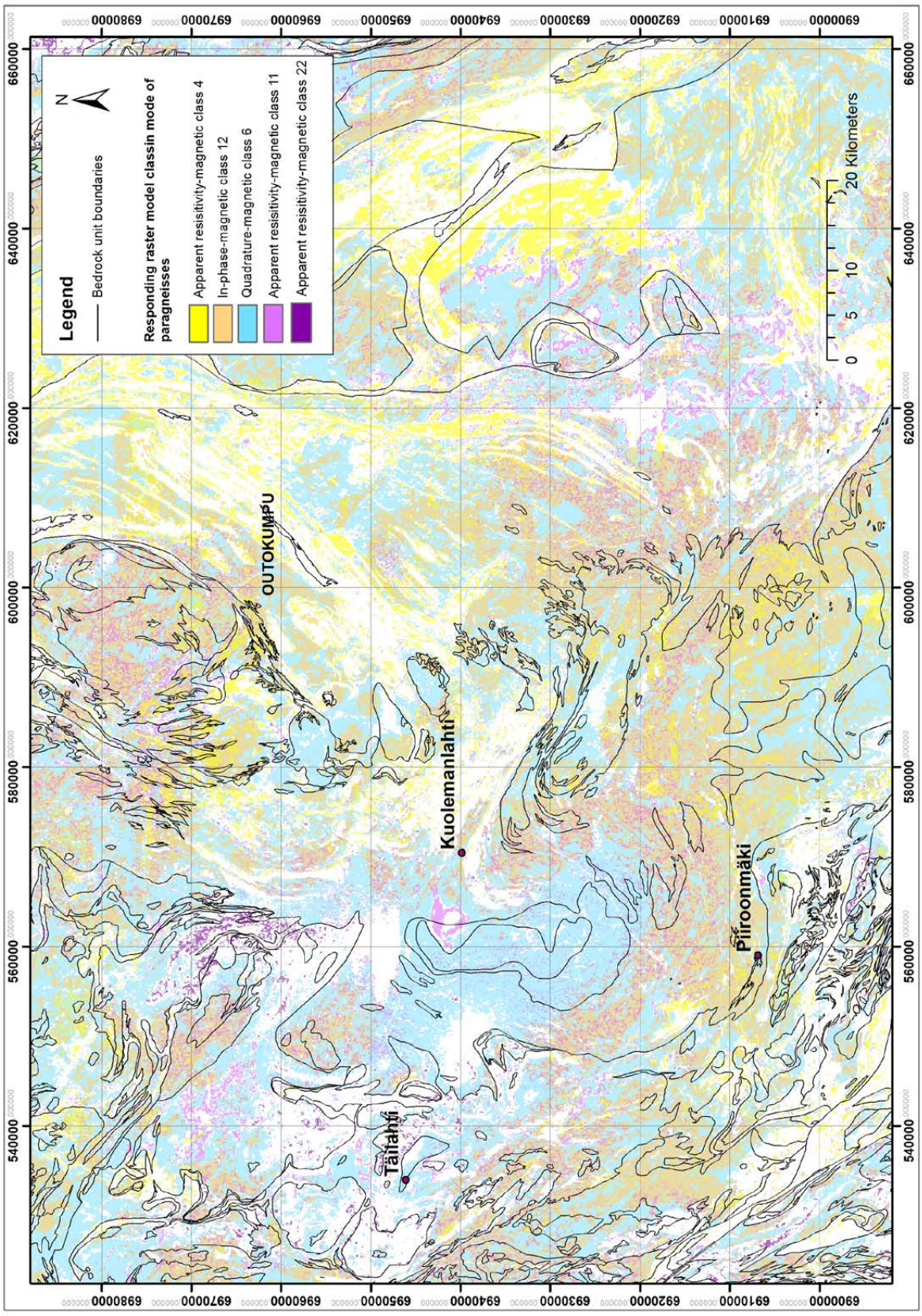

Fig. 61. Different areas related to paragneisses can be visualised with selected raster model classes preliminary interpreted with the aid of lithogeochemical REE (+ Zr) cluster model introduced in Table 10. Some of the response types characterising the Viinijärvi suite exist SW of Piiroonmäki and further east in North Karelia, although the geological domains are of different age and stratigraphy. Bedrock unit boundaries originate from Bedrock of Finland – DigiKP.

Table 10. Lithogeogeochemical REE evaluation data were processed with a statistical k-means tool to produce clusters. The dataset consisted of 1,109 data rows of which the number of valid sample cases for clustering was 602. The number of missing cases was 507. The number of the final REE cluster center vectors was 4. Main element oxide and minor element concentration of main bedrock group paragneisses related to each cluster were presented as median values (n of valid cases).

Cluster (valid 283, missing 363 in total)	**1**	**2**	**3**	**4**
Number of cases in each cluster (n)	57	84	11	131
Zr ppm	112,8	208,7	318,6	156,5
La ppm	20,6	33,2	37,2	30,8
Ce ppm	42,2	65,6	71,9	61,6
Pr ppm	5,2	7,8	8,3	7,3
Nd ppm	19,5	29,0	30,3	27,4
Sm ppm	4,08	5,44	5,50	5,22
Eu ppm	0,93	1,14	1,22	1,11
Gd ppm	3,71	4,80	4,83	4,69
Tb ppm	0,56	0,70	0,70	0,68
Dy ppm	3,32	3,92	3,91	3,84
Ho ppm	0,67	0,77	0,75	0,75
Er ppm	2,00	2,27	2,26	2,23
Tm ppm	0,29	0,33	0,32	0,32
Yb ppm	1,99	2,25	2,18	2,19
Lu ppm	0,31	0,33	0,33	0,32
Concentration (n)	**1**	**2**	**3**	**4**
SiO_2 %	63.73 (57)	69.68 (84)	69.73 (11)	67.19 (131)
TiO_2 %	0.684 (57)	0.714 (84)	0.771 (11)	0.725 (131)
Al_2O_3 %	13.56 (57)	13.58 (84)	13.64 (11)	14.34 (131)
FeO %	6.97 (57)	5.31 (84)	5.26 (11)	5.87 (131)
MnO %	0.07 (57)	0.08 (84)	0.08 (11)	0.07 (131)
MgO %	3.38 (57)	2.40 (84)	2.21 (11)	2.82 (131)
CaO %	2.03 (57)	2.36 (84)	2.76 (11)	2.23 (131)
Na_2O %	1.97 (57)	2.87 (84)	3.10 (11)	2.83 (131)
K_2O %	2.89 (57)	2.47 (84)	2.39 (11)	2.84 (131)
P_2O_5 %	0.12 (57)	0.16 (84)	0.19 (11)	0.15 (131)
Zr ppm	118 (57)	205 (84)	307 (11)	157 (131)
Co ppm	22.0 (56)	14.6 (82)	13.0 (11)	16.2 (119)
Cr ppm	120 (57)	110 (83)	100 (11)	112 (131)
Cu ppm	64.00 (49)	24.00 (61)	24.70 (8)	39.25 (110)
Ni ppm	81.25 (56)	43.80 (81)	39.85 (10)	52.70 (1309
S ppm	3745 (52)	568 (78)	800 (9)	1365 (120)
Pseudolithological model class in mode of paragneisses (n)				
Apparent resistivity-magnetic	Class 22, PARAGNEISS (6)	Class 4, MICA GNEISS (7)	Class 21, MICA SCHIST (1) and PARAGNEISS (1)	Class 11, MICA GNEISS (4) and MICA SCHIST (4)
Quadrature-magnetic	Class 5, PARAGNEISS (8)	Class 6, MICA GNEISS (18)	Class 8, MICA SCHIST (3)	Class 6, MICA GNEISS (17)
In-phase-magnetic	Class 12, PARAGNEISS (4)	Class 12, MICA GNEISS (23)	Class 12, GNEISS (2) and MICA SCHIST (2)	Class 12, MICA GNEISS (24)
Pseudolithological-litho-geochemical interpretation paragneisses by rock types	PARAGNEISS (+graphite-and/or sulphide bearing rocks), with higher levels of MgO, FeO, Cu and Ni concentration	Quartz bearing MICA GNEISS	Quartz and possibly albite bearing MICA SCHIST with slightly higher level of Zr concentration	MICA GNEISS (+migmatitic rocks), may contain sulphides

12.2.4 Discussion

Multivariate data analytical methods were applied to computing of airborne geophysical originated GIS raster models and evaluating them with lithogeochemical data with sample-wise bedrock geological labelling. The results were suitable for qualitative or semi-quantitative interpretation. The uncertainties of the modelling were also dependent of the quality of the original bedrock geological sampling and labelling, data, and chemical analytical methodologies chosen. Anthropogenic anomalies may be difficult to distinguish from natural geophysical responses in the interpretation, especially conductive powerlines.

The Outokumpu assemblage, and some metasedimentary rock units were identifiable or distinguishable from the modelling results introduced in this study. The methodology can be considered as a holistic approach to pseudolithological mineral potential mapping of a mineral system compared to more atomistic types of mineral potential modelling that emphasise using individual geochemical element distributions as GIS modelling parameters. Use of lithogeochemical data instead of geochemical data of secondary origin (e.g. geochemistry of till) in evaluation of modelling results is one approach in quest of a less complicated interpretation of regional bedrock geology.

12.3 Flake graphite

Graphite has been mined from several small pits in Haapamäki and Rääpysjärvi areas in the end of 19th and the beginning of 20th century. At that time the exploited deposits were a few metres wide shear zone -hosted graphite lenses with exceptionally high graphite contents (Fig. 62), with graphite contents locally exceeding 50%, when the black schists of East Finland on average contain ca. 7% graphite (Loukola-Ruskeeniemi 1992). Nygård (2017) reported bedrock samples exceeding 9% graphite from the Haapa_mäki area. GTK drillings on the west side of the Suvasvesi granite yielded zones of 4–9% graphite up to 40 m wide (Romu & Nousiainen 2020).

Although exploitation has historically been on a miniscule scale, the potential of finding sufficiently large flake graphite deposits suitable for modern economic extraction can be considered as reasonably high. The graphite-bearing schists in the study area have been metamorphosed in medium to high amphibolite facies (Hölttä & Heilimo 2017), metamorphic degree increasing towards the south-west. This high-grade metamorphism is an important factor in creation of large-sized flake graphite, as purification and crystallisation of graphite in a regional metamorphosis is mainly temperature dependent. The gneisses together with migmatitic melts and granite bedrock have been considerably folded and deformed in tectonic processes (Koistinen 1993a). These deformation events further improve the area's prospectivity for graphite as they can lead to significant thickening of the originally relatively narrow black schist layers (e.g. Puronaho 2018).

The Aitolampi graphite project managed by Beowulf Mining is located in the south-east corner of the study area, 13 km north of Heinävesi village (Fig. 6). This deposit is the most thoroughly studied in the area and the only one for which a modern resource estimate has been made. Drill results show an indicated and inferred mineral resource of 26.7 Mt at 4.5% total graphitic carbon. This mineralisation occurs in folded lenses > 500 m long and up to 100 m thick. Within the deposits are local zones of 10-20 m with 7% graphite. Beneficiation test shows well-developed crystalline graphite with a 97% recovery rate and >99% graphite purification (Beowulf Mining 2019).

The mineralogy of the black schists in the region is basically the same as that of the host gneisses, with the addition of graphite and associated sulphides. Pyrrhotite and magnetite are common minerals (Koistinen 1993a). The magnetic properties together with graphite being highly conductive make the black schists suitable for detecting with magnetic and electromagnetic geophysical methods.

Based on the abundant electromagnetic anomalies in aeromagnetic data and bedrock observations, the greatest potential for finding new graphite deposits in the study area is east of the Suvasvesi granite, extending from Heinävesi to northern parts of Tuusniemi. The metamorphic degree in this whole area is suitably high (Hölttä & Heilimo 2017) and the locally isoclinal folding could have resulted in significant thickening of the deposits. The graphite contents in the area can be regarded as relatively low as they rarely exceed 10%, but the slightly lower grade is potentially compensated by high crystallinity of the graphite.

Fig. 62. A) Historic graphite mine in Haapamäki, width of the mined exceptionally rich graphite layer was less than 5 metres. B) Ore from the Haapamäki mine, width of compass 6 cm.

13 DISCUSSSION

13.1 Archaean evolution

Despite limitations in the data from the Archaean units, certain interpretations regarding their relationship with the main Archaean segments of East Finland can be drawn. Especially the amount of post-crystallisation alteration would warrant closer studies. Based on available geochemical data, the Sotkuma and Juojärvi domes consist of TTGs representing all three geochemical subtypes. Compositional heterogeneity is also observable in the southern parts of the Lentua complex (Mikkola et al. 2013) where, additionally, the southwesternmost parts of the Sivakkavaara area belong to the sanukitoid suite (Fig. 12) based on geochemical data.

Within the Kuopio complex, sanukitoids are, based on both geochemical data and field observations, common north of the Suvasvesi shear zone, while different TTG types dominate south of it and in the smaller Archaean segments, Saamanen, Konnuslahti and Vasikkasaaret, further south. West of the present study area, the situation changes again as the domes in the Kuopio area contain abundant sanukitoids (Heilimo et al. 2012, Fig. 12).

The two age determinations from the Sotkuma dome, A37 and A38, yielded ages (2774±2 and 2784±2 Ma respectively) consistent with the younger end of the main TTG magmatism (2.75–2.85 Ga of the Lentua complex (e.g. Käpyaho et al. 2007, Mikkola et al. 2011, 2013). The two samples (A356, A362) from the Kotalahti dome only yielded rough estimates for their crystallisation ages, also

falling within the age range of the observed main TTG phase. Such ages have not been reported from neither Iisalmi nor Rautavaara complexes, but it should be noted that the age data from these is limited and concentrated on certain units, whereas the TTGs forming the bulk of the bedrock have received relatively little attention.

The ages of high-HREE-type samples A75 from the Juojärvi dome and A2532 from the Kuopio complex (2704±2 Ma and 2708±7 ma) are anomalously low for TTG-type granitoid in East Finland where TTGs display ages 2.75 Ga or older, with only one 2.72 Ga exception being dated so far (Mikkola et al. 2011). It should be noted that, within the Iisalmi block, uplifted lower crustal amphibolites indicate generation of TTG-type melts close to 2.70 Ga (Nehring et al. 2009).

The acquired additional data from sanukitoids and quartz diorites (A1033, A448, A449) of the Kuopio complex do not allow determination of exact ages but seems to be in accordance with ages obtained earlier for these suites, i.e. ~2.72 Ga for sanukitoids and ~2.70 Ga for the quartz diorites (Hölttä et al. 2000, Lukkarinen 2008, Heilimo et al. 2011).

What seems to be lacking or at least less voluminous in the currently studied areas are the 2.7 Ga migmatisation and anatectic leucogranites of the Konivaara suite, both characteristic features of the Lentua complex but insignificant in Rautavaara and Iisalmi complexes (Bedrock of Finland – DigiKP). However, confirming this would require a separate geochemical and geochronological study based on more extensive field work.

Based on similarities in geochemical composition and ages, we interpret the Sotkuma dome as part of the Lentua complex. The above-discussed similarities in age data support, in our opinion, the correlation of the Juojärvi domes with the Kuopio complex as suggested by Hölttä et al. (2012a). On similar bases, we tentatively suggest the correlation of the Iisalmi and Kuopio complexes.

Due to the intensity of Palaeoproterozoic deformation events, Archaean structures in the study area could not be recognised.

13.2 Initiation of a rift, from basal conglomerates to pillow lavas and arkosites

In its main aspects, the variably preserved volcano-sedimentary sequence covering the Archaean gneisses is alike that of the Kuopio region. The sequence commences in the Konnuslahti area with coarse-grained conglomeratic unit, which quickly grades upwards to arkositic sandstones and to immature quartzites containing aluminium silicates. However, it would require further studies to reliably distinguish to which extent the quartzites have been hydrothermally altered during later stages. In most places the preserved sequence starts from these quartzites, which are covered by mafic volcanic rocks locally displaying well-preserved pillow structures. Carbonatite rocks between the silicate sediments and volcanic units occur locally. In pre-existing maps based on work carried out by Outokumpu Ltd., the locally abundant dolerite dykes were interpreted as volcanic rocks, causing significant changes in the bedrock map in the Konnuslahti and Räsälä areas. The arkosite rocks overlaying the mafic volcanic units in Kohma have not been described from the Kuopio region, although slightly further north, a similar sequence could exist (Paavola 1984).

Most of the volcanic rocks and diabases in the study areas display compositions similar to ocean floor basalts and within plate basalts. This is in line with the interpretation by Lukkarinen (2008) from the Siilinjärvi and Kuopio areas: the tholeiitic magmatic rocks originated in an underwater rift environment on the continental crust. Compositional and mineralogical similarity of the diabases and volcanic rocks link them as part of the same event(s). Exception is the Juojärvi-Kohma low-TiO_2 samples area, which can be classified as island arc basalts. According to Kontinen et al. (2006), the low-Ti Losomäki-type mafic volcanic rocks could be part of the Outokumpu ophiolite assemblage but alternatively represent a parautochthonous Lower Kaleva assemblage. Additional detailed work in the Kohma area where both types are present in close vicinity could provide additional insigths to this question.

13.3 Paragneisses

Out of the paragneisses the Levänen group displays the largest chemical scatter and also deviates in certain aspects from the two other units. Higher Cr contents of the more mafic samples can be interpreted as a result of material from a more mafic source, e.g. the volcanic rocks underlaying the unit. These samples also have highest CIA values, which explains the relative abundance of the aluminium-bearing porphyroblast in the unit. On the other hand, the samples richest in SiO_2 indicate locally a highly felsic source, Archaean granitoids and/or quartzites. Overall, the high chemical variability is in line with the observed well-developed layering on the outcrops, which contrast strongly with the more uniform characteristics of the Suonenjoki and Viinijärvi suites in both aspects.

As noted earlier, the compositions, on average, tend to be more pelitic in the Suonenjoki suite than in the Viinijärvi suite, but no single boundary can be identified as individual samples from the Viinijärvi and Suonenjoki suites cannot be distinguished chemically. Within the Viinijärvi suite, the most notable variation is the lower LREE contents, on average, of the samples along the western boundary of the unit. Main element or other trace element patterns of these samples do not deviate from the main group. Therefore, verifying whether these small differences indicate variation in source characteristics would require isotopic work, e.g. Sm-Nd whole rock analyses.

Interestingly, similar low-LREE characteristics cannot be found from the eastern parts of the Suonenjoki suite where the clearest deviations from the typical patterns are the samples with low LREE/HREE and/or HREE from the vicinity of the Konnuslahti dome. As samples with typical LREE/HREE ratios and HREE levels for the Suonenjoki suite exist in the same area, these samples likely represent small domains. It would be tempting to state that they indicate proximity during deposition to the Archaean crust and its cover rocks, like the Levänen group, but the current dataset does not allow such comparison, as based on the current observation data, these samples do not significantly deviate from the main goup. However, this is something that should be studied in more detail in the future.

Scatter in LILE, Na_2O and, to a smaller extent, also in K_2O could represent variation in protolith composition or be an artefact of postcrystallisation alteration and migmatisation. As some of the samples contain variable amounts of veining, at least the latter option is likely. Samples with overrepresentation of granitoid neosome veining could explain the samples with high Na_2O and K_2O and samples which have lost melt fraction would be the samples with lower concentrations of the aforementioned elements.

In respect of detrital zircon populations, the situation is similar, as both the Suonenjoki and Viinijärvi suites display detrital populations characterising rocks of this type in the whole of Central and Southern Finland, i.e. Neoarchaean peak at 2.7–2.8 Ga and Palaeoproterozoic peak at 1.95–2.05 Ga (e.g. Lahtinen et al. 2002, 2010, 2015, Kotilainen et al. 2016, Mikkola et al. 2018b). The relative size of the peaks varies, but both are present in all of the samples (Figs. 49 and 63). The westernmost samples from the Suonenjoki suite and Piiroonmäki differ from the other four in one aspect: they do not seem to contain detrital zircons yielding ages from 2200 to 2600 Ma, which could indicate small differences in source regions. However, it should be noted that the number of analysed spots is not high enough to state with statistical certainty that this phenomenon is not a result of an inadequate number of analysed points.

In respect to the paragneisses, the most significant change to earlier interpretations is that, based on field observations, geochemistry and especially the detrital zircon data, large areas in Kohma and around the Juojärvi domes are parts of the Viinijärvi suite and not of the Karelia group as interpreted earlier (e.g. Nironen et al. 2016).

Detrital Archaean zircons display ages which correspond well with the two main felsic phases of the Lentua complex and the whole Karelia Province, TTG magmatism peaking at ca. 2.8 Ga and 2.7 Ga granitoid magmatism consisting of leucogranitoids and sanukitoids (e.g. Heilimo et al. 2011, Mikkola et al. 2011, 2013, this study). More problematic is the source of the 1.95–2.05 Ga zircons for which Lahtinen et al. (2010) suggested the Lapland-Kola orogeny as a possible source. However, the ages reported from Lapland-Kola orogeny are <1.95 Ga (Meriläinen 1976, Kesola 1995, Tuisku et al. 2006) and therefore the ~2.0 Ga zircons must have a different source, one possibility being the poorly known Central Russian Fold Belt, from where ~2.0 Ga magmatic ages have been preliminarily reported

(Samsonov et al. 2016). Zircon crystals with ages between 1.93 and 1.91 Ga and thus possibly representing older Svecofennian magmatism are present but not in significant proportions. This indicates that the approaching arc did not form a significant source for the paragneisses, a phenomenon already noted earlier (e.g. Lahtinen et al. 2015, Mikkola et al. 2018b), especially when the possibility of observed ages being "younged" by lead loss is taken into account.

It is relatively clear that the younger sedimentation phase with a maximum deposition age (1.89–1.88 Ga) described northwest of our study area (Lahtinen et al. 2015) is not present among the samples of the study area. In respect to zircon populations, the more extensively studied parts of the Savo supersuite (Näläntöjärvi suite) display a similar zircon population to the Suonenjoki suite for which the first data is presented in this study (Fig. 63). On unit level, the detrital populations from Pirkanmaa and Häme migmatite belts are identical to those from Viinijärvi and Suonenjoki suites. Although the first mentioned units should present a different deposition stage (e.g. Nironen 2017, Mikkola et al. 2018a), this similarity has been suggested as being a result of the older paragneiss units forming a significant source region for the slightly younger units (Lahtinen et al. 2009).

Division of paragneisses between the Suonenjoki and Viinijärvi suites was one of the main research questions of this project. Based on the current data, it seems that the location or even existence of this division in our study area is questionable. Detrital zircon populations are similar and individual whole rock analyses are indistinguishable between the suites. If proven presence of rocks belonging to the Outokumpu assemblage is taken as key identifier of the Viinijärvi suite, large areas around the Suvasvesi granite could actually be interpreted as belonging to the Suonenjoki suite. Now the boundary between the units is formed by the Outokumpu decollement thrust (see below), which as an unarguably post-depositional structure does not necessarily mark a shift from one depositional basin to another. Thus, the spatial extent of the Viinijärvi suite could also be continued significantly further west to the core of the Raahe-Ladoga suture zone, e.g. to the level marking the location of the westernmost Archaean thrust sheets or easternmost rocks interpreted as belonging to the older Svecofennian magmatism (Bedrock of Finland – DigiKP).

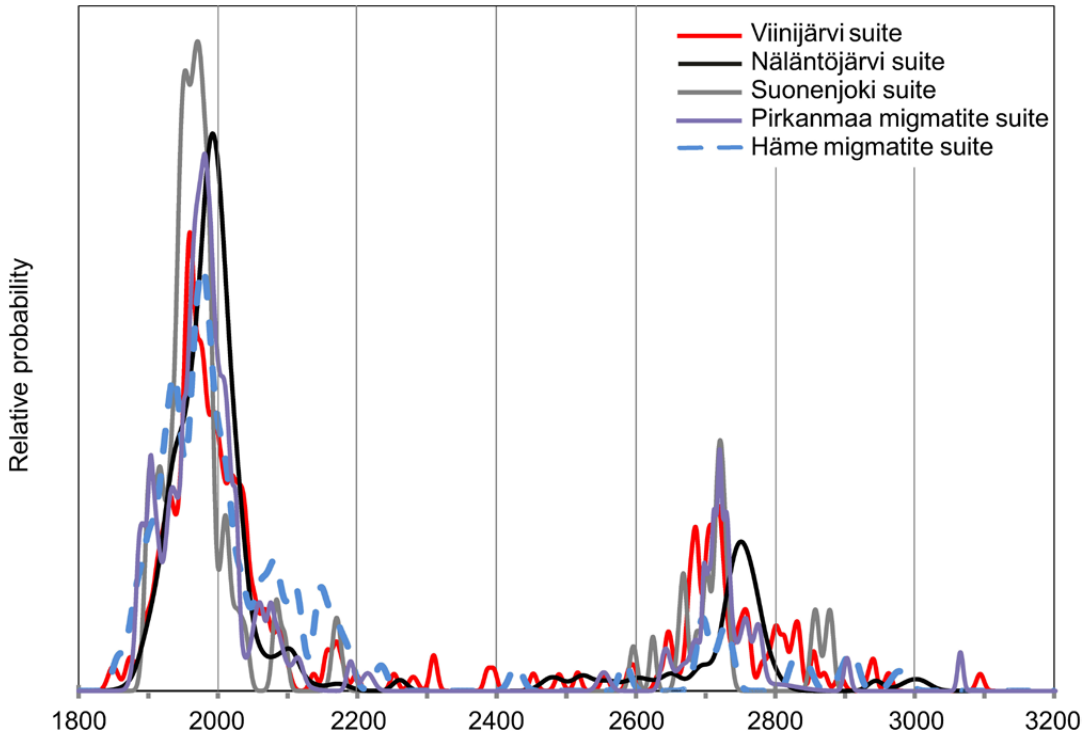

Fig. 63. Probability density plot of paragneiss units in the study area and paragneiss units in its vicinity. Data for Viinijärvi and Suonenjoki suite from this study. Data for the Näläntöjärvi suite from Lahtinen et al. (2015), for Pirkanmaa and Häme migmatite belts from Mikkola et al. (2018a). Only spots interpreted as representing detrital ages and with less than 10% central discordancy are plotted.

The exploratory data analysis managed to produce certain differences between the paragneisses in the study area (Fig. 61), e.g. those interpreted as part of the Viinijärvi suite and located north and west of the Suvasvesi granite clearly stand out from those east of it and known to host the rocks of the Outokumpu assemblage. This is an interesting phenomenom as none of the "traditional" geological data collected diplay such drastic differences. Confirmation of the ultimate reason between the different responses in modelling would require collection of more detailed data from smaller areas.

13.4 The first deformation phase and distribution of the Outokumpu assemblage

The youngest detrital zircons in the Viinijärvi and Suonenjoki suite paragneisses yield ages between 1.93–1.91 Ga (this study, Claesson et al. 1993). This can be held as the most reliable timing for rift inversion and beginning of the Svecofennian orogeny. In the most recent tectonic model by Kohonen et al. (2021), the first event is designated to a collision of Iisalmi, Rautavaara and Kuopio complexes against Lentua complex (See Fig. 1). This led to basin inversion and emplacement of rocks of the Outokumpu allochthon over the Archaean basement and its autochthonous cover. Kontinen & Paavola (2006) suggested an alternative model where ophiolites and associated supracrustal rocks were thrust over the Iisalmi block from the west. We associate isoclinal, recumbent folds in the paragneisses of the Viinijärvi suite (Fig. 42A) with this phase and interpret that the Outokumpu allochthon was thrusted over the attenuated Archaean basement in a thin-skinned manner.

Additional data verifies that the Kuolemanlahti, Piiroonmäki, and Täilahti occurrences that were known earlier, but studied only limitedly, belong to the Outokumpu assemblage. Out of these, Täilahti is part of a klippe of the Viinijärvi suite rocks, separated from the Suonenjoki suite by Outokumpu decollement thrust. It is likely that the Täilahti klippe was originally connected to the Outokumpu assemblage, and is preserved from erosion in bottom of a synform formed in younger deformation phase.

The mineral potential modelling for the Outokumpu assemblage is mainly in good agreement with the observational data. The smaller targets (Täilahti, Piiroonmäki) are difficult or impossible to identify from regional data, but areas with larger number of occurrences show up. Based on both observational data and modelling, we conclude that areas north and west of the Suvasvesi granite do not possess any significant potential for hosting Outokumpu-type ores, which could however potentially exist along the structural trend hosting Kuolemanlahti and Piiroonmäki and bend by the Suvasvesi shear zone. However, the amount of rocks belonging to the Outokumpu assemblage, at least in the present erosion surface, is significantly smaller than in the Outokumpu–Tuusniemi region.

13.5 The second deformation phase

The tectonic evolution continued with accretion of microcontinents or island arcs from the south or south-west 1.91–1.90 Ga ago (Nironen 2017). We associate the second deformation phase (D2) with accretion of the Savo arc formed of Pyhäsalmi and Vihanti group supracrustal rocks and Venetpalo suite orthogneisses in the current erosion level (Mikkola et al. 2018a). The Savo arc has also been interpreted as being formed on the edge of a (Keitele) microcontinent which then accreted to Karelian province (Lahtinen et al. 2005). Deformation continued in a thick-skinned manner, and Archaean basement and autochthonous cover rocks were also deformed during the second deformation phase. The most compelling evidence of this phase comes from the Kaavi area where also basement is deformed in east-verging folds (Park & Bowes 1983). Pervasive foliation and lineation developed in the rocks of Outokumpu allochthon (Koistinen 1981, Park & Bowes 1983, Ward 1987). East-verging, subhorizontal folds have also been observed on the western side of the Vehmasmäki dome in the Suonenjoki suite paragneiss (Forss et al. 1999). Slightly east-verging folds and thrusts were observed at the eastern margin of the Kuopio complex and associated with this phase. In the study area these consist of Honkajärvi and Tomperi antiforms, Ylä-Nurjonen and Kolonjärvi synforms and the Kohma thrust (Figs. 39 and 41). We also interpretate that the Saamanen and Konnuslahti domes were originally folded in this phase and later refolded in NW-SE compression (D3).

13.6 The third deformation phase

Svecofennian orogeny continued with accretion of additional volcanic arcs and microcontinents between 1.90–1.87 Ga ago (Nironen 2017). This caused transposition of structural trends in a clockwise manner, formation of folds with SW-NE-trending fold axes and activation of SE-NW-trending shear zones in the study area. As indicated by transposition of structural trends, the tectonic compression at this stage must have been trending NW-SE. The current interpretation is that rotation of the previously collated micro-continent caused the transposition 1.87 Ga ago (Nironen 2017).

Transposed structural trends are discordant with metamorphic isograds, which are defined from the Outokumpu-type peridotites (Säntti et al. 2006). Sorjonen-Ward (2006) related metamorphic facies at the Outokumpu allochthon to regional advection of heat from granitoids of the Heinävesi and Kaarakkala suites. This implies that the transposition and the NE-SW-trending folding must have occurred before magmatism caused the peak metamorphic conditions. Syntectonic granitoid ages from the Outokumpu allochthon reinforce the interpretation by Nironen (2017) that the age of the transposition event is ca. 1.87 Ga.

SW-NE-trending, open F3 folds and crenulations with horizontal fold axes were observed in the field (Figs. 42F and 43A) and can be seen on a regional scale at Konnuslahti (Fig. 10). An interesting observation was made of granitoid veins in axial plane of F3 folds at Kohma (Fig. 40). We interpret that these folds formed in the same deformation phase as the Konnuslahti folds. Granitoid veins intruded while the tectonic stress formed the folds, or soon after. These veins are yet to be dated and their age might reinforce the age of the deformation phase indicated in the previous paragraph.

At Kohma, sequence from folding to shearing can be seen on the outcrops (Figs. 40D–F). As the deformation progressed, first strike-slip shear zones developed also within the Suonenjoki suite paragneisses (Jokela 1994, Forss et al. 1999). Folding ceased as the strain focused in the shear zones and enhanced metamorphic fluid flow along the shear zones increased migmatisation of the paragneisses (Forss et al. 1999). The minor Kohmanvesi shear zone (Fig. 39), along with major shear zones of Suvasvesi, Iisvesi, Haukivesi and Airaksela, were active. We interpret that the transposition along the Suvasvesi shear zone occurred asymmetrically: the SW side of the zone moved markedly towards NW after initial transposition of the structural trends. The asymmetric interpretation is based on drag folding of the pre-existing foliation at the southwest side of the Suvasvesi shear zone, east of Suvasvesi granite, together with the approximately 15 km step in the north-south-trending eastern contact of the Archean Kuopio complex . At the northeast side of the Suvasvesi shear zone, schistosity trends are mostly north-south-oriented and very little transposition parallel to the Suvasvesi shear zone is apparent. Here the trend of schistosity also deviates from the NE-SW trend of the Outokumpu area. Simultaneously with the dextral movement of Suvasvesi shear zone, or slightly later, Kermajärvi granitoid intruded in to the drag fold structure east of Suvasvesi granite.

13.7 Palaeoproterozoic granitoid rocks

Based on the available geochemical data, the Heinävesi and Kaarakkala suites are compositionally similar with dominantly I-type characteristics, being peraluminous, but display relatively low ASI values and only rarely contain garnet or other aluminium-enriched minerals. The Heinävesi suite displays deviations towards higher ASI values which could be indicative of either assimilation of Viinijärvi suite paragneisses during emplacement or of them forming the source locally. However, as based on field observations, the abundant dykes are, at least in most cases, not anatectic melts from the current erosion level and the paragneiss cover is not sufficiently thick to allow sourcing from significantly deeper levels, the assimilation option seems more likely. Intrusive contacts between paragneisses and granitoid veins are sharp and the dykes do not show decrease in grain size towards the contact. Neither do the contact zones of the paragneisses with larger intrusions display contact-metamorphic aureoles, all of these features indicate that the dykes intruded in near-peak metamorphic conditions.

The highly heterogeneous REE patterns observed from the Heinävesi suite indicate fractionation at various stages. The few P_2O_5-enriched dioritic samples display high total REE, together with a less

fractionated pattern, a combination most likely caused by cumulation of apatite in relatively early stages, as the apatite has high Kd values for REEs (Fujimaki 1986). The scatter in most silica- enriched compositions is likely associated with fractionation and accumulation of feldspars, samples with strong positive Eu anomalies likely represent crystal mushes from which the remaining melt has been largely removed and those with strongly negative anomalies the removed melt. Due to high viscosity, fractionation in silica-rich melts is normally not a significant process, but emplacement during deformation could have facilitated separation of crystals from the remaining melt. As the K_2O and Na_2O concentrations do not correlate with the Eu anomaly, it can be interpreted that both K-feldspar and plagioclase contributed to the fractionation.

The, on average, more mafic composition of the Haukivesi suite and the weaker Nb, P and Ti anomalies set it apart from the Kaarakkala suite. It is also, on average, more metaluminous than the other suites, although it includes a few members that have ASI values above 1.2, and, in the case of Juurikkamäki intrusion, also garnet. Based on these observations and the fact that the Suonenjoki suite displays stronger migmatisation, the situation could be that this poorly defined suite currently includes both S- and I-type granitoids. The differences displayed by the more mafic I-type intrusions compared to the Savo supersuite indicate differences in source composition. This change in composition of granitoid suites (1.88–1.86 Ga) overlapping in age is further emphasised if the A-type intrusions of the Sorsakoski area belonging to the Saarijärvi suite are taken into account. Based on observations and 3D modelling, the Savo supersuite is present in the area where Archaean craton is either outcropping or hidden beneath a relatively thin paragneiss layer. The Haukivesi suite occurs in the core of the Raahe-Ladoga suture zone where Archaean crust exists but does not necessarily form a continuous sublayer and the Sorsakoski intrusions are present in an area having entirely Svecofennian crust (e.g. Sorjonen-Ward 2006, Lahtinen et al. 2016, this study). The more mafic compositions from diorite to gabbro also indicate addition of material from mantle sources at this time, especially when the Kotalahti suite (~1.88 Ga), spatially overlapping with the marginally younger Haukivesi (~1.87 Ga) suite, is taken into account.

13.8 The fourth deformation phase

There was a break in igneous activity in southern Finland between 1.86 and 1.85 Ga (Vaasjoki 1996). The next tectonic event occurred between 1.84-1.80 Ga ago, which is indicated by an intrusion of microcline granites and local granulite-facies metamorphose in southern Finland (Vaasjoki & Sakko 1988, Ehlers et al. 1993). Lahtinen et al. 2005 modelled continent-continent collision to explain this tectonic event, while Kärki et al. (1993) related activation of the Oulujärvi shear zone to this event. This is the fourth deformation phase (D4) in the study area. Previously formed shear zones were reactivated during this event and possibly new zones were formed. Folds of this phase were not observed; which indicates that the strain concentrated in (pre-existing) shear zones.

Postorogenic granitoids intruded in the major shear zones at 1.8 Ga ago and their undeformed character indicate that tectonic processes of the Svecofennian orogeny had permanently ceased (Vaasjoki et al. 2001). Of these postorogenic granitoids, the Puruvesi granite that intersects the SE end of the Suvasvesi shear zone (monazite U-Pb age 1797±19 Ma, Huhma 1986) and the Parikkala granodiorite at Mikkeli (zircon U-Pb age 1794±5 Ma, Patchett & Kouvo 1986) are closest to the study area.

14 FURTHER WORK

Based on the results of this study, the main Kuopio complex, as well as the domes and thrust sheets south of the complex seem to be a continuum of the larger Archaean areas of East Finland and not exotic terrains assembled during the Svecofennian orogeny. Still, a detailed study for more precise determination of the granitoid types present and their ages is required to confirm this.

Based on the current data, the Haukivesi intrusive suite does not display significant differences in composition and age with the Heinävesi and Kaarakkala suites occurring east of it. Still, cer-

tain small geochemical differences are present and should be looked at in more detail as they could be indicative of differences in source region compositions and thus provide further information on the deeper structure and composition of the Raahe-Ladoga suture zone.

Detailed geophysical studies could provide more insight to the "seam" running from Kuolemanlahti to Piiroonmäki and the hosting rocks clearly belonging to the Outokumpu assemblage. For example, surveying reflection seismic lines across the structure at selected locations could help in further development of the regional 3D models, structural interpretations and evaluating of whether the seam could host serpentinites large enough to have associated economically viable deposits in depth.

The observed major gravity anomaly not explained by observations of surficial geology should first be further studied with geophysical measurements (reflection seismic and AMT methods). If modelling with these additional data indicates that the anomaly source is relatively shallow (<2 km), a deep drill hole should be drilled to solve the source.

The observed major northwest-southeast-trending gravity anomaly is an evident target for further studies. Based on density modelling, the depth of its source is not deeper than 400–500 metres. Also the short reflection seismic line shows reflections at roughly similar depths. A longer reflection seismic line together with audio-magnetotelluric measurements would allow more precise modelling of the structure, after which its source could be confirmed with a single, most likely ca. 1,000 m long drillhole. Confirmation of the cause of the gravity anomaly would be significant for better understanding of the large geological structures and ore potential in the area.

15 CONCLUSIONS

The new data from Archaean rocks gives further support to the models in which the smaller domes and thrust sheets are continuations of the larger complexes and not exotic terrains tectonically emplaced during early phases of the Svecofennian orogeny.

Karelia group clastic sediments of the study area display stratigraphy and development from rift conglomerates to quartzites and through mafic volcanites to carbonate rocks and turbidites similar to those previously described from the Kuopio-Siilinjärvi area, the most significant addition being the locally observable arkosites between the mafic volcanic rocks and the paragneisses on top of them.

The Viinijärvi and Suonenjoki suites cannot be distinguished from each other based on their whole-rock chemistry or detrital zircon populations, although the Suonenjoki suite is, on average, slightly more pelitic than the Viinijärvi suite. It is thus likely that the current border between them, formed by the Outokumpu detachment fault, is a structural one and does not represent a difference in depositional basin or timing.

The new data confirms the earlier interpretations that the Outokumpu assemblage is constrained to areas NE of the Suvasvesi shear zone, excluding the Hanhisalo klippe and the seam hosting Kuolemanlahti and Piiroonmäki occurrences.

The new data did not reveal any previously unknown members of the Kotalahti suite, which is spatially strictly limited to and connected with the Raahe-Ladoga suture zone.

Structural observation made from the western part of the Outokumpu allochthon correlates with earlier observations made on the eastern and western side of the current study area. Structural interpretation, together with age data from granitic igneous rocks, indicates that folding and shearing in the third deformation phase occurred before 1.87 Ga. This phase is seen as NE-SW-trending folds in Konnuslahti and Kohma, and the first activation of the major Suvasvesi and Airaksela shear zones. The third deformation had a major impact on the present geology of the study area and reached further away towards NW along the Suvasvesi shear zone.

Based on both age and geochemical data, granitoids of the Kaarakkala suite intruding into the Archaean Kuopio complex and Heinävesi suite intruding into the Viinijärvi suite paragneisses correlate with each other in the study area. The units are not however combined as it would require closer studies concerning the northern continuations of the Kaarakkala suite.

REFERENCES

Aarnisalo, J. 1990. Keski-Lapin harvapistemoreeniaineiston kuvankäsittely. Outokumpu Oy ore exploration, Archive report 060/27,37/JA/90. 44 p., 45 app. pages. (in Finnish). Available at: https://tupa.gtk.fi/raportti/arkisto/060_27_37_ja_1990.pdf

Äikäs, O. 2000. Juankoski. Geological Map of Finland 1:100 000. Pre-Quaternary Rocks, Sheet 3333. Geological Survey of Finland. Available at: https://tupa.gtk.fi/kartta/kallioperakartta100/kp_3333.pdf

Airo, M.-L. 1999. Aeromagnetic and petrophysical investigations applied to tectonic analysis in the northern Fennoscandian shield. Geological Survey of Finland, Report of Investigation 145. 51 p., 1 appended map. Available at: https://tupa.gtk.fi/julkaisu/tutkimusraportti/tr_145.pdf

Airo, M.-L. 2005. Aerogeophysics in Finland 1972–2004: Methods, System Characteristics and Applications. Geological Survey of Finland, Special paper 39. 197 p. Available at: https://tupa.gtk.fi/julkaisu/specialpaper/sp_039.pdf

Airo, M.-L., Hyvönen, E., Lerssi, J., Leväniemi, H. & Ruotsalainen, A. 2014. Tips and tools for the application of GTK's airborne geophysical data. Geological Survey of Finland, Report of Investigation 215. 33 p. Available at: https://tupa.gtk.fi/julkaisu/tutkimusraportti/tr_215.pdf

Aumo, R. 1983. Kuopion Pienen Neulamäen ympäristön kallioperä ja stratigrafia. Unpublished Master's thesis, University of Turku, Department of Geology and Geography, 113 p. (in Finnish). Available at: http://tupa.gtk.fi/opinnayte/aumo_raili_gradu.pdf

Bedrock of Finland – DigiKP. Digital map database [Electronic resource]. Espoo: Geological Survey of Finland [referred 31.12.2020]. Version 2.1.

Belousova, E. A., Griffin, W. L. & O'Reilly, S. Y. 2006. Zircon crystal morphology, trace element signatures and Hf isotope composition as a tool for petrogenetic modeling: examples from Eastern Australian granitoids. Journal of Petrology 47, 329–353.

Beowulf Mining plc 2019. Annual Report. Available at: https://beowulfmining.com/

Boynton, W. V. 1984. Cosmochemistry of the rare earth elements: meteorite studies. In: Henderson, P. (ed.) Rare earth element geochemistry. Amsterdam: Elsevier, p. 63.

Claesson, S., Huhma, H., Kinny, P. D. & Williams, I. S. 1993. Svecofennian detrital zircon ages – implications for the Precambrian evolution of the Baltic shield. Precambrian Research, 64, 109–130.

Dohmen, R., Marschall, H. R., Ludwig, T. & Polednia, J. 2018. Diffusion of Zr, Hf, Nb and Ta in rutile: effects of temperature, oxygen fugacity, and doping level, and relation to rutile point defect chemistry. Physics and Chemistry of Minerals 46, 311–332.

Donadini, F., Plado, J., Werner, S. C., Salminen, J., Pesonen, L. J. & Lehtinen, M. 2006. New evidence for impact from the Suvasvesi South structure, central east Finland. In: Cockell, C., Koeberl, C. & Gilmour, I. (eds) Biological Processes Associated with Impact Events, Impact Studies. Berlin: Springer, 287–307.

Ehlers, C., Lindroos, A. & Selonen, O. 1993. The late Svecofennian granite–migmatite zone of southern Finland – a belt of transpressive deformation and granite emplacement. Precambrian Research 64, 295–309.

Eilu, P. (ed.) 2012. Mineral deposits and metallogeny of Fennoscandia. Geological Survey of Finland, Special Paper 53. 401 p. Available at: https://tupa.gtk.fi/julkaisu/specialpaper/sp_053.pdf

Ekdahl, E. 1977. Raportti Vehmersalmen Puutosmäellä 1973–75 suoritetuista U-malmitutkimuksista. Geological Survey of Finland, archive report M19/3244/77/1/10. 6 p., 10 app. pages. (in Finnish). Available at: https://tupa.gtk.fi/raportti/arkisto/m19_3244_77_1_10.pdf

Ekdahl, E. 1993. Early Proterozoic Karelian and Svecofennian formations and the Evolution of the Raahe-Ladoga Ore Zone, based on the Pielavesi area, central Finland. Geological Survey of Finland, Bulletin 373. 137 p. Available at: https://tupa.gtk.fi/julkaisu/bulletin/bt_373.pdf

Elliott, B. A., Rämö, O. T. & Nironen, M. 1998. Mineral chemistry constraints on the evolution of the 1.88–1.87 Ga post-kinematic granite plutons in the Central Finland Granitoid Complex. Lithos 45, 109–129.

Eskola, P. 1949. The problem of mantled gneiss domes. Quarterly Journal of Geological Society of London 104, 461–476.

Forss, H., Kontoniemi, O., Lempiäinen, R., Luukas, J., Makkonen, H. & Mäkinen, J. 1999. Ni-vyöhyke ja 1.9 Ga magmatismi-hankkeen (12204) toiminta vuosina 1992–1998 Tervo–Varkaus alueella. Geological Survey of Finland, archive report CM19/3241/-99/1/10. 152 p., 57 app. pages. (in Finnish). Available at: https://tupa.gtk.fi/raportti/arkisto/m19_3241_99_1_10.pdf

Frosterus, B. & Wilkman, W. W. 1924. Joensuu. The General Geological Map of Finland 1:400 000, Pre-Quaternary Rocks, Sheet D3. Geological Survey of Finland.

Fujimaki, H. 1986. Partition coefficients of Hf, Zr, and REE between zircon, apatite, and liquid. Contributions to Mineralogy and Petrology 94, 42–45.

Gaál, G. 1980. Geological setting and intrusion tectonics of the Kotalahti nickel-copper deposit, Finland. Bulletin of the Geological Society of Finland, 52, 101–128. Available at: https://doi.org/10.17741/bgsf/52.1.005

Gaál, G. (ed.) 1988. Exploration target selection by integration of geo data using statistical and image processing techniques: an example from Central Finland. Geological Survey of Finland, Report of Investigation 80. 156 p. Available at: http://tupa.gtk.fi/julkaisu/tutkimusraportti/tr_080.pdf

Gaál, G., Koistinen T. & Mattila, E. 1975. Tectonics and stratigraphy of the vicinity of Outokumpu, North Karelia, Finland, including a structural analysis of the Outokumpu ore deposit. Geological Survey of Finland, Bulletin 271. 67 p. Available at: https://tupa.gtk.fi/julkaisu/bulletin/bt_271.pdf

Glumoff, T. 1987. Outokummun alueen kiilleliuskeista. Unpublished master's thesis, University of Turku, Department of geology and mineralogy. 97 p. (in Finnish)

Grieve R. A. F., Langenhorst F. & Stoffler D. 1996. Shock metamorphism of quartz in nature and experiment. 2. Significance in geoscience. Meteoritics & Planetary Science 31, 6–35.

Haapala, P. 1936. On serpentinite rocks in Northern Karelia. Geological Survey of Finland, Bulletin 114. 80 p. Available at: https://tupa.gtk.fi/julkaisu/bulletin/bt_114.pdf

Halden, N. M. 1982. Structural, metamorphic and igneous history of migmatites in the deep levels of a wrench fault regime, Savonranta, eastern Finland. Royal Society of Edinburgh Transactions, Earth Sciences 73, 17–30.

Halla, J., van Hunen, J., Heilimo, E. & Hölttä, P. 2009. Geochemical and numerical constraints on Neoarchean plate tectonics. Precambrian Research 174, 155–162

Hanski, E. & Melezhik, V. A. 2013. Litho- and chronostratigraphy of the Paleoproterozoic Karelian formations. In: Melezhik, V., Prave, A. R., Fallick, A. E., Kump, L. R., Strauss, H., Lepland, A. & Hanski, E. J. (eds) Reading the Archive of Earth's Oxygenation, Volume 1: The Palaeoproterozoic of Fennoscandia as Context for the Fennoscandian Arctic Russia – Drilling Early Earth Project. Springer-Verlag, 39–110.

Hanski, E., Huhma, H. & Vuollo, J. 2010. SIMS zircon ages and Nd isotope systematics of the 2.2 Ga mafic intrusions in northern and eastern Finland. Bulletin of the Geological Society of Finland 82, 31–62. Available at: https://doi.org/10.17741/bgsf/82.1.002

Heilimo, E., Halla, J. & Hölttä, P. 2010. Discrimination and origin of the sanukitoid series: geochemical constraints from the Neoarchean western Karelian Province (Finland). Lithos 115, 27–39.

Heilimo, E., Halla, J. & Huhma, H. 2011. Single-grain zircon U-Pb age constraints of the western and eastern sanukitoid zones in the Finnish part of the Karelian Province. Lithos 121, 87–99.

Heilimo, E., Halla, J. & Mikkola, P. 2012. Overview of Neoarchaean sanukitoid series in the Karelia Province, eastern Finland. In: Hölttä, P. (ed.) The Archaean of the Karelia Province in Finland. Geological Survey of Finland, Special Paper 54, 214-225. Available at: https://tupa.gtk.fi/julkaisu/specialpaper/sp_054_pages_214_225.pdf

Herron, M. M. 1988. Geochemical classification of terrigenous sands and shales from core or log data. Journal of Sedimentary Petrology 58, 820–829.

Hietava, J. 2022. Geochemistry, lithology and mineralogy of the Outokumpu assemblage rocks in Kuolemanlahti, Leppävirta, eastern Finland. Geological Survey of Finland, Open File Work Report 16/2022. Available at: https://tupa.gtk.fi/raportti/arkisto/16_2022.pdf

Hölttä, P. & Heilimo, E. 2017. Metamorphic map of Finland. In: Nironen, M. (ed.) Bedrock of Finland at the scale 1:1 000 000 – Major stratigraphic units, metamorphism and tectonic evolution. Geological Survey of Finland, Special Paper 60, 77–128. Available at: https://tupa.gtk.fi/julkaisu/specialpaper/sp_060_pages_077_128.pdf

Hölttä, P., Heilimo, E., Huhma. H., Juopperi, H., Kontinen, A., Konnunaho, H., Lauri, L., Mikkola, P., Paavola, J. & Sorjonen-Ward, P. 2012a. Archaean complexes of the Karelia Province in Finland. In: Hölttä, P. (ed.) The Archaean of the Karelia Province in Finland. Geological Survey of Finland, Special Paper 54, 9-20. Available at: https://tupa.gtk.fi/julkaisu/specialpaper/sp_054_pages_009_020.pdf

Hölttä, P., Heilimo, E., Huhma, H., Kontinen, A., Mertanen, S., Mikkola, P., Paavola, J., Peltonen, P., Semprich, J., Slabunov, A. & Sorjonen-Ward, P. 2012b. The Archaean of the Karelia Province in Finland. In: Hölttä, P. (ed.) The Archaean of the Karelia Province in Finland. Geological Survey of Finland, Special Paper 54, 21-73. Available at: https://tupa.gtk.fi/julkaisu/specialpaper/sp_054_pages_021_073.pdf

Hölttä, P., Huhma, H., Mänttäri, I. & Paavola, J. 2000. P-T-t development of Archaean granulites in Varpaisjärvi, central Finland. II. Dating of high-grade metamorphism with the U–Pb and Sm–Nd methods. Lithos 50, 121–136.

Huhma, A. 1971a. Outokumpu. Geological Map of Finland 1:100 000, Pre-Quaternary Rocks. Sheet 4222. Geological Survey of Finland. Available at: https://tupa.gtk.fi/kartta/kallioperakartta100/kp_4222.pdf

Huhma, A. 1971b. Sivakkavaara. Geological Map of Finland 1:100 000, Pre-Quaternary Rocks, Sheet 4311. Geological Survey of Finland. Available at: https://tupa.gtk.fi/kartta/kallioperakartta100/kp_4311.pdf

Huhma, A. 1971c. Karsinäytteenotto Outokummun alueella. Outokumpu Oy, report OKU_1290. 11 p., 20 app. pages. Available at: https://tupa.gtk.fi/raportti/arkisto/020_4221_3243_3333_ah_1971.pdf

Huhma, A. 1975. Outokummun, Polvijärven ja Sivakkavaaran kartta-alueiden kallioperä. Summary: Precambrian rocks of the Outokumpu, Polvijärvi and Sivakkavaara map-sheet areas. Geological Map of Finland 1:100 000, Explanation to the Maps of Pre-Quaternary Rocks, Sheets 4222, 4224 and 4311. Geological Survey of Finland. 151 p. Available at: https://tupa.gtk.fi/kartta/kallioperakartta100/kps_4222_4224_4311.pdf

Huhma, A. 1976. New aspects to the geology of the Outokumpu region. Bulletin of the Geological Society of Finland 48, 5–24. Available at: https://doi.org/10.17741/bgsf/48.1-2.002

Huhma, A. 1981. Youngest Precambrian dyke rocks in North Karelia, East Finland. Bulletin of the Geological Society of Finland 53, 67–82. Available at: https://doi.org/10.17741/bgsf/53.2.001

Huhma, A. & Huhma, M. 1970. Contribution to the geology and geochemistry of the Outokumpu region, Bulletin of the Geological Society of Finland 42, 57–88. Available at: https://doi.org/10.17741/bgsf/42.007

Huhma, H. 1986. Sm-Nd, U-Pb and Pb-Pb isotopic evidence for the origin of the Early Proterozoic Svecokarelian crust in Finland. Geological Survey of Finland, Bulletin 337. 48 p. Available at: https://tupa.gtk.fi/julkaisu/bulletin/bt_337.pdf

Huhma, H., Hanski, E., Kontinen, A., Vuollo, J., Mänttäri, I. & Lahaye, Y. 2018. Sm–Nd and U–Pb isotope geochemistry of the Palaeoproterozoic mafic magmatism in eastern and northern Finland. Geological Survey of Finland, Bulletin 405. 150 p. Available at: https://tupa.gtk.fi/julkaisu/bulletin/bt_405.pdf

Huhma, H., Mänttäri, I., Peltonen, P., Kontinen, A., Halkoaho, T., Hanski, E., Hokkanen, T., Hölttä, P., Juopperi, H., Konnunaho, J., Layahe, Y., Luukkonen. E., Pietikäinen. K., Pulkkinen, A., Sorjonen-Ward, P., Vaasjoki, M. & Whitehouse, M. 2012. The age of the Archaean greenstone belts in Finland. In: Hölttä, P. (ed.) The Archaean of the Karelia Province in Finland. Geological Survey of Finland, Special Paper 54, 74-175. Available at: https://tupa.gtk.fi/julkaisu/specialpaper/sp_054_pages_074_175.pdf

Jensen, L. S. 1976. A new cation plot classifying subalkalic volcanic rocks. Ontario Geological Survey Miscellaneous Paper 66. 22 p. Available at: http://www.geologyontario.mndmf.gov.on.ca/mndmfiles/pub/data/imaging/MP066/MP066.pdf

Jokela, J. 1994. Itä-Suomen Ni-vyöhykkeen kartoitus ja rakennetulkinta raportti kenttätöistä 1993–1994. Geological Survey of Finland, archive report M19/3241/94/1/10. 26 p. (in Finnish). Available at: https://tupa.gtk.fi/raportti/arkisto/m19_3241_94_1_10.pdf

Juurela, S. 2012. Tutkimustyöselostus Sarkalahti 8167/1. Altona Mining Ltd / Vulcan Kotalahti Oy, claim report 8167/1. 4 p. (in Finnish). Available at: https://tupa.gtk.fi/raportti/valtaus/8167_1.pdf

Käpyaho, A., Hölttä, P. & Whitehouse, M. J. 2007. U-Pb zircon geochronology of selected Archaean migmatites in eastern Finland. Bulletin of the Geological Society of Finland 79, 95–115. Available at: https://doi.org/10.17741/bgsf/79.1.005

Kärki, A., Laajoki, K. & Luukas, J. 1993. Major Paleoproterozoic shear zones of the central Fennoscandian Shield. Precambrian research 64, 207–223.

Karppanen, T. 1982. Yhteenveto: Kotalahden kaivoksen ympäristön malminetsintäprojekti. Outokumpu Oy,

report 001/3241, 3423, 3234/KTK/1982. 13 p. (in Finnish). Available at: https://tupa.gtk.fi/raportti/arkisto/001_3241_3243_3234_ktk_1982.pdf

Kesola, R. 1995. Näätämön kartta-alueen kallioperä. Summary: Pre-Quaternary rocks of the Näätämä maps-sheet area. Geological Map of Finland 1:100 000, Explanation to the Maps of Pre-Quaternary Rocks, Sheets 3934+4912+4914. Geological Survey of Finland. 88 p. Available at: https://tupa.gtk.fi/kartta/kallioperakartta100/kps_3934_4912_4914.pdf

Kohonen, J., Kontinen, A. & Luukas, J. in prep. Proterozoic stratigraphy and basin evolution in North Karelia and Kainuu, Eastern Finland: a review.

Kohonen, J., Lahtinen, R., Luukas, J. & Nironen, M. 2021. Classification of regional-scale tectonic map units in Finland. In: Kohonen, J. & Tarvainen, T. (eds) Developments in map data management and geological unit nomenclature. Geological Survey of Finland, Bulletin 412, 33–80. Available at: https://tupa.gtk.fi/julkaisu/bulletin/bt_412_pages_033_080.pdf

Koistinen, A. 1981. Structural evolution of an early Proterozoic strata-bound Cu-Co-Zn deposit, Outokumpu, Finland. Transaction of the Royal Society of Edinburgh: Earth Sciences 72, 115–158.

Koistinen, T. 1993a. Heinäveden kartta-alueen kallioperä. Summary: Pre-Quaternary rocks of the Heinävesi map-sheet area. Geological Map of Finland 1:100 000, Explanation to the Maps of Pre-Quaternary Rocks, Sheet 4211. Geological Survey of Finland. 64 p. Available at: https://tupa.gtk.fi/kartta/kallioperakartta100/kps_4221.pdf

Koistinen, T. 1993b. Heinävesi. Geological Map of Finland 1:100 000, Pre-Quaternary Rocks, Sheet 4221. Geological Survey of Finland. Available at: https://tupa.gtk.fi/kartta/kallioperakartta100/kp_4221.pdf

Koistinen, T. 1996. Explanation to the Map of Precambrian basement of the Gulf of Finland and surrounding area 1:1 million. Geological Survey of Finland, Special Paper 21. 141 p. Available at: https://tupa.gtk.fi/julkaisu/specialpaper/sp_021.pdf

Kontinen, A. 1998. The nature of the serpentinites, associated dolomite-skarn-quartz rocks and massive Co-Cu-Cn sulphide ores in the Outokumpu area, eastern Finland. In: Hanski, E. & Vuollo, J. (eds) International Ophiolite Symposium and Field Excursion, Oulu, Finland. Abstracts, Excursion Guide. Geological Survey of Finland, Special Paper 26, p. 33. Available at: https://tupa.gtk.fi/julkaisu/specialpaper/sp_026_pages_033_033.pdf

Kontinen, A. & Paavola, J. 2006. A preliminary model of the crustal structure of the eastern Finland Archaean complex between Vartius and Vieremä, based on constraints from surface geology and FIRE 1 seismic survey. In: Kukkonen, I. T. & Lahtinen, R. (eds) Finnish Reflection Experiment FIRE 2001–2005. Geological Survey of Finland, Special Paper 43, 223–240. Available at: https://tupa.gtk.fi/julkaisu/specialpaper/sp_043_pages_223_240.pdf

Kontinen, A. & Sorjonen-Ward, P. 1991. Geochemistry of metagraywackes and metapelites from the Palaeoproterozoic Nuasjärvi Group, Kainuu schist belt and the Savo province, North Karelia; implications for provenance, lithostratigraphic correlation and depositional setting. Geological Survey of Finland, Special Paper 12, 21–22. Available at: https://tupa.gtk.fi/julkaisu/specialpaper/sp_012_pages_021_022.pdf

Kontinen, A., Peltonen, P. & Huhma, H. 2006. Description and genetic modelling of the Outokumpu-type rock assemblage and associated sulphide deposits. Final technical report for GEOMEX J.V., Workpackage Geology. Geological Survey of Finland, archive report M10.4/2006/1. 378 p. Available at: https://tupa.gtk.fi/raportti/arkisto/m10_4_2006_1.pdf

Korsman, K. & Pääjärvi A. 1980. Varkaus. Geological Map of Finland 1:100 000, Pre-Quaternary Rocks, Sheet 3234. Geological Survey of Finland. Available at: https://tupa.gtk.fi/kartta/kallioperakartta100/kp_3234.pdf

Korsman, K. & Pääjärvi A. 1988. Varkauden kartta-alueen kallioperä. Summary: Pre-Quaternary rocks of the Varkaus map-sheet area. Geological Map of Finland 1:100 000, Explanation to the Maps of Pre-Quaternary Rocks, Sheet 3234. Geological Survey of Finland. 35 p. Available at: https://tupa.gtk.fi/kartta/kallioperakartta100/kps_3234.pdf

Korsman, K., Koistinen, T., Kohonen, J., Wennerström, M., Ekdahl, E., Honkamo, M., Idman, H. & Pekkala, Y. 1997. Bedrock map of Finland 1:1 000 000. Espoo: Geological Survey of Finland.

Kotilainen, A. K., Mänttäri, I., Kurhila, M., Hölttä, P. & Rämö, O. T. 2016. Evolution of a Palaeoproterozoic giant magmatic dome in the Finnish Svecofennian; New insights from U–Pb geochronology. Precambrian Research 272, 39–56.

Krogh, T. 1973. A low-contamination method for hydrothermal decomposition of zircon and extraction of U and Pb for isotopic age determinations. Geochimica et Cosmochimica Acta 37, 485–494.

Krogh, T. E. 1982. Improved accuracy of U-Pb zircon ages by the creation of more concordant systems using an air abrasion technique. Geochimica et Cosmochimica Acta 46, 637–649.

Kukkonen, I. T., Heikkinen, P., Ekdahl, E., Hjelt, S. E., Ylinimiemi, J., Jalkanen, E. & FIRE Working Group 2006. Acquisition and geophysical characteristics of reflection seismic data on FIRE transects, Fennoscandian Shield. In: Kukkonen, I. T. & Lahtinen, R. (eds) Finnish Reflection Experiment FIRE 2001–2005. Geological Survey of Finland, Special Paper 43, 13–43. Available at: https://tupa.gtk.fi/julkaisu/specialpaper/sp_043_pages_013_043.pdf

Kuosmanen, V. (ed.) 1988. Exploration target selection by integration of geodata using statistical and image processing techniques: an example from Central Finland. Part 11, Atlas. Geological Survey of Finland, Report of Investigation 84. 47 p. Available at: http://tupa.gtk.fi/julkaisu/tutkimusraportti/tr_084.pdf

Laajoki, K. 2005. Karelian supracrustal rocks. In: Lehtinen, M., Nurmi, P. & Rämö, T. (eds) The Precambrian Bedrock of Finland – Key to the Evolution of the Fennoscandian Shield. Elsevier Science B.V., 279–342.

Lahtinen, R., Huhma, H., Kähkönen, Y. & Mänttäri, I. 2009. Paleoproterozoic sediment recycling during multiphase orogenic evolution in Fennoscandia, the Tampere and Pirkanmaa belts, Finland. Precambrian Research 174, 310–336.

Lahtinen, R., Huhma, H., Kontinen, A., Kohonen, J. & Sorjonen-Ward, P. 2010. New constraints for the source characteristics, deposition and age of the 2.1–1.9 Gametasedimentary cover at the western margin of the Karelian Province. Precambrian Res. 176, 77–93.

Lahtinen, R., Huhma, H. & Kousa, J. 2002. Contrasting source components of the Palaeoproterozoic Svecofennian metasediments: detrital zircon U–Pb, Sm–Nd and geochemical data. Precambrian Research 116, 81–109.

Lahtinen, R., Huhma, H., Lahaye, Y., Kontinen, A., Kohonen, J. & Johanson, B. 2013. Long-lived LREE mobility in the cratonic, rift and foredeep to foreland sedimentary cover at the western margin of the Karelia Province. Lithos 175–176, 86–103.

Lahtinen, R., Huhma, H., Lahaye, Y., Kousa, J. & Luukas, J. 2015. Archean–Proterozoic collision boundary in central Fennoscandia revisited. Precambrian Research 261, 127–165.

Lahtinen, R., Huhma, H., Lahaye, Y., Lode, S., Heinonen, S., Sayab, M. & Whitehouse, M. J. 2016. Paleoproterozoic magmatism across the Archean-Proterozoic boundary in central Fennoscandia: Geochronology, geochemistry and isotopic data (Sm-Nd, Lu-Hf, O). Lithos 262, 507–525.

Lahtinen, R., Korja, A. & Nironen, M. 2005. Palaeoproterozoic tectonic evolution of the Fennoscandian Shield. In: Lehtinen, M., Nurmi, P. & Rämö, T. (eds) The Precambrian Bedrock of Finland – Key to the evolution of the Fennoscandian Shield. Amsterdam: Elsevier Science B.V., 418–532.

Lakanen, E. 1983. Leppävirta, Kotkatsuo 1982 – tunnetun pienialaisen Ni-mineralisaation syvyysjatkeiden etsintä. Outokumpu Oy, report 040/3243 02/ENL/1983. 3 p., 12 app. pages. (in Finnish). Available at: https://tupa.gtk.fi/raportti/arkisto/040_3243_02_enl_1983.pdf

Laurent, O, Martin, H., Moyen, J.-F. & Doucelance, R. 2014. The diversity and evolution of late-Archean granitoids: Evidence for the onset of "modern-style" plate tectonics between 3.0 and 2.5 Ga. Lithos 205, 208–235.

Lehtinen, M., Pesonen, L. J., Stehlik, H. & Kuulusa, M. 2002. The Suvasvesi South structure, Central Finland: New evidences for impact (abstract # 1188). 33rd Lunar and Planetary Science Conference. CD-ROM.

Leväniemi, H., Hulkki, H. & Tiainen, M. 2017. SOM guided fuzzy logic prospectivity model for gold in the Häme Belt, southwestern Finland. Journal of African Earth Sciences 128, 72–83.

Loukola-Ruskeeniemi, K. 1992. Geochemistry of Proterozoic metamorphosed black shales in eastern Finland, with implications for exploration and environmental studies. Espoo: Geological Survey of Finland. 97 p. Available at: https://tupa.gtk.fi/julkaisu/erikoisjulkaisu/ej_009.pdf

Ludwig, K. R. 1991. PbDat 1.21 for MS-dos: A computer program for IBM-PC Compatibles for processing raw Pb-U-Th isotope data. Version 1.07. U.S. Geological Survey, Open File Report 88–542. 35 p.

Ludwig, K. R. 2003. User's manual for Isoplot/Ex, Version 3.00. A geochronological toolkit for Microsoft Excel. Berkeley Geochronology Center, Special Publication No. 4.

Lukkarinen, H. 2000. Siilinjärvi. Geological Map of Finland 1:100 000, Pre-Quaternary Rocks, Sheet 3331. Geological Survey of Finland. Available at: https://tupa.gtk.fi/kartta/kallioperakartta100/kp_3331.pdf

Lukkarinen, H. 2002. Kuopio. Geological Map of Finland 1:100 000, Pre-Quaternary Rocks, Sheet 3242. Geological Survey of Finland. Available at: https://tupa.gtk.fi/kartta/kallioperakartta100/kp_3242.pdf

Lukkarinen, H. 2008. Siilinjärven ja Kuopion kartta-alueiden kallioperä. Summary: Pre-Quaternary rocks of the Siilinjärvi and Kuopio map-sheet areas. Geological Map of Finland 1:100 000, Explanation to the Maps of Pre-Quaternary Rocks, Sheets 3242 and 3331. Geological Survey of Finland. 196 p., 34 app. pages. Available at: https://tupa.gtk.fi/kartta/kallioperakartta100/kps_3331_3242.pdf

Lundqvist, T., Bøe, R., Kousa, J., Lukkarinen, H., Lutro, O., Roberts, D., Solli, A., Stephens, M. & Weihed, P. 1996. Bedrock map of Central Fennoscandia. Scale 1:1 000 000. Geological Survey of Finland, Mid-Norden Maps 01.

Luukas, J. & Kohonen, J. 2021. Major thrusts and thrust-bounded geological units in Finland: definitions and descriptions. In: Kohonen, J. & Tarvainen, T. (eds) Developments in map data management and geological unit nomenclature. Geological Survey of Finland, Bulletin 412, 81–114. Available at: https://tupa.gtk.fi/julkaisu/bulletin/bt_412_pages_081_114.pdf

Luukas, J., Kousa, J., Nironen, M. & Vuollo, J. 2017. Major stratigraphic units in the bedrock of Finland, and an approach to tectonostratigraphic division. In: Nironen, M. (ed.) Bedrock of Finland at the scale 1:1 000 000 – Major stratigraphic units, metamorphism and tectonic evolution. Geological Survey of Finland, Special Paper 60, 9-40. Available at: http://tupa.gtk.fi/julkaisu/specialpaper/sp_060_pages_009_040.pdf

Luukkonen, E. & Lukkarinen, H. 1985. Stratigraphic map of Middle Finland 1:1 000 000. Espoo: Geological Survey of Finland.

Luukkonen, E. & Lukkarinen, H. 1986. Explanation to the stratigraphic map of Middle Finland. Geological Survey of Finland, Report of Investigation 74. 47 p. Available at: https://tupa.gtk.fi/julkaisu/tutkimusraportti/tr_074.pdf

Mäkinen, J. 1995. Migmatiittien geokemiallinen koostumus Leppävirran ja Varkauden ympäristössä. Geological Survey of Finland, archive report S/42/3241/1/95. 3 p., 16 app. pages. (in Finnish). Available at: https://tupa.gtk.fi/raportti/arkisto/s42_3241_1_1995.pdf

Martin, H., Smithies, R. H., Rapp, R., Moyen, J.-F. & Champion, D. 2005. An overview of adakite, tonalite–trondhjemite–granodiorite(TTG), and sanukitoid; relationships and some implications for crustal evolution. Lithos 79, 1–24.

Mattinson, J. M. 2005. Zircon U-Pb chemical abrasion ("CA-TIMS") method: Combined annealing and multi-step partial dissolution analysis for improved precision and accuracy of zircon ages. Chemical Geology 220, 47–66.

McDonough, W. F. & Sun, S.-S. 1995. The composition of the Earth. Chemical Geology 120, 223–253.

Meinhold, G., Anders, B., Kostopoulos, D. & Reischmann, T. 2008. Rutile chemistry and thermometry as provenance indicator: An example from Chios Island, Greece. Sedimentary Geology 203, 98–111.

Meriläinen, K. 1976. The granulite complex and adjacent rocks in Lapland, northern Finland. Geological Survey of Finland, Bulletin 281. 129 p. Available at: https://tupa.gtk.fi/julkaisu/bulletin/bt_281.pdf

Mikkola, P., Heilimo, E., Luukas, J., Kousa, J., Aatos, S., Makkonen, H., Niemi, S., Nousiainen, M., Ahven, M., Romu, I. & Hokka, J. 2018a. Geological evolution and structure along the southeastern border of the Central Finland Granitoid Complex. In: Mikkola, P., Hölttä, P. & Käpyaho, A. (eds) Development of the Paleoproterozoic Svecofennian orogeny: new constraints from southeast boundary of the Central Finland Granitoid Complex. Geological Survey of Finland, Bulletin 407, 5–27. Available at: https://tupa.gtk.fi/julkaisu/bulletin/bt_407_pages_005_027.pdf

Mikkola, P., Heilimo, E., Paavola, J., Halkoaho, T., Äikäs, O. & Huhma, H. 2013. Lentuan kompleksin eteläosan kallioperä. Summary: Bedrock of the southern part of the Lentua complex. Geological Survey of Finland, Report of Investigation 202. 97 p. (in Finnish). Available at: https://tupa.gtk.fi/julkaisu/tutkimusraportti/tr_202.pdf

Mikkola, P., Huhma, H., Heilimo, E. & Whitehouse, M. J. 2011. Archean crustal evolution of the Suomussalmi district as part of the Kianta Complex, Karelia: Constraints from geochemistry and isotopes of granitoids. Lithos 125, 287-307.

Mikkola, P., Huhma, H., Romu, I. & Kousa, J. 2018b. Detrital zircon ages and geochemistry of the metasedimentary rocks along the southeastern boundary of the Central Finland Granitoid Complex. In: Mikkola, P., Hölttä, P. & Käpyaho, A. (eds) Development of the Paleoproterozoic Svecofennian orogeny: new constraints from southeast boundary of the Central Finland Granitoid Complex. Geological Survey of Finland, Bulletin 407, 28–55. Available at: https://tupa.gtk.fi/julkaisu/bulletin/bt_407_pages_028_055.pdf

Mikkola, P., Kontinen, A., Huhma, H. & Lahaye, Y. 2010. Three Paleoproterozoic A-type granite intrusions and associated dykes from Kainuu, East Finland. Bulletin of the Geological Society of Finland 82, 81–100. Available at: https://doi.org/10.17741/bgsf/82.2.002

Mikkola, P., Lauri, L. S. & Käpyaho, A. 2012. Neoarchean leucogranitoids of the Kianta Complex, Karelian Province, Finland: source characteristics and processes responsible for the observed heterogeneity. Precambrian Research 206-207, 72-86.

Mikkola, P., Lukkarinen, H. & Luukas, J. 2016. Suonenjoen kartta-alueen 3241 kallioperä ja kivilajiyksiköt. Geological Survey of Finland, archive report 29/2016. 29 p. (in Finnish). Available at: https://tupa.gtk.fi/raportti/arkisto/29_2016.pdf

Molnár, F., Middleton, A., Stein, H., O'Brien, H., Lahaye, Y., Huhma, H., Pakkanen, L. & Johanson, B. 2018. Repeated syn- and post-orogenic gold mineralization events between 1.92 and 1.76 Ga along the Kiistala Shear Zone in the Central Lapland Greenstone Belt, northern Finland. Ore Geology Reviews, 936–956.

O'Connor, J. T. 1965. A classification for quartz-rich igneous rocks based on feldspar ratios. U.S. Geolological Survey, Professional Paper 525-B, 79–84.

Nehring, F., Foley, S. F., Hölttä, P. & van den Kerkhof, A. M. 2009. Internal differentation of the Archean Continental Crust: Fluid-Controlled Partial Melting of Granulites and TTG–Amphibolite Associations in Central Finland. Journal of Petrology 50, 3–35.

Niiranen, T., Nykänen, V. & Lahti, I. 2019. Scalability of the mineral prospectivity modelling – An orogenic gold case study from northern Finland. Ore Geology Reviews 109, 11– 25.

Nironen, M. 2017. Guide to the Geological Map of Finland – Bedrock 1:1 000 000. In: Nironen, M. (ed.) Bedrock of Finland at the scale 1:1 000 000 – Major stratigraphic units, metamorphism and tectonic evolution. Geological Survey of Finland, Special Paper 60, 41–76. Available at: http://tupa.gtk.fi/julkaisu/specialpaper/sp_060_pages_041_076.pdf

Nironen, M., Kousa, J., Luukas, J. & Lahtinen, R. (eds) 2016. Geological Map of Finland – Bedrock 1:1 000 000. Espoo: Geological Survey of Finland. Available at: http://tupa.gtk.fi/kartta/erikoiskartta/ek_097_300dpi.pdf

Nygård, H. 2017. Kvalitetsbestämning av flakgrafit i Haapamäki, Leppävirta, Norra Savolax. Unpublished master's theses, Åbo Akademi University, Faculty of Science and Engineering. 69 p. (in Swedish)

Nykänen, V. M. 2008. Spatial data analysis as a tool for mineral prospectivity mapping. Espoo: Geological Survey of Finland. 27 p. Available at: http://tupa.gtk.fi/julkaisu/erikoisjulkaisu/ej_075_synopsis.pdf

Öhman, T., Badjukov, D., Raitala, J., Petrova, T. & Stehlik, H. 2003. Impactites of the Paasselkä and Suvasvesi S craters, Finland (abstract #1571). 34th Lunar and Planetary Science Conference. CD-ROM.

Pääjärvi, A. & Äikäs, O. 2005. Suonenjoki. Geological Map of Finland 1:100 000, Pre-Quaternary Rocks, Sheet 3241. Geological Survey of Finland. Available at: https://tupa.gtk.fi/kartta/kallioperakartta100/kp_3241.pdf

Paavola, J. 1984. Nilsiän kartta-alueen kallioperä. Summary: Pre-Quaternary Rocks of the Nilsiä Map-Sheet area. Geological Map of Finland 1:100 000, Explanation to the Maps of Pre-Quaternary Rocks, Sheet 3334. Geological Survey of Finland. 57 p. Available at: https://tupa.gtk.fi/kartta/kallioperakartta100/kps_3334.pdf

Papunen, H. & Koskinen, J. 1985. Geology of the Kotalahti nickel-copper ore. In: Papunen, H. & Gorbunov, G. I. (eds) Nickel-copper deposits of the Baltic Shield and Scandinavian Caledonides. Geological Survey of Finland, Bulletin 333, 228–240. Available at: https://tupa.gtk.fi/julkaisu/bulletin/bt_333_pages_228_240.pdf

Park, A. F. & Bowes, D. R. 1983. Basement-cover relationships during polyphase deformation in the Svecokarelides of the Kaavi district, eastern Finland. Transaction of the Royal Society of Edinburgh: Earth Sciences 74, 95–118.

Parkkinen, J. 1974. Raportti Leppävirran aluetutkimuksesta 1968–73. Outokumpu Oy, report 020/3241,3242,3234/OJP/74. 250 p. (in Finnish). Available at: https://tupa.gtk.fi/raportti/arkisto/020_3241_3242_3234_ojp_74.pdf

Patchett, J. & Kouvo, O. 1986. Origin of continental crust of 1.9-1.7 Ga age: Nd isotopes and U-Pb zircon ages in the Svecokarelian terrain of South Finland. Contributions to Mineralogy and Petrology 92, 1–12.

Pekkarinen, L. 2002. Haukivuoren ja Pieksämäen kartta-alueiden kallioperä. Summary: Pre-Quaternary Rocks of the Haukivuori and Pieksämäki Map-Sheet areas. Geological Map of Finland 1:100 000, Explanation to the Maps of Pre-Quaternary Rocks, Sheets 3231, 3232. Geological Survey of Finland. 98 p. Available at: http://tupa.gtk.fi/kartta/kallioperakartta100/kps_3231_3232.pdf

Peltonen, P. 2005a. Ophiolites. In: Lehtinen, M., Nurmi, P. & Rämö, T. (eds) The Precambrian Bedrock of Finland – Key to the Evolution of the Fennoscandian Shield. Elsevier Science B.V., 237–278.

Peltonen, P. 2005b. Svecofennian mafic-ultramafic intrusions. In: Lehtinen, M., Nurmi, P. & Rämö, T. (eds) The Precambrian Bedrock of Finland – Key to the Evolution of the Fennoscandian Shield. Elsevier Science B.V., 407–441.

Peltonen, P., Kontinen, A., Huhma, H. & Kuronen, U. 2008. Outokumpu revisited: new mineral deposit model for the mantle peridotite-associated Cu–Co–Zn–Ni–Ag–Au sulphide deposits. Ore Geology Reviews 33, 559–617.

Pesonen, L. J., Donadini, F., Salminen, J. & Lehtinen, M. 2003. The Suvasvesi South structure, central Finland: Further evidences of impact (abstract #4074). 3rd Large Meteorite Impacts Conference.

Pesonen, L. J., Lehtinen, M., Deutsch, A., Elo, S. & Lukkarinen, H. 1996. New geophysical and petrographic results of the Suvasvesi N impact structure, Finland (abstract). 27th Lunar and Planetary Science Conference, p. 1021.

Pettijohn, F. J., Potter, P. E. & Siever, R. 1972. Sand and Sandstone. Berlin: Springer-Verlag. 600 p.

Pietilä, M. 2020. Petrography, Geochemistry and Geochronology of the Post-kinematic A-type Intrusions of the Sorsavesi Area, Central Finland. Unpublished master's theses, University of Helsinki, Department of Geosciences and Geography. 61 p., 19 app. pages. Available at: http://tupa.gtk.fi/opinnayte/pietila_maija_gradu.pdf

Pirinen, H. & Niskanen, M. 2020. Piiroonmäen kairaukset Varkaudessa 2019. Geological Survey of Finland, Open File Work Report 36/2020. 10 p., 5 app, pages. (in Finnish). Available at: https://tupa.gtk.fi/raportti/arkisto/36_2020.pdf

Puronaho, L. 2018. Structural interpretation of graphite-bearing black schist in Aitolampi area, Eastern Finland. Unpublished master's theses, Åbo Akademi University, Faculty of Science and Engineering. 64 p. Available at: https://urn.fi/URN:NBN:fi-fe20180424184 03

Puura, V. & Plado, J. 2005. Settings of meteorite impact structures in the Svecofennian crustal domain. In: Koeberl, C. & Henkel, H. (eds) Impact Tectonics. Berlin, Heidelberg: Springer-Verlag, 211–245.

Puustjärvi, H. 1984. OKU-länsialueen 3244 07-12, 4221 01 karsikivien paljastumanäytteiden petrografiasta ja litokemiasta. Outokumpu Oy, report OKU_4227. 3 p., 4 app. pages. Available at: https://tupa.gtk.fi/raportti/arkisto/020_3244_07_12_4221_01_hop_84.pdf

Rämö, O. T. & Haapala, I. 2005. Rapakivi granites. In: Lehtinen, M., Nurmi, P. & Rämö, T. (eds) The Precambrian Bedrock of Finland – Key to the evolution of the Fennoscandian Shield. Elsevier Science B.V., 533–562.

Rantanen, H. 2021. Mineralogy, Petrology, and Petrogenesis of the Suvasvesi Granitoid Intrusion. Unpublished Master's thesis, University of Helsinki, Department of Geosciences and Geography. 77 p. Available at: http://tupa.gtk.fi/opinnayte/rantanen_hanna_gradu.pdf

Rasilainen, K., Eilu, P., Äikäs, O., Halkoaho, T., Heino, T., Iljina, M., Juopperi, H., Kontinen, A., Kärkkäinen, N., Makkonen, H., Manninen, T., Pietikäinen, K., Räsänen, J., Tiainen, M., Tontti, M. & Törmänen, T. 2012. Quantitative mineral resource assessment of nickel, copper and cobalt in undiscovered Ni-Cu deposits in Finland. Geological Survey of Finland, Report of Investigation 194. 514 p. Available at: https://tupa.gtk.fi/julkaisu/tutkimusraportti/tr_194.pdf

Rasilainen, K., Lahtinen, R. & Bornhorst, T. J. 2007. The Rock Geochemical Database of Finland Manual. Geological Survey of Finland, Report of Investigation 164. 38 p. Available at: http://tupa.gtk.fi/julkaisu/tutkimusraportti/tr_164.pdf

Robertson, S. 1999. BGS Rock Classification Scheme Volume 2 Classification of metamorphic rocks. British Geological Survey, Research Report 99-02. 26 p. Available at: http://nora.nerc.ac.uk/id/eprint/3226/1/RR99002.pdf

Romu, I. & Nousiainen, M. 2020. Soisalon kairaukset kesällä 2019. Geological Survey of Finland, Open File Work Report 15/2019. 17 p., 20 app. pages. (in Finnish). Available at: https://tupa.gtk.fi/raportti/arkisto/15_2020.pdf

Romu, I., Mikkola, P., Nousiainen, M. & Niskanen, M. 2020. Case Island Of Soisalo, Eastern Finland: From Rift Related Volcanism To Siliciclastic Continental Margin. In: GSA 2020 Connects Online. Geological Society of America. Available at: http://dx.doi.org/10.1130/abs/2020am-357884

Saksela, M. 1948. Outokummun kuparimalmin löytö. Summary: The discovery of Outokumpu ore field. Geological Survey of Finland, Geotechnical publications 47. 36 p. Available at: https://tupa.gtk.fi/julkaisu/geoteknillinen/gt_s_047.pdf

Samsonov, A. V., Spiridonov, V. A., Larionova, Y. O. & Larionov, A. N. 2016. The Central Russian fold belt: Paleoproterozoic boundary of Fennoscandia and Volgo-Sarmatia, the East European Craton. In: Abstracts of the 32nd Nordic Geological Winter Meeting. Bulletin of the Geological Society of Finland, Special Volume 162. Available at: http://www.geologinenseura.fi/bulletin/Special_Volume_1_2016/BGSF-NGWM2016_Abstract_Volume.pdf

Säntti, J., Kontinen, A., Sorjonen-Ward, P., Johanson, B. & Pakkanen, L. 2006. Metamorphism and Chromite in Serpentinized and Carbonate-Silica-Altered Peridotites of the Paleoproterozoic Outokumpu-Jormua Ophiolite Belt, Eastern Finland. International Geology Review 48, 494–546.

Sawyer, E. W. 2008. Working with migmatites: Nomenclature for the constituent parts. In: Sawyer, E. W. & Brown, M. (eds) Mineralogical Association of Canada Short Course 38, 1–28. Available at: https://www.mineralogicalassociation.ca/publications/topics-in-mineral-sciences/sc38/

Schmieder, M., Schwarz, W. H., Trieloff, M., Buchner, E., Hopp, J., Tohver, E., Pesonen, L. J., Lehtinen, M., Moilanen, J., Werner, S. C. & Öhman, T. 2016. The two Suvasvesi impact structures, Finland: Argon isotopic evidence for a "false" impact crater doublet. Meteoritics and Planetrary Science 51, 966–980.

Simonen, A. 1980. The Precambrian in Finland. Geological Survey of Finland, Bulletin 304. 58 p. Available at: https://tupa.gtk.fi/julkaisu/bulletin/bt_304.pdf

Sorjonen-Ward, P. 2006. Geological and structural framework and preliminary interpretation of the FIRE 3 and FIRE 3A reflection seismic profiles, Central Finland. In: Kukkonen, I. T. & Lahtinen, R. (eds) Finnish Reflection Experiment FIRE 2001–2005, Geological Survey of Finland, Special Paper 43, 105–159. Available at: https://tupa.gtk.fi/julkaisu/specialpaper/sp_043_pages_105_159.pdf

Spear, F. S., Kohn, M. J. & Cheney, J. T. 1999. P -T paths from anatectic pelites. Contributions to Mineralogy and Petrology 134, 17–32.

Stacey, J. S. & Kramers, J. D. 1975. Approximation of terrestrial lead isotope evolution by a two-stage model. Earth and Planetary Science Letters 26, 207–221.

Sun, S. S. & McDonough, W. F. 1989. Chemical and isotopic systematics of oceanic basalts; implications for mantle composition and processes. Geological Society, Special Publications 42, 313–345.

Torppa, J., Chudasama, B., Hautala, S. & Kim, Y. 2021. GisSOM for clustering multivariate data. Geological Survey of Finland, Open File Research Report 52/2021. 27 p. Available at: https://tupa.gtk.fi/raportti/arkisto/52_2021.pdf

Torppa, J., Nykänen, V. & Molnár, F. 2019. Unsupervised clustering and empirical fuzzy memberships for mineral prospectivity modelling. Ore Geology Reviews 107, 58–71.

Tuisku, P., Mikkola, P. & Huhma, H. 2006. Evolution of migmatitic granulite complexes : implications from Lapland Granulite Belt, Part 1 : Metamorphic geology. Bulletin of the Geological Society of Finland 78, 71–105. Available at: https://doi.org/10.17741/bgsf/78.1.004

Vaasjoki, M. 1996. Explanation to the geochronological map of southern Finland: The development of the continental crust with special reference to the Svecofennian orogeny. Geological Survey of Finland, Report of Investigation 135. 30 p. Available at: https://tupa.gtk.fi/julkaisu/tutkimusraportti/tr_135.pdf

Vaasjoki, M. & Sakko, M. 1988. The evolution of the Raahe-Ladoga zone in Finland: Isotopic constraints. In: Korsman, K. (ed.) Tectono-metamorphic evolution of the Raahe-Ladoga zone. Geological Survey of Finland, Bulletin 343, 7–32. Available at: https://tupa.gtk.fi/julkaisu/bulletin/bt_343.pdf

Vaasjoki, M., Kärki, A. & Laajoki, K. 2001. Timing of Palaeoproterozoic crustal shearing in the central Fennoscandian Shield according to U-Pb data from associated granitoids, Finland. Bulletin of the Geological Society of Finland 73, 87–101. Available at: https://doi.org/10.17741/bgsf/73.1-2.007

Vihreäpuu, U. 1985a. Kaivoslain 19 §:n mukainen tutkimustyöselostus Tuusniemi, "Vuorinen", kaivosrekisterinumero 3680/2. Outokumpu Oy, claim report OKU_3592. 2 p., 5 app. pages. (in Finnish). Available at: https://tupa.gtk.fi/raportti/valtaus/3680_2.pdf

Vihreäpuu, U. 1985b. Kaivoslain 19 §:n mukainen tutkimustyöselostus Tuusniemi, "Mansikkamäki", kaivosrekisterinumero 3680/1. Outokumpu Oy, claim report OKU_3591. 2 p., 6 app. pages. (in Finnish). Available at: https://tupa.gtk.fi/raportti/arkisto/080_3244_10_a_umv_1985.pdf

Vihreäpuu, U. 1993. Tutkimustyöselostus, Leppävirta, Häikiä-valtaus (kaiv.rek.nro 4115/1). Outokumpu, claim report. 3 p., 7 app. pages. (in Finnish). Available at: https://tupa.gtk.fi/raportti/valtaus/4115_1.pdf

Vorma, A. 1971. Pieksämäki. Geological Map of Finland 1:100 000, Pre-Quaternary Rocks, Sheet 3232. Geological Survey of Finland. Available at: https://tupa.gtk.fi/kartta/kallioperakartta100/kp_3232.pdf

Vuollo, J. & Huhma, H. 2005. Paleoproterozoic mafic dikes in NE Finland. In: Lehtinen, M., Nurmi, P. A. & Rämö, O. T. (eds) Precambrian Geology of Finland – Key to the Evolution of the Fennoscandian Shield. Amsterdam: Elsevier B.V., 195–236.

Ward, P. 1987. Early Proterozoic deposition and deformation at the Karelian craton margin in southeastern Finland. Precambrian Research, 35, 71–93.

Watson, E. B., Wark, D. A. & Thomas, J. B. 2006. Crystallisation thermometers for zircon and rutile. Contributions to Mineralogy and Petrology 151, 413–433.

Wegmann, C. E. 1928. Über die Tektonik der jüngeren Faltung in Ostfinnland. Fennia 50, 1—22.

Werner, S. C., Plado, J., Pesonen, L. J., Janle, P. & Elo, S. 2002. Potential fields and subsurface models of Suvasvesi North impact structure, Finland. Physics and Chemistry of the Earth, Parts A/B/C 27, 1237–1245.

Wetherill, G. W., Kouvo, O., Tilton, G. R. & Gast, P. W. 1962. Age measurements on rocks from the Finnish Precambrian. Journal of Geology 70, 74-88.

Wilkman, W. W. 1935. Kuopio. The General Geological Map of Finland 1:400 000, Pre-Quaternary Rocks, Sheet C3. Geological Survey of Finland.

Wilkman, W. W. 1938. Kuopio. The General Geological Map of Finland 1:400 000, Explanation to the Map of Rocks, Sheet C3. Geological Survey of Finland. 171 p. (in Finnish). Available at: http://tupa.gtk.fi/kartta/kivilajikartta400/kls_c3.pdf

Zack, T., Moraes, R. & Kronz, A. 2004a. Temperature dependence of Zr in rutile: empirical calibration of a rutile thermometer. Contributions to Mineralogy and Petrology 148, 471–488.

Zack, T., von Eynatten, H. & Kronz, A. 2004b. Rutile geochemistry and its potential use in quantitative provenance studies. Sedimentary Geology 171, 37–58.

APPENDICES

Appendix 1: Bedrock, aeromagnetic and Bouguer anomaly maps

Appendix 2: Airborne electromagnetic map, quadrature component

Appendix 3: Airborne electromagnetic map, in-phase component

Appendix 4: Magnetic residual from aeromagnetic data

Appendix 5: Type section from Kohma

Electronic appendix 1: Analytical data

Electronic appendix 2: 3D pdf of the regional voxet model

BEDROCK MAP OF THE WESTERN BOUNDARY OF THE OUTOKUMPU ALLOCHTON

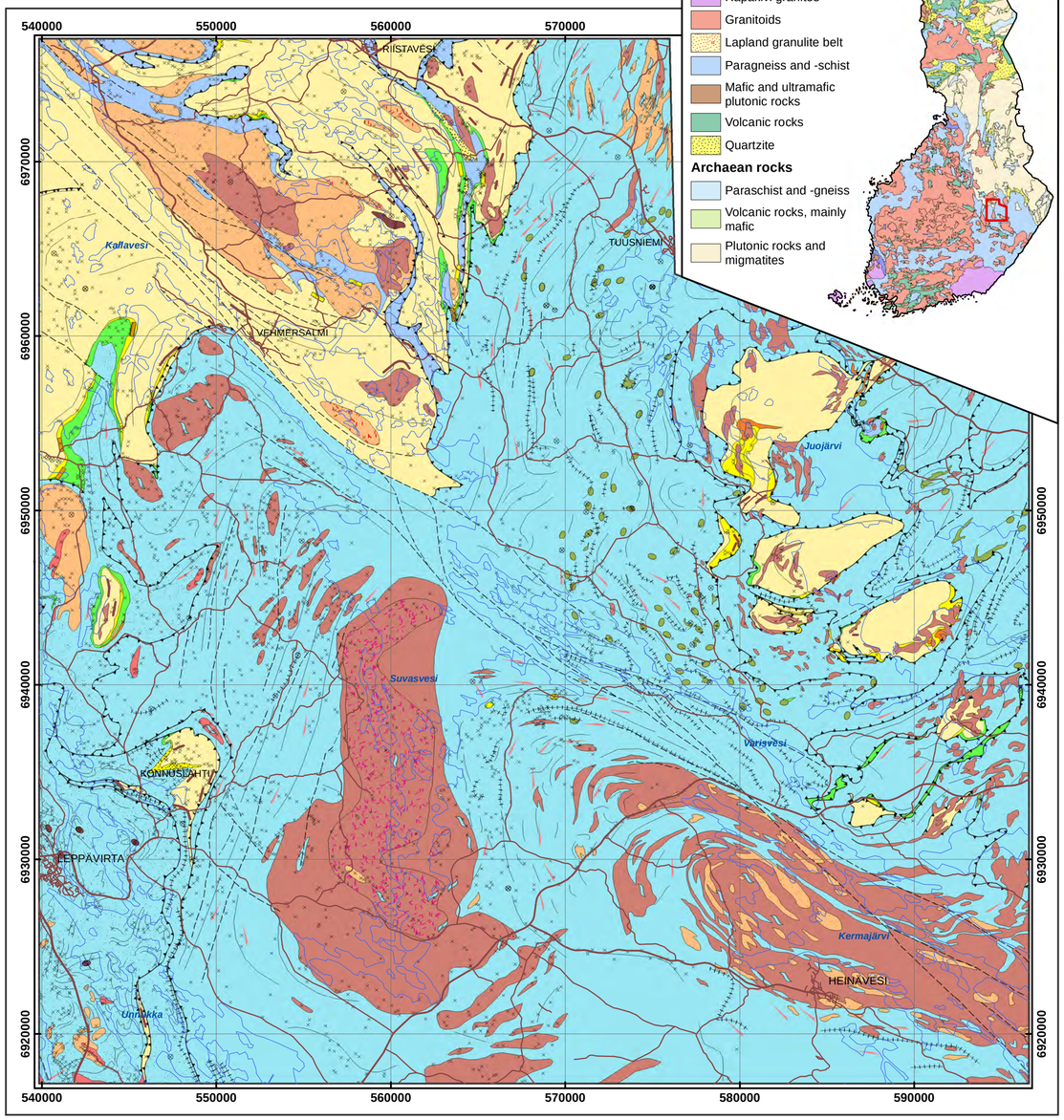

Proterozoic rocks
- Unmetamorphosed sedimentary rocks
- Rapakivi granites
- Granitoids
- Lapland granulite belt
- Paragneiss and -schist
- Mafic and ultramafic plutonic rocks
- Volcanic rocks
- Quartzite

Archaean rocks
- Paraschist and -gneiss
- Volcanic rocks, mainly mafic
- Plutonic rocks and migmatites

Haukivesi suite, ca. 1.87 Ga
- Granite, granodiorite
- Tonalite, quartz diorite
- Diorite, gabbro

Kaarakkala and Heinävesi suites, ca. 1.87 Ga
- As dykes
- Granite, granodiorite
- Porphyritic granite, granodiorite
- Tonalite, quartz diorite

Kotalahti suite ca. 1.88 Ga
- Gabbro, diorite body
- Gabbro, diorite

Suonejoki suite, maximum deposition age 1.90 - 1.92 Ga
- Black schist interbeds
- As enclaves in younger rocks
- Paragneiss, mainly migmatitic

Outokumpu association
- Quartz rock bodies
- Serpentinite, skarn bodies
- Serpentinite

Viinijärvi suite, maximum deposition age 1.90 - 1.92 Ga
- Black schist interbeds
- As enclaves in younger rocks
- Paragneiss, mainly unmigmatized

Dykes associated with rifting of the Archaean craton
- Diabase
- Diabase

Karelia supergroup
- Garnet paragneiss, Levänen group
- Arkosite, Levänen group
- Mafic volcanic rock, Neulamäki group, Juojärvi suite
- Carbonate rock, skarn interbed
- Carbonate rock, skarn, Neulamäki group
- Quartzite, arkosite interbed
- Quartzite, arkosite, Nilsiä group, Juojärvi suite
- Conglomerate, arkosite, Lippumäki Formation

Archaean rocks
- Porphyritic granodiorite, Koitere suite
- Tonalite, granodiorite, quartz diorite, mainly TTG-series

Other Symbols
- Outcrop observation
- Diamond drill hole
- Trend of schistosity
- Lithologic contact
- Fault or fracture, tectonic contact
- Thrust or thrust zone

Low-altitude aeromagnetic anomaly map

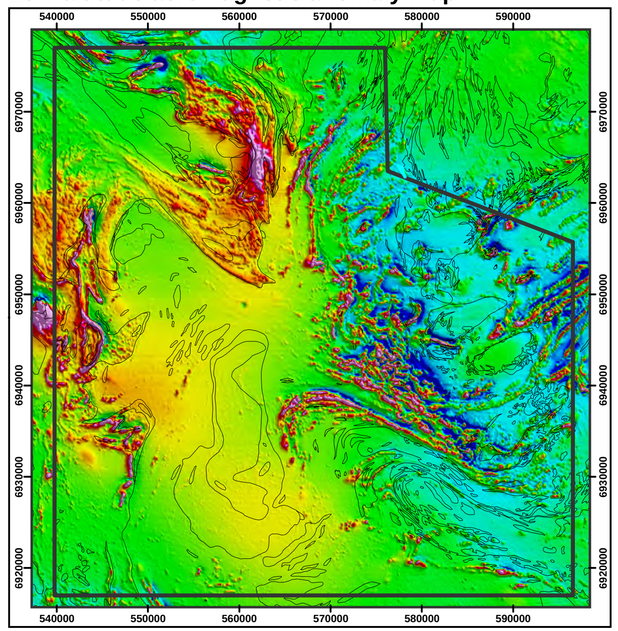

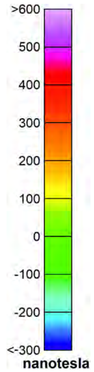

Low-altitude aeromagnetic survey by GTK
DGRF corrected anomaly [nT]

Bouguer anomaly map of the gravity measurements

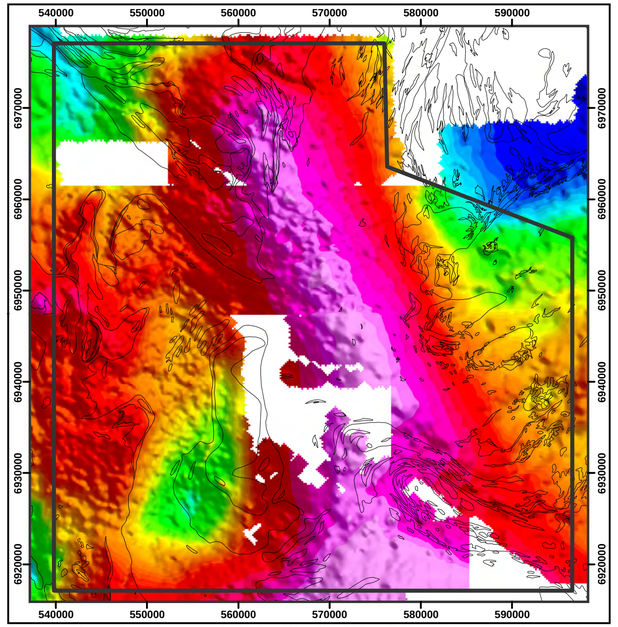

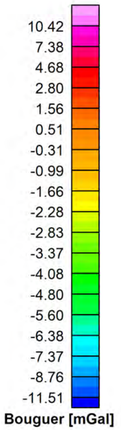

Regional gravity map. Ground measurements (4 to 6 points/km2) by GTK and Outokumpu Oy included with calculated bouguer-anomaly from airborne gradiometric measurements by ABI Holdings limited.

0 5 10 20 km

Bibliographic reference: Mikkola, P., Jäsberg, J. & Luukas, J. 2021. Bedrock map of the western boundary of the Outokumpu allochton. In: Mikkola, P., Aatos, S., Halkoaho, T., Heinonen, S., Hietava, J., Hietala, S., Kurhila, M., Jäsberg, J., Laine, E.-L., Luukas, J., Niskanen, M., Nousiainen, M., Nygård, H., Piispanen, A., Pirinen, H., Rantanen, H. & Romu, I. 2022. Geological evolution and structure along the western boundary of the Outokumpu allochton. Geological Survey of Finland, Open File Research Report 23/2022.

Coordinate system:
Map-datum EUREF-Fin
Map projection ETRS-TM35FIN
Central meridian E27

Compiled by and GIS-production: Perttu Mikkola, Jani Jäsberg, Jouni Luukas
Legend and layout: Riitta Turunen
Base map production: Jyrki Kokkonen

Appendix 2

Low-altitude airborne electromagnetic survey by GTK, quadrature component [%]

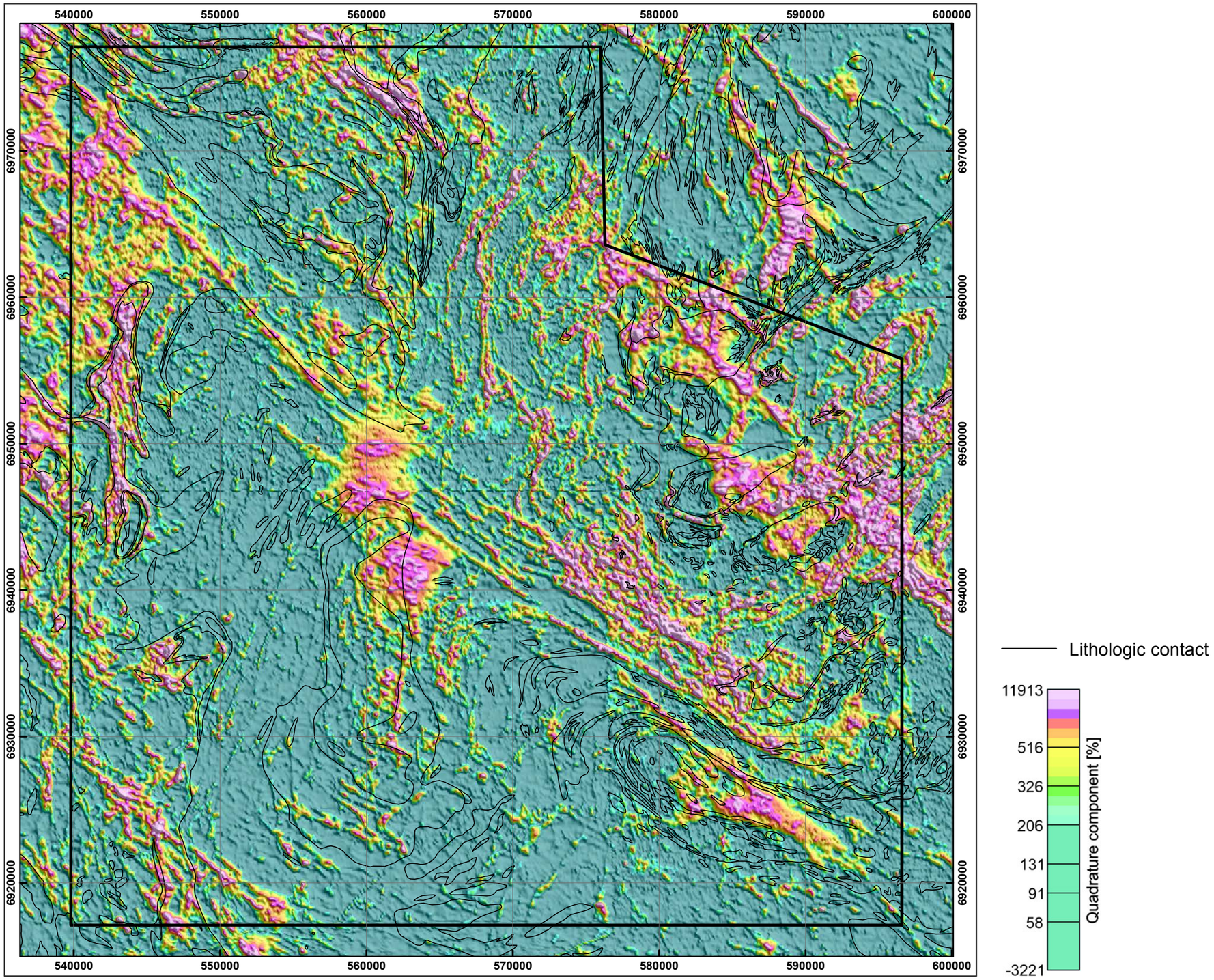

Quadrature component is related to weak electrical conductors such as swamps.

Appendix 3

Low-altitude airborne electromagnetic survey by GTK, in-phase component [%]

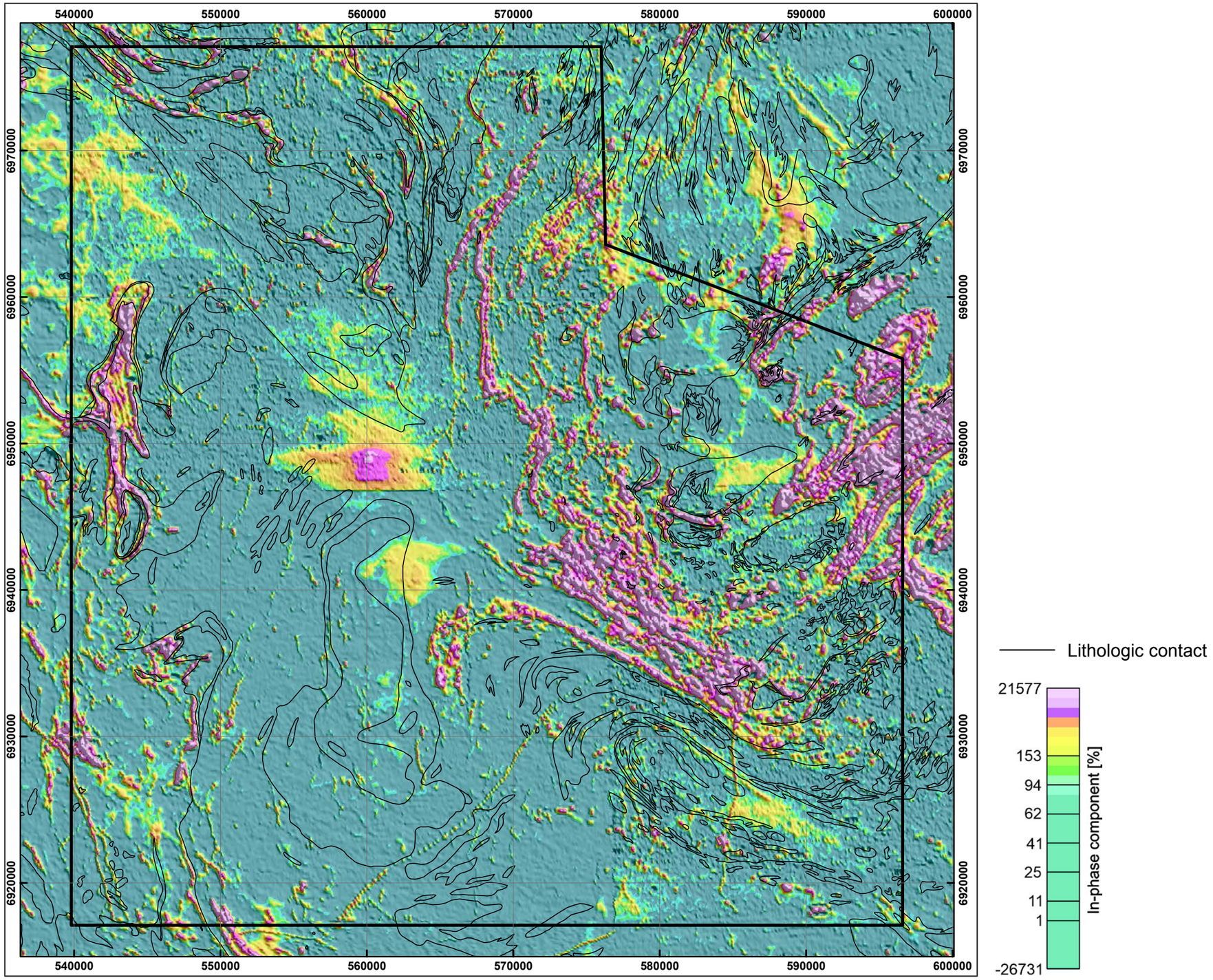

In-phase component is related to good conductors such as mineralisations.

Appendix 4

Low-altitude aeromagnetic survey by GTK, magnetic residual [nT]

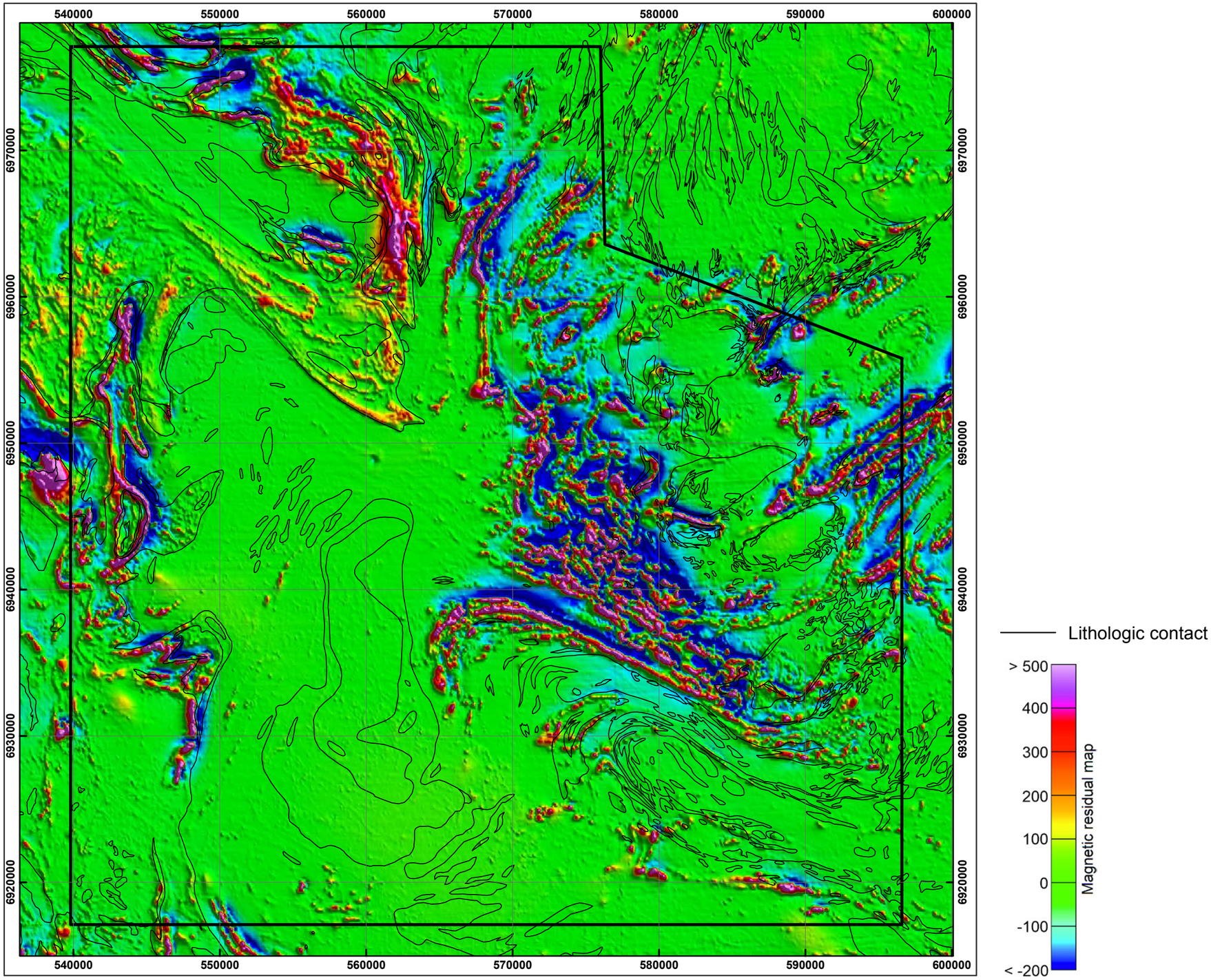

Magnetic trend is removed from the IGRF65-corrected anomaly map to further highlight local, near surface features.

Appendix 5:

1 BACKGROUND

In the Kohma syncline, 12 km west of Tuusniemi, an intact stratigraphy from Archaean basement through Jatulian quartzites and Ludicovian mafic volcanic rocks, arkosites and paragneisses has been preserved. New stratigraphic units have been defined for the area and these are described in this appendix. Location of the section is shown in Figure 1 and inferred cross section through the syncline in Figure 2.

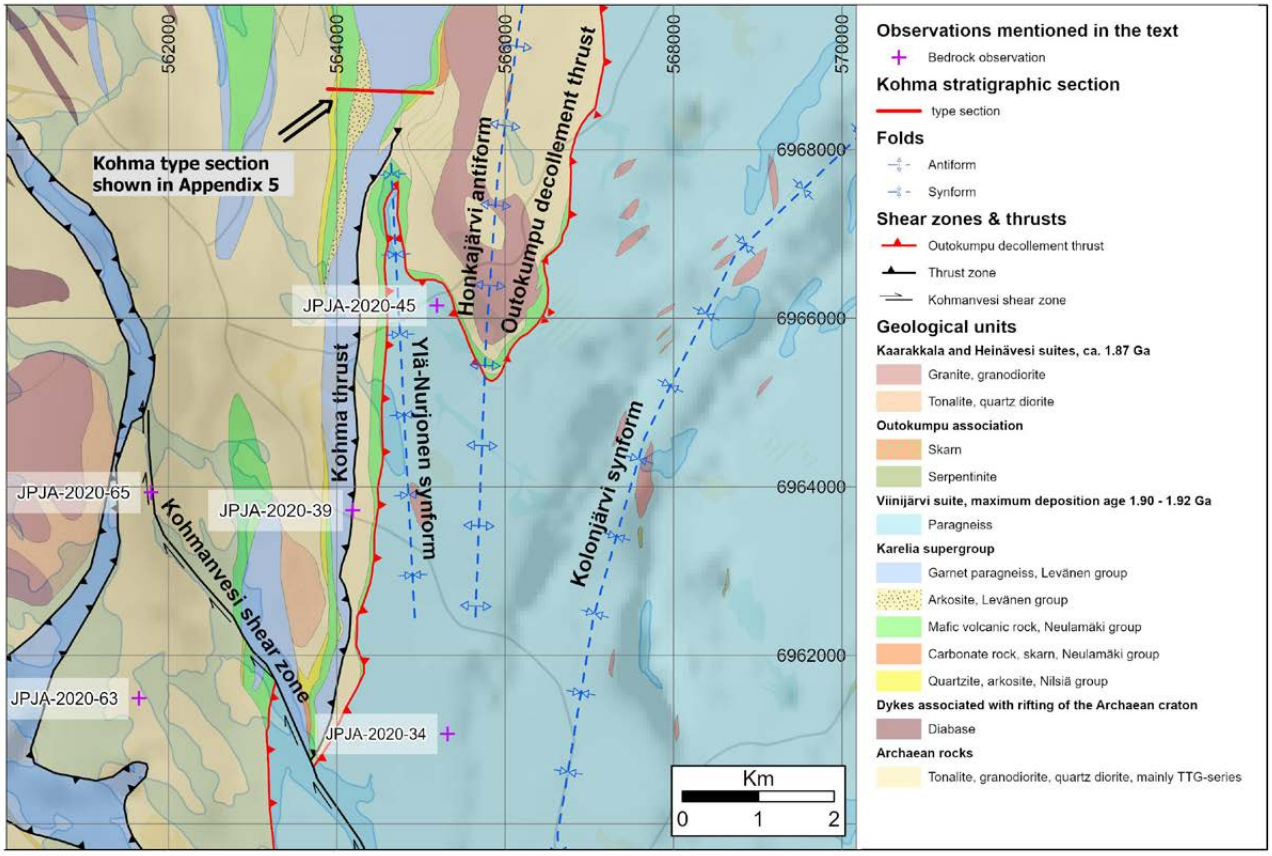

Fig. 1. Location of the type section on geological map (Bedrock of Finland – DigiKP).

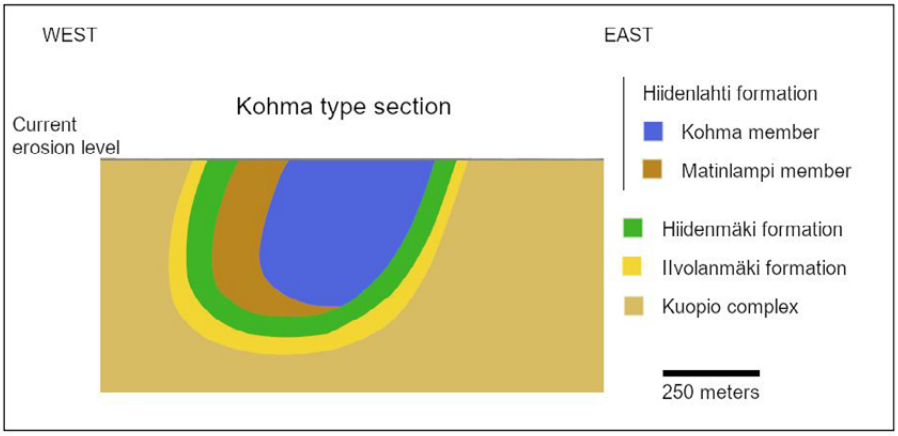

Fig. 2. Cross section of a syncline from Kohma with preserved supracrustal rock of Jatulian and Ludicovian. Location of the cross section is shown in Figure 1. Horizontal scale shown on the right side of the figure. Vertical dimensions not on scale.

1.1 Iivolanmäki formation

The Iivolanmäki formation, consisting of variably pure quartzites (Fig. 3), is interpreted as part of the Nilsiä group. It overlies conformably on top of Archean basement. All primary structures have been destroyed during metamorphism and deformation. The formation belongs to the upper part of the Jatulian period. The thickness of the formation varies from a few tens of meters up to several hundred metres.

Fig. 3. Iivolanmäki formation quartzite with coarse, recrystallised texture from observation location MTL2-2020-23 (E=563 972, N=696 8352). Width of the compass 6.5 cm.

1.1.1 Hiidenmäki formation

The mafic volcanic rocks of the Hiidenmäki formation of the Neulamäki group are deposited on top of Iivolanmäki formation. On the outcrops the unit consists of heterogeneous, relatively fine-grained rocks of volcanic origin (Fig. 4). Due to deformation in the type area nature of the primary structures is questionable, but in other locations pillow lava structures have been preserved. The Hiidenmäki formation belongs to Ludicovian period. The formation's thickness is from 50 to over 200 metres.

Fig. 4. Heterogeneous mafic volcanic rock of the Hiidenmäki formation, observation location JPJA-2020-70 (E=563 960, N=696 6935).

1.1.2 Hiidenlahti formation of Levänen group

The Hiidenlahti formation consists of two members, arkosites of the Matinlampi member and garnet-paragneisses of the Kohma member (Figs. 4–6). Light grey-coloured arkosites form beds of varying thickness above the mafic volcanic rocks of the Hiidenmäki formation. Arkosite beds alternate with beds of garnet-bearing paragneisses of the Kohma member. When moving up in the stratigraphy, the abundance of garnet-paragneiss beds increases, and the upper parts of the Hiidenlahti formation is dominated by the Kohma member. The Hiidenlahti formation belongs to the Ludicovian period and is the uppermost unit in the section shown in Figure 2.

Fig. 5. Matinlampi member arkosite, with cm scale interbeds of Kohma member garnet-paragneiss at observation location JPJA-2020-41 (E=564 010, N=696 2191). Width of the compass 6.5 cm.

Fig. 6. Arkosite (Matinlampi member) and garnet-paragneiss (Kohma member) beds intertwined in the upper parts of the Hiidenlahti formation. Observation location JPJA-2020-68 (E=564 207, N=696 7268).

All GTK's publications online at hakku.gtk.fi